AN ABSTRACT OF THE THESIS OF

David S. Twining for the degree of Doctor of Philosophy in Atmospheric Sciences presented on February 24, 1995. Title: The Relationship of Precipitation in the Western United States to Variations in the Outgoing Long-Wave Radiation field over the Tropical Pacific: The Role of the Mid-Latitude Circulation.

Abstract approved: Redacted for Privacy

The relationship between the outgoing long-wave radiation (OLR) field over the tropical Pacific and wintertime monthly precipitation for the western U. S. is investigated, using the mid-latitude upper-air circulation as an intermediary. Principal components (PC's) of the 500mb monthly averaged height field over the NE Pacific and western North America are compared with those of the monthly tropical Pacific OLR field. It is found that, of the first 6 PC's of the height field, five are correlated significantly with the first 3 OLR field PC's at lags of between two and six months. Canonical correlations between the two sets of PC's are greatest at a lag of four months and are highly significant. When stratified by different levels of the OLR field PC's, the separations between means of the height field PC's are highly significant as well. Differing distributions of the height field PC ensemble are also found to be associated with different OLR field PC levels.

The relationship between the 500mb height field and concurrent western district precipitation is examined. Using a hybrid model including both linear statistical and non-linear physical components it is found that considerably more of the variance in the precipitation can be explained by that of the height field alone than when the precipitation is inferred directly from a linear statistical model.

A set of reconstructed height field PC's is predicted from OLR values based on the height field/OLR stratification associations compiled for a period separate from that of the forecast. Applied to the precipitation

model, this results in predicted western district precipitation which is better correlated with the observations than is the equivalent precipitation forecast from the linear statistical relationship of precipitation to the Southern Oscillation Index.

The Relationship of Precipitation in the Western United States to Variations in the Outgoing Long-Wave Radiation field over the Tropical Pacific: The Role of the Mid-Latitude Circulation

by

David S. Twining

A THESIS

submitted to

Oregon State University

in partial fulfillment of
the requirements for the
degree of

Doctor of Philosophy

Completed February 24, 1995
Commencement June 1995

Doctor of Philosophy thesis of David S. Twining presented on February 24, 1995

APPROVED:

Redacted for Privacy

Major Professor, representing Atmospheric Sciences

Redacted for Privacy

Dean of College of Oceanic and Atmospheric Sciences

Redacted for Privacy

Dean of Graduate School

I understand that my thesis will become part of the permanent collection of Oregon State University libraries. My signature below authorizes release of my thesis to any reader upon request.

David S. Twining, Author

To my father

ACKNOWLEDGMENTS

Throughout the lengthy period of time between the beginning of my research and the presentation of this dissertation I have been guided and advised by my major professor, Dr. Steven K. Esbensen. He has patiently corrected my tendency to follow an initial approach without careful consideration of the alternatives and has always encouraged me to apply more objective measures to better assess otherwise overly intuitive determinations. To his efforts and extensive review I owe much of the validity of the final product. I should also like to thank the other members of my committee and, in particular, Professors Ronald Guenther and Larry Mahrt for a number of helpful suggestions during the final phases of the project.

As an unsupported student, I was given access to the Atmospheric Sciences Computer Facility, through a grant, arranged by Professor Esbensen, at that time Chair of the department. Without such a grant I could have no longer continued my research. The AtS Computer Facility Manager, Dean Vickers, has assisted me on many occasions with the numerous problems that inevitably arise with such an effort.

It was essential for the success of this project that I had access to a number of large data sets which are archived at The National Center for Atmospheric Research (NCAR) in Boulder, Colorado. By the donation of 20 General Accounting Units of computer time, provided without charge through their program to aid unsupported students such as myself, this was made possible. In particular, I wish to thank Dennis Joseph of NCAR's Data Support Division for his kind assistance in providing me both instruction and the necessary data extraction programs for the task.

The precipitation related data sets that I required are archived on the computer systems of the Oregon Climate Service. I am indebted to George Taylor, the Oregon State Climatologist, for the free donation, not only of access to the data but also considerable computation time as well. Much additional help and advice in this area was kindly given by his assistant, Wayne Gibson.

Even for a dissertation, the time required for the research and reworking of this project has been of unusual length. My friends and

family have given me their constant and uncomplaining support over this period and have been understanding in my neglect of many other duties. Longest of all has been the support of my father, to whom this work is dedicated. Well over fifty years ago, he recognized my fascination with weather and gave me my first barometer and first weather textbook. Ever since, he has patiently listened to my speculations on the subject.

Finally, I wish to thank my wife, Shirley. Not only did she assume a major share in the necessary disruptions in both schedule and finances but also was of great assistance in formatting and proofing the thesis itself. Without her steadfast and loyal encouragement my efforts could never have been carried to completion.

TABLE OF CONTENTS

TABLE OF CONTENTS (Continued)

TABLE OF CONTENTS (Continued)

LIST OF FIGURES

LIST OF FIGURES (Continued)

LIST OF FIGURES (Continued)

LIST OF FIGURES (Continued)

LIST OF TABLES

The Relationship of Precipitation in the Western United States to Variations in the Outgoing Long-Wave Radiation field over the Tropical Pacific: The Role of the Mid-Latitude Circulation

CHAPTER 1: INTRODUCTION AND PURPOSE

To those living in the western United States and, particularly, west of the crest of the Cascades and Sierra Nevada ranges, seasonal precipitation is arguably the most important meteorological variable. Destructive storms are infrequent and the occasional hot and cold spells are of but passing interest. The availability of water affects agriculture, sport and commercial fisheries, hydroelectric power and recreation. The bulk of this water, stored in reservoirs and mountain snow packs, is used throughout the year but is principally the result of rain and snow that falls from November through March. The sparse summer rains are of less consequence to the region. It is the cumulative precipitation of the winter months that determines the availability of water for the entire year and the timing and intensity of individual storms are of but transitory interest.

For those who manage water resources, the inability to forecast precipitation on a seasonal or even a monthly basis, poses a dilemma. Total reservoir storage is insufficient to contain the runoff from precipitation of even an average year. One would like to begin the summer dry season with full reservoirs and, as these take months to fill, water managers anticipating a dry winter would prefer to begin containment early by limiting outflow. Should the late winter precipitation be heavy, however, reservoirs would become filled beyond capacity resulting in destructive springtime flooding. Accordingly, the cautious manager delays containment and, for winters that stay or end dry, risks starting the summer with half filled reservoirs. There are many others, managers and users alike, that need to make water related decisions that cannot be delayed until the winter is over and the final totals are recorded. For the present, such decisions must be based on forecasts for which the confidence level is so low as to make them of little assistance.

In the past few decades the skill and utility of short-range forecasts have improved to the point that they can be used as a reliable factor in weather related decisions. Forecasts of five days, which were of little use prior to 1980, have become reasonably accurate in so far as the general circulation pattern is concerned. For example, 500mb anomaly correlations between five-day forecasts and observations have improved from 0.62 in 1985 to 0.73 in 1989 (Caplan and White, 1989).

Unfortunately, the situation is quite different for forecast periods of a month or a season. Other than some small success with some statistical approaches by the NMC which will be described in the next section, the little skill demonstrated has been due to the inclusion, in the beginning of the forecast period, of the last vestiges of dynamic predictability (Epstein, 1988) and the assumption of persistence.

1.1 The nature of the extended forecast problem

The National Meteorological Center (NMC) provides forecasters with a number of products. For the synoptic forecaster there are various model outputs which may be used as important aids in predicting conditions up to about three days in advance. Discussed at some length by Hoke et al. (1989), they include the Limited Fine Mesh model (Garrity, 1977), the Nested Grid Model (NGM) (Phillips, 1979) and various spectral models of increasing resolution (Sela, 1982,1988). For the United States, the NGM not only provides the 500mb and 700mb height forecasts for 12, 24, 36 and 48 hours in advance but also concomitant surface pressures, thickness, vorticity, vertical motion and 700mb relative humidity. Even quantitative precipitation is forecast, based upon orography, vertical motion and available moisture. Beyond 48 hours the spectral models provide 500mb height forecasts out to 72, 84 and 108 hours in advance with decreasing reliability and with increasingly truncated wave numbers used for graphic presentation (the short-waves associated with specific disturbances are not resolvable for the five-wave representation used in the 108 hr forecast). Using the 18 layer, 80-wave triangular truncation (T80) version of the spectral model the NMC Medium-Range Forecast Group also produces a

number of 6-day and 10-day 500mb forecasts, again presented with a resolution limited so as to suppress the unreliable short-wave features (Petersen and Stackpole, 1989). As the models have improved and the initialization has become more accurate the skill of these forecasts has risen steadily.

Caplan and White (1989) provide graphic and objective evidence of the improvement over the years in the quality of the height forecasts. They show, in addition, that the reduction in forecast height error for forecast periods of five days or more is greater for levels between 700mb and 250mb than for either the lower levels or for the stratosphere.

For specific local forecasts of temperature and precipitation, forecasters at the national level have compared, historically, the outputs of these circulation models with the temperatures and precipitation which actually occurred, accumulating Model Output Statistics (MOS) for each station which may then be applied to current model outputs for generating local MOS forecasts (Glahn and Lowry, 1972). As a minimum, such forecasts can serve as a guide to the skilled local forecaster who may modify them based upon specific local experience or disagreement with the outputs of the models themselves. The introduction of MOS (in 1972) to the probability of precipitation (PoP) 48-hour forecasts effectively doubled the precipitation skill scores for individual stations over those produced directly from the dynamic models (Carter et al., 1989).

Comparison of the current forecasts with the actual observations shows the observer that, beyond 48 hours in advance, forecasts of the timing of onset and intensity of individual synoptic-scale disturbances are not reliable. Junker et al. (1989) shows that by 48 hours the mean error for forecast positions of surface cyclone and anticyclone centers over the US has already grown to about 500 km (1987-1988 data). However, forecasts of change or continuation of more general upper air flow regimes which indicate the *probability* of passage and intensity of such synoptic events for a given region are now forecast with reasonable skill for periods of on the order of a week. Tracton et al. (1988) shows how the Dynamical Extended Range Forecast model (DERF) maintains at least some residual skill in the forecasting of flow regimes out to about ten days. Beyond that period the model results are only slightly better than persistence. They show, additionally, that the model skill is dependent on the flow regime. For

example, the initiation of blocking is not well forecast and skill varies with the PNA index.

Beyond ten days there remains but small residual skill in the prediction of even the planetary-scale structure of the upper air flow by dynamic models alone. Indeed, there have been many studies, beginning with that of Lorenz (1969b) up to that of Epstein (1988), which have shown that the theoretical limit to dynamic predictability, at least on the *synoptic* scale, is on the order of about two weeks. Model development has not yet reached this theoretical limit and there are still gains in dynamic predictability to be realized. Nevertheless, as the model boundaries are expanded, with more physical processes included, and as the resolution in time and space is improved, the computational cost rapidly becomes enormous. A global model capable of resolving meso-scale processes is beyond our present capability. Bonner (1989) states that the next generation of computers should permit meso-scale resolution for individual storm systems but would be unlikely to permit expansion to the scale of the United States. Shuman (1989) remarks that an order of magnitude increase in computer power is required for a doubling of resolution and that experience shows that with such a doubling the forecast skill appears to increase only about 15%. Resolution necessary to model directly the evolution of cloud elements would require a further increase of many orders of magnitude. There have been advances in our ability to parameterize sub-grid processes but this approach also has limitations.

As cited above, however, even with a hypothetical "perfect" model it can be easily shown that the effect of small errors in initialization, on the order of the resolution limits of our instruments of measurement, will amplify sufficiently to obscure the "true" forecast over an interval dependent on the time-scale of the feature which is forecast (e.g., Schubert et al., 1992). It is this last point that provides some amelioration of an otherwise bleak prospect for substantive progress. As stated by Tracton et al.(1989), there is a residual degree of dynamic predictability that does not fall off at the same rate as does the initial predictability. They speculate that this may be associated with atmospheric modes of considerably longer time-scale, for which the theoretical limits of predictability must be commensurately extended. These modes may, in addition, be influenced

by external forcing from adjacent systems (such as the oceans) which operate on yet longer time-scales. As compared to the more rapidly evolving mid-latitude circulation, persistence alone makes the oceanic circulation more predictable on the seasonal time-scale.

Despite the problem of our present inability to extend *dynamic* predictability beyond about ten days, the NMC has taken advantage of the *statistical* relationships between these modes and various boundary conditions and also within the modes at different time lags to produce extended range forecasts of regional temperatures and precipitation for periods of a month or season. Wagner (1989) describes the process as a combination of applying the month-to-month autocorrelation statistics of 700mb anomaly fields, the statistical effects of the Quasi-Biennial Oscillation (QBO) and Sea-Surface Temperatures (SST's), while also considering the statistical relation of anomalous positions, and strengths of the major surface centers of action such as the Aleutian Low. The weights given to each of these relationships are determined subjectively, and the combination determines the predicted 700mb height field.

The effect of this field on regional temperature and precipitation may be determined subjectively from meteorological experience. However, this is now supplemented by a simple statistical model developed by Klein and Bloom (1989) which, by regressing temperature and precipitation anomalies against 700mb heights at several geographic positions (for a given district), obtains weighting coefficients necessary to infer temperatures and precipitation. The skill of this model, assuming a perfect forecast of the 700mb height field, is modest, depending on the season and the district. For precipitation it is most accurate in the western US. and for the winter season, explaining about 40 percent of the variance for the best correlated district, but this is for categorical forecasts divided into three approximately equal groups of below normal, normal and above normal amounts.

Klein and Bloom (1989) note that predictions of above normal monthly precipitation using this model and the NMC 700mb height forecast are correct an average of about 37% of the time, for example, whereas by chance the success rate should be about 30%. In terms of a skill score referenced to climatology such that SSC =(F-C)/(1-C), where F is the fraction for an event forecast correctly and C is the fraction for that event

expected by climatology, Epstein (1988) reports that seasonal precipitation forecasts generally (but not always) have positive skill scores but seldom greater than 0.1. This is not particularly useful, even for a categorical forecast, and extended-range *quantitative* precipitation forecasts are not normally attempted. Any additional understanding of processes which may contribute, even to a limited degree, to future changes in the height field; or how the height field determines precipitation may thus represent a substantial advance in extended-range forecasting.

1.2 Purpose and rationale of the investigation

The general purpose of this study has been to investigate the influence of conditions over the tropical Pacific on the distribution of monthly and seasonal precipitation across the weather districts of the western US. The key element of the investigation was that of the role of the upper-air circulation over the NE Pacific and western North America as a necessary intermediary between tropical conditions and western US precipitation. In particular, the investigation examined both the relationship of the Outgoing Long-wave Radiation (OLR) field of the tropical Pacific to the five-day time averaged 500mb height field over the NE Pacific and western North America and also the relationship of this height field to wintertime monthly district precipitation in the western United States.

1.2.1 Motivation

The study was motivated, originally, by a study concerning, in part, the association between the Southern Oscillation Index (SOI) and western precipitation (Wade et al., 1989) in which this investigator participated. For the western US. weather districts, they have shown significant correlations between the SOI and monthly and seasonal precipitation in the Pacific Northwest (positive) and in the lower Colorado Valley (negative). Correlations are highest at a lag of four to six months after the SOI measurement. Ropelewski and Halpert (1989), note that cold El Niño-

Southern Oscillation (ENSO) events (with positive SOI) are weakly associated with subnormal precipitation in the southern portions of the Great Basin whereas more warm events are associated with years of above normal precipitation in the same region. They report no significant associations with warm and cold ENSO events elsewhere in western North America, however. Figure 1.1, taken from Wade et al. (1989) shows correlations between district precipitation and the SOI for the winter seasons (Oct.- Feb.) from 1933 to 1985 with a five months lag. Figure 1.2 is from the same data set showing the probability of these apparent correlations occurring by chance. It can be seen that the correlations along the coastlines of Oregon and Washington are significant while those across Arizona, south Nevada and much of Southern California are highly significant. For the great remainder of the western districts, however, the correlations are small and not significant. Those portions of the correlations shown in Fig. 1.1 which *are* significant, however, imply a relationship between western precipitation and the remote tropical Pacific that would appear to require intermediate links; the adjacent link to western precipitation is clearly the circulation over and upstream of this region. Not only is predicted circulation (or height field) the primary input to most precipitation forecasting systems, but, as is demonstrated in the following chapters, most of the variance in the precipitation field can be explained by that in the circulation field.

The SOI/ precipitation correlations discussed above led to the question of whether tropical related changes to the mid-latitude circulation pattern would be found consistent with precipitation changes to the same or greater extent as those associated directly with the SOI. Using the mid-latitude circulation as an intermediary between the tropics and western precipitation would permit the employment of a regional, circulation based precipitation model which might forecast precipitation for more western districts than those for which the direct SOI/precipitation correlations were significant. On the other hand, if contrary to the assumptions of our study, the mid-latitude circulation were *not* a useful intermediary then the precipitation predictions based on the circulation would be inferior to those directly from the SOI.

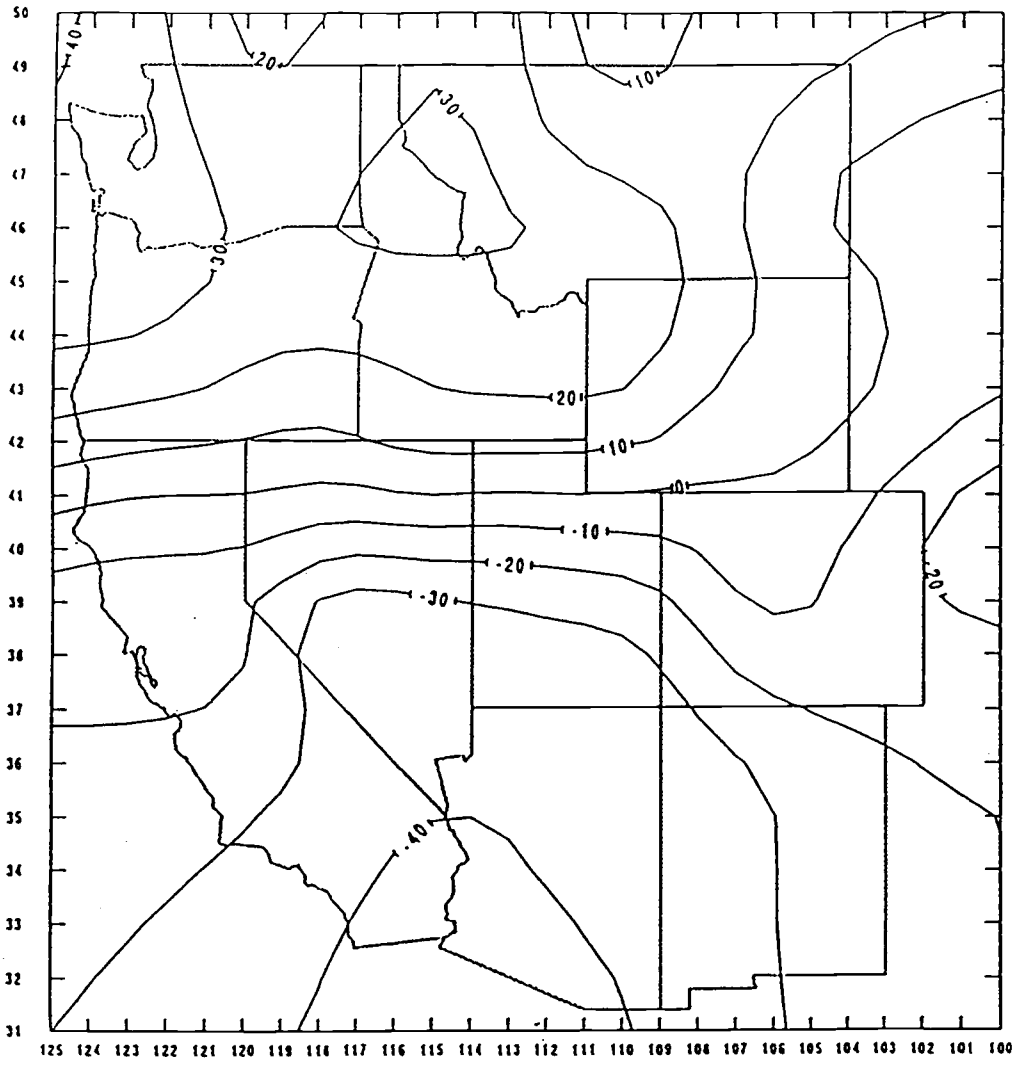

Fig. 1.1 Correlation (in percent) of western district precipitation for the months Oct. through Feb. for years 1933 through 1985 with the Southern Oscillation Index (SOI). Precipitation lags SOI by five months.

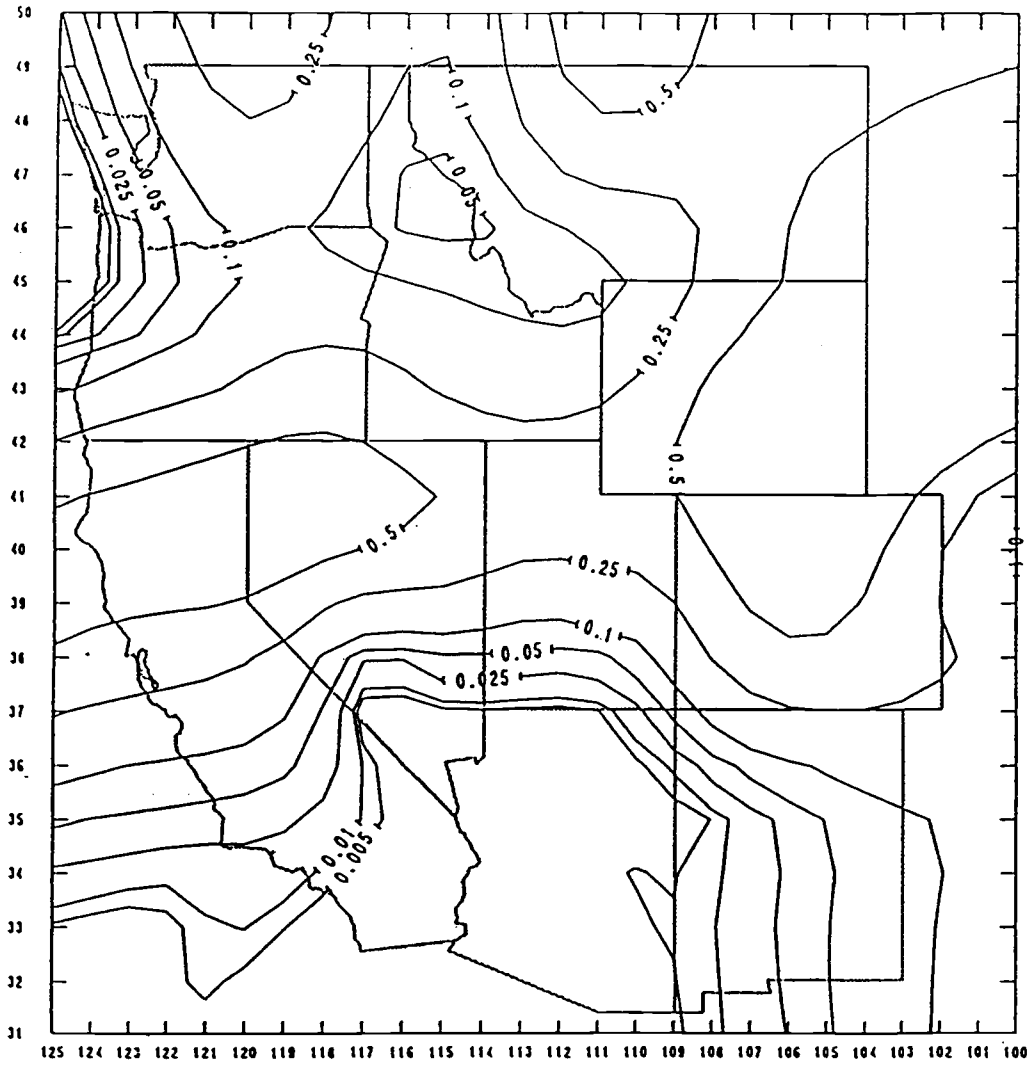

Fig. 1.2 Probability that correlations shown in Fig. 1.1 are actually zero.

An additional advantage to the two-phased approach of this study is that the physical relationship of the circulation to precipitation is determinable and it may be possible (although beyond the scope of this investigation) to find the dynamical basis for the link between the tropical and mid-latitude circulations as well. Conversely, there appears to be no reasonable direct physical link between the SOI and western district precipitation which could be exploited.

There is little expectation of extended-range forecasting of the day-to-day evolution of the synoptic-scale mid-latitude height field. For the time-averaged long-wave or planetary-scale circulation, as discussed in Section 1.1, there presently exists some limited skill using a combination of the last vestiges of dynamical predictability, persistence and statistical inference. Some of the history of the progress in understanding the nature and the difficulties involved is related in the following chapter. Common to both observational studies, such as that of Horel and Wallace (1981) and also model studies such as Hoskins and Karoly (1981) or Kushnir and Lau (1992), is the implication that predictability of the mid-latitude height field from external forcing (such as it is) is in the slowly varying long-wave component of the circulation rather than in the rapidly varying synoptic-scale component. Accordingly, a precipitation model developed to exploit circulation forecasts should be able to use, as its sole variable input, the long-wave circulation or height field and not require synoptic-scale detail.

As set forth in the opening paragraphs of Section 1.2, we are here focused on monthly time-averaged and district space-averaged precipitation and will show that, with this limitation, the indices computed by our model from the slowly varying long-wave approximation to the 500mb height field will explain more than half of the variance in the precipitation field.

1.2.2 The influence of the tropics on the mid-latitude height field

The response of the mid-latitude height field to changes in various tropical fields has been studied by a number of investigators but the results have been of limited use in their application to forecasting rainfall along

the Pacific coast. The steady linear response (as seen in mid-latitude height anomalies) associated with tropical thermal forcing (Hoskins and Karoly, 1981) and similar effects linked to interannual variability of the equatorial sea-surface temperature (SST) by Horel and Wallace (1981) appeared to result in an insufficient change to the height field directly over the far western U.S. to account for the precipitation anomalies associated with the SOI. While both of the above studies show increased heights over the northern Rockies and decreased heights well off the north Pacific coast associated with the warm phase of the ENSO, there is little change along the coast itself or in the lower Colorado Valley where the SOI/precipitation correlation is the greatest. These are the same regions for which the operational extended-range precipitation forecasting system (Klein and Bloom, 1989) best correlates local height anomalies with district precipitation. It should be noted, however, that this configuration of height anomalies *is* consistent with an anomalous coastal southerly wind. We believed that a more sophisticated precipitation model with a region-wide circulation pattern as its input might better utilize the height anomalies associated with tropical change.

It was also considered possible that, if more information on the tropical configuration than that represented by a single scalar variable (such as the SOI) could be included in the comparison, the associated mid-latitude circulation might be determined in greater detail. The importance of eddy fluxes in the poleward transfer of angular momentum from the tropics increases with latitude (Palmen and Newton, 1969); and while a zonally symmetric Hadley cell, with momentum transfer solely by mass flux of air aloft, is mathematically possible, it would be baroclinically unstable (Holton, 1979). Starr and White (1951) have demonstrated that at the latitude of maximum momentum transfer (about 30° for the winter season) the contribution of the asymmetric eddies is much greater than that of the mass flow. The location and intensity of the injection of momentum into the westerlies is thus influenced by the structure of the these eddies which extend from the region of ascent near the ITCZ into the subtropics. We believe it reasonable, then, to expect a relationship between the configuration of the circulation over the tropics and that of the mid-latitudes. While the SOI is related to the *strength* of the east-west Walker circulation component over the tropical Pacific, it cannot, by itself, be

indicative of the low-latitude eddy *structure*. A number of different eddy structures, with differing effects on the mid-latitude circulation could be associated with the same SOI value. An adequate representation would necessarily require more than a single parameter.

Additionally, it appeared likely that the *distributions* of the various mid-latitude circulation states associated with different tropical conditions might differ as much or more as the *means* of the states. For example, if a specific distribution included even a small proportion of circulation states with the Polar Jet through Southern California, its effect on the total precipitation there would be far greater than the small shift in the mean circulation would suggest. An alternate distribution might even show the *mean* position of the jet to be shifted further southward, with heavy rains for the central California districts, but without any occurrences of the jet axis through Southern California. Were such relationships determinable, the differences in states on the extrema of the distributions might be found to have a greater effect on district precipitation than the differences in the means. Accordingly, we have attempted to relate differing mid-latitude circulation state *distributions*, as well as differing means, to tropical conditions.

There are other probable forcing mechanisms for the Pacific mid-latitude circulation such as mid-latitude sea-surface temperatures (Kushnir and Lau, 1992) and other mechanisms which will be discussed later. Tropical forcing has been selected for this study, however, not only due to its already demonstrated statistical linkage with western precipitation but also due to the fortuitous time lag (Ropelewski and Halpert, 1989) between the change in the tropical pacific and that of the western precipitation pattern. Moreover, the time-scale of state evolution over the tropical Pacific basin is much longer than that of the mid-latitudes. This may be demonstrated immediately by an autocorrelation of the SOI, shown in Fig. 1.3, which shows positive autocorrelations for lags of up to nine months and negative autocorrelations for lags between one and two years implying quasi-periodic behavior. Additionally, the composite of a number of El Niño episodes (Rasmusson and Carpenter, 1982) demonstrates that many warm episodes appear to have a characteristic progression which implies predictability.

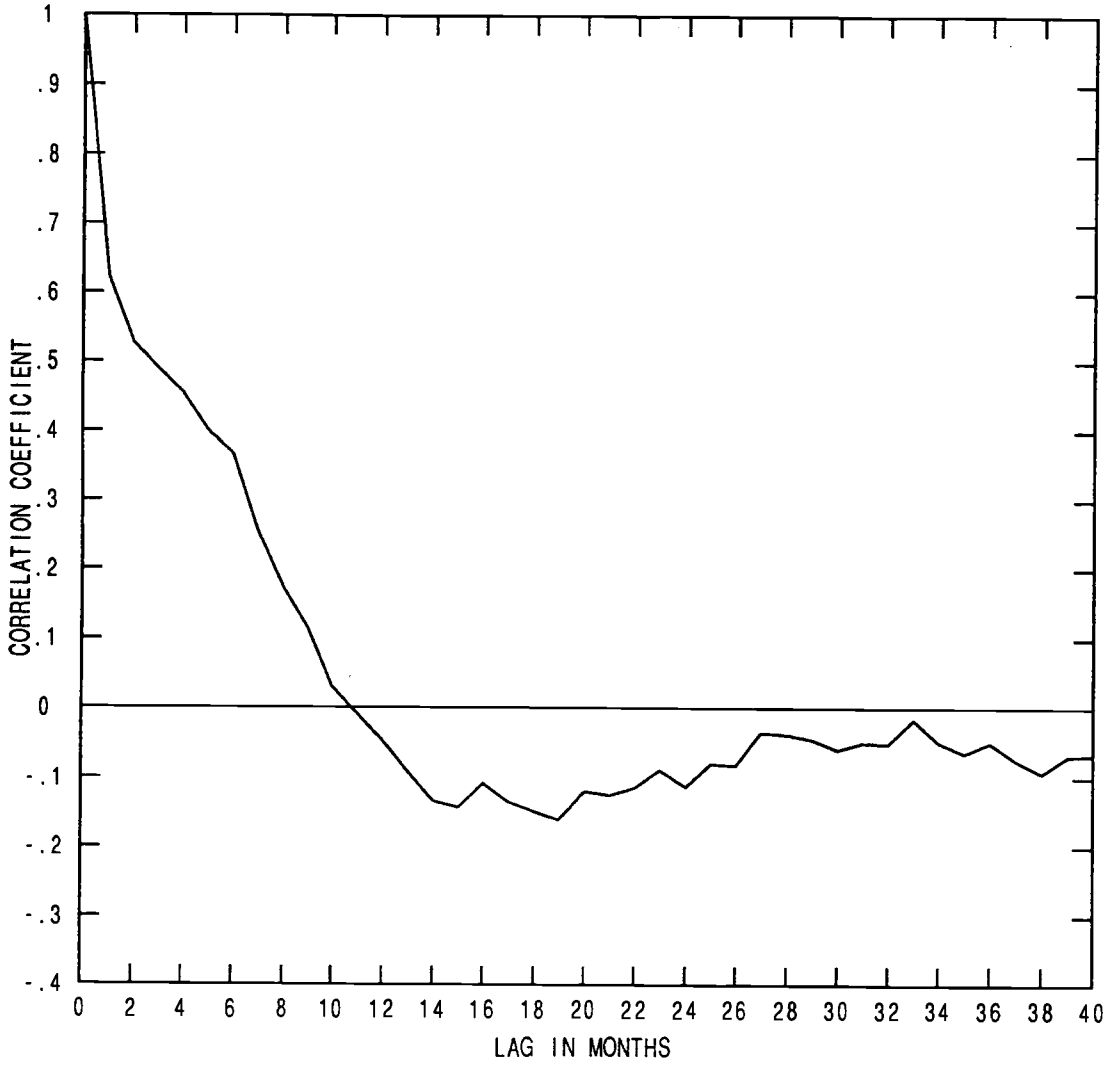

Fig. 1.3 Autocorrelation of SOI for lag times of zero to 40 months for years 1933 through 1985.

The ENSO model of Cane and Zebiak (1987) has had some success with deterministic prediction, once the warm episode has commenced, although the model has not correctly predicted the evolution of the most recent (1992) El Niño. Nevertheless, the period of deterministic predictability of large-scale conditions over the tropical Pacific is clearly far longer than it is for even the planetary-wave structure of the mid-latitudes. Finally, from a philosophical aspect, as the main source of energy to power the mid-latitude circulation is in the release of latent heat in tropics, the choice of this region for a forcing mechanism is attractive.

In selecting a field variable for representing conditions over the tropical Pacific, it was considered that the upper-level circulation has the best potential for being directly linked to that of the adjacent mid-latitudes. The energy of tropical convection from the meso-scale convective cloud clusters (MCC's) along the Inter-Tropical Convergence Zone (ITCZ) far exceeds local dissipation (Hastenrath, 1985) and is exported poleward to power the Subtropical and Polar Jets and, to a large extent, the entire mid-latitude westerly circulation. Hoskins and Pearce (1983) discuss how convergence in this poleward flow in the extra-tropics is consistent with jet acceleration. The poleward outflow varies in longitude (being greatest over the western Pacific and Indonesia in the northern winter and over SE Asia in the summer) but also interannually, with an eastward displacement associated with the warm or El Niño phase of the ENSO. Rasmusson and Mo (1993) show a specific tropical to mid-latitude 200mb circulation anomaly linkage for the warm and cool phases of one ENSO cycle.

Comparisons which include a two-component field, such as the horizontal wind, are more complex than for a single-component field, such as the geopotential height and we accordingly use the height field in the mid-latitudes as a surrogate for the circulation there, assuming the geostrophic wind to be a reasonable approximation. This is not true in the tropics, where the Coriolis parameter is small and geostrophic control weak. The ageostrophic wind component is particularly important in the deep tropics, in the vicinity of the upwelling air from the MCC's along the ITCZ (Webster, 1983). Tropical wind fields are depicted, typically, by streamline plots, which show winds diverging from the regions of upwelling (Hastenrath, 1985). Candidate single-component surrogates for this wind field include the velocity potential, indicative of the irrotational

component of the wind, and the divergence field (Webster, 1983). The computation of either of these measures from observations requires a very accurate determination of the horizontal winds or a reasonable estimation of the vertical wind field (Holton, 1979).

Until the availability of satellite observations, measurement of winds over the tropical oceans was limited to widely spaced RAOB stations on islands or on ships or from transient aircraft. For short periods, dense observational networks have been established, such as in GATE and MONEX (Hastenrath, 1985) which provided high quality wind field data; the periods of observation, however, were insufficient for the purposes of our comparisons. For more than twenty years, wind measurements of high-level tropical winds have been determined from satellite observation of cloud motion and with increasing accuracy. From initial determinations (about 1970) to 1979 the mean high-level wind errors decreased from about 10 ms^{-1} to about 2.5 ms^{-1} (Hasler et al., 1979). Error sources include the uncertainty of target cloud height, non-advective cloud motion and poor cloud point identification from scan to scan (Hubert and Whitney, 1971). By the early 1980's a number of analysis techniques (Stout and Young, 1983) had further reduced the mean velocity errors to about 1.7 ms^{-1}.

The tropical field comparisons in this study are already handicapped by the brevity of the observational record. Were 20 years of wind observations available, with an accuracy attainable today, we would probably use the horizontal wind-derived velocity potential field or the divergence field for our comparative variable. However, the wind velocity accuracies for the earlier portion of the period appear to be insufficient for this purpose (Krishnamurti and Low-Nam, 1986) and the remainder of the period is too brief.

The vertical wind field may also be used to compute horizontal divergence and the requirement for accuracy is not as stringent as that for the horizontal wind (Holton, 1979) but direct measurements of vertical wind are difficult to obtain. Charney (1963) noted that, from scaling considerations, the tropical atmosphere must be virtually non-divergent and barotropic outside of areas of precipitation; the principal divergence fields must be concentrated in the regions of deep convection. This has permitted an estimate of the divergence field by associating deep convection

intensity, determined by the cloud top heights, with vertical velocity. Krishnamurti and Low-Nam (1986) have used the Outgoing Long-wave Radiation (OLR) field, indicative of cloud top height and convection intensity, to determine the divergence field. They have found a linear formulation with terms of both the OLR and its Laplacian which yields a value of divergence correlated at 0.76 with divergence computed directly using winds from the FGGE IIIb data set. Puri and Miller (1990) have extended this approach with a non-linear model inferring rainfall, divergence, velocity potential and moisture fields from the OLR field.

From such considerations it was decided to use the structure of the OLR field to represent that of the tropical circulation configuration. The level of detail in the monthly averaged record available gives a depiction of the upper-level tropical cloud structure which contains far more information than a single index (such as the SOI) but sufficiently compact to be conveniently decomposed into a small number of indices which explain most of the variance in the field and may be compared with similar indices from the mid-latitude height field.

It is possible to compare the tropical OLR and mid-latitude 500mb height fields directly by means such as combined principal component analysis (Kutzbach, 1967), canonical correlation (Barnett and Preisendorfer, 1987) and singular value decomposition, which is well suited to the comparison of large data sets (Prohaska, 1976). Singular value decomposition is particularly applicable for cases in which the data are collocated on a common grid (which is not the case for this comparison). It was decided, however, to first reduce the two fields, separately, by principal component analysis into a number of EOF's and associated principal component score matrix time-series (for convenience these will hereafter be referred to as PC's or PC time-series). These PC's are then compared in individual pairs by simple linear correlation and, in addition, each of the height field PC's are compared to a combination of OLR PC's by multiple linear correlation. Finally, five height field PC's are compared jointly with three OLR field PC's by canonical correlation. This procedure gives us the ability to examine the association of specific features of one field with those of the other either separately or in combination. Furthermore, a number of the components can then be

related to observable physical modes so that the nature of the associations between them may be better understood.

1.2.3 The precipitation model

As discussed above, the precipitation model must be able to infer the wintertime monthly western district precipitation from the long-wave 500mb height field. For monthly precipitation there is no necessity for specifying the time of onset, duration or intensity of individual storms. The monthly accumulated precipitation totals can be inferred from a determination of the *expectation* of precipitation for a given district. For the model, this expectation will be determined by relating the five-day averaged 500mb height field to the probability of orographic precipitation and to that resulting from synoptic-scale disturbances propagating along the storm track. The specific precipitation mechanisms and their implementation in the model will be discussed in Chapter 4 and in the appendices.

In general, the model uses a combination of direct computation and statistical inference to determine wind fields and temperature and moisture profiles over the district for which the precipitation is forecast. Orographic precipitation is computed directly, by an estimation of moisture condensed due to cooling by lifting of air as it passes over the district terrain. Synoptic storm precipitation is estimated from the configuration, position and strength of the band of maximum 500mb winds in relation to the forecast district.

The NMC operational model of Klein and Bloom (1989), with 700mb heights spaced at approximately 5° intervals as inputs, uses weighting coefficients determined by multiple linear regression to proceed directly to district precipitation. We believe, however that the simplifying assumption of linearity of precipitation with height results in a considerable loss of skill for this model. As will be shown in Chapter 4, the orographic precipitation mechanism is a highly nonlinear function of winds, terrain and moisture and the distribution of precipitation across the storm track is a complex and nonlinear function of flow configuration as well. While the

intermediate wind, moisture and temperature variables are not strictly linear functions of the 500mb height field, such a large proportion of their variance is explained that the assumption of linearity here contributes little to loss of skill. In summary, the physically based nonlinear computational step between the intermediate variables and the indices preserves a good proportion of the variance lost in the NMC model.

1.3 Outline of the dissertation

In the following chapter, some of the applicable prior approaches to the general problem addressed initially in this introduction are reviewed. This is followed by a description of the data sets used. In Chapter 3, we discuss the western district precipitation pattern, its relation to the 500mb height field over the NE Pacific and western North America and some general mechanisms of western wintertime precipitation. In Chapter 4, we present our western district precipitation model, first discussing the specific precipitation mechanisms applicable to the western US and how a number of these are included in the model and then the model methodology. Much of the specific model implementation is detailed in Appendix A and a supporting study of circulation types and baroclinic (storm track) precipitation is presented in Appendix B. The model is next evaluated, assuming a perfect 500mb height forecast, comparing the model skill using the actual height fields with that resulting from representing the height fields by various numbers of EOF's. In Chapter 5, the association of variations in the OLR field of the tropical Pacific with those of the 500mb height field over the NE Pacific and western North America is assessed by various comparisons of the principal components of the two fields at different lag times. The fields are compared by correlations between individual PC time-series, by multiple correlations of each height PC series against the first three OLR PC series and then by canonical correlation between the set of the first 5 PC's of the height field and set of the first 3 PC's of the OLR field. The differences in the means of the height PC's are determined when stratified by values of the OLR PC's. Additionally, we show differences in the distributions of the height PC's

resulting from this stratification. Finally, wintertime monthly district precipitation is forecast for the years 1980-1988 using the OLR field of four months prior to the month of each forecast. This is compared with the observations and evaluated. Chapter 6 summarizes the study and concludes with suggestions for further investigation.

CHAPTER 2: BACKGROUND AND DATA SETS

Before describing and evaluating the precipitation model it is appropriate to review some of the previous approaches to the extended-range forecasting problem. A discussion of the primary data sets and their initial processing follows this review.

2.1 Historical review

For as long as observations of weather in the mid-latitudes have been recorded, episodes of persistent abnormal conditions for periods of up to a season in length have been noted. Many observers were aware that, in addition to the day-to-day fluctuations in wind, temperature and precipitation, which we now associate with the passage of synoptic-scale disturbances, there appeared to be more general variations of a considerably longer time-scale. Moreover, there has long been the impression that this sort of variation is not merely an extension of the day-to-day variability but something separate and distinct.

A number of approaches to explaining and forecasting the long-term variability have been attempted. One of the earliest, as discussed by Namias (1968), was the work of Teisserenc de Bort (1883) who formulated the concept of "centers of action", further developed by Clayton (1935) and by Namias (1936) who extended the concept to a broader consideration of circulation classifications.

The complexity of the spatial and temporal structure of the total variability made real progress in its analysis impossible prior to the availability of synoptic surface data and, only after synoptic upper air charts were available on a routine basis, was it possible to observe the different scales with clarity. The possibility of extended-range forecasting by associating current upper-air charts with previous chart sequences was examined by Elliot (1944), who, although unsuccessful in actual forecasting, was able to discern that certain sequences appeared to be similar. By comparing large numbers of sequential charts he noted that

although there was a continuum of structure at all scales, a significant proportion of the variability appeared to be grouped into a number of "types".

An early attempt at type categorization was the *Grosswetterlagen* of Baur (1951). Baur divided the northern temperate zone into longitudinal sectors and described a number of "characteristic" weather types for each sector. He further postulated that the weather could be characterized by rather abrupt transitions between types and that these transitions tended to occur near "key" dates. Most of these conclusions were based on a statistical examination of the limited data available at that time and cannot be substantiated by a similar examination of the more extensive data accumulated since. His initial conclusion, however, that *Grosswetter* exists, appears to be valid; that the long term anomalies are large, comparable to the climatological differences due to change of season, and that the time scale of these anomalies is well separated from that of the synoptic-scale fluctuations. This is related to the later determined but now well known separation in both space and time scales between the short and long waves in the circumpolar vortex (Sawyer, 1970).

The search for repeating weather sequences led to the method of "analogues" (Craddock, 1958). The concept is that similar weather situations should evolve similarly and the more closely a past circulation pattern is duplicated by a current situation, the longer will the current evolution match that of the past (Lorenz, 1969a). While the analogue method has the appeal of representing real events in the past and, in a sense, constitutes an "easy solution" to the forecast problem, it is greatly restricted by the near impossibility of actually finding an actual, sufficiently accurate, match in the past records (Namias, 1968).

Direct external forcing from cosmic influence, such as solar constant variations and the sun-spot cycle has been investigated by Walker (1915), Clayton (1934) and Abbot (1935). Even the lunar synodical period has received some attention (Brier and Bradley, 1964). While some intriguing relationships have emerged from these studies, their validity remains controversial (Namias, 1968).

A more general approach to the characterization of weather patterns was based on variations in the mean circumpolar vortex structure

between zonal and meridional extremes. Rossby (1939) had quantified this behavior with an "index value". Namias (1950) extended the concept and remarked that while the angular momentum of the westerly vortex, integrated from the subtropics to the Arctic, is relatively constant for a particular season, the mean latitude of the maximum westerly winds changes considerably. As a "high" index is associated with strong zonal winds in the latitude of the traditional "polar front", the zonal flow in the equatorward portion of the temperate zone must be correspondingly reduced. During periods of "low" index, for which the zonal flow in the poleward portion of the zone is reduced, the vortex maximum would necessarily be displaced equatorward. The flow in the poleward portion would then also be more meridional with associated polar and tropical outbreaks.

Namias (1950) believed that the index had a typical progression from high to low and back again, an index "cycle", which had a time-scale of on the order of a month or more and occurred with a certain degree of regularity at least once for every winter season. He also postulated the types of synoptic-scale circulations to be expected with various phases of the "cycle". A detailed example of an extreme low index situation was reported by Namias (1951) for the early winter of 1949-1950, during which a large anomalous anti-cyclone moved from the subtropical central Pacific northward into western Alaska. The associated flow southward through the eastern Gulf of Alaska and eastward across the US Pacific coast resulted in episodes of below freezing weather in the Los Angeles basin and unprecedented snowfalls in the valleys of western Washington and Oregon.

Lorenz (1952) was able to relate the flow of angular momentum, poleward from the tropics, to the strength of the zonal westerlies and found that the changes in the zonal index could be anticipated thereby. Later, Van Loon and Rogers (1981) related the mean latitude of the wintertime westerlies at 700mb to the phase of the Southern Oscillation, comparing the latitude of the maximum height gradient for years of the cool phase (for which the mean westerlies were displaced poleward) as contrasted with that for the warm phase. They showed that the maximum low-latitude transports of eddy heat and momentum occurred during winters for which the SOI was lower than normal.

As for the "key dates" in the Grosswetterlagen of Baur (1951), the accumulated data since 1950 has made any regularity in the index "cycle" difficult to substantiate. Julian (1966) performed a spectral analysis of the sequential variations of the zonal index and found little evidence for specific periodicity; the changes were better associated with broad ranges of periods.

There have been other attempts to discover true periodic behavior in meteorological variables but, other than the diurnal and annual cycles and the quasi-biennial oscillation (not strictly periodic) in the tropical stratosphere, the search has been unsuccessful. A systematic attempt at this was a pioneering spectral study of atmospheric variability by Ward and Shapiro (1961) which found no new significant periodicities but did establish that power in the low frequency variability was greater than previously estimated. Studies such as this have shown that if precise periodic variability exists (other than for those cases already mentioned) it is either too subtle to be discovered by today's methods or occurs on a time-scale that exceeds our historical record. Very low-frequency astronomical periodicities (Milankovitch, 1941) may be an exception but verification by the geological record is not sufficiently reliable as to make a clear determination. There do appear to be corresponding climatic responses indicated in the record of deep-sea cores (Crowley, 1983); and Kutzbach (1981), in a study of the monsoon climate of the early Holocene, has found significant correlations with the Earth's orbital parameters. The effect of orbital forcing on climate is complicated and to some extent obscured, however, by the effects of volcanism (Kutzbach, 1976).

Insofar as seasonal or sub-seasonal variability is concerned, there appear to be no useful periodicities although less precise quasi-repetitive sequences such as the index "cycle" have not been completely invalidated. Clearly, this index and the corresponding character of the circulation varies within wide limits and with a time scale considerably longer than that of the synoptic disturbances, but prior values of the index during any "cycle" do not appear to be good predictors of future values. Transitions between high and low states may occur rather abruptly and without reliable precursor indications. Nevertheless, the early attempts to find regularity, both in the index "cycle" and also in other weather patterns,

have provided useful concepts in the characterization of anomalous circulation on the seasonal time-scale.

Yet another early approach to the problem of long-term variability was that of persistent "blocking" (Elliot and Smith, 1949 and Rex, 1950). This extratropical phenomenon has the structure of a dipole pair of geopotential height anomaly centers, and has a strong tendency to occur in the eastern Atlantic and Pacific Oceans with profound meteorological effects upon the regions immediately downstream. Dole (1985) has studied the geographic distribution and statistics of such anomalies. From his statistics on their duration and evolution one may conclude that while there is some evidence of regularity the most useful feature, insofar as prediction is concerned, is in their persistence.

More recently, in order to compare more effectively the state of the circulation and its evolution with potentially influential factors, a number of investigators have sought methods to reduce the complex circulation patterns and their temporal evolution to as simple a set of numerical values as can represent the salient aspects of the circulation. By making maps of the correlation of the geopotential height of each point with all other points, Wallace and Gutzler (1981) were able to show that there existed certain sequences of regions which had alternate positive and negative correlations. These regions, which appeared to be aligned along great circle paths were described as "teleconnections", the most prominent of which, known as the Pacific-North American (PNA), began in the central tropical Pacific with other nodes in the northern Pacific, North America and southeastward into the Atlantic.

Horel and Wallace (1981) examined the atmospheric phenomena associated with the Southern Oscillation, with emphasis on vertical structure and teleconnections to middle latitudes. They found fluctuations in mean tropospheric temperatures and 200mb heights varying simultaneously with equatorial Pacific SST's. The teleconnection patterns were well defined and consistent with those of Wallace and Gutzler (1981). Using a linearized steady-state primitive equation model, Opsteegh and Van Den Dool (1980) were able to demonstrate that the responses of upper-level mid-latitude stationary waves to tropical surface heating were significant and postulated that such a model might assist in mid-latitude circulation forecasts.

Hoskins and Karoly (1981) were able to show that the PNA pattern could be simulated by a heat source in the tropical Pacific, using a five layer baroclinic model with a climatological wintertime zonal flow, and that the resulting perturbations corresponded to Rossby waves propagating on a sphere. The relationship of the simulated heat source to anomalous heating in the El Niño phase of the Southern Oscillation was considered significant. By simulating a deep heating mechanism in the sub-tropics, Webster (1981) also demonstrated that the strongest response was in the mid-latitudes. Hendon and Hartmann (1982), however, showed by including deep heating with an ocean-atmosphere sensible heat feedback, that mid-latitude forcing has a stronger remote response than does tropical forcing and have concluded that tropical forcing should not be considered of preeminent importance. Simmons et al.(1983), using a global barotropic model linearized about the climatological mean January flow, determined, by perturbing the basic state at key tropical locations with forcing comparable to that of the anomalous heating of the Southern Oscillation, that circulation patterns similar to those of the Pacific-North American (PNA) resulted. The most rapidly growing modes resulted from barotropic instability and were found to account for an appreciable fraction of the observed low-frequency variance of the geopotential height field.

Another, but statistically oriented, method of describing variability is that of Principal Component Analysis (PCA) in which the total variance is decomposed into a number of orthogonal component fields, ordered by the proportion of the variance that they "explain". The patterns produced by maps of such components (or EOF's) are interesting and often instructive, particularly when little is known concerning the mechanism of the variability, but do not necessarily correspond to underlying physical causes. In the case of the NE Pacific 500mb height field, a number of the EOF maps are suggestive of observed anomaly patterns and, when combined with the mean height field, resemble (as will be shown in the next chapter) many of the fields associated with common precipitation patterns.

Horel (1981) was able to demonstrate that, by an orthogonal rotation of the EOF's, the map of the magnitudes of the first rotated EOF field resembled the PNA pattern and a number of investigators have

subsequently used rotated EOF's to characterize the circulation. Molteni et al. (1990) have used amplitudes from the first three rotated EOF score matrices as coordinates in phase space to classify each of 576 five-day-mean eddy fields of the 500mb observed wintertime height. They show that the points corresponding to these pentads are not spaced uniformly but are in clusters. Six rather diffuse clusters were identified, the largest of which was located in the region of phase space with positive values of the rotated EOF (REOF) #1. This REOF coordinate corresponded (approximately) to the PNA index. The cluster contained about 40 percent of the total points and most of the points in this cluster were also in the positive PNA region. Other clusters with smaller numbers of points were shown to correspond to circulation regimes suggestive of various less commonly occurring wave patterns.

In our analysis of variations in the 500mb height field, discussed in Chapter 3, we computed rotated EOF's in a manner similar to that of Molteni et al.(1990) but for a more limited spatial domain and over a longer time-span. While our spatial EOF patterns were similar we were unable to observe the well defined clusters directly from our scatter plots that Molteni et al. (1990) had extracted using a clustering algorithm. We did not require such cluster positions in our analysis. Nevertheless, we found the concept of a single point or vector in n-dimensional phase space with coordinates of the principal component scores a useful simplification in the approximation of the circulation state.

There has been much speculation regarding the nature of the transitions between the various circulation regimes. It may be noted by an observer of the performance of the current forecasting models that there is little success in anticipating major transitions more than 72 hours in advance, while, within a regime, the essential features of the long-wave pattern are more predictable. Tracton et al.(1989) show, from an analysis of forecasts and verifications, that the evolution of a zonal flow into a blocking event and the converse are relatively poorly predicted, with little skill after three days. In contrast, while within a settled regime, the period of comparable predictive skill is much longer. Lorenz (1969b) has demonstrated that the length of time over which dynamic predictability is effective should be approximately proportional to the time-scale of evolution of the phenomena. Van Den Dool and Saha (1990), however,

show that while dynamic predictability is better for the long-waves than for the synoptic-scale disturbances, the actual improvement is much less than one would expect from the theoretical considerations of Lorenz (1969b). They remark that we appear to lack models for long-wave evolution comparable in skill to those for synoptic-scale development.

Although the abruptness and magnitude of the transitions between long-wave circulation states might have led to the conclusion that some form of external forcing must be responsible, a number of investigators have demonstrated that internal processes alone can cause a system to undergo this sort of vacillation. Using a very simple convection model described by three non-linear differential equations, Lorenz (1963) was able to show that the state of the system, as projected on a phase space with coordinates of the system parameters, underwent non-periodic vacillations, switching between orbits on a complex attractor. The nature of this attractor was determined by these system parameters which, over certain ranges, resulted in complicated fluctuations for which the system would spend a considerable time orbiting in one portion of the attractor and then would abruptly switch over to orbits about a different position. The analogy of this behavior to that of the change in circulation regimes was evident.

An attempt to simulate such changes in the context of transitions between high and low index states was made by Charney and DeVore (1979) using a barotropic channel model with zonal flow, externally driven over simplified orography and with a highly truncated spectral expansion of the model algorithm. This was later extended to the baroclinic case with zonally symmetric heating driving the flow (Charney and Straus, 1980). Considering the simplicity of these models, the simulated variability of the flow resembled remarkably the behavior of the actual circulation. In particular, the simulated circulation appeared to make transitions between various states of relative equilibrium corresponding to different zonal and blocking regimes in the atmosphere. As the time spent in transition was less than that spent in the vicinity of an equilibrium state, there resulted a bimodality in the distribution in both the zonal flow (index value) and in the wave amplitude. While bimodality in the amplitude of planetary waves in the actual circulation has been confirmed, that for the zonal flow index has not (Sutera, 1986).

Vautard and Legras (1988a and 1988b) have investigated the forcing of low-frequency variability by synoptic transient perturbations using a quasi-geostrophic channel model forced by a baroclinic jet and studying the various flow regimes. They concluded that persistence properties were distributed inhomogeneously in phase space, although not confined to sharply defined regions. There was persistence simulated in both zonal and blocking flows. They noted that the transient eddies weaken considerably during propagation around a block, suggesting a maintenance mechanism for this regime. The immediate mechanism for an initiation of transition to a *new* regime, however, remained unclear. They noted that the variation in the paths of the simulated disturbances are in good agreement with the observational study of Dole (1985).

In fact, the circulations simulated by these and other models (e.g., Vautard et al., 1988 and Mukougawa, 1988) all show strong qualitative similarities to the actual atmosphere in the quasi-stationary nature of the various regimes, their distribution in phase space and the abrupt and non-periodic transitions between them. As these models exhibit these characteristics while their boundary conditions are fixed, there is an implication that, for the actual atmosphere as well, external forcing is not required to explain transitions between circulation regimes. Indeed, the time-scales of most boundary forcing mechanisms are not commensurate with that of the transitions. Yet, in all of the models, the locations of the envelopes or means of the various quasi-stationary states appear to be functions of system parameters and related to the external boundaries. For the model of Vautard et al.(1988), for which low-frequency variability is forced by synoptic-scale transient perturbations, the structure of the low-frequency variability is seen to change with differences in the mean velocity and vertical shear of the basic flow.

The distribution of quasi-stationary zonal and blocking circulation regimes varies in both time and space with changes in the basic westerly flow. Mukougawa (1988) uses a two layer quasi-geostrophic model with a mid-latitude β-plane channel and rudimentary surface topography. External thermal forcing representing the differential solar heating between the Equator and pole and dissipative processes are included. With this model, a complex system of quasi-stationary circulation states

are examined. The distribution of these states is found to be highly dependent on the differential-heating forcing parameter.

We have not yet been able to estimate the proportion of the total system variability that is due to external forcing as compared to non-deterministic internal vacillation, and this question has an important bearing on our future success in long-range forecasting. Nevertheless, it appears highly probable that at least *some* of the variability is the result of external forcing. Although much less complex than the actual mid-latitude circulation, the behavior of the models suggests that changes in boundary conditions are influential in the structure of the circulation state ensemble. The model of Charney and Straus (1980), discussed above, has differing patterns of vacillation corresponding to different zonal heating. A model of Pedlosky and Frenzen (1980) shows differing envelopes of the chaotic circulation state (associated with the development of baroclinic waves) as a function of damping. Both this energy sink term and the energy source terms of the Charney and Straus and Mukougawa (1988) models may be related to external forcing.

Many of the potential forcing mechanisms, such as sea-surface-temperatures (Webster, 1981), snow and ice extent (Namias, 1985), (Barnett et al., 1989) or polar or stratospheric conditions (McGuirk and Douglas, 1988), as well as the structure of the adjoining tropical upper-air circulation, are more predictable than is the mid-latitude circulation itself, and most have much longer time-scales. This would imply that while the problem of long-range forecasting of specific transitions between regimes may remain intractable, there is a reasonable probability of improving forecasts of the cumulative *effects* of such transitions on a seasonal or sub-seasonal basis. There is some indirect support for such predictability from a study by Farrel (1990) on small error dynamics. He finds that while there is an asymptotic divergence of circulation state trajectories in phase space, the rate of envelope growth is less than expected from that of synoptic-scale perturbations and that there exist envelope structures that can be identified with the preferred responses of the system. Two companion studies (Molteni and Palmer, 1993 and Mureau, et al., 1993) show a certain degree of ensemble predictability by the use of dynamically conditioned perturbations. All three of these studies focus on the predictability of the ensemble or envelope of the

evolving circulation state rather than on the circulation state itself. As stated throughout this investigation, it is upon this aspect of the circulation that we are focused as well.

2.2 Data sets and initial processing

2.2.1 The 500mb height fields and domains for computation and display

The primary data set from which height and circulation fields over the NE Pacific and western North America were extracted is that of the National Meteorological Center (NMC) series of twice-daily 500mb geopotential height fields. These are archived at the National Center for Atmospheric Research (NCAR) on a 47x51 octagonal grid covering most of the Northern Hemisphere in data set DS060.0 (Jenne, 1975 and 1989). For convenience, both in computation and also for graphical presentation, these fields were interpolated, using a 16 point Bessel interpolation scheme, to a 23x17 Cartesian 3°x3° grid covering the region from 22°N to 70°N and 172°W to 106°W. The zonal and latitudinal extent of this domain is more than sufficient for the precipitation model but was considered necessary to be commensurate with the scale of the long-wave features to be compared with the tropical effects. A secondary display region, from 31°N to 49°N and from 125°W to 106°W was used for plotting data and the results of various computations for the US western weather districts. Fig. 3.1 is an example of this domain. An example of the larger computational and circulation display domain is found in Fig. 3.6.

To obtain the slowly evolving long-wave pattern in isolation from the transitory effect of the more rapidly moving synoptic-scale disturbances, ten successive fields (spanning a five day period) were averaged. Some investigators (Blackmon, 1976 and Sawyer, 1970) have suggested that 10 days might be a more appropriate cut-off due to the life-cycle time of these disturbances, but their purpose was somewhat different from ours and required total removal of the energy of the short-wave systems from the long. This is neither necessary nor desirable in our case. In five days most synoptic-scale disturbances move through at least a half wavelength

of the long-wave pattern and through many wavelengths of their own. Consequently, a five day averaging period should remove most of the apparent transitory effect of the short-waves on the long-wave configuration. Moreover, during periods of rapid transition between long-wave regimes, the use of a longer averaging period may result in the loss of significant information concerning the transition. Thus, as for other investigators interested in related long-wave phenomena (e.g.., Vautard and Legras, 1988a, and Molteni et al., 1990), we have adopted the five day or "pentad" average. This removes the *transitory* effects of the short-waves on the circulation configuration while retaining the averaged influence of the synoptic disturbances. Following Molteni, et al. (1990), we consider the resultant circulation more appropriate to our purposes than one resulting from the removal of short-wave energy by filtering.

We have formed 30 pentad averages of the 500mb height fields for each of the 42 winter seasons from 1949-50 to 1990-91. The first pentad for each season begins on November 2nd and the last ends on March 31st (March 30th for leap years).

2.2.2 Western district precipitation data

The monthly district precipitation used for the study was taken from a climatological data base originally maintained by The Oregon State Climatologist on the Atmospheric Sciences computer system at Oregon State University. This record had been obtained from The National Climatic Data Center, Asheville, N. C. Records were extracted for the 60 western weather districts extending from the Pacific coast to the vicinity of the Continental Divide for the November through March period from 1931 to 1984. The record was later extended to 1988, extracting the data from the World Weather Disc (Reference Technology Inc., 1988).

District precipitation is a simple average of the individual stations of each district which have records of sufficient length and is necessarily biased toward the more populated and less mountainous areas. The subject of how this bias effects representation is discussed briefly in Chapter 3.

2.2.3 The OLR field of the tropical Pacific

Regions of strong upper air outflow are associated with convective activity as indicated by concentrations of high cold cloud tops. These are observed from satellites as areas of depressed outgoing long-wave radiation (OLR) with values well below those for the tropical or subtropical clear sky oceanic background. Monthly averages of the tropical OLR field on a 2.5° grid, expressed in units of W m^{-2}, are available from an updated NCAR (DS761.1) data base (Jenne, 1989) from June of 1974 to January 1992 with a ten month record gap from March through December 1978. From 1979 onwards, the data is from the Nimbus-7 Earth Radiation Budget (ERB) satellite which has been combined with other satellite records and recalibrated so as to produce a consistent data set (Kyle, 1990).

For our purposes, a subset of these fields extending from 15°S to 20°N and from 135°E to 120°W was extracted for each of the 212 months in the record. For the computations in extracting EOF's and associated principal components, these fields were sampled at 5° intervals on an 8 x 22 array. The processing is discussed in Chapter 5.

2.2.4 Supplemental data

There were a number of additional data files that were necessary in the determination of statistical relationships between the 500mb height fields and the intermediate variables used in the precipitation model. These were all archived at NCAR and consisted of the 850 mb height fields, extracted from the primary data set (DS082.0) in the same manner as the 500mb height fields and also vertical sounding data of temperature and relative humidity. The sounding data came from the NCAR RAOB data set DS390.1. Terrain elevation data necessary for the precipitation model was a subset of the US Navy 10' terrain data set, also archived at NCAR in data set DS754.0.

2.2.5 Computer resources

The primary height field data discussed in section 2.2.1 and supplemental data discussed in section 2.2.4 were extracted from the Mass Storage System (MSS) at NCAR and pre-processed with the CRAY Y-MP CPU. The resulting files were transmitted to Oregon State University (OSU) via the NCAR remote job entry system over the internet to the OSU Atmospheric Sciences SUN work stations.

The bulk of the file processing and computation of results was performed on the SUN workstation of the Oregon State Climatologist, collocated with the Atmospheric Sciences portion of The College of Atmospheric Sciences and Oceanography (COAS) at OSU. Post-processing for graphic presentation was accomplished on the Atmospheric Sciences SUN work stations.

CHAPTER 3: WESTERN WINTER PRECIPITATION AND ITS RELATIONSHIP TO THE 500MB HEIGHT FIELD

As discussed in the introduction, we are focusing on the monthly and seasonal wintertime precipitation for the various western weather districts of the US and its relationship to low frequency variations in the 500mb height field over the NE Pacific and western North America. In this chapter the nature and variability of both the precipitation and the height field are examined. We will demonstrate that the relationship between them is sufficiently strong (for the time and space scales examined) that district precipitation may be inferred from the first 6 principal components of the 500mb height field alone, using a linear regression model. The inferred precipitation will be shown to have an average district correlation with that from the observations of about 0.40 and, with a probability that there is no true relationship of less than $p = 0.05$, the relationship is considered significant. In the following chapter a more physically based model, with intermediate inputs of wind, moisture and temperature (all inferred from the 500mb height field) will be shown to improve the correlation between observed and inferred precipitation to an average of about 0.62 for the same districts and, with a probability of no true relationship less than $p=0.01$, the relationship is considered highly significant. Such correlations are sufficient to demonstrate that the future prediction of even a rough approximation of the tropospheric height field (as represented by a few of its principal components) would translate into a more useful forecast of monthly or seasonal precipitation than is now possible.

We have selected the 60 contiguous weather districts which extend from the US Pacific Coast to the Continental Divide. These are listed in Table 3.1 and mapped in Fig. 3.1. The plotted district boundaries are approximate.

If the district precipitation were computed as the total precipitation over a district divided by its area, it would be better related to stream flow, a particularly useful input to reservoir level forecasts, and a better representative measure. It is actually the average of a number of station

Table 3.1 The Western Weather Districts. District code, latitude and longitude in degrees and minutes, mean elevation in meters and district name are listed.

Code	Latitude		Longitude		Elev	District Name	St
0201	35	10	114	05	1000	Northwest Piedmont	AZ
0202	35	30	111	30	1800	Northeast Plateau	AZ
0203	35	10	113	00	500	Western Rim	AZ
0204	33	30	112	00	500	Central Rim	AZ
0205	32	53	114	10	25	Southwest Low Desert	AZ
0206	33	20	112	40	250	Central Low Desert	AZ
0207	32	00	111	00	350	Southeast Desert	AZ
0401	40	45	124	05	0	North Coast	CA
0402	39	05	121	30	20	Sacramento Valley	CA
0403	40	00	120	20	1000	North Sierra Nevada	CA
0404	35	55	121	37	0	Central Coast	CA
0405	36	30	119	50	20	San Joaquin Valley	CA
0406	33	54	118	00	0	South Coast	CA
0407	35	00	117	00	600	Southeast Deserts	CA
0502	39	15	108	10	2000	Western Mountains	CO
1001	48	00	116	30	400	Northern Panhandle	ID
1002	47	00	116	55	500	West Central Lowlands	ID
1003	40	00	116	50	500	Clearwater Valley	ID
1004	45	40	115	40	1100	Central Highlands	ID
1005	44	00	116	30	600	West Snake River Plain	ID
1006	42	40	116	00	1300	Southwest High Desert	ID
1007	43	00	114	00	700	Central Snake River Plain	ID
1008	44	15	113	40	1950	Salmon River Valley	ID
1009	43	40	112	00	1300	Henrys River Plain	ID
1010	43	00	112	00	1350	East Snake River Valley	ID
2401	47	55	114	10	700	Flathead River Valley	MT
2402	45	30	112	20	1700	Southwest Highlands	MT
2601	41	00	119	00	1300	Northwest Highlands	NV
2602	41	00	116	00	1500	Northeast Highlands	NV
2603	38	00	116	30	1600	Central Highlands	NV
2604	36	00	115	00	450	Southern Lowlands	NV
3501	44	15	124	02	0	Oregon Coast	OR
3502	44	50	122	50	20	Willamette Valley	OR
3503	42	20	123	00	450	Southwest Interior Valleys	OR
3504	44	30	122	15	600	North Cascades	OR
3505	43	00	121	40	1300	South Central Highlands	OR
3506	45	30	121	00	200	Columbia Plateau	OR
3507	43	00	119	30	1500	Southeast Highlands	OR
3508	45	30	118	50	600	Blue Mountains	OR
3509	43	00	117	20	500	Owyhee Valley	OR
4201	40	00	113	30	1500	Western Desert	UT
4202	37	10	113	50	400	Santa Clara Valley	UT
4203	40	30	111	50	1200	Salt Lake Valley	UT
4204	38	00	112	40	1600	South Central Uplands	UT
4205	40	40	111	30	1550	Uinta Mountains	UT
4206	39	40	109	40	1200	Green River Valley	UT
4207	38	00	110	00	1700	Southeast Highlands	UT
4501	47	00	124	00	0	Washington Coast	WA
4502	48	25	122	30	0	San Juan Islands	WA
4503	47	30	122	30	0	Puget Sound	WA
4504	46	40	123	00	50	Southwest Interior	WA
4505	47	40	121	30	400	Western Cascades	WA
4506	47	30	121	00	600	Eastern Cascades	WA
4507	48	00	119	30	400	Okanogan Valley	WA
4508	46	30	120	00	300	Columbia Basin	WA
4509	48	00	117	50	400	Northeast	WA
4510	47	00	117	20	450	Southeast	WA
4801	44	40	110	40	2200	Yellowstone Plateau	WY
4802	43	40	110	50	1700	Tetons and Wind River	WY
4803	42	00	110	00	1600	Southwest	WY

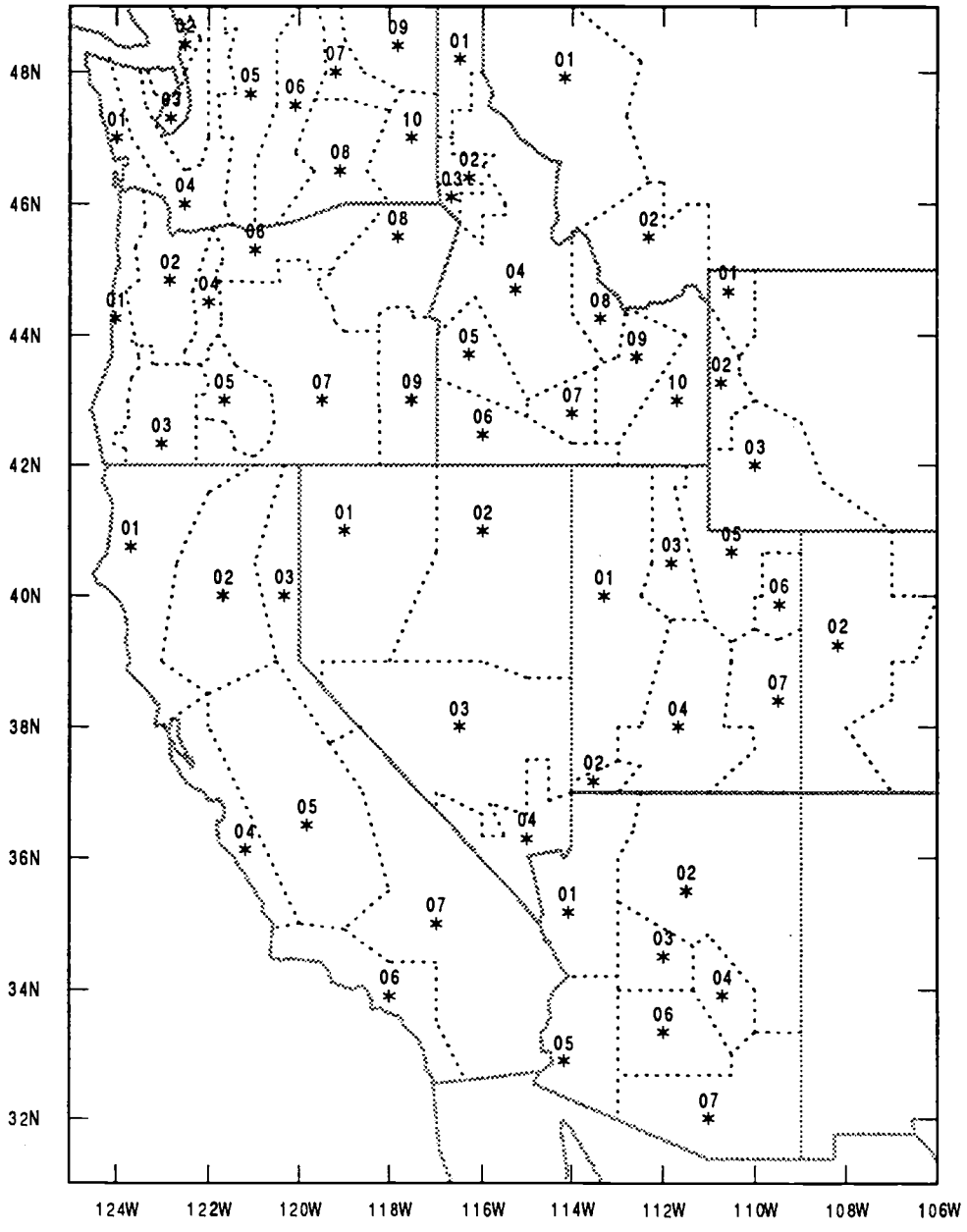

Fig. 3.1 Map of 60 weather districts of the western US. Boundaries are approximate. Asterisks are locations of district centroids for use in precipitation model.

records at locations which are convenient and have been selected, until recently, on the basis of historical settlement. Accordingly, as the mix of contributing stations changes with time, the rainfall statistics are not stationary; moreover, they are biased negatively as the majority of the observations have been taken in the lower occupied regions which are less favored for orographic precipitation. This is a particular problem in the high relief regions of the west. Nevertheless, the district record is still the most representative area-wide measure of precipitation and will probably remain so until precipitation models such as PRIZM (Daly et al., 1994), applied to Oregon precipitation by the State Climatologist, are used for all districts. Such models can realistically extrapolate lowland station measurements to other areas taking into account the orography, and a better measure of district precipitation can be made by integrating over the area. In Oregon this has resulted not only in an increase in the estimate of precipitation for the state as a whole but also in shifts of relative precipitation between regions.

The monthly western district precipitation record begins in 1931 and the portion of the record used for comparison with the 500mb height field in this study is for the months November through March, 1949 to 1988. Even a casual observer of this record becomes aware immediately of the variability of precipitation both in time and space. The temporal variability will be discussed in the next section.

Mean winter precipitation appears to increase to the north, particularly for the coastal districts, and also with elevation. The increase with elevation is most apparent in cases for which no higher elevations are to the west. Conversely, low lying regions to the east of much higher terrain, such as Owens Valley, east of the Sierra Nevada and Death Valley, east of the lofty Inyo Range (4300m), are exceptionally dry. This behavior is not unexpected, as the major moisture source for the western US is the Pacific and the westerly flows necessary to advect this moisture must rise and fall as they traverse the terrain. The general increase to the north may be explained by the observation that winter storms are, on the average, more frequent to the north, at least up to the latitude of the Washington Coast. These storms are often accompanied by strong westerlies, enhancing orographic lifting and also generating dynamic

lifting, both effects contributing to precipitation. Such mechanisms will be discussed in more detail in the next chapter.

3.1 The temporal variability of district precipitation.

Both natural and human cultural development has accommodated itself to the spatial variability of mean precipitation. Sitka spruce grows in the Coast Range and not in the valley of the Malheur. Farmers depend on irrigation systems, rather than gambling on possible rainfall, in the drylands. Temporal variability of precipitation, on the other hand, may cause disruption of ecological and manmade systems. Unlike the eastern and central US districts, for which rainfall during the summer growing season is critical, wintertime precipitation variability on a time-scale shorter than a month or so is not as significant. In the west it is the accumulated winter seasonal precipitation that is of primary importance. Except for the immediate coast and the coastal valleys, the bulk of the winter precipitation is stored in mountain snowpacks which maintain stream flows and irrigation systems throughout the summer. Even along the coast, where summer rainfall, alone, is normally insufficient for crops except in the most northern districts, ground water reserves accumulated during winter must supply the deficit. Thus, it is the long term and seasonal variability that is of greatest interest.

In Chapter 2, a number of unsuccessful attempts to find regularity in the precipitation related circulation patterns were mentioned. This apparent lack of regularity, however, does not imply that the variability is not organized. In fact, the spatial organization of the wintertime precipitation variability is simple to determine and instructive to display. To do so we must first normalize the precipitation records for each district, both so that the differences in mean precipitation between districts will not affect the results and also that the "gamma" distribution common to precipitation records will not invalidate the results of statistical operations that assume normal distributions. This problem and its solution is discussed in Section 4.2.4.

When one compares the monthly precipitation records of adjacent districts, it is found that the linear correlation coefficient is on the order of 0.90 for most geographically adjacent pairs (e.g., Oregon Coast and Willamette Valley). As the physical separation between districts increases the correlation generally declines, although not necessarily monotonically. Table 3.2 is a listing of the correlations between representative districts.

Table 3.2 Correlations between observed monthly precipitation from 1949 to 1988 for selected western districts.

Districts	#	0203	0206	0407	0401	0502	1001	3501	3502	4501	4504
AZ western rim	0203	1.00	0.96	0.81	0.20	0.55	-.07	-.11	-.14	-.24	-.24
AZ low desert	0206		1.00	0.74	0.16	0.44	-.13	-.15	-.19	-.27	-.28
CA SE desert	0407			1.00	0.39	0.51	0.01	0.03	-.02	-.17	-.08
CA north coast	0401				1.00	0.36	0.51	0.72	0.65	0.38	0.34
CO west mtns	0502					1.00	0.09	0.18	0.15	-.08	-.04
ID N panhandle	1001						1.00	0.82	0.85	0.80	0.88
OR Coast	3501							1.00	0.97	0.75	0.85
OR W. valley	3502								1.00	0.79	0.85
WA Coast	4501									1.00	0.93
WA SW interior	4504										1.00

On the basis of the SOI/precipitation correlations discussed in Chapter 1, it was suspected that distant district pairs (such as those from the far northwest vs. those in the lower Colorado Valley) might be negatively correlated. Some negative correlations are seen for distant district pairs in Table 3.2, although perhaps not as large as expected. This is not necessarily inconsistent with the SOI/precipitation correlation finding, for it is likely that there exist various competing modes of precipitation variability which, in combination, may sum to reduce the total correlation.

To separate the modes of variability we use the method of empirical orthogonal functions (EOF's). The eigenvectors of the covariance matrix of the district precipitation time-series are the EOF's, each of which is orthogonal to the others and represents a decreasing proportion of the total

variance. For this 60 district sample the first EOF explains 44% of the variance and the first 4 EOF's explain 82% of the variance. By summing the individual EOF's point by point with the original district array for each month we get a corresponding principal component (PC) time series, the time varying amplitude of the associated EOF. Computation of the EOF's and PC's was by applying the PRINC program from the IMSL library (IMSL, 1979) to the covariance matrix. For display, the EOF's, each point of which is associated with a district location, were interpolated to a regular grid which was then contour plotted on a map of the western US.

There are a number of deficiencies in the analysis of individual modes of variability by an examination of unmodified EOF's. As discussed by Richman (1986), the imposed orthogonality restriction in both component loadings and score matrices may create a number of artificial attributes which can lead to misinterpretation. In particular, he has shown how the shape of the domain can influence the EOF patterns and how the EOF pattern is not invariant for changes in domain extent. For individual mode analyses he recommends either the orthogonal rotation of the EOF's by procedures such as "varimax" or an oblique rotation by the "DAPPFR" or "Procrustes" method. The ability to resolve some "simple structure" in the variance by such methods depends upon the particular situation and on whether or not a simple structure is really present at all. Following other analysts of meteorological fields beginning with Horel (1981), we have applied the varimax rotation method to the precipitation EOF's using the FROTA program from the IMSL library (IMSL, 1979).

For the rotated EOF's, the initial covariance matrix is a "T-mode" matrix (Richman, 1986). The elements of this matrix are the variance/covariance values formed from pairs of the entire space series at each combination of times. This is in contrast to the "S-mode" matrix formed from the variance/covariance of time series at each pair of points in the spatial field. While the "S-mode" matrix is satisfactory for finding unrotated EOF's, its use as the starting point for rotated EOF's concentrates the displayed variance for each EOF into different small regions which provide little insight into the behavior of the field as a whole. As suggested by Richman (1986) we used the "T-mode" covariance matrix instead and found that the displayed fields had a structure with a scale comparable to the extent of the domain. We rotated the first 24 EOF's,

which explained 99% of the total variance, as suggested by Horel (1981), and after rotation the first 4 EOF's now explained 74% of the variance (as compared to 82% for the first 4 unrotated EOF's). When we use PC amplitude time-series in comparisons of different fields it is advantageous to use those explaining the greater proportion of the total variance. As there is no particular advantage, in that case, to using those associated with the rotated EOF's, we use the unrotated EOF's and PC's individually and in combination for our statistical analysis.

The first 4 rotated EOF's are shown in figures 3.2 to 3.5. The first two REOF's are rather similar, both modes of variability showing alternations between southeast and northwest. However, for REOF#1, the negative nodal region is along the California-Oregon border. It is noted that this is an area for which the precipitation to SOI correlation (Fig. 1.1) is low. Apparently, although the largest proportion of the total variability results from contrasting wet and dry seasons between here and southern Arizona, this is not associated with variations in the SOI. North of the nodal zone the seasonal variability decreases. It is likely that the effect of persistent storm-blocking ridges is greatest at the nodal latitude. Northward, ridges of increasing magnitude and of less frequent occurrence are required to block precipitation.

The second REOF (Fig. 3.3) shows a mode of variance resembling the SOI/precipitation correlation pattern shown in Fig. 1.1 and it is possible that ENSO related circulation anomalies may be associated with it. For this mode the precipitation variations in the Pacific Northwest and in the Southern California-Arizona region are directly out of phase. A possible explanation for this sort of pattern is a variation in the mean latitude of the Pacific storm track when it is oriented zonally. The individual storms ordinarily yield most of their rainfall along or just to the north of the axis of maximum upper-level winds, by which the storms are steered. Additionally, this is coincident with the band of baroclinic instability which can transfer energy from the zonal current to the eddy circulation of the storm. The latitude of the resulting precipitation band is thus dependent on that of the axis of zonal circulation and, for periods of time for which the zonal axis is relatively stationary and displaced to the north, enhanced precipitation in the northern latitudes is accompanied by a deficit in the

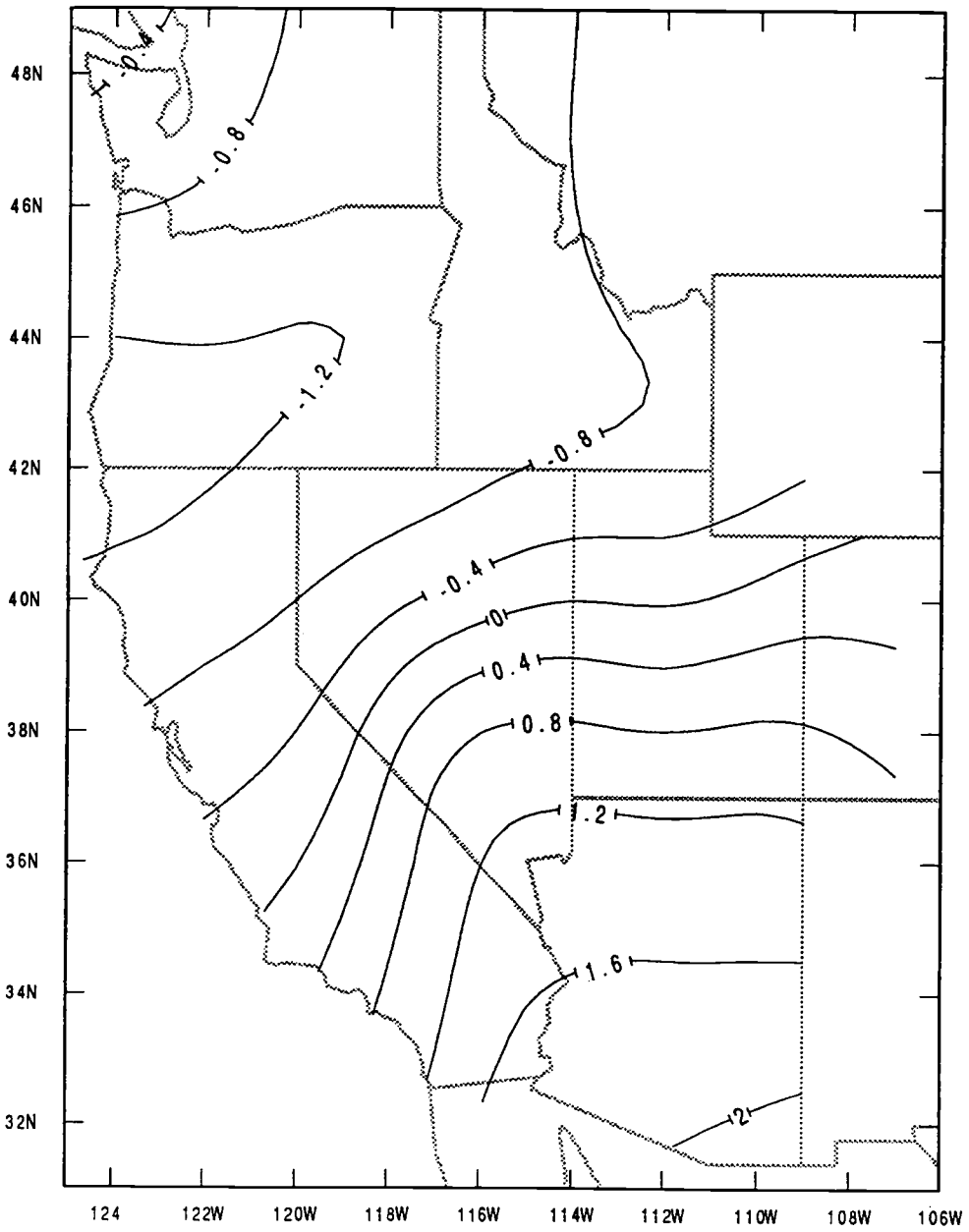

Fig. 3.2 Plot of rotated EOF #1 (REOF #1) of the 60 district Nov.-Mar. monthly precipitation record for years 1950-1988. REOF has been interpolated to the geographic grid for contouring.

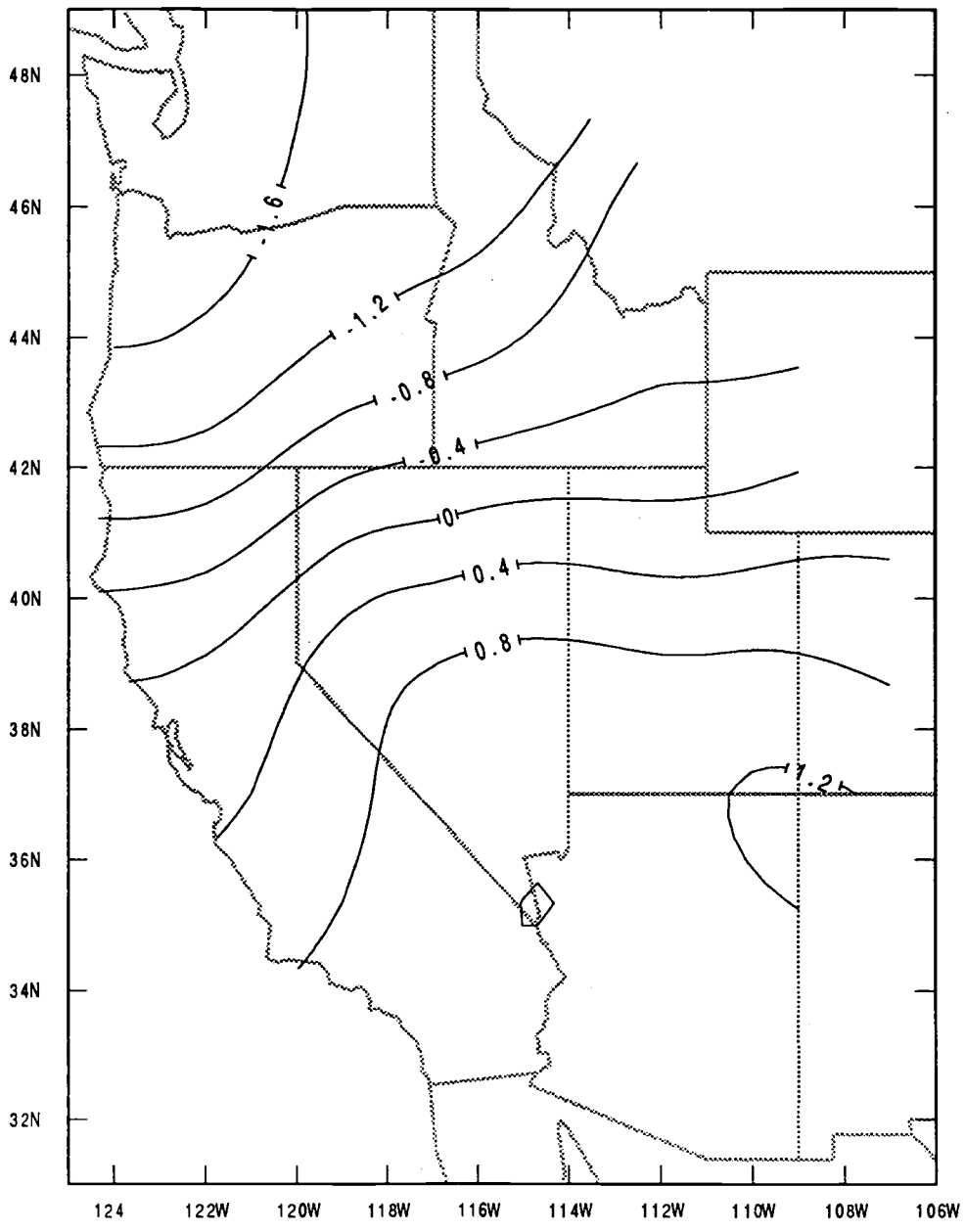

Fig. 3.3 Same as Fig. 3.2 but for REOF #2

south. The converse situation occurs when the zonal wind axis is displaced to the south. Such an alternation would result in the variance displayed in Fig. 3.3.

The major feature displayed by the third REOF (Fig. 3.4) is the steep gradient in the southern portion of the domain between large positive values in eastern Arizona and negative values along the central California coastline. There are also positive values seen north of about 45°N. Meridional flows of relatively short wavelength which occasionally develop quasi-stationary troughs just off the California coast or, in an alternate situation, over the southern Rockies, may produce this sort of variation in precipitation. With the trough located southwest of California the storm track is well removed from the far northwest. With the trough over the southern Rockies, however, the southwesterly flow out of the upstream trough may well influence the precipitation in the northwest, possibly explaining the variance there being in-phase with that of eastern Arizona.

The fourth REOF (Fig. 3.5) shows a mode of precipitation anomalies which are generally in phase for the far northwestern and the southern districts but which are both out of phase with those along the 42nd parallel, particularly in SE Wyoming. A possible explanation for this sort of variability is a high amplitude (meridional) upper-air circulation pattern alternating with a zonal flow. In the prior situation, ridges, for which storms can only approach the west coast in the far north, are succeeded by deep troughs, extending to low latitudes, consistent with rainfall in the southern districts. For the latter (zonal) circulation, the heaviest precipitation would then be expected near the axis of maximum winds which is often near the California-Oregon border (see Fig. 4.7). It should be emphasized, however, that the distribution of variance displayed by these EOF's need not be related to coherent circulation regimes at all. A variety of circulation anomalies can be responsible for the total variance and the method of separation of the variance into modes by EOF's does not insure that the modes are real; there may *be* no "simple" structure. Richman (1986) demonstrates that if a number of simulated simple structures are combined, a decomposition by rotated EOF's may recover them but the inverse is not necessarily true. We can only say that the presence of simple structure in a precipitation EOF *may* be indicative of

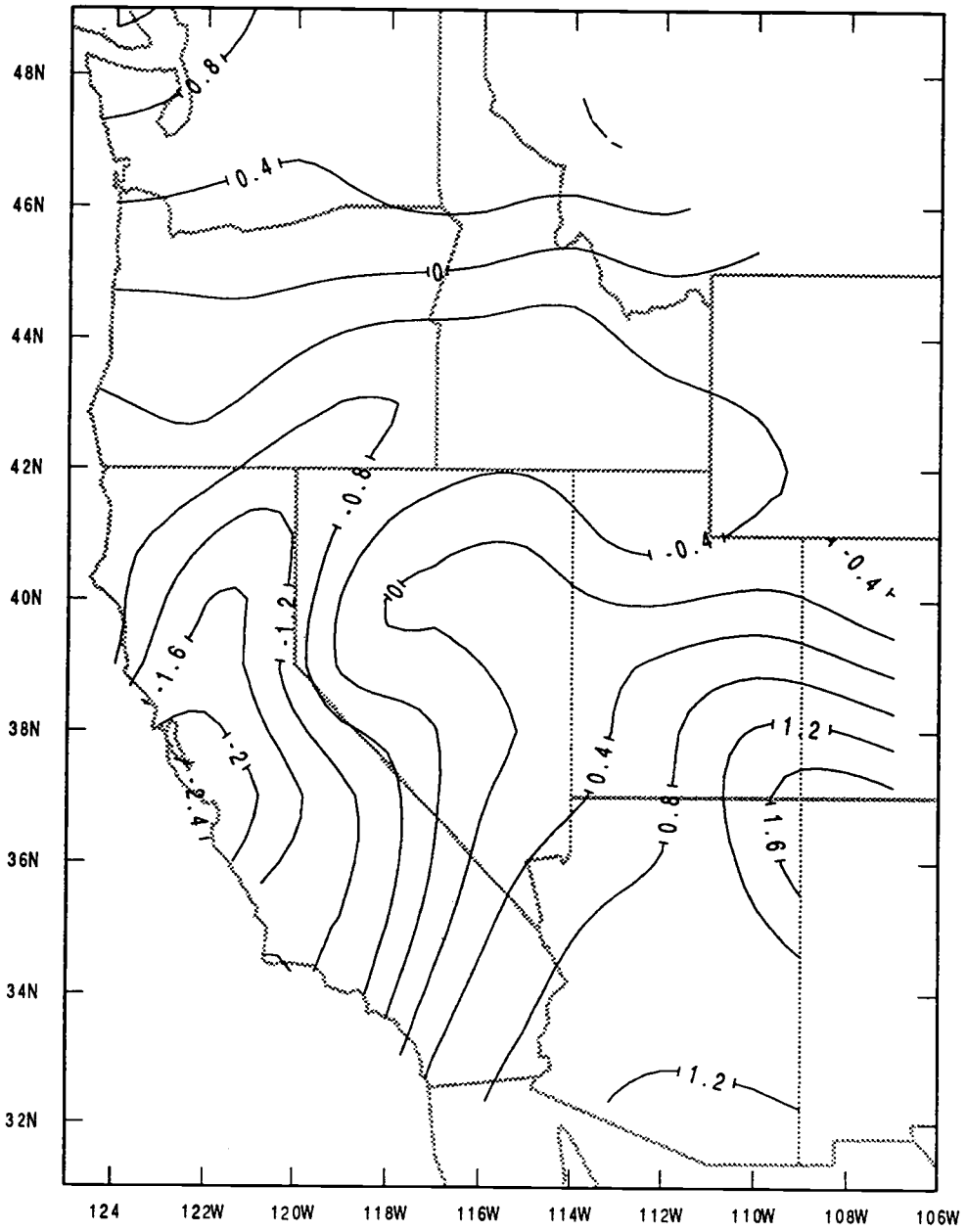

Fig. 3.4 Same as Fig. 3.2 but for REOF #3

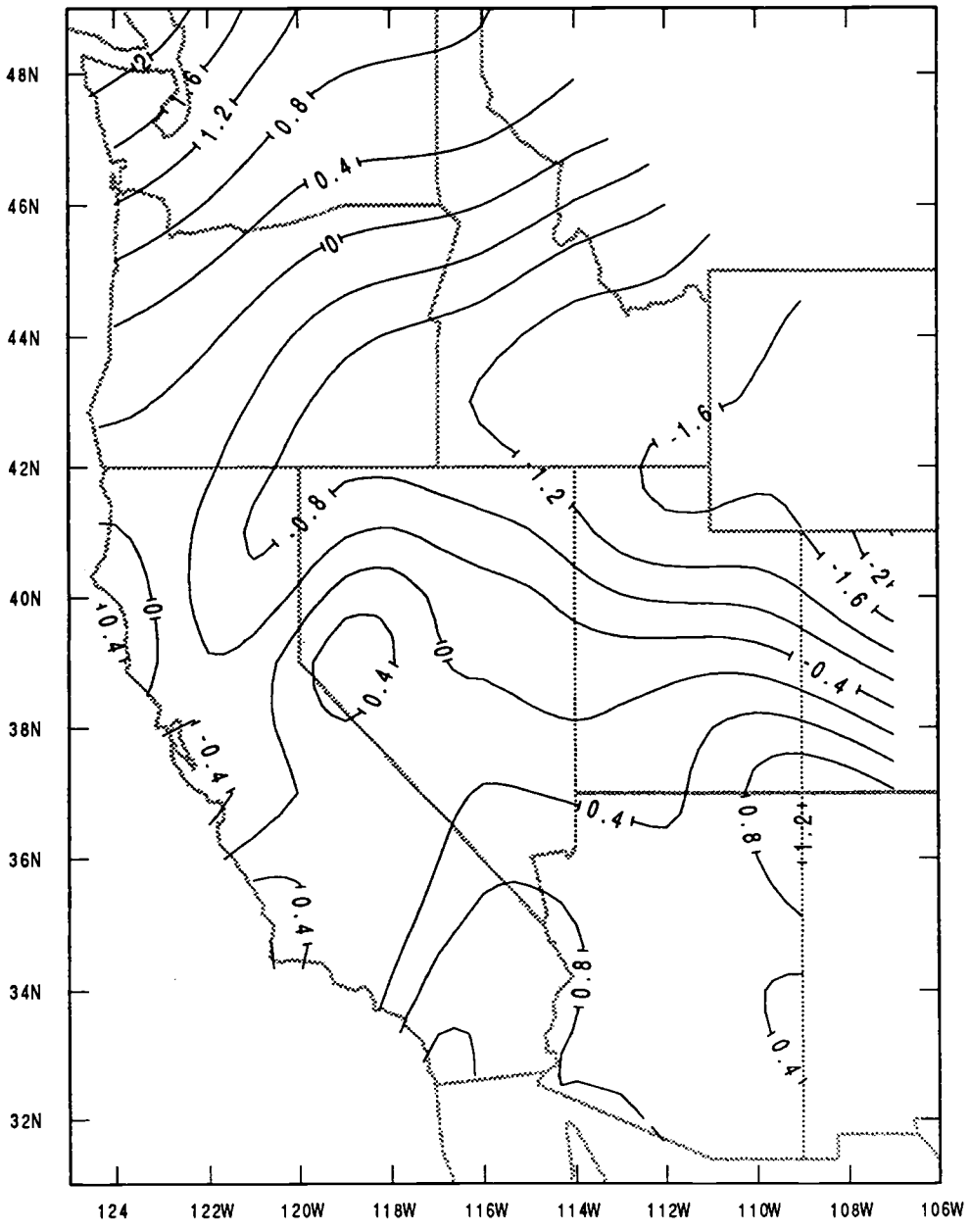

Fig. 3.5 Same as Fig. 3.2 but for REOF #4

a real circulation regime. If there is other compelling corroborating evidence, such as the SOI/precipitation pattern in the case of EOF #2, the case for this is stronger.

Some quantitative statistical connections between the precipitation pattern and the circulation will be examined after first making an analysis of the variance in the height field similar to that of the precipitation.

3.2 Variability of the 500mb height field

As stated in the introduction, the two-fold focus of this study is first, to better quantify the linkage between atmospheric changes over the tropical Pacific and those in the upper-air circulation over the NE Pacific and second, to demonstrate that even an approximate knowledge of the mid-latitude upper-air circulation is, by itself, sufficient to infer district-scale monthly precipitation to a useful degree. The typical short-range precipitation forecaster uses all available information. There are models that predict the winds, temperature and moisture of the atmosphere at many levels; and secondary attributes, such as vorticity and thermal advection, are used to advantage. Nevertheless the quantitative precipitation forecasts for specific storms are imperfect, as most comparisons between forecasts and observations reveal. It appears reasonable to expect, however, that for a district, rather than a station, and a month or season rather than a day (assuming the same atmospheric inputs) one could forecast far more accurately. Were the errors, in fact, random, this expectation would be a statistical truism. We ask if this statistical advantage would permit useful monthly and seasonal precipitation forecasts if a foreknowledge of some minimal representation of the atmosphere were available. The 500mb height field is a useful representation for this purpose. It is at a level sufficiently high to be free of complications caused by surface effects and is a good choice for determining the motions of embedded synoptic systems. Forecasters typically examine the 500mb prognostic fields in their initial assessment of future trends in the circulation pattern and, as a consequence, it is the level chosen most frequently for display by numerical forecast models.

The performance of the existing forecast models is better at the middle and upper-tropospheric levels than for the surface. Anomaly correlations for mid-range 500mb height forecasts are at least 10% higher than corresponding forecasts for 1000mb (Caplan and White, 1989). For the purposes of this study the 300mb or 700mb level could have probably been used instead, but the 500mb level appeared to be a reasonable compromise between the higher level, more representative of the polar jet and the lower level, better representative of pressure integrated moisture and temperature.

The imposed restriction to the of use of the minimum information necessary to represent a single level is due to our expectation that progress in extended forecasting of the atmospheric circulation will probably be, if at all, in the large-scale features of the circulation, such as the positions and amplitudes of the major ridges and troughs, and the occurrence of blocks, rather than in synoptic-scale features. As discussed in Section 1.1, the limits to dynamic predictability by present methods are influenced by the time-scale of the forecast phenomena and the time-scale of the long-waves is considerably greater than for the short-waves. Moreover, it is the long- or planetary-wave structure that has been most successfully related to external forcing by boundary conditions (such as SST's, soil moisture and snow or ice extent) with still longer evolutionary periods (Hoskins and Pearce, 1983).

We have chosen as this minimal representation a small set of numbers that can approximate the 500mb height field. These are the first few principal components (PC's) corresponding to the EOF's of the height field. Representation by EOF's insures that any desired proportion of the variance can be accounted for by a minimum number of orthogonal fields and that the associated PC time-series are an efficient set of numbers for comparison with prospective related phenomena.

To validate this approach we must demonstrate that these first few EOF's are sufficient to regenerate an approximation of the height field that can be used to infer a useful estimate of district precipitation. Utility is, to some extent, subjective but there are a number of objective measures which will be discussed in the next chapter. The accuracy of the precipitation forecast is, of course, contingent upon that of the 500mb height field PC's. As we are assuming a long-range height field forecast

which is limited to an approximation of the long-wave structure, it is necessary to devise a precipitation forecast methodology that can make effective use of this minimum information.

We begin by limiting the domain over which the height field is represented to the "target" area, the western US and to the adjacent NE Pacific, a distance of 66° of longitude (106°W-172°W). The latitude band spans a bit more than the temperate zone (22°N-70°N). This domain is computationally convenient and appears to be a reasonable compromise between a wider domain, which might improve the accuracy of the forecast model but would require more EOF's to represent it, and a narrower domain which could be more accurately represented by the same number of EOF's but which might not include some key circulation features. The covariance matrix from which the EOF's are determined is computed from the anomalous height time series of each of the 391 points in a 23x17 array with 3° spacing covering this domain.

As discussed in Chapter 2, we wish to minimize the complications caused by representation of transitory short-waves in the height field and so have formed "pentad" five-day averages of the 10 twice-daily 500mb fields. As for the space domain limitation, this reduction in detail has further decreased the total variance and has permitted a greater proportion to be represented by a small number of components. This point may be illustrated by a study by Penland and Ghil (1993) who found that for the daily hemispheric 700mb height field, 27 EOF's were required to explain 90% of the total variance while for the more limited domain and pentad time-scale of this study, 90% of the variance is explained by the first 6 EOF's.

As for the precipitation field, we have decomposed the height field variance into its principal components using both unrotated and rotated solutions. For reasons previously described, it is advantageous to use the rotated PC loadings when attempting to interpret "simple" structure in the spatial field and we have accordingly used individual rotated PC loadings combined with the mean field to detect typical height field patterns. For the statistical analysis, however, for which we relate combinations of height field PC's to those from the precipitation or OLR fields, the differences in the distribution of variance between the PC's are

not relevant and, as more of the total variance is explained by an equal number of unrotated PC's, we use these for this purpose.

Figure 3.6 is a depiction of the mean 500mb height field for the pentad centered on 18 January, a mid-winter date. The mean field is little different, qualitatively, on other winter dates, although the heights increase about 100 meters in November and in March. The January flow is nearly zonal with a broad, low amplitude ridge centered approximately along the west coast. The November and March ridge positions (not shown) are about 8° further to the east and the flow is a little weaker.

A number of characteristic height patterns may be simulated by adding or subtracting the individual rotated EOF's multiplied by a selected value of the PC amplitudes. To emphasize the differences in the circulation types we have chosen a multiplier of three times the RMS value of each PC time-series. A number of these simulated circulations resemble those catalogued in Appendix B, taken from observed 500mb flows for the winters of 1976 to 1987. Figs. 3.7 and 3.8 are for REOF #1, which are for the mean field combined with the positive and negative REOF anomaly field respectively. The first figure shows a large, high amplitude ridge, negatively tilted, in the eastern Gulf of Alaska with northwesterly flow across western North America. This rather dry cold flow resembles circulation category V of Appendix B.

Figure 3.8, the negative case, depicts a strong zonal flow, diffluent along the Pacific coastline. Here, from the position of the mean storm track, one would expect to see heavy rainfall in the northern sections, diminishing to the south and ending at the latitude of central California. For REOF #2, the positive combination with the mean field (Fig. 3.9) simulates a circulation similar to that of circulation category III of Appendix B. The Pacific coastline north of the California-Oregon border is under the influence of a strong southwesterly flow, while the interior Northwest and Great basin are under a ridge. One would expect precipitation to be confined to the northwest coastal districts and the elevated 500mb heights suggest correspondingly high snow levels. For the negative REOF #2 combination (Fig. 3.10), with the ridge in the western Gulf of Alaska, the northwesterly flow has an over-water trajectory and the flow, resembling category VI of Appendix B, would be expected to advect

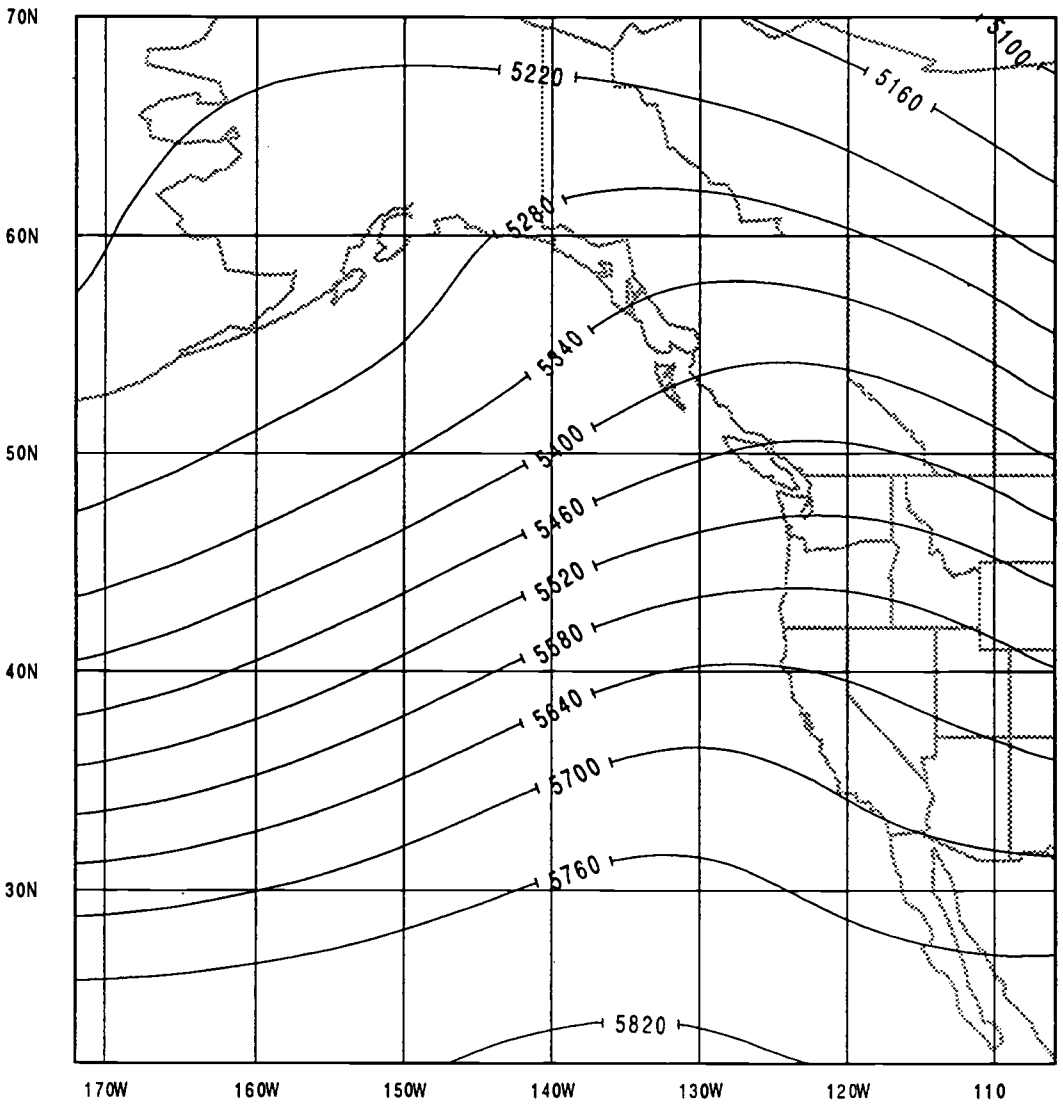

Fig. 3.6 Mean 500mb height field over NE Pacific and western North America for five day period centered on Jan. 18. Heights are in meters.

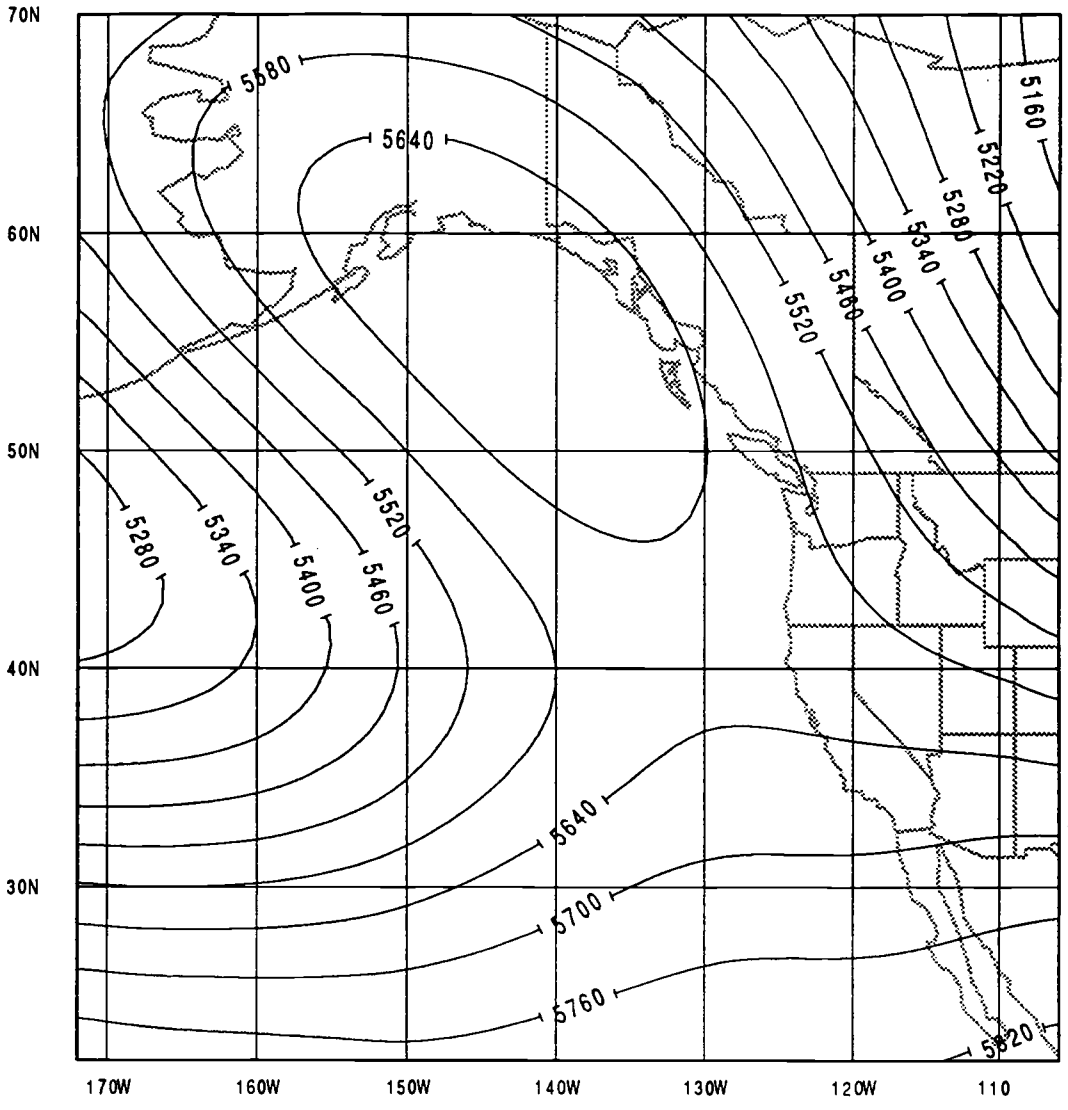

Fig. 3.7 Sum of mean height field of Fig. 3.6 plus REOF #1 of the anomalous height field at the amplitude of three times rms. value of the corresponding 1st principal component.

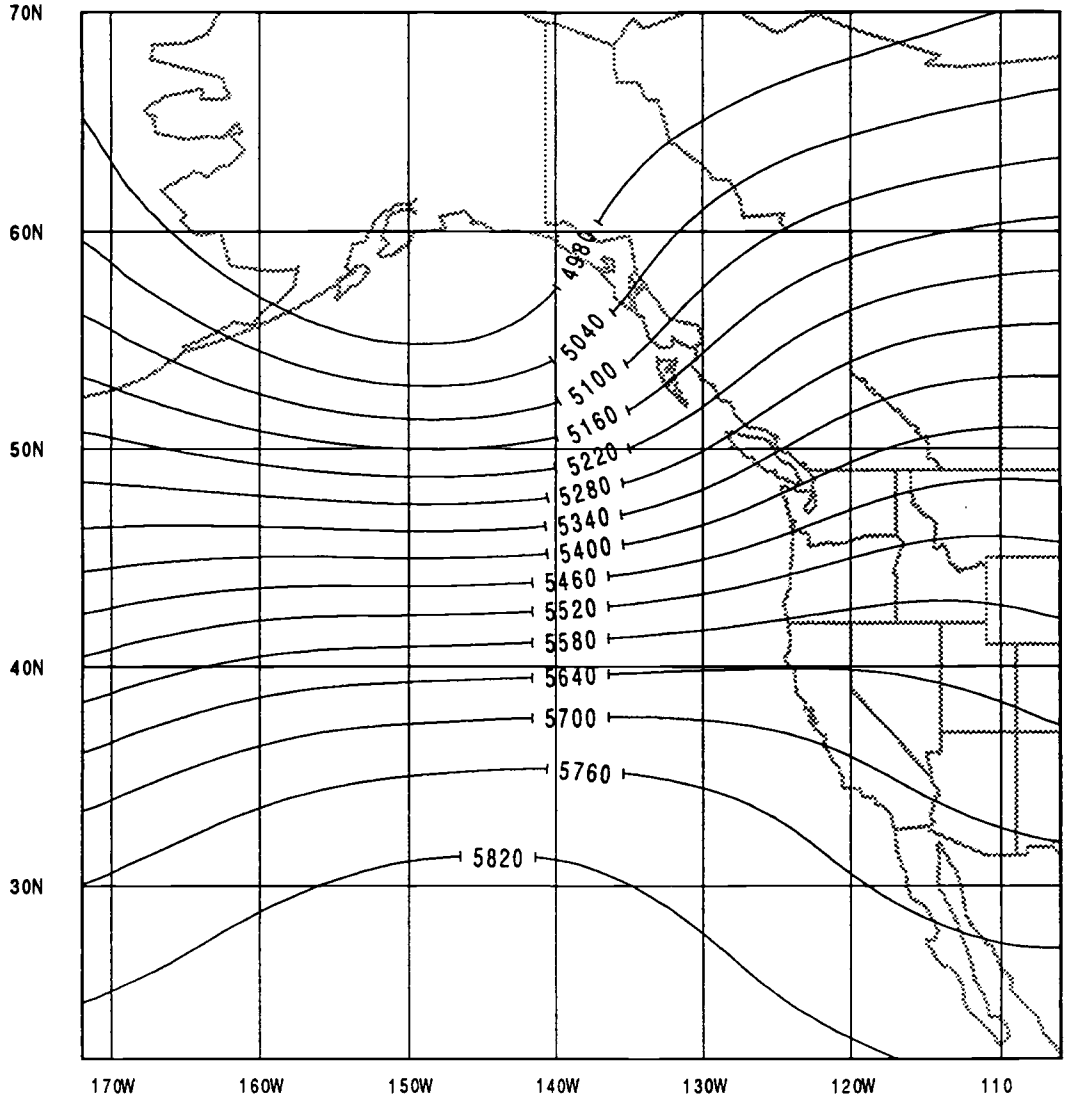

Fig. 3.8 Same as for Fig. 3.7 but for a negative amplitude.

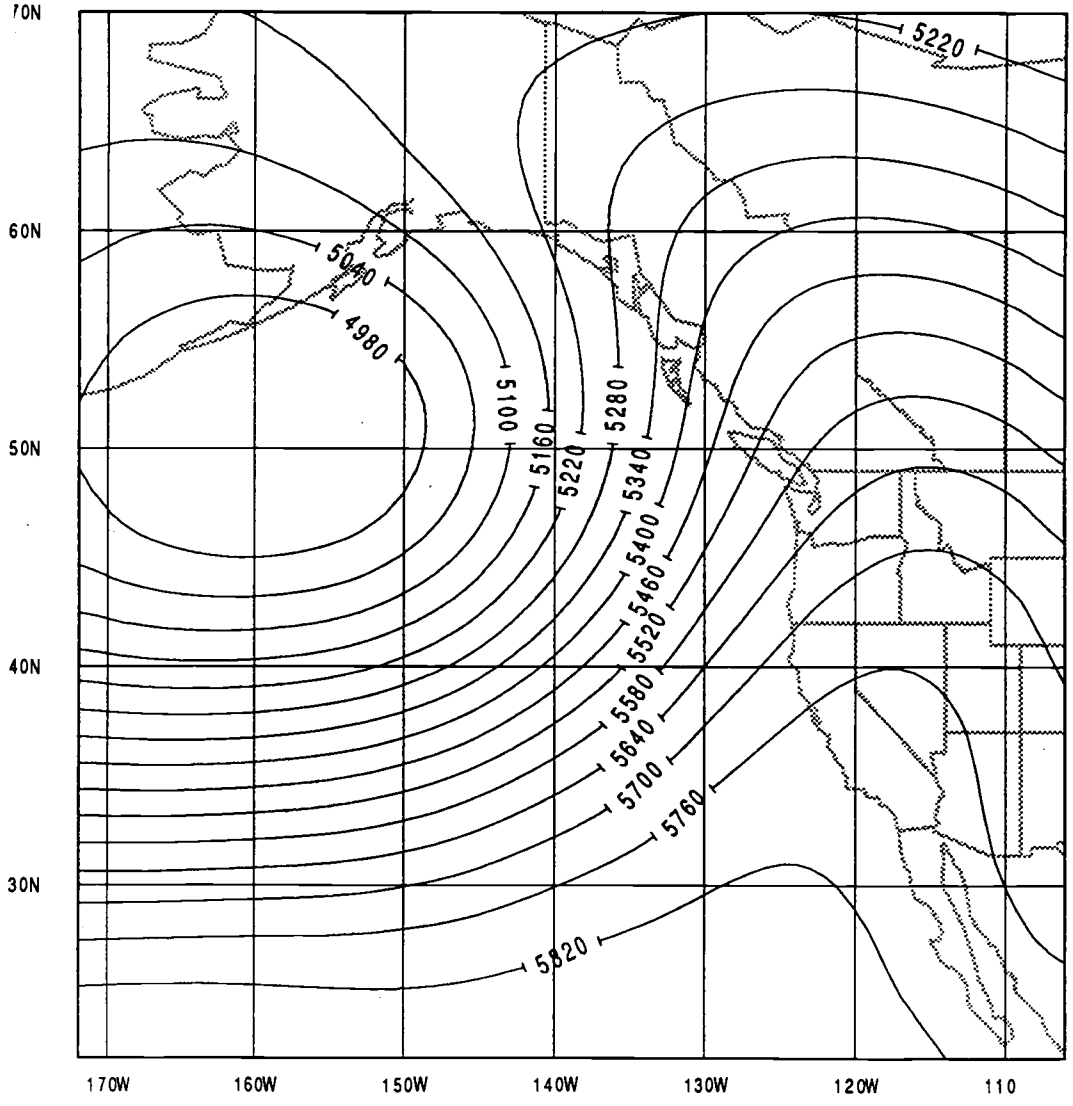

Fig. 3.9 Same as for Fig. 3.7 but for positive REOF #2.

polar maritime air over the coast with convective showers and lower snow levels.

The combination of positive REOF #3 with the mean flow (Fig. 3.11) simulates a low amplitude trough in the eastern Gulf of Alaska with a near zonal WSW flow over the entire western US. Despite the weak southerly flow component, the 500mb heights are below normal, particularly for the northernmost districts, and the flow would appear to be consistent with a wet and cool weather regime. Nevertheless, this flow pattern, while appearing reasonable, was not observed (in the preparation of Appendix B) with sufficient frequency to be one of the designated flow circulation categories, illustrating that this particular "simple structure" (the EOF of which explains 17% of the variance) may not be representative of a real circulation regime. The negative REOF #3 combination with the mean height field (Fig. 3.12) simulates a positively tilted ridge with its axis extending NE across British Columbia. The southwesterly flow across SE Alaska and northerly flow over the US Pacific coast was occasionally observed in the preparation of Appendix B but the more common similar circulation regime had a considerably greater tilt with northeasterly flow over the Pacific Northwest and a cutoff low, west of Southern California. While that circulation was associated with rainfall in Southern and Baja California and in Arizona, the circulation depicted in Fig. 3.12 appears to be dry for all the US western districts.

The combinations of REOF's #4, #5 and #6 with the mean height field (not shown) were examined and found to resemble plausible height fields, similar to examples which could be found in the height field records. None, however, were characteristic of the frequently observed and often persistent height field categories we found in the preparation of Appendix B. In particular, Category II, which is that of a large amplitude ridge with its axis between 115°W and 125°W and is the second most frequently occurring circulation category, is not represented by *any* of the individual EOF/mean field combinations. This is a limitation of this sort of analysis. There is no guarantee that the segregation of the variance by the method of EOF's (rotated or not) will result in the depiction of the actual modes of variability (Richman, 1986). At least, in this case, we have reproduced four of the six circulation types that we observed in the height field data for Appendix B.

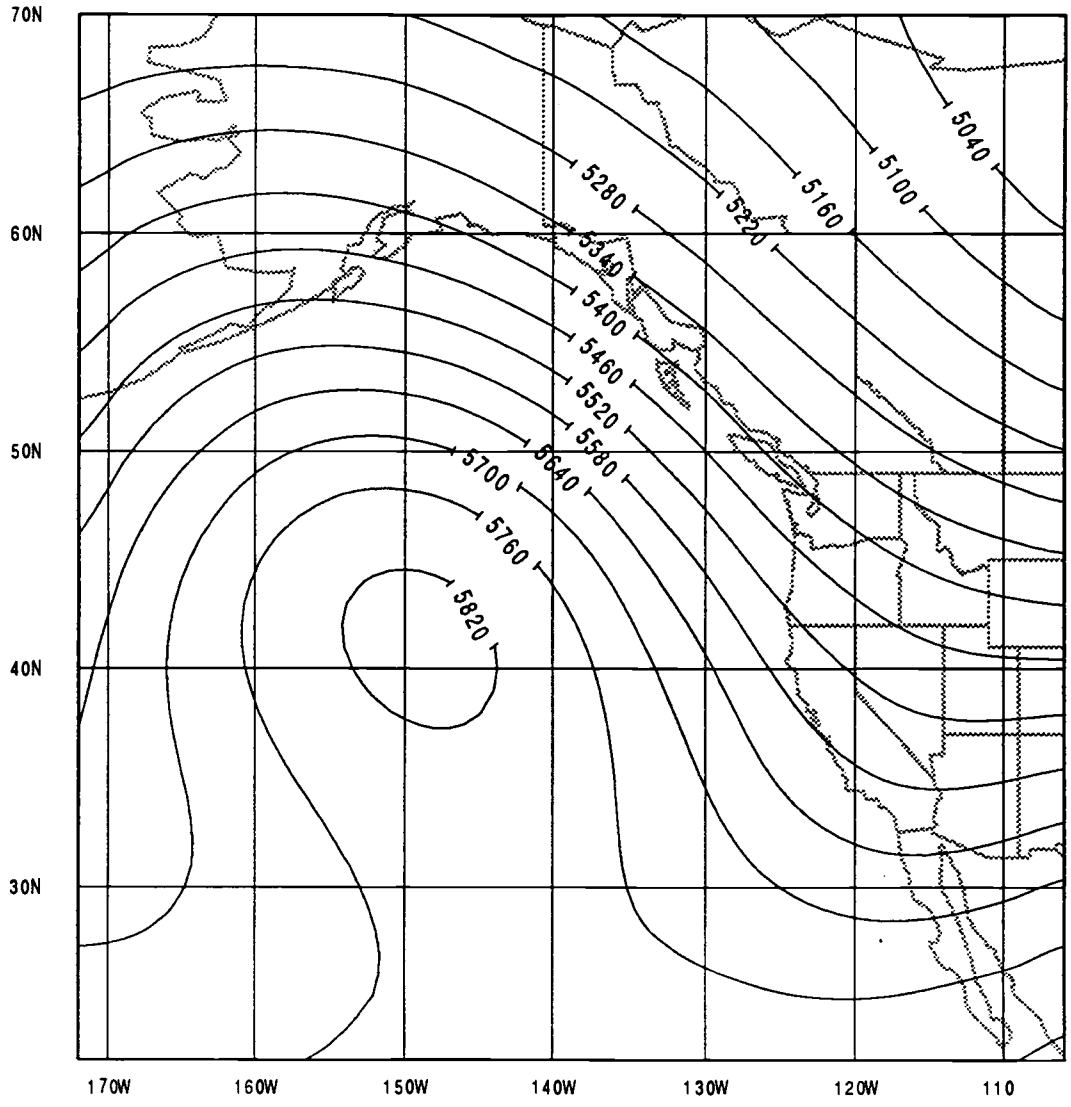

Fig. 3.10 Same as for Fig. 3.7 but for negative REOF #2.

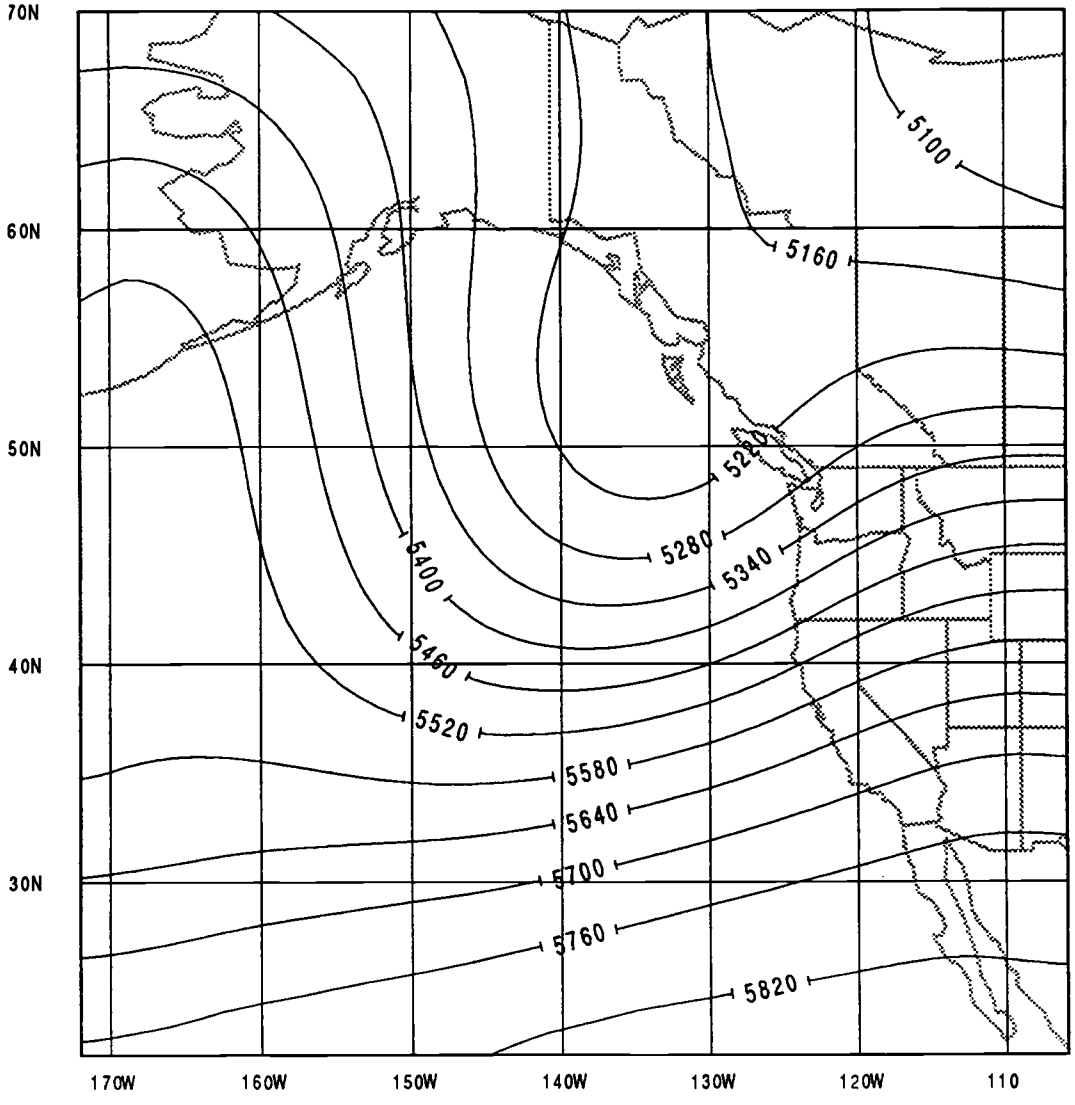

Fig. 3.11 Same as for Fig. 3.7 but for positive REOF #3

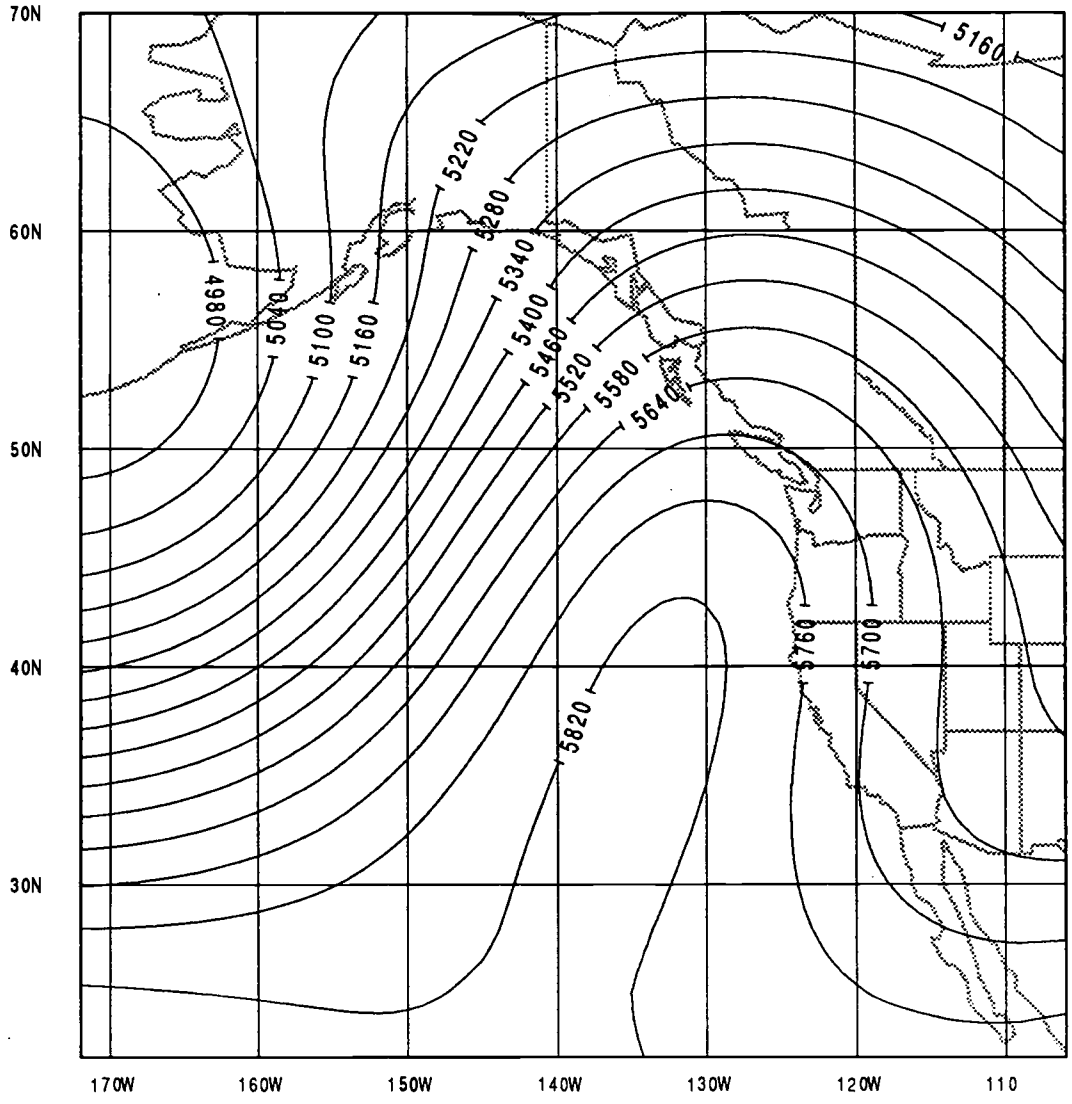

Fig. 3.12 Same as for Fig. 3.7 but for negative REOF #3

While we may attempt to show relationships between the height field and precipitation field EOF patterns descriptively, it is more productive to demonstrate them quantitatively. We first examine the linear correlations between the precipitation and height fields for individual PC pairs. Table 3.3 is a listing of these correlations and a number of them are found to significant (a probability of no real correlation less than .05).

Table 3.3 Linear correlation coefficients between height field and precipitation principal component time series. Columns are precipitation PC's and rows are height PC's. Significant (p>0.05) correlations are marked *.

ht/precip	PC 1	PC 2	PC 3	PC 4	PC 5
PC 1	.007	.318 *	-.095	-.261	.136
PC 2	.334 *	-.004	-.007	-.156	-.178
PC 3	-.588 *	-.280	-.043	-.398 *	-.089
PC 4	.123	-.514 *	-.037	-.202	.068
PC 5	-.173	-.046	-.012	.261	-.034
PC 6	.074	-.386 *	-.102	.016	-.104
PC 7	.189	-.007	-.238	-.118	-.057

For precipitation PC 1 we note a significant positive correlation with height PC 2 and a negative correlation with height PC 3. Similarly, for precipitation PC 2, the positive correlation for height PC 1 and the negative correlations for PC's 4 and 6 are also significant. There are no significant correlations for precipitation PC's 3 and 5. There is a single significant negative correlation for PC 4 with height PC 3.

To further extend the relationship of the precipitation field to the height field we now model each of the first 5 precipitation PC's as a linear combination of the first 6 height PC's. The model may be expressed as

$$\hat{Y}(t) = b_0 + \sum_{i=1}^{6} b_i X_i(t) \qquad (3.1)$$

where the estimated time-series for Y(t), one of the precipitation PC's, is given as the sum of a constant term, b_0, and the first 5 height field PC's, $X_i(t)$, each multiplied by a weight, b_i. The weights can be determined by multiple linear regression, a brief discussion of which is included here for

completeness. The method has been extracted from Hoel (1947) and Harris (1985). As for simple linear regression, we wish to minimize the sum of the squared difference between the estimated and actual Y's. Thus if the difference, E, is given by

$$E = \sum\left(\hat{Y} - Y\right)^2 = \sum Y^2 - 2\sum Y\hat{Y} + \sum \hat{Y}^2 \qquad (3.2)$$

We may find the b's by setting dE/db to zero. In order to facilitate this it is convenient to express these relationships in matrix form. Then the time-series, Y(t), with mean subtracted, becomes the column vector, **Y**, the five time-series, $X_i(t)$, become the matrix, **X**, and the five component weights, b_i, become the vector **b**. From 3.1 we can then rewrite 3.2 as:

$$E = \mathbf{Y'Y} - 2\mathbf{b'S}_{xy} + \mathbf{b'S\,b} \qquad (3.3)$$

where the column vector, $\mathbf{S}_{xy}$, is the covariance of the predictor variables, X with the outcome variable, **Y**, and **S** is the covariance matrix for the predictor variables. Then:

$$dE/d(\mathbf{b}) = -2\mathbf{S}_{xy} + 2\,\mathbf{S\,b} = 0 \qquad (3.4)$$

which can only be true if:

$$\mathbf{S\,b} = \mathbf{S}_{xy} \quad \text{or}$$

$$\mathbf{b} = \mathbf{S}^{-1}\mathbf{S}_{xy} \qquad (3.5)$$

The bias term, b_0, is given by $b_0 = Y_{ave} - \mathbf{X}_{ave}\,\mathbf{b}$ where Y_{ave} is the average of the outcome variable and $\mathbf{X}_{ave}$ is the row vector of the predictor variable averages. To determine how well the estimated values for Y(t) correspond to those observed we may compute the multiple correlation coefficient, R from:

$$R^2 = \mathbf{b'}\,\mathbf{S}_{xy}/\sigma^2 \qquad (3.6)$$

where σ is the standard deviation of Y(t).

With the weights thus determined for each of the precipitation PC's separately, by multiple regression, the precipitation time series can be reconstructed by summing the products of the model-computed PC's with the associated EOF's. The district correlations of the reconstructed precipitation record with the observations are interpolated to the western US grid for contour plotting and display, as for the district precipitation EOF's, and shown in Fig. 3.13.

If the computed weighting coefficients reflect a valid relationship, this can be demonstrated by determining the weights from one data set and

applying them to another. In this case we use the height and precipitation data for the winters of 1950-1969 to determine the weights for the model and apply them to the height PC's for the winters of 1970-1988. The "predicted" precipitation record for the 60 weather districts is reconstructed from the computed PC's and the correlations with the observed record are displayed in Fig. 3.14.

As might be expected, Fig. 3.14 shows that the correlations between the observations and inferred precipitation are slightly degraded when separate data are used to evaluate the model relationships. Nevertheless, this plot is quite similar to Fig. 3.13. From either plot, it appears that the height field PC's are better predictors of precipitation in the western sections of the domain, particularly, north of Southern California. As discussed above, the easternmost districts are on the edge of our height data and it may be that the circulation is not as well defined by the EOF's in this area. Moreover, there are a number of possible precipitation mechanisms in these regions not as well related to the 500mb circulation, such as the injection of tropical moisture into the Arizona districts and the effect of surface upslope winds on the Montana plains.

We have now demonstrated that a 6 EOF approximation to the pentad 500mb height field over the NE Pacific and western North America can be used as a sole predictor of district wintertime monthly precipitation. The correlations of inferred to observed precipitation, however, in no case exceed 0.52 and are often much less (0.16 in western Colorado). We now will show that much better predictability can result from the same input data with a more physically based model. The model discussed above assumed a direct linear relationship between height field and precipitation components. We propose a different model for which intermediate atmospheric variables, such as winds, moisture and temperature, are computed either directly from the height field or from linear statistical inference. It will be shown that the inferred intermediate variables are better correlated with the height field than are the directly inferred precipitation components discussed above. As the

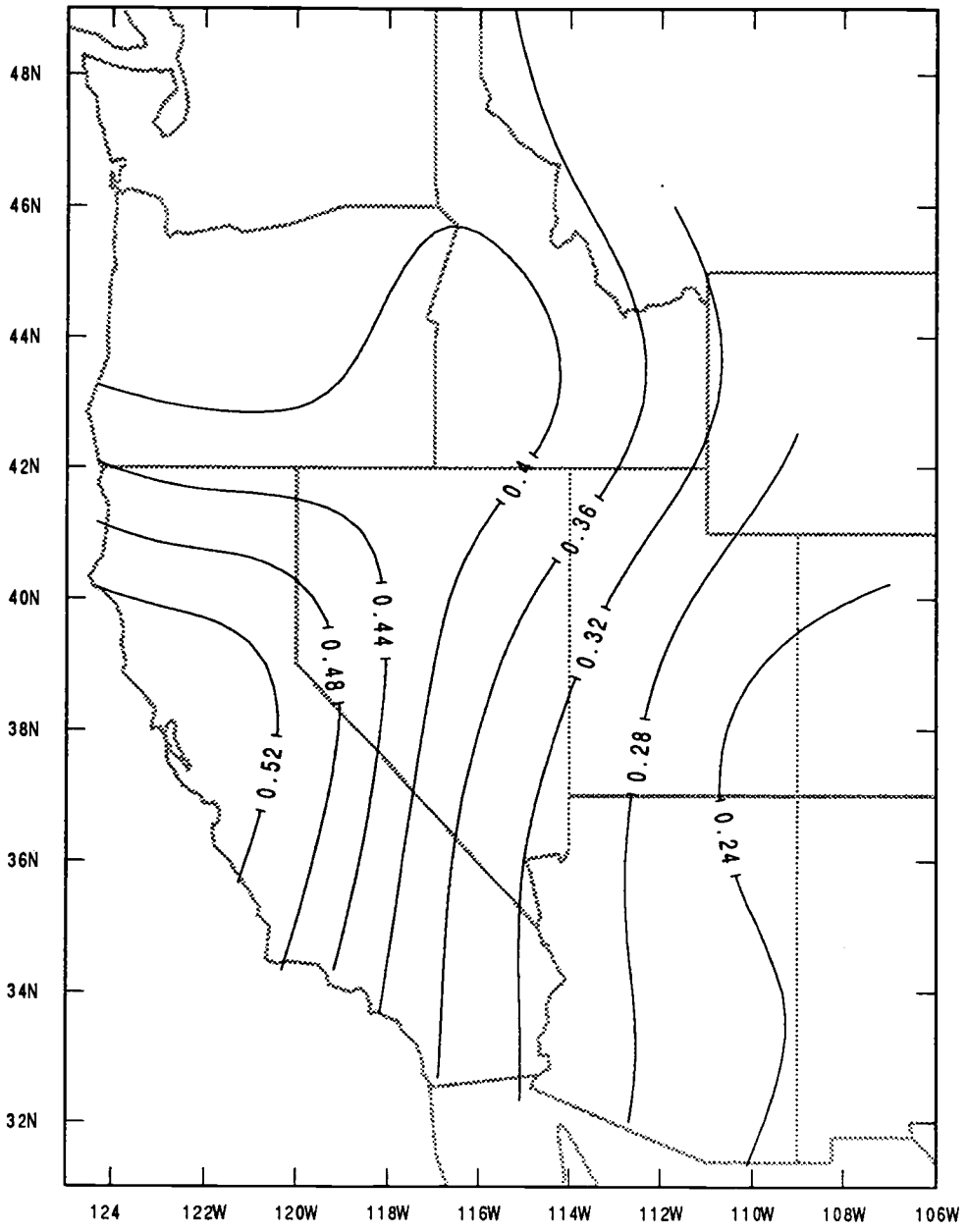

Fig. 3.13 Plot of district correlations between observed wintertime monthly precipitation and that reconstructed from the first 5 precipitation PC's inferred from the first 6 500mb height field PC's. The reconstruction uses the linear model weights derived through multiple regression analysis for each of the precipitation PC's against the 6 height PC's for the period 1950-1988. Same data set used for reconstruction as for determining model weights. The district correlations were interpolated to the geographic grid for contouring.

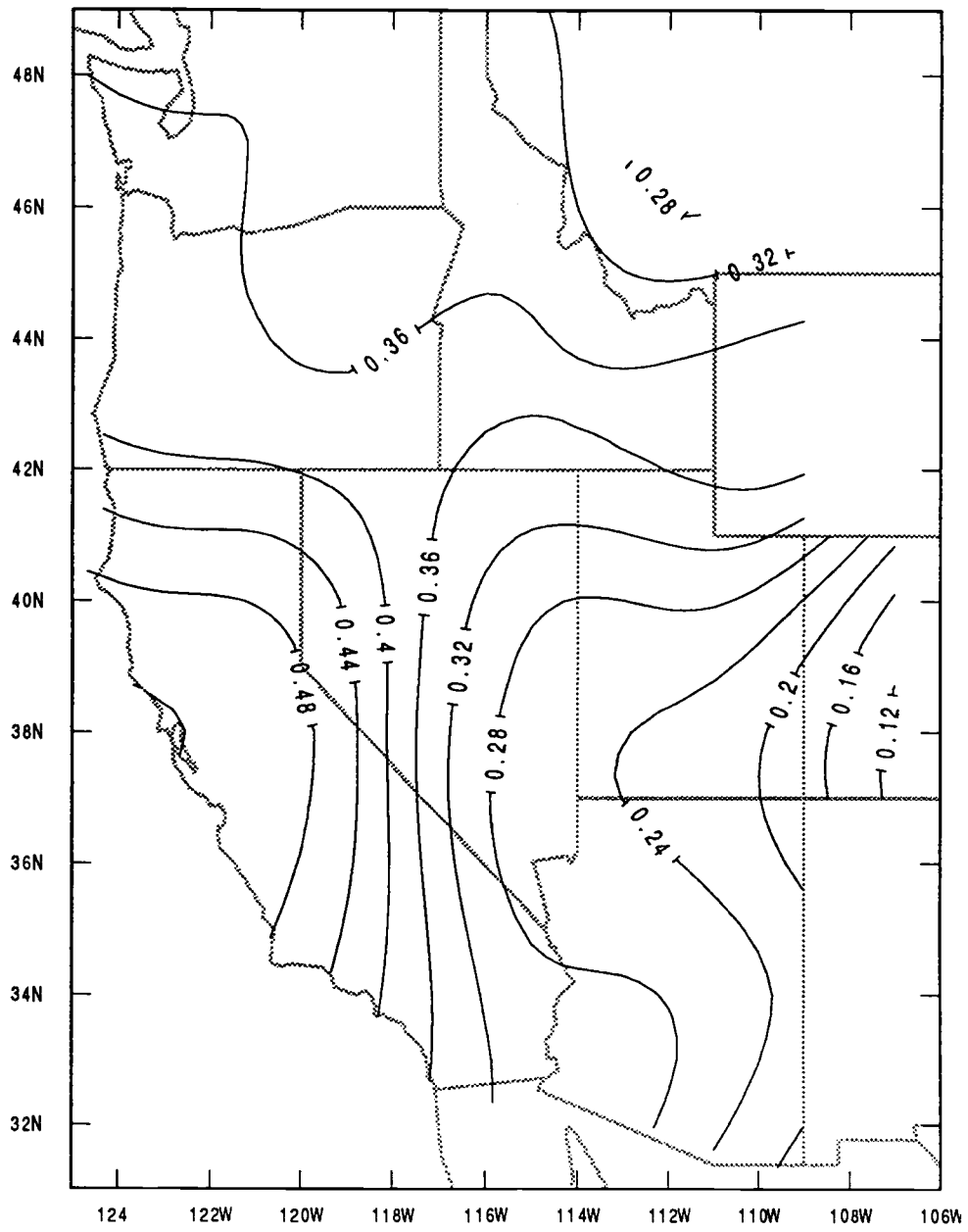

Fig. 3.14 Plot of correlations between observed wintertime monthly precipitation and that inferred from the 6 height field principal components. The time series of the first 5 precipitation PC's were used, with the associated EOF's, to generate a 60 district inferred precipitation time series for the years 1971-1988. Each precipitation PC is a linear combination of the first 6 height PC's with the weighting coefficients derived from multiple regression of the height and precipitation series for the years 1950-1970. The district correlations were interpolated to the geographic grid for contouring.

modeled precipitation includes non-linear functions of these intermediate variables, the limitations of a purely linear statistical model are ameliorated, resulting in an inferred precipitation record better correlated with the observations.

CHAPTER 4: A WESTERN DISTRICT PRECIPITATION MODEL

The purpose of the precipitation model discussed in this chapter is to determine the wintertime district precipitation expected over a five-day period consistent with the pentad averaged 500mb height field. We shall first discuss the limitations of the linear statistical approach of the previous chapter and the advantages of introducing objective, physically based processes into the model. In Section 4.1 we discuss the general mechanisms for wintertime precipitation over the western US and their relationship to the 500mb circulation. The model itself is covered in Section 4.2, with a more detailed description in Appendix A and with an additional observational precipitation study presented in Appendix B. The model results, comparing outputs to actual observations, are presented in Section 4.3.

In the previous chapter we have demonstrated a purely statistical connection between western district precipitation and the pentad 500mb height field by modeling each of the first 5 precipitation PC's (from which the precipitation field may be recovered) as a linear combination of the first 6 PC's of the height field. The results were comparable to those of Klein and Bloom (1989) who modeled monthly precipitation for each district as separate linear combinations of 700mb heights at different sets of selected locations.

The assumption of linearity in either case has not been justified and, indeed, appears unlikely (considering the non-linear physical processes involved in precipitation) but the alternative of determining the functional form and coefficients of a *non-linear* model by statistical means does not yet appear to be practical. While methodologies (such as Levenberg-Marquardt) are well known and programs have been written (Press et al., 1988) which generate the functions and coefficients from the data sets by nonlinear χ^2 reduction routines, it necessarily follows that each increase in the complexity of the assumed relationship must be accompanied by a loss of significance. Press et al. (1988) demonstrate, using Monte Carlo simulations, a rapid increase in the spread of the confidence limits for the coefficients of the non-linear terms resulting from a small increase in the proportion of random errors in the observations.

Applied to the district precipitation problem, we would expect that an increase in correlation between observed precipitation and height fields by the use of a non-linear model, *generated statistically*, would not be sustained when applied to new data. The effect of meteorological variables not directly relatable to the 500mb height field is to cause variations in precipitation which tend to obscure the true non-linear components of the height-precipitation relationship. Accordingly, curvilinear relationships, generated from data sets which include such extraneous precipitation components, are likely to have fortuitous features that will degrade the correlations when applied to *new* height fields. As this extraneous component of the precipitation is, by definition, unrelated to the 500mb height field, its effect on detection of the actual curvilinear relationship can be minimized by using data sets of sufficient length. This is, of course, true for the best fitting linear relationship as well, but much less data is required to generate significant coefficients for the linear solution.

We have selected the alternative approach of determining the expectation of precipitation by modeling the lifting of moist air by orographic, convective or synoptic-scale dynamic processes and computing the resultant condensation. It is still necessary to infer various temperature and moisture variables from the 500mb height field, statistically, but many of these appear to have closer and more linear relationships to the height field than does the precipitation itself. The link between these intermediate variables and precipitation is objective and many of the modeled processes are non-linear. In this manner, the deficiencies of the purely statistical and linear model discussed above are ameliorated and the precipitation is better related to the 500mb height field.

The fields are either input directly from a file containing the pentad heights derived from the 500mb NMC gridded heights for the 43 winters from 1950 to 1992 or, alternatively, regenerated from the time series of the principal component scores (PC's) for these fields and the associated loadings. The direct height field input mode is used to evaluate the model and to provide a baseline by which to compare the results of inputs of alternative height fields reconstructed from forecast PC series.

4.1 Western wintertime precipitation and the 500mb circulation

In this section we examine the relationship between wintertime precipitation for the western weather districts and the 500mb circulation pattern. The general mechanism for precipitation is the lifting, and consequent cooling of moist air. Lifting may occur as a consequence of a number of processes but it is convenient, here, to classify them as synoptic-scale dynamic, orographic and convective. Cooling due to other causes, such as by radiation or conduction is usually either insufficient or affects too limited a depth of air to produce significant precipitation. Sufficient moisture must be present for the cooling to bring the vapor to its condensation point and beyond so that liquid water can result. Additionally, various micro-physical processes, such as nucleation on aerosols and droplet growth by collision and coalescence, must take place. The preponderance of western wintertime precipitation is from clouds that reach heights sufficient so that some of the nucleation is in the form of ice particles with the remainder supercooled liquid droplets. This requires temperatures considerably below 0°C (typically about -15°C) and the differential in vapor pressure between droplet and crystal at this temperature causes the crystal to grow at the expense of the droplet (Hobbs, 1974). The resultant differential in fall speeds causes rapid accretion through contact nucleation. While these latter processes have an important effect on precipitation (Wallace and Hobbs, 1977), they are not easily related to the large-scale circulation and will not be considered further in this study.

The large-scale flow over the western districts, however, *can* be related to moisture availability, orographic lifting (by relating the flow to the terrain) and also to the probability of synoptic storm development. Moisture availability, particularly in the lower levels, may be related to flow direction, for the generally mountainous terrain (Fig. 4.6) causes air following long overland trajectories to be exposed to moisture loss by orographic precipitation with little replenishment due to passage over a cold and often dry land surface.

The geography of the western United States has a profound influence on the relative importance of the various mechanisms for precipitation.

The high mountain ranges of the west, oriented predominately in a north-south direction, inhibit low-level moisture advection. Air from the Gulf of Mexico source region, of key importance for the eastern two thirds of the United States, is found only rarely west of the Continental Divide. Polar Continental air is occasionally forced westward across the northern Rockies but the principal "continental" air found in the west is either maritime air of Pacific origin, modified by passage over the mountains, or dry subsident air associated with upper-level ridges and surface high pressure regions (Saucier, 1959).

The additional restriction of the scope of this study to the winter months permits a number of further simplifications. The moist air affecting the region in the winter is almost exclusively from the Pacific, with trajectories originating over source regions from the subtropics to the Gulf of Alaska. The west, particularly inland of the Sierra Nevada and Cascades, is subject to summertime flows of moist air from the tropical Pacific. These "monsoon" flows extend to the upper troposphere and provide the moisture source for much of the summer precipitation in the form of convective storms. In the winter, however, with cold surface temperatures, such air-masses are generally too stable to make an important contribution to the seasonal precipitation. Moreover, the mean mid-level circulation in the winter is such that trajectories extending from the tropics are less common (Palmen and Newton, 1969). In summary, the Pacific (from the subtropics to Alaska) is the only important source region for maritime air and significant moisture is thus restricted to flows from westerly directions or from eddies with moisture derived from such Pacific maritime flows. East of the Continental Divide the moisture source direction is less restricted as moist air from the Atlantic or Gulf of Mexico can be advected overland for great distances without encountering terrain that removes moisture by orographic lifting.

Except for the highest elevations (for which orographic precipitation may occur with the transit of moist air in flows of almost any configuration) most western wintertime precipitation can be associated with synoptic storm systems. Such systems, even the large decaying barotropic disturbances, act to produce moisture convergence, thus enhancing the effect of lifting. Synoptic-scale dynamic lifting and frontal lifting are, of course, directly associated with storm systems. Orographic

and convective lifting are only indirectly linked; but without sufficient moisture these lifting mechanisms can produce no rainfall.

Simmons and Hoskins (1977a) have studied the development of synoptic-scale disturbances by means of a series of integrations of the primitive equations with spherical geometry. They show that, starting with a small-amplitude perturbation of the balanced basic flow, the system grows by baroclinic instability from an initial, essentially linear, structure of the "normal mode form" to a large, non-linear, disturbance with the structure of an occluding synoptic system. They find that baroclinic processes are replaced by barotropic processes as the system develops. With increasing radial symmetry of the temperature and velocity fields, both vorticity and thermal advection decrease in importance. Growth ceases first in the lower portions of the system and vertical motion diminishes. As the system decays, its eddy kinetic energy is transferred to the zonal flow.

In Appendix B, we show that zonal 500mb flow (over Oregon) is associated with about 90% of the small but developing baroclinic disturbances. The much larger decaying barotropic systems are found in zonal flow as well, but are also found in quasi-stationary states in deep 500mb meridional troughs and cut-off lows. We show that while the majority of the large rainfall events (daily precipitation in excess of 1.5 inches) are for the few days with transits of baroclinic storms across the state, the greater fraction of the total precipitation is accumulated during days with zonal flow but with baroclinic systems absent.

The distribution of precipitation in extratropical cyclonic storms is influenced by the configuration of the associated frontal boundaries separating contrasting air-masses. As described by Wallace and Hobbs (1977), however, the classical "Norwegian" model of tropical air riding up over the denser, colder polar air, thus producing continuous regions of precipitation along the frontal surface, is overly simplified. There is considerable meso-scale structure of the precipitation along, but also well removed from the frontal surfaces; the precipitation being typically concentrated in bands both aligned with and at various angles to the fronts. Moreover, the tropical air streamlines in the vertical plane are often not parallel to the frontal surface. Citing a study of cloud structure and vertical motion in storms over western Europe, Palmen and Newton

(1969) show that such streamlines rise at a much steeper angle than that of the frontal surface. Additionally, many of the thicker cloud layers were found to overlie the surface well to the tropical side of the surface front.

Well defined fronts are less common in the west than in the mid-western or eastern portions of the US. The mean wintertime north-south thermal gradient is less in the west (Palmen and Newton, 1969) and the necessary low-level convergence, which must act on this gradient to produce frontogenesis, is restricted by the rough terrain. Additionally, fronts which do exist are often difficult to detect from surface observations, due to the presence of strong valley inversions. As less dense tropical air can seldom displace the cold air underneath such inversions, unless the overrunning winds can generate sufficient mechanical turbulence, it is not uncommon for temperatures to rise only after a vigorous *polar* maritime invasion.

The contribution of fronts to precipitation distribution is influenced by the temperature gradient across them and by their orientation with respect to the thermal wind (Palmen and Newton, 1969). Surface temperature contrasts in the maritime flows of the western US are seldom as great as those of the east and mid-west, due to the differences in terrain and proximity to source region. For strong upper-level zonal flows, however, the north-south altitude averaged temperature gradient is considerable, consistent with the thermal wind which is parallel to the baroclinic zone. In the initial stages of baroclinic system development the associated fronts are nearly aligned with the upper-level flow, but as the system grows and deepens the frontal orientation becomes more transverse.

Sansom (1951), in a study of 50 cold fronts passing over the British Isles, found that in the initial stages of system development, with the cold front of the disturbance essentially parallel to the thermal wind, the tropical air above the frontal surface had a horizontal wind component normal to the front slower than that of the front itself with concomitant general ascent. In contrast, for later stages of development and with the cold front *across* the thermal wind, the normal component of the tropical air typically exceeded that of the frontal surface below, resulting in descent in most cases. For this latter situation there was little or no rain and rapid clearing after frontal passage; in the former there was prolonged postfrontal rain. In this former case, despite the greater temperature

contrast and slower frontal speed, the upper portion of the frontal surface had a steeper slope than for the fronts across the thermal wind as a consequence of the much greater differential in the wind component parallel to the front.

Some consequences of these findings, as applied to the precipitation mechanisms of the western US can be illustrated by studies of two extratropical cyclones. The first (Hobbs et al., 1975) is a study of a large decaying system with an occluded front. The surface low center moved ashore over central British Columbia while the southern portion of the front extended to the latitude of central California. The 500mb flow over Washington was from the WSW, essentially zonal, although there was a considerable depth to the following trough which was almost vertically aligned over the surface low. Typical of many of the systems of this type (see our own analysis in Appendix B.), it moved slowly out of the Gulf of Alaska and weakened in the coastal mountains. Its strong surface winds south of the center were parallel to those aloft but almost perpendicular to the front. Hobbs et al.(1975) analyzed the wind, thermal and moisture structure of that portion of this system over western Washington and found the structure related to the accompanying cloud and rain patterns. They found a radial band of surface convergence oriented north-south and parallel to the front that swept eastward across the state.

In its motion over the relatively flat terrain south of the Olympics and west of the Cascades most of the precipitation, with a maximum rate of approximately 1 mm hr^{-1}, was in a narrow band near but ahead of the pressure minimum. This was coincident with a low-level tongue of moist air ahead of the front. The front itself was difficult to distinguish at any level and there was relative flow from the east that passed through the frontal surface. A considerable portion of the prefrontal and almost all of the postfrontal precipitation was considered to be convective.

As the front ascended the slopes of the Cascades, the precipitation ahead of the front diminished, apparently due to the interference of low-level moisture flux from the south by the rough and elevated terrain. In contrast, the post frontal precipitation increased markedly. Here, the moisture, advected from the flatter terrain to the west, was subject to orographic lifting. Total storm precipitation along the west slopes of the Cascades was approximately three times what it was over the low altitude

region to the west. This is consistent with the comparison of the kinematic (orographic) vertical velocity of 36 cm s^{-1} and the dynamically induced large-scale lifting of 12 cm s^{-1}. In summary, orographic and convective processes dominated in the production of precipitation for this essentially barotropic system. The chief role of the storm itself was to generate horizontal winds and moisture concentrations favorable to these processes.

The second and contrasting storm system study was of an open-wave developing baroclinic depression by Browning and Harrold (1969). The meridional extent of the frontal pattern for this storm was about 5°, as was that of the precipitation belt. Precipitation rates were much greater for this system than for that of the preceding example, exceeding 8 mm hr^{-1} in bands parallel to the warm front. Here, the vertical velocity was computed to be as great as 50 cm s^{-1}. Other precipitation bands were in the warm sector, parallel to the 850mb tropical wind. These latter bands were found to be aligned with topographic features and thus considered to have orographic components but the orographic contribution to the total storm precipitation was not determined. The heavy precipitation from the bands was in addition to a general region of continuous moderate precipitation in advance of the storm. Within the warm sector bands there were small areas of very heavy precipitation associated with convection. From their analysis, however, Browning and Harrold (1969) determined that the role of convection in this system was to concentrate, rather than to enhance, the total rainfall. They noted, in addition, that there appeared to be no orographic influence in either the region of continuous rain or for the prefrontal rain bands parallel to the warm front, due to the weak low-level winds beneath the frontal surface.

The primary precipitation mechanism for this baroclinic system was considered to be dynamically induced large-scale ascent, with orography a secondary factor. The 500mb flow regime, with a jet axis just to the south of the track of the surface center and with maximum winds of 75 m s^{-1}, is typical of those for which, in Appendix B, we associate the baroclinic storm systems transiting the west coast of the US.

4.2 The precipitation model

The output of the precipitation model is the expected precipitation, over a period of five days, for each of the 60 weather districts west of the Continental Divide. This expected precipitation is generated by the model from a five-day-averaged (pentad) 500mb height field which may be actual or forecast. The height field consists of the 500mb geopotential heights on a 23 x17 Cartesian 3°x3° grid covering the NE Pacific and western North America, from 22°N to 70°N and from 106°W to 172°W. This field may also be input in the form of selected EOF's and corresponding pentad time series of Principal Component amplitudes. From these, an approximation to the height field can be regenerated.

A key aspect of this precipitation model is that it is not necessary to determine the onset, duration or intensity of particular storms. As we shall show, the pentad 500mb height field contains sufficient information to determine the *expectation* of precipitation over each five day period with sufficient accuracy so that, summed over a month, the modeled precipitation is linearly correlated with that precipitation observed to about .80 for the coastal districts and to an average of about .60 for the districts east of the Cascades and Sierra Nevada ranges.

An expression for determining precipitation as a result of moisture convergence is developed by Palmen and Newton (1969) as follows: For a unit mass of air, the precipitation contributed can be represented as

$$P_i = -\frac{\partial q}{\partial t} - V \bullet \nabla q - \omega \frac{\partial q}{\partial p} \tag{4.1}$$

then, using

$$\nabla \bullet V = -\frac{\partial \omega}{\partial p}$$

(4.1) may be rewritten as

$$P_i = -\frac{\partial q}{\partial t} - \nabla \bullet qV - \frac{\partial (q\omega)}{\partial p} \tag{4.2}$$

Not considering evaporation, this expression may be integrated through the vertical column to yield

$$P = -\frac{1}{g}\int_0^{p_s} \frac{\partial q}{\partial t} dp - \frac{1}{g}\int_0^{p_s} \nabla \bullet qV dp - \frac{1}{g}\int_0^{p_s} \frac{\partial q\omega}{\partial p} dp \tag{4.3}$$

At the top of the atmospheric column, ω may be considered as zero but due to kinematic boundary condition the horizontal flow over the surface will result in vertical motion. Hence, the last term, neglected over flat terrain, must be included here and may be considered as the orographic contribution to precipitation.

Palmen and Holpainen (1962) computed the moisture and precipitation budget for a baroclinic system centered on the Mississippi Valley on 18 Nov., 1957. Neglecting the orographic term and expanding the divergence term they obtained

$$P - E = -\frac{1}{g}\int_0^{P_0} \frac{\partial q}{\partial t} dp - \frac{1}{g}\int_0^{P_0} V \bullet \nabla q dp - \frac{1}{g}\int_0^{P_0} q \nabla \bullet V dp \qquad (4.4)$$

For a six hour period, for which the area averaged precipitation was 7.6 mm, they found that evaporation and the local rate of change in q were both negligible and that the last term, controlled by the velocity divergence, was far greater than the advection term, accounting for 6.2 mm of the total precipitation. This last term can be related, for a given moisture content, to ω at the level of non-divergence (about 600mb) and is further evidence that the ω field is a reasonable surrogate for that of the precipitation in a synoptic system. For the elevated terrain of the western US, however, it is necessary to include the orographic term as well.

At a given location, the time-scale of the synoptic dynamic lifting is such that over a period of five days ascent is, for the most part, countered by descent so that, as determined from the pentad mean flow, moisture convergence is not representative of precipitation. The mean flow *is* useful, however, in estimating the *expectation* of such precipitation. Accordingly, in our model, synoptic storm precipitation will be parameterized based on the relationships discussed in Section 4.1 and in Appendix B.

Orographic precipitation, on the other hand, can be well estimated from the mean flow. This may be illustrated by an example. We consider a uniform westerly flow across elevated terrain with a velocity $U_o = 10$ ms^{-1}. Let this flow be modulated by a sinusoidal variation with wavelength λ so that $U = U_o + U_i \cos(\omega t - 2\pi x/\lambda)$ where ω is the frequency and x is the distance east of the point of maximum wind. This modulation is consistent with alternating bands of convergence and divergence.

$$\nabla \bullet U = \frac{\partial u}{\partial x} = \frac{2\pi}{\lambda} U_i \sin\left(\omega t - \frac{2\pi x}{\lambda}\right) \qquad (4.5)$$

For typical (medium intensity) synoptic systems the maximum divergence is on the order of 0.8 $x10^{-5}$ sec^{-1} (Palmen and Newton, 1969). For a wavelength of 1000 km, this equates to a Ui of about 1 m sec^{-1}, only 10% of the mean flow. As the vertical velocity induced by orography is approximately linear with horizontal velocity and the relative variation is small, it can be seen that estimating orographic precipitation from the mean flow will result in a total very little different from that resulting from an integration of the instantaneous flow over the time period. In contrast, as the mean flow divergence is zero, the synoptic storm precipitation from dynamic lifting would not be represented at all.

In the model, we compute the effects of orographic lifting separately from those of synoptic-scale dynamically induced lifting. The preliminary outputs of the model are two indices, Io and Ic, proportional to the contributions of orographic and synoptic storm precipitation, respectively. For convenience, we have denoted the latter the "baroclinic index", for, as discussed above, the principal vertical motions in developing baroclinic disturbances are associated with synoptic-scale dynamics, whereas those in decaying systems (which are essentially barotropic) are, in the high relief terrain of the west, largely orographic.

To combine the two indices in order to obtain district precipitation we weight the relative contributions according to the individual characteristics of the district. The rationale and method for this procedure is discussed in Section 4.2.4

4.2.1 The orographic index

The orographic precipitation term in equation (4.3) may be rewritten as

$$P_o = -\frac{1}{g}\int_{p_s}^{p_t} \frac{\partial(q\omega)}{\partial p} dp \qquad (4.6)$$

where p_s and p_t are the surface and atmospheric "lid" pressures, respectively. At the bottom of the atmospheric column ω may be computed from the kinematic boundary condition as a function of surface wind and

the slope of the underlying terrain. At the top of the column, ω is considered as zero. The estimation of the variation of both ω and q with pressure is discussed in Section 4.2.1.3 and in Appendix A. We integrate numerically, dividing the column into 20 "sigma" layers and summing each layer's contribution to the column precipitation. The estimation of the surface wind is discussed in Section 4.2.1.1 and the modeling of the profiles of temperature and moisture, necessary to the calculation, is discussed in Section 4.2.1.2, with more detail included in Appendix A.

We have found it convenient to include augmentation of precipitation by convection in the orographic index and discuss this in Section 4.2.1.4. A more complete discussion is presented in Appendix A.

As stated at the beginning of this chapter, the general philosophy of the model is that many necessary intermediate variables such as lower level winds, temperatures and moisture can be inferred, statistically, by linear regression of observations against the 500mb height field, with more variance explained than can that of the end product, precipitation. These intermediate variables can then be used in the evaluation of non-linear expressions, such as (4.6), obtaining better estimates of precipitation than could be inferred, by linear regression, directly from the 500mb height field. The method of calculating the various regression coefficients of the linear model used for the intermediate variables is the same as that discussed in Chapter 3, equations (3.1) to (3.6), and this general procedure is used in the following sections (4.2.1.1 and 4.2.1.2).

4.2.1.1 The estimation of lower-level winds from the 500mb flow

We have chosen the 850mb level as a representative height for determining orographic lifting. The actual surface winds in the rough terrain of the western US are affected by terrain features too small for the scale of the model and cannot be well inferred from the 500mb flow, particularly over the land. Moreover, 850mb is a reasonable compromise level, being at about the altitude of the peaks of the higher coast ranges, the pass levels of the Cascades and the mid-levels of the Sierra Nevada. It is

also a reasonable "mean" level for the range and basin country of the western interior.

We have constructed the following linear model for the 850 mb winds in terms of the 500mb wind components:

$$U_{850} = a_o + a_1U_{500} + a_2V_{500} \quad (4.7)$$

$$V_{850} = b_o + b_1U_{500} + b_2V_{500} \quad (4.8)$$

This simple model is based on the assumption that the mean thermal structure between the two levels is relatively coherent and that the thermal wind varies rather slowly as a function of distance. The equivalent wintertime thickness gradient, with the temperature increasing to the south and toward the sea, would be consistent with a westerly shear with height over the open ocean and with an added northerly shear component along the west coast. It is neither expected nor necessary that this mean relationship hold for individual cases.

The coefficients of the model are derived from multiple linear regression, the technique of which was discussed in the previous chapter, using observations of both the 500mb and 850mb winds at various locations over the NE Pacific and along the west coast and interior. The proportion of variance explained by the 500mb wind components is also derived. It will be shown that the estimate is a reasonable one and better to use in our case (for which the precipitation estimates are for periods exceeding those of individual storms) than are climatological means.

We have compared 4440 sets of winds at 77 locations over the NE Pacific and western North America at 500mb and at 850mb. These are geostrophic winds derived from twice daily height fields for the 15 winter seasons from 1966 through 1980. By regressing lower level u and v components separately against both 500mb components we have found that between 55 and 74 percent of the total variance is explained over oceanic locations for the 850mb winds, decreasing to a minimum of 27 percent over the Yukon territory.

It was found that the coefficients varied slightly with location, illustrating associated variations in the mean temperature gradient. It is instructive to compute and plot the thermal wind, in terms of the thickness gradient, as a function of the difference between the 500mb and 850mb wind components as predicted from the regression coefficients. The relationship used is:

$$\frac{\partial \overline{T}}{\partial y} = -\frac{R}{f \ln\left(\frac{850}{500}\right)}\left(u_{500} - u_{850}\right)$$

$$\frac{\partial \overline{T}}{\partial x} = \frac{R}{f \ln\left(\frac{850}{500}\right)}\left(v_{500} - v_{850}\right) \qquad (4.9)$$

These temperature gradients were computed using the mean winter season 500mb winds and the inferred 850mb winds from equations (4.7) and (4.8), at latitudes from 31° to 61°N and for longitudes from 160° W to 110°W at 5° intervals and plotted as vectors in Fig. 4.1. Both the effect of the normal north-south thermal gradient and also that of the wintertime land-sea contrast appear to be represented as expected by the vector field. For the precipitation model, the coefficients appropriate to the various geographic locations are stored in a matrix and interpolated for computation of the 850mb wind at a given point. The relationship between the inferred and observed 850mb winds is illustrated by scatter plot diagrams (Figs. 4.2 through 4.5) for the u and v components of 440 pentad wind cases at one point just off the coast and another just east of the northern Sierra Nevada.

4.2.1.2 The inference of the vertical profiles of moisture and temperature

In addition to the winds, it is necessary to infer the vertical temperature and moisture profiles below the 500mb level in order to model orographic precipitation. The alternative of using mean wintertime profiles, perhaps including an adjustment for geographical location, would not make use of the information available from the 500mb height field which will be shown to explain a significant portion of the variance in both profiles. The details of the computation are discussed in Appendix A but the rationale and outline of the procedure are given here.

We designate the vertically averaged or "mean" temperature as that equivalent to the 1000mb-500mb thickness. The 500mb height, which explains the larger portion of the thickness variance, is available directly.

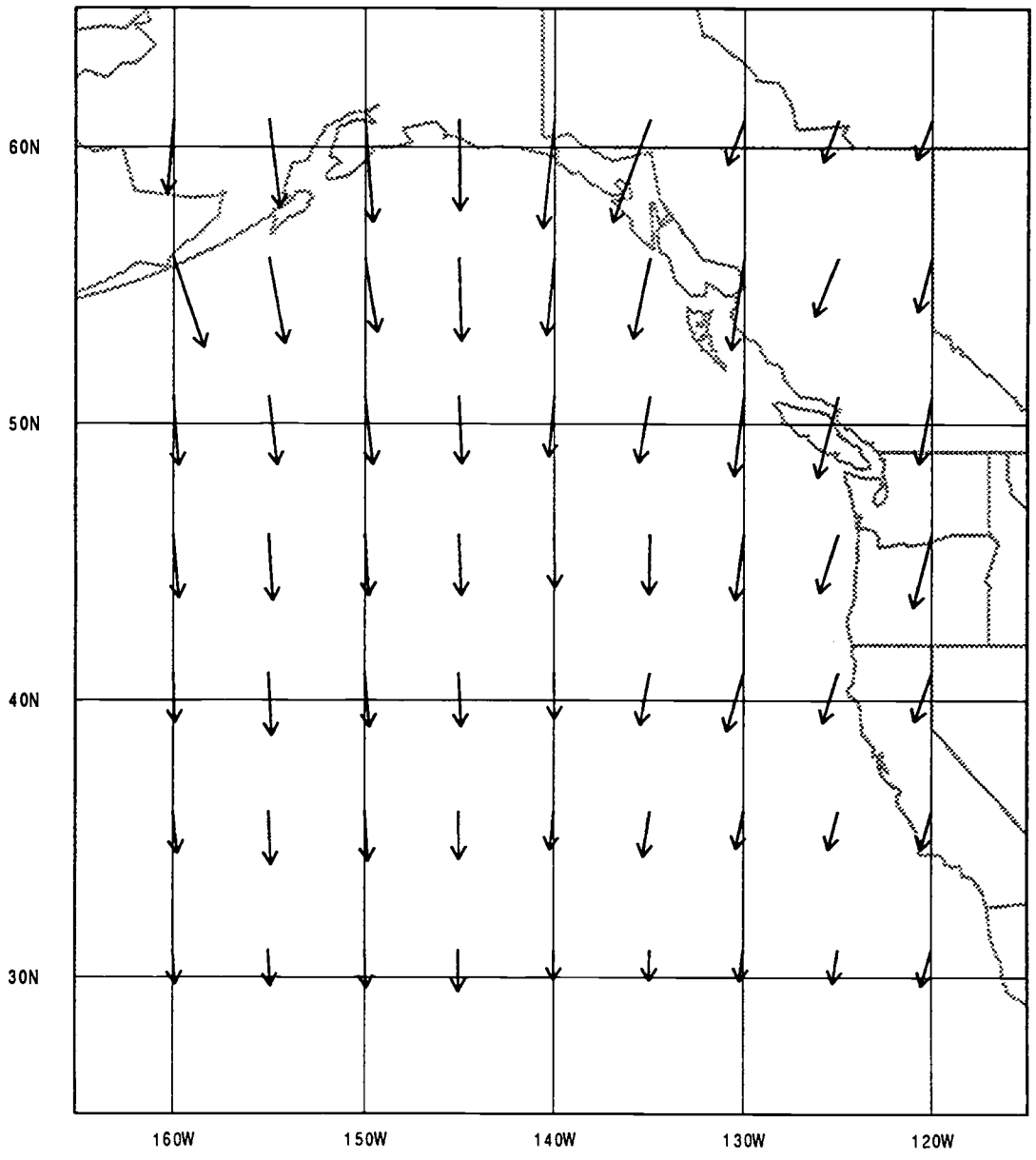

Fig. 4.1 Mean 850-500mb thickness gradient vectors over NE Pacific and western North America. Thickness computed in terms of thermal gradient from differences in mean 500mb and 850mb wind fields. Vector length proportional to temperature change such that a vector of 1° (lat) length represents a temperature increase of 0.2°C per 10° (lat) distance in direction of vector.

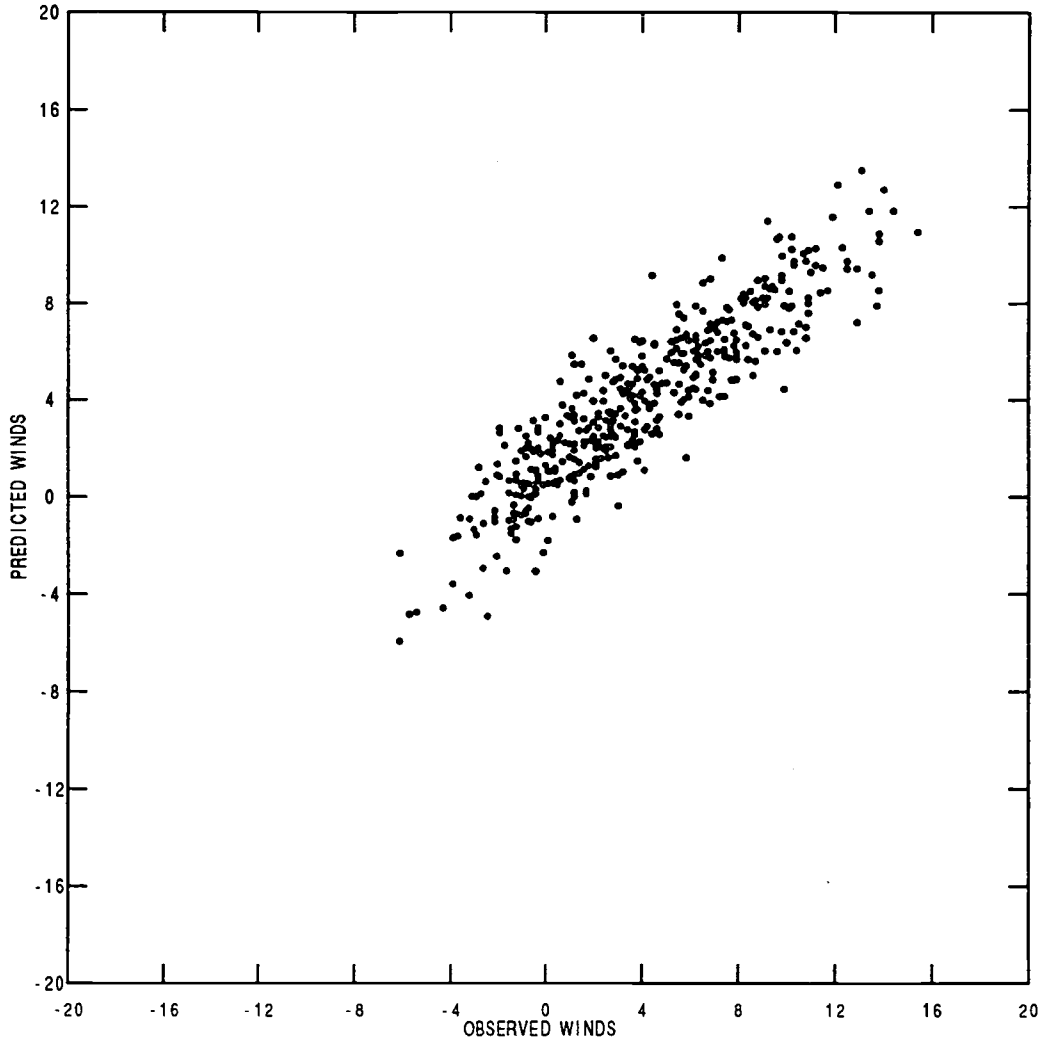

Fig. 4.2 Scatter plot of u-component of inferred 850 mb winds vs. observed over point at 36° N,125° W. Winds inferred from linear model using both u and v 500 mb winds over same point with weights from regression analysis of observed data 1966-1980.

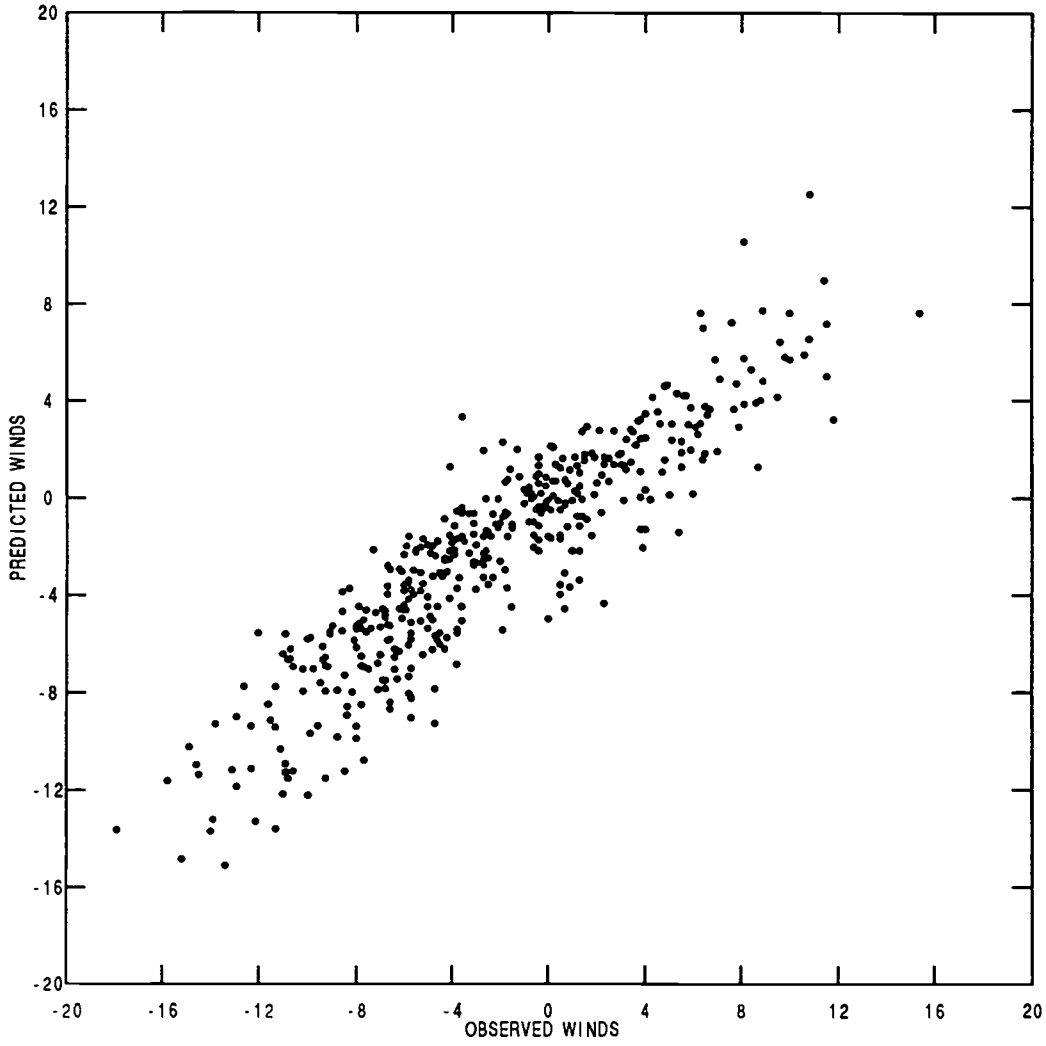

Fig. 4.3 Same as Fig. 4.2 but for v-component winds.

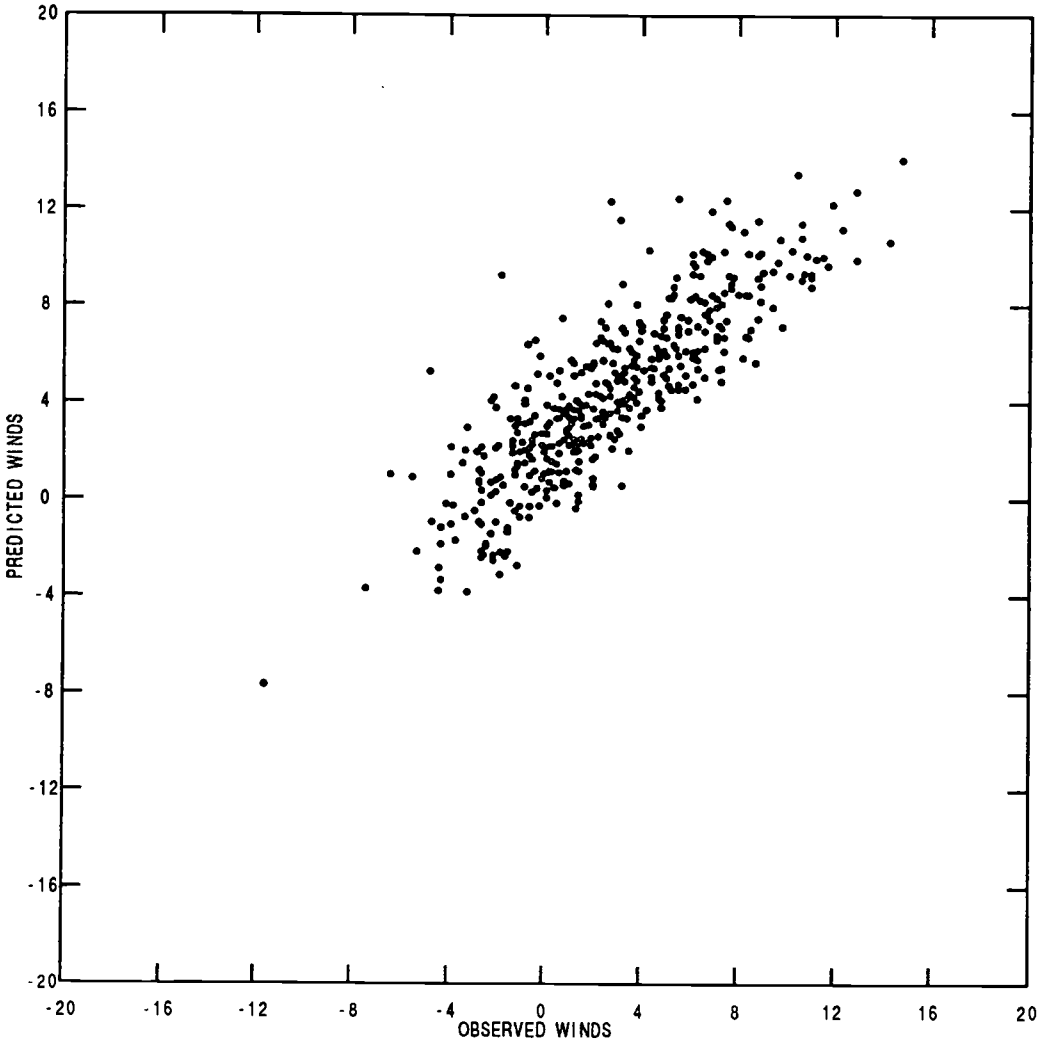

Fig. 4.4 Same as Fig. 4.2 but for 41° N, 120° W.

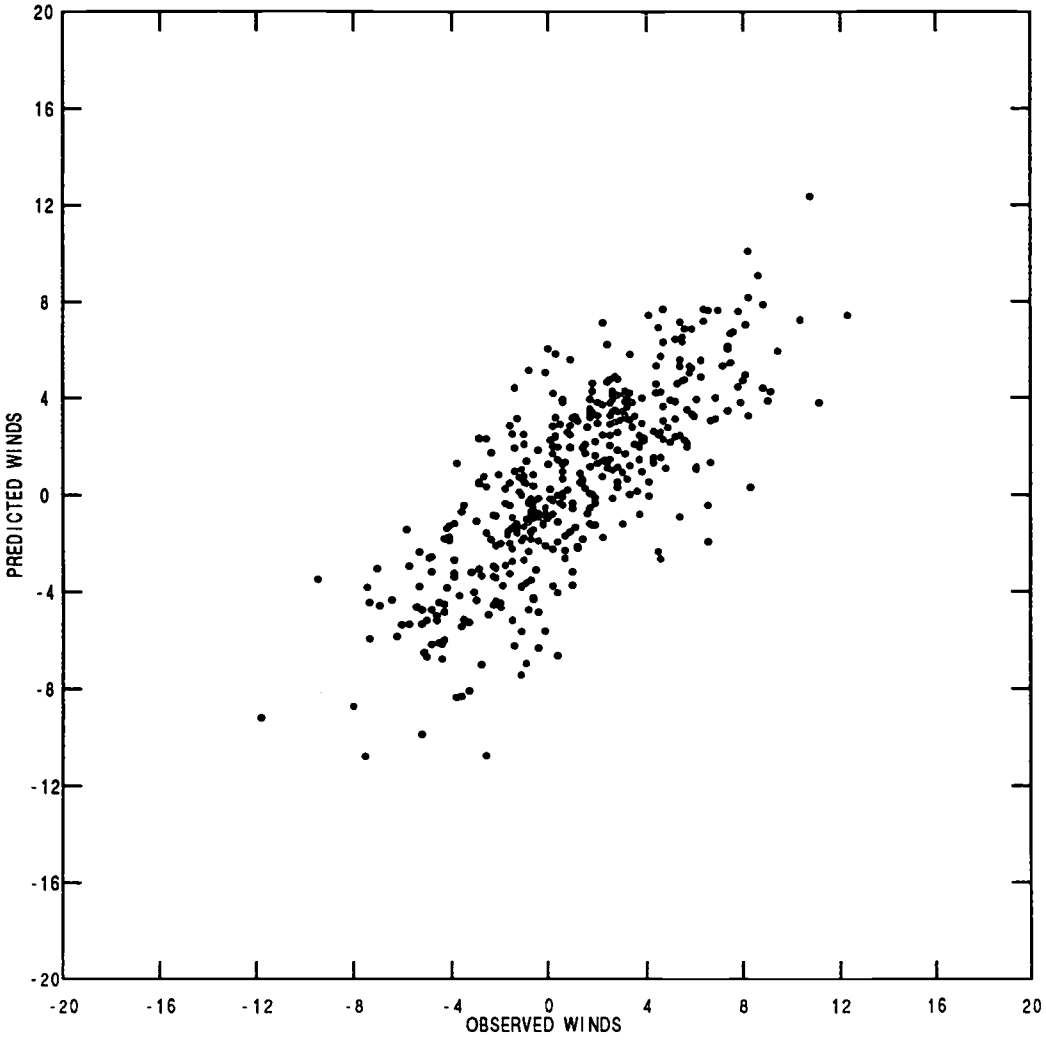

Fig. 4.5 Same as Fig. 4.4 but for v-component winds.

The 1000mb height is determined from sea-level pressure (SLP), which is inferred from the 500mb winds. As these were found to explain about 50% of the SLP variance (northerly winds being associated with higher SLP), the combined proportion of thickness variance explained by the 500mb data was found to be in excess of 0.8.

To construct the temperature profile an estimation of the lapse rate is required in addition to the mean temperature. Our model temperature profile has two slopes, one from the surface to 850mb and another from 850mb to 500mb. The slopes are generated from the stability index, using an algorithm detailed in Appendix A.

As maximum moisture content is limited by the temperature, in accordance with the *Clausius-Clapeyron* relationship, it would seem that a useful approximation of moisture might also be inferred, even using standard profiles of relative humidity. It appeared, however, that such profiles, and lapse rates as well, might both be related to the 500mb winds and height. If even a small portion of the variance in relative humidity and stability could be explained by the 500mb field, the model could be improved. A determination of stability would permit the modeling of a more realistic temperature profile and, combined with a relative humidity profile, the specific humidity profile as well. Additionally, an estimation of stability would permit the modeling of convective precipitation.

An air-mass flowing from a relatively colder source region over a warmer surface is expected to become less stable and conversely. In fact, it is commonly observed that air of polar Pacific origin, flowing over the warmer waters off the US west coast, contains scattered convective cloud systems. As the lower layers are warmed this convection appears to be sufficient to transport heat and moisture aloft so that the air mass maintains a condition of marginal stability. The air remains sufficiently cold and dry at upper levels, however, so that it is both conditionally and convectively unstable and any forced lifting, such as the crossing of the Coast Range, is observed to trigger intense convection with significant precipitation. In contrast, an air mass of subtropical Pacific origin arriving at the coast after passing over relatively colder water is generally observed to have stratiform clouds typical of stable air. Although such air contains more moisture than does the polar air, considerable lifting is required to produce precipitation due to its stability.

Such considerations suggested that a useful approach would be to make a statistical comparison between actual profile temperature, moisture and stability and coincident 500mb height and wind components. Temperatures and relative humidities were extracted from the wintertime soundings at 13 western RAOB stations having records extending from 1949 to 1988. Surface pressure and pressure-weighted mean relative humidity and stability were regressed against the 500mb wind components. For stability, the 500mb heights were also included. For convenience, stability was designated as a function of the temperature differences between the sigma surfaces corresponding to the 1000mb, 850mb, 700mb and 500mb pressure surfaces such that a zero index indicated a profile with a moist adiabatic lapse rate while an index of -1.0 indicated a dry adiabatic lapse rate. On this scale, the mean index for the 13 RAOB stations combined was determined to be approximately +0.22. For each station, surface pressure, mean relative humidity and stability were thus modeled as linear combinations of the local 500mb wind components and, in the case of stability, the 500mb height as well.

The sets of coefficients relating pressure, humidity and stability to the 500mb variables were qualitatively in agreement from station to station but varied with the both the latitude and longitude of the station in a manner sufficiently systematic to suggest interpolation to a regular grid in the same way in which the coefficients for the 850mb winds were tabulated. The "Barnes" two-pass interpolation algorithm was used (Barnes, 1964). As for the 850mb winds, the coefficients for a particular location (such as a district centroid) could now be interpolated from the tabular data and the local profile variables could then be immediately determined from the local 500mb height and wind.

To construct the temperature and moisture profiles we begin with the actual temperature profile averaged over all cases and adjust the temperature differences between levels to conform to the derived stability index. The mean temperature of this preliminary profile is then computed from a digitized (see Appendix A) approximation of

$$\overline{T} = \frac{1}{\ln(2)} \int_{1000}^{500} \frac{T(p)}{p} dp \qquad (4.10)$$

Next, the thickness is determined from the heights of the 500mb and 1000mb levels, the latter determined from the surface pressure. This is then converted to actual mean temperature and the entire profile is shifted by the difference between the actual and preliminary mean temperatures.

As for the regression coefficients, the mean standard relative humidities and standard deviations of the humidity for each level are interpolated to the location of the district. These relative humidities are then adjusted so that the vertically averaged relative humidity is the same as that computed from the 500mb wind model. Specific humidity at each level is the product of the saturation specific humidity (a function of temperature and pressure at the particular level) and the relative humidity. This completes the formation of the basic district profile.

4.2.1.3. Computation of the orographic index

Air forced to rise by a general flow over elevated terrain is lifted as a rather complex function of terrain rise, original height within the air mass and the vertical temperature and moisture structure of the air. If not blocked, the flow adjacent to the surface will follow the contour of the underlying terrain. For the case of an air mass constrained on the top by a "rigid lid" approximation at the tropopause, the relationship of the streamline surfaces, between the terrain features and the flat "lid", to the shape and slope of the underlying terrain is a complicated function dependent on the scales of the terrain features and the flow. Merkine (1975) has studied the case of a steady inviscid vertically sheared flow past a mountain ridge in a rotating, stratified atmosphere. He has found, in general, that the streamline surfaces are depressed below the levels they would assume in the case of neutral buoyancy. These levels are "sigma" surfaces; surfaces for which the ratio $\sigma=(p-p_t)/(p_s-p_t)$ is conserved, where p_s is the pressure at the elevation of the underlying terrain and p_t is that at the top of the atmospheric column.

The most important parameters influencing this depression are the Burger number, $S = (Lr/L)^2$, where L is the length-scale of the mountain cross-section and Lr is the radius of deformation (NH/f), and α, the ratio of

mountain height to atmospheric depth. The Burger number can be seen to be proportional to the square of the buoyancy frequency and becomes larger as the vertical stability increases. With increasing S, the intermediate-level flow becomes concentrated near the surface at the top of the mountain ridge with correspondingly less upward displacement in the upper portions of the flow. At still further increases in S, and with sufficiently large α, the flow becomes "blocked" and is deflected parallel to the ridge. One of the assumptions of Merkine (1975) is that the cross-terrain flow remains adiabatic. Diabatic heating, due to moisture condensation, would lift the streamlines to a higher surface, countering the streamline depression.

In our precipitation model we lack the information necessary to assess the depression or elevation of the streamlines and, accordingly, use the sigma surfaces to compute orographic lift. Except for the problem of failure to detect complete blocking of the flow, this simplification should not greatly affect the orographic precipitation budget. The lowest layers, closest to the terrain surface, which have both the highest moisture content and are subject to the greatest elevation change are also little affected by streamline depression. Those layers most affected are midway up the atmospheric column where the specific humidity is low and can make little contribution to the total column precipitation.

Actual orographic lifting is greatly complicated by the rough and irregular terrain of the Coast, Cascade and Sierra Ranges as well as by that of the complex range and basin structures of the interior western districts. The influence of nearby peaks or passes on precipitation at specific stations, due to orographic lifting, is complex and would require information on the meso-scale level of detail. For precipitation averaged over a district and for time periods of a month or more, however, much of the variation due to such complexities is averaged out.

For the model orography, the western topography is represented by a filtered version of the US Navy 10 minute terrain data base, obtained from NCAR. The filter is a single-pass adaptation of the method of Barnes (1964), an interpolation for which the elevations at each grid point are represented by the sum of those at nearby points weighted by an exponential function of their distance. The degree of smoothing is set by the magnitude of a relaxation constant by which the distance is multiplied.

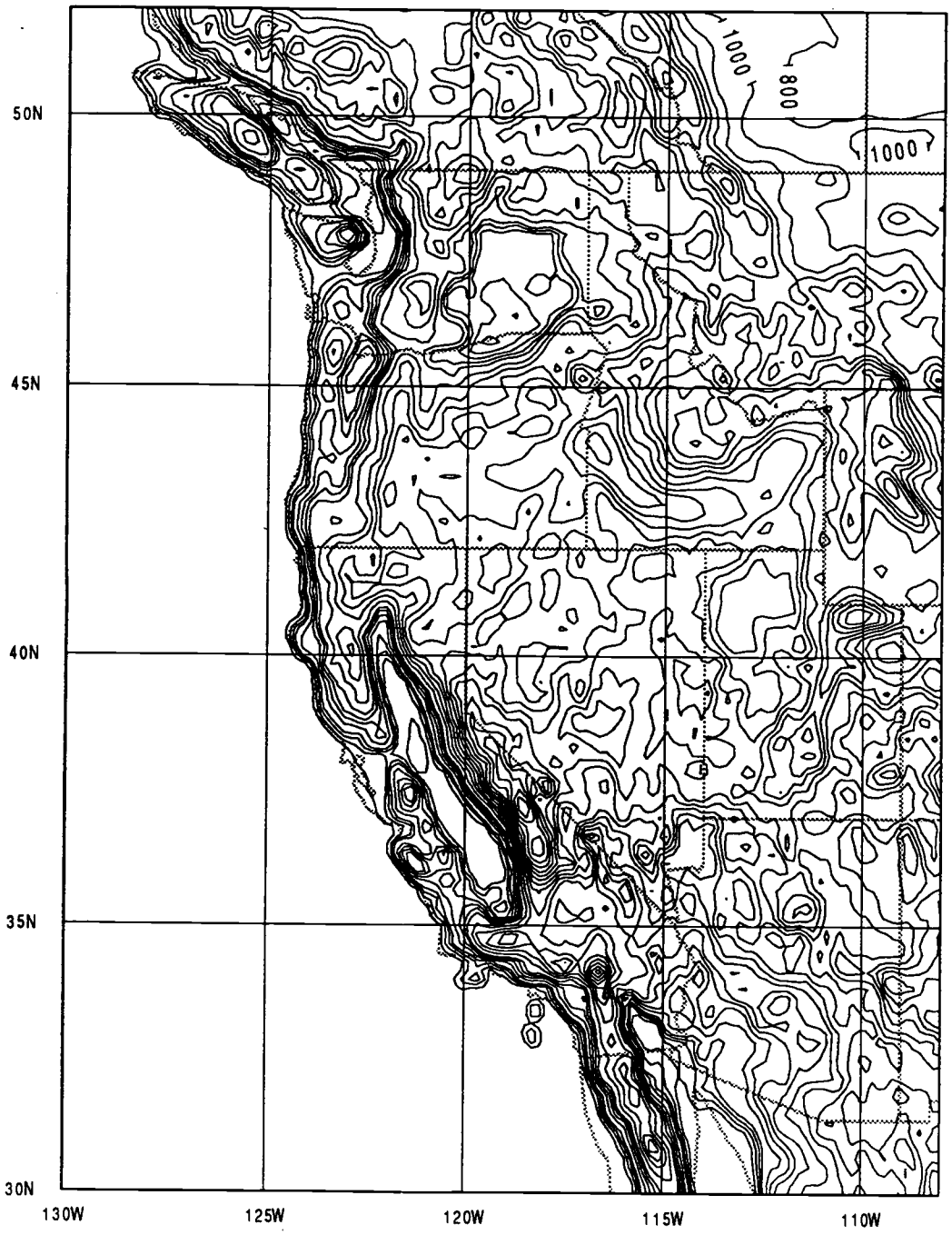

Fig. 4.6 Contour plot of terrain elevation in meters used in precipitation model. Basic data set from US Navy 10 min. terrain data base, then smoothed with one-pass Barnes filter as discussed in text.

For this case the constant is set so that major terrain features, such as the Coast Range, Willamette Valley and the Cascades are resolved with representative elevations, while minor features, such as the Salem Hills (an isolated terrain rise of about 200 meters and of 10 km extent in the mid Willamette Valley) or the Sutter Buttes (a similar feature in the eastern Sacramento Valley) are not. Figure 4.6 is a contour plot of the filtered terrain height.

With lifting determined as a function of σ for a given combination of wind and terrain, the expected precipitation can then be estimated using the vertical temperature and moisture profile. For the model, the air-mass is divided vertically into 20 layers with $\delta\sigma$ of .05. Moisture and temperature for each layer is set as discussed above. The height change over a length of 75 km (determined by experiment to be consistent with the scale of the major terrain features of the topographic model) across the target district is computed in the direction of the 850mb wind. This is converted into a pressure change and adiabatic temperature change for each layer. Should the layer become saturated, the temperature change thereafter is computed at the moist adiabatic rate and water content is correspondingly reduced. The water loss, if any, is summed over all layers. Details of the above procedure are given in Appendix A (Section A.5).

4.2.1.4 Convective augmentation

In the colder and less stable flows of polar Pacific origin, orographic precipitation is augmented by convection, triggered by lifting. While still over the ocean, convective activity is generally modest, serving to maintain a condition of marginal stability by transport of heat and moisture aloft. When a mountain barrier such as the Coast Range is encountered, however, even minor lifting may be sufficient to cause a significant enhancement to the precipitation total. Such convective activity is suppressed by the descent into the Willamette or Sacramento valleys but recommences on the western slopes of the Cascades or Sierra at about the altitude of the Coast Range. In the model, as detailed in Appendix A (Section A.6), this convective augmentation is parameterized as a function

of summed moisture, stability and orographic lift. The inclusion of convective augmentation in the orographic index (Section A.7 of Appendix A) causes a modest but significant increase in the correlation of the orographic index, Io, with the observed precipitation (about 16% when averaged across all districts).

4.2.2 The baroclinic index

When applied to the problem of modeling the precipitation from baroclinic disturbances, considering only the 500mb flow, it is necessary to determine a relationship between the strength and concentration of the flow and the most probable location, intensity and meridional extent of precipitation resulting from the expected systems. Precipitation intensity, related to the dynamically induced ascent, is a function of the disturbance growth rate (Palmen and Newton, 1969). This, in turn, may be related to jet strength and width.

In the theory of growth of extratropical disturbances it is generally agreed (Palmen and Newton, 1969) that their kinetic energy is derived from the release of available potential energy inherent in the baroclinic structure of the basic flow (Eliassen, 1956). Sutcliffe (1947) had demonstrated that the growth of vorticity in the lower levels was related to divergence aloft and convergence below. Petterssen (1955) formulated the concept of high-level positive vorticity advection, superposed on a low-level frontal region, leading to system development. This was extended, in the framework of quasi-geostrophy, to the "tendency equation" and its complement, the "omega equation", for which the Laplacian of ω is equated to differential vorticity advection and temperature advection (Holton, 1979).

For the most rapidly developing storms, associated with major precipitation events, the vertical velocities appear to be greater than those explained by the quasi-geostrophic omega equation. In a comparison with such lifting using the full or generalized omega equation, Pauley and Nieman (1992), applying the Limited-Area Meso-scale Prediction System (LAMPS) model initialized with the QE II storm conditions, found that

various other factors had a comparable effect in determining the net lifting. In particular, the diabatic heating due to condensation and the ageostrophic advection of both heat and vorticity not only greatly augmented the rising motion in the forward portions of the system but also tended to suppress the sinking motion in the rear. While, for the case studied, these effects contributed to explosive development they should, under more normal circumstances, lead to greater rising motion and hence more precipitation than would be expected from the quasi-geostrophic omega equation alone.

Pauley and Nieman (1992) relate the ageostrophic advective wind to the secondary circulation in the vicinity of fronts. For the case of the nascent developing wave, the front lies along the baroclinic zone under the jet. There is far more temperature contrast across this sort of front than for those fronts discussed earlier in connection with mature storm systems (Hobbs et al., 1975).

As demonstrated in Appendix B, precipitation events for any particular location which are associated with developing baroclinic storms are far less common in the western United states than those resulting from large mature or decaying systems. Nevertheless, as discussed above, baroclinic system precipitation is often very heavy and thus makes an important contribution to seasonal totals.

In Appendix B it is shown that the typical (canonical) developing baroclinic system crossing the Oregon Coast from the west has a band of precipitation of about 300 km in north-south extent centered about 200 km north of the jet axis. During the winter, as this axis meanders from Baja California to Alaska, the "residence" time for any one location is normally short. We determined the number of occurrences of the pentad averaged 500mb wind maximum for 3° latitude bins along the Pacific Coast out of a total of 1272 pentads from 1950 to 1992. These occurrences are presented as a bar chart in Fig. 4.7. It can be seen that, even for the most favored latitudes, the jet is sufficiently close to a given location for baroclinic precipitation from the "canonical" system only about 10% of the time. This residence behavior of the jet varies markedly between winters. In 1985, for example, only three baroclinic systems crossed the coast between 41°N and 47°N; in the following year there were twelve such transits. In a particular location, Corvallis, Oregon, the rainfall totals for these years

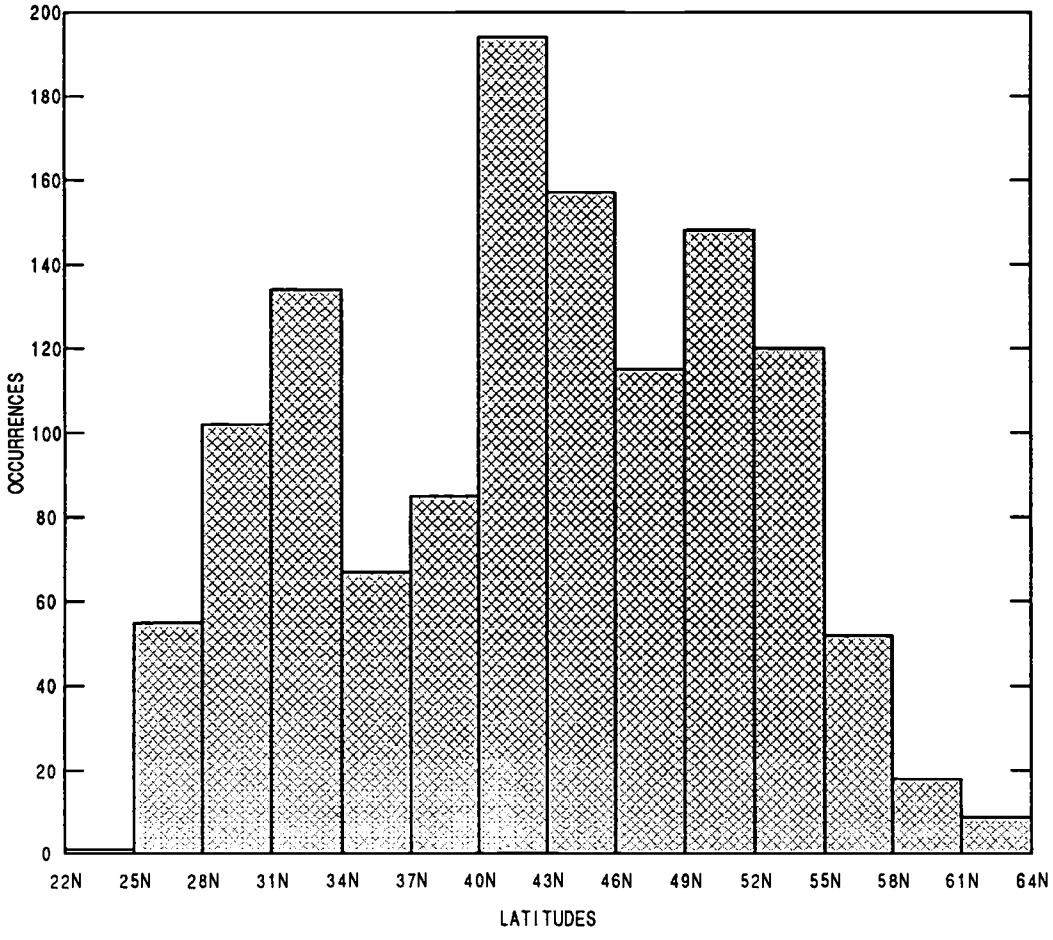

Fig. 4.7 Bar chart of occurrences of the latitudes of pentad averaged jet crossings of the 122°W meridian for November through March, years 1949 to 1992.

were 27.15 and 43.75 inches, respectively. While we have not been able to isolate, definitively, the contribution of precipitation from synoptic-scale dynamic lifting to these totals, we believe the contribution to be manifestly important and necessary to include in our model.

As the pentad averaged 500mb height field contains insufficient information to determine the development of specific baroclinic systems we will relate the *expectation* of baroclinic precipitation to the 500mb flow by parameterizing applicable portions of the following theoretical and observational relationships.

4.2.2.1 Relationship between 500mb flow and location and meridional extent of baroclinic precipitation

In this section the results of a number of observational and theoretical studies, which provide the framework for the model baroclinic precipitation parameterization, are summarized. In particular we wish to determine factors, relatable to the upper-level flow configuration, which can be used to infer the location of both the center of the expected baroclinic precipitation and also its meridional extent.

Large-scale processes, such as differential heating and the mean circulation, tend to concentrate the horizontal temperature gradient in the mid-latitudes. In general, the synoptic-scale eddies, initiated when the baroclinity becomes sufficient, tend to reduce this baroclinity and to transfer their eddy kinetic energy into the zonal kinetic energy of the polar jet. Stone (1978) refers to this process as " baroclinic adjustment" and demonstrates that for baroclinity greater than some critical value, unstable waves will grow to large amplitudes and will thus become more effective in reducing the baroclinity. Below this critical value, the waves tend to remain shallow.

Using realistic zonal flows with jet maxima at various latitudes, Simmons and Hoskins (1977b) have employed a primitive equation model with special geometry to determine wave numbers for maximum growth rates. They find that for latitudes between 30° and 55°, wave numbers for maximum growth range from 9 to 5 respectively, with wave number 7 for a

45° jet. Here, the e-folding time is a little less than two days. They also find a slower growth rate and a bias toward shorter waves for narrower jets.

James (1987) shows that increasing *barotropic* shear reduces the growth rate of the most unstable mode. Moreover, the transfer of momentum into the jet core (as a consequence of the growing disturbance) further increases the horizontal shear, thus acting as a "barotropic governor" which limits further development.

The meridional extent of baroclinic waves and associated precipitation is dependent on the characteristics of the flow in which they are imbedded. In his pioneering work on baroclinic instability, Eady (1949) found that with no variation of the basic flow in the horizontal, and a number of other simplifying assumptions, the most rapidly growing wave has a specific zonal wavelength but is of infinite latitudinal extent when the flow is unbounded. When the flow is confined between vertical walls, however, the wave assumes a meridional scale equal to the width of the channel.

With a two-layer β-plane model, Stone (1969) determined, that for zonal flows with large latitudinal extent, the meridional scale of baroclinic systems should be limited by the radius of deformation, L = NH/f, where N is the *Brunt-Väisälä* or buoyancy frequency, H is the depth of the fluid and f is the Coriolis parameter. Simmons (1977), expanding on the work of Stone (1969) by adding meridional shear to the model and obtaining numerical solutions, determined that the shape of the cross-jet velocity profile also influences the meridional scale, S_m, of the disturbance and that this scale should be the geometric mean of the radius of deformation, L, and a curvature term, R.

Then

$$S_m = \sqrt{LR} \tag{4.11}$$

where:

$$R = \left(\frac{\bar{u}}{\frac{d^n u}{dy^n}} \right)^{1/n} \tag{4.12}$$

and n determines the degree of the curvature function. For a parabolic velocity profile (n=2) this may be related directly to the width of the jet.

In addition, Simmons (1977) shows that for disturbances in basic flows of latitudinal extent much greater than the radius of deformation, the amplitude of the upper-level streamfunction is given by

$$A = A_0 \exp\left[-\frac{k(2y - y_0)^2}{y_0}\right] \tag{4.13}$$

where y_0 is the channel width, $y = .5\ y_0$ is the channel center and k is a function of the wave number. With a more concentrated jet this gaussian amplitude shape is modified but not significantly.

The meridional scale of the precipitation in a baroclinic system should be comparable to that of the vertical motion field. Lim and Wallace (1991) have studied the structure and evolution of "generic" baroclinic systems through regression analysis of high-pass filtered NMC analyses over the mid-Pacific for the winters of 1975-1984. Omega field analyses were made directly from the data set and also by computation from both the quasi-geostrophic omega equation and by the divergence of the "Q" vector (Hoskins et al., 1978). The space-scale of the ω field is seen to be somewhat smaller than that of the height field. While the meridional extent of the height perturbation appears to be about 8° north and south of the disturbance center (to the half-maximum perturbation extent), that for the ω field appears to be about 5° for the directly analyzed data and 4° for the fields computed by the two ω-equation methods. Lim and Wallace (1991) remark that problems with the data assimilation system may have contributed to some diffusion in the apparent scales of the disturbances.

A number of investigators, as discussed by Palmen and Newton (1969), have found that baroclinic development is typically initiated near or a little to the south of the jet axis but then moves to the north as the disturbance intensifies. Anderson and Gyakum (1989) have segregated cyclone tracks in the mid-Pacific by upper-level circulation types. For well defined zonal flow, the cyclone track data shows that, when first identified, the tracks are rather closely grouped near the jet axis and then diverge, generally to the north. On the second day after detection the disturbances average 3.5° north of the jet. By the third day of development the cyclone centers average about 5° north of the jet with a standard deviation of about 5°. For weaker flows, and particularly for those flows with less parallel streamlines, the tracks of the cyclone centers are more erratic and dispersed.

As applied to the precipitation patterns for baroclinic systems crossing the west coast, there is the additional question of whether or not the typical storm of the western US is as fully developed as are those mid-Pacific systems analyzed above. An inspection of US synoptic surface and 500mb map sequences gives the impression that the majority of the open-wave systems crossing the coastline south of the US-Canadian border originate within about 20° longitude from the coastline. Such systems have but a few days of development before they reach the coast and appear to be of lesser amplitude and with heavy precipitation zones of narrower meridional extent than are the typical fully developed storms that originate further to the west. We have verified this impression by making a separate analysis of precipitation events, baroclinic systems and accompanying 500mb circulation types. This is detailed in Appendix B and provides additional data upon which to base the baroclinic portion of the precipitation model.

4.2.2.2 Application to the baroclinic algorithm

The details of the application of the results of the studies discussed above (and also from Appendix B) are given in Appendix A, where the specific baroclinic precipitation algorithms are presented. In summary, the expected position of the baroclinic system centers is determined to be 3.3° north of the pentad averaged axis of maximum 500mb winds. The meridional extent of the precipitation for these centers is only about 2.5° north-to-south and the distribution shape is approximately normal. To this dispersion, however, must be added the uncertainty in the 3.3° bias, which is a combination of that of the cyclone centers in reference to the instantaneous position of the 500mb maximum wind axis and also that of the instantaneous axis to the pentad averaged axis. The combined dispersion is modeled as a gaussian distribution with a standard deviation varying from 5° at 48°N, to 6° at 34°N for a jet in excess of 12° width (between half power points) and commensurately less for narrower jets.

As discussed in Appendix B, an additional factor related to the expectation of baroclinic development appears to be that of the inclination

of the streamlines of the basic flow to the east-west (zonal) orientation. Baroclinic development was found to diminish sharply for flows inclined more than 45° and this has been incorporated in the algorithm.

The combined baroclinic index algorithm, the development of which is detailed in Appendix A, is

$$I_c = A \cdot \cos^2\left(\frac{90\alpha}{75}\right) e^{-\frac{1}{2}\left(\frac{d+b}{\sigma}\right)^2} \qquad (4.14)$$

where A is a constant of proportionality, chosen for convenience (as Ic itself is relative, rather than absolute), α is the angle of streamline inclination, d is the distance of the district centroid from the jet axis along a line perpendicular to the flow at the jet axis, b is the precipitation pattern center bias (+3.3° if the district is south of the jet, -3.3° if north) and σ is given as

$$\sigma = C\left(6.0 - \frac{\varphi - 34^\circ}{14^\circ}\right) \qquad (4.15)$$

C is a function of the cross-jet velocity profile which is limited to a maximum value of 1 but is otherwise, C = Vs/0.85 Vmax, where Vs is the jet velocity 6° from the axis (on the side of the district), Vmax is that along the jet axis and ϕ is the jet axis latitude.

4.2.3 Combining indices to obtain district precipitation

The two indices developed in the preceding section are designed to be proportional to the orographic and baroclinic components of precipitation at a district location. The individual characteristics of the various districts, however, have an effect on the relative contribution of the two components that is not easily incorporated directly into the model. This may be due to the lack of resolution of small-scale terrain features and to unresolved interactions of these features with the pressure gradient field near the surface. Even when forecasters have access to models which output synoptic-scale fields of wind, temperature and moisture, it has been found that forecasts for individual stations are much improved by the use of a statistical relationship between the model output and the forecast variables. This methodology, (Glahn and Lowry, 1972), (Carter et al., 1989), known as model output statistics (MOS), is to assume that the

predicted variable is a linear function of the model output variables and to determine these relationships by regression against the historical station records. Hence, for the orographic and baroclinic indices, I_o and I_c,

$$P = a_0 + a_1 I_o + a_2 I_c \qquad (4.16)$$

This method is easily adapted to the orographic and baroclinic index values generated by the model. Multiple linear regression, discussed in Chapter 3, is used to generate a table of weights, a constant term (a_0), an orographic coefficient (a_1) and a baroclinic coefficient (a_2), for each district which are applied to the two indices to yield an inferred monthly district precipitation value in terms of standard deviations. At this point it is necessary to discuss an additional procedure that is required.

If the distributions of the indices and of district precipitation were even approximately normal the weighting coefficients could be optimized by a standard multiple regression analysis (MRA). This, however, is not the case. Not only are these distributions highly positively skewed but their modal values are occasionally zero. In some of the southern districts of the west it is evident from an inspection of the monthly precipitation record that, whatever divisions are made in the precipitation amounts, the lowest division (that starting at zero) occurs with the greatest frequency. Even in northern coastal districts, where this is not true, there is still a substantial frequency of occurrence of the lowest division and the distribution is always positively skewed. As the indices were developed so as to be proportional to precipitation, it is not surprising to find that these distributions are similar.

This problem with comparisons of precipitation has been recognized for many years. Recently, Leathers et al. (1991), in his comparison of US temperatures and precipitation with the PNA index, discussed the problem and noted that previous studies (e.g. Thom, 1958) had shown that precipitation is well represented by a gamma distribution. In a study of monthly and seasonal precipitation distributions, as compared to 30 and 90 day outlooks, Wilks and Eggleston (1992) also have found that a gamma

distribution is appropriate. It may be expressed in terms of the parameters β and γ as

$$f(x) = \frac{1}{\beta^{\gamma}\Gamma(\gamma)} x^{\gamma-1} e^{\frac{-x}{\beta}} \quad \text{where } \beta > 0 \text{ and } \gamma > 0 \tag{4.17}$$

Thom (1958) showed how, for an actual distribution, β and γ may be obtained from the method of Maximum Likelihood Estimates. Following this procedure, which he discusses in detail, we arrive at an estimate for γ:

$$\hat{\gamma} = \frac{1+\sqrt{1+4A/3}}{4A} \quad \text{where } A = \log\bar{x} - \frac{1}{n}\sum \log x \tag{4.18}$$

then β is estimated from the relation

$$\frac{\bar{x}}{\hat{\beta}} = \hat{\gamma} \tag{4.19}$$

For each district, the precipitation and the two indices will have individual gamma distributions specified by the derived parameters β and γ.

For comparison purposes we wish to convert the precipitation and index variables into new equivalent variables which are normally distributed. We choose distributions with zero mean and unit variance, hence:

$$g(z) = \frac{1}{\sqrt{2\Pi}} e^{-\frac{1}{2}z^2} \tag{4.20}$$

Then, to map any point x_i in the gamma distribution into an equivalent point z_i in the unit normal distribution we note that for equivalent points the cumulative frequency distributions must be the same. The relationship can be stated as

$$\int_{-\infty}^{z_i} g(z)dz = \int_{0}^{x_i} f(x)dx \tag{4.21}$$

As a zero value for x_i would result in a singularity for z_i, a small increment (.001) is added to all precipitation and index values (x_i). For the particular precipitation distributions encountered in the districts evaluated, a monthly precipitation of zero would then result in a z of about -1.0 in the dryer southern districts and as low as -3.9 in the more normally distributed and wetter districts of the north coast.

To determine a specific z_i, the gamma distribution function, f(x), is integrated from zero to x_i, numerically, and the corresponding integral of g(z) computed for increasing values of z until the two integrals become equal. The relation (4.21) is then satisfied. In this manner the series of

indices and actual precipitation are normalized and the estimated transformed precipitation may be better represented by a linear combination of the precipitation indices.

4.3 Evaluation of the precipitation model

The precipitation model as described above was run both with actual 500mb pentad height fields and also with fields regenerated from varying numbers of principal components and associated EOF's. As has been stated before, a distinction should be made between comparisons of model outputs used for evaluating the effect of differing input data, such as the number of PC's used, and comparisons made to evaluate the utility of the model as a forecast tool. In the former case, the inclusion of the entire data set is appropriate; in the latter, the data set used to derive the various weighting coefficients by regression, not only for the final indices but also for the intermediate variables, must be separate from that used to evaluate the model. The comparisons discussed in the following section are for the entire data set.

4.3.1 Comparisons

The model was first run with 500mb pentad height fields interpolated from the 1977 point octagonal NMC NCAR data set for 00Z and 12Z. The resulting orographic and baroclinic indices were averaged for each month, mapped into a normal distribution as discussed above and regressed against the similarly transformed observed monthly district precipitation record. The coefficients of multiple linear correlation between the indices and the precipitation record, obtained as discussed in Chapter 3, are used as a baseline for further comparisons. The correlations vary from over .80 in some of the north coastal districts to about .40 in the southeastern districts of Utah and Arizona. Figure 4.8 shows these correlations

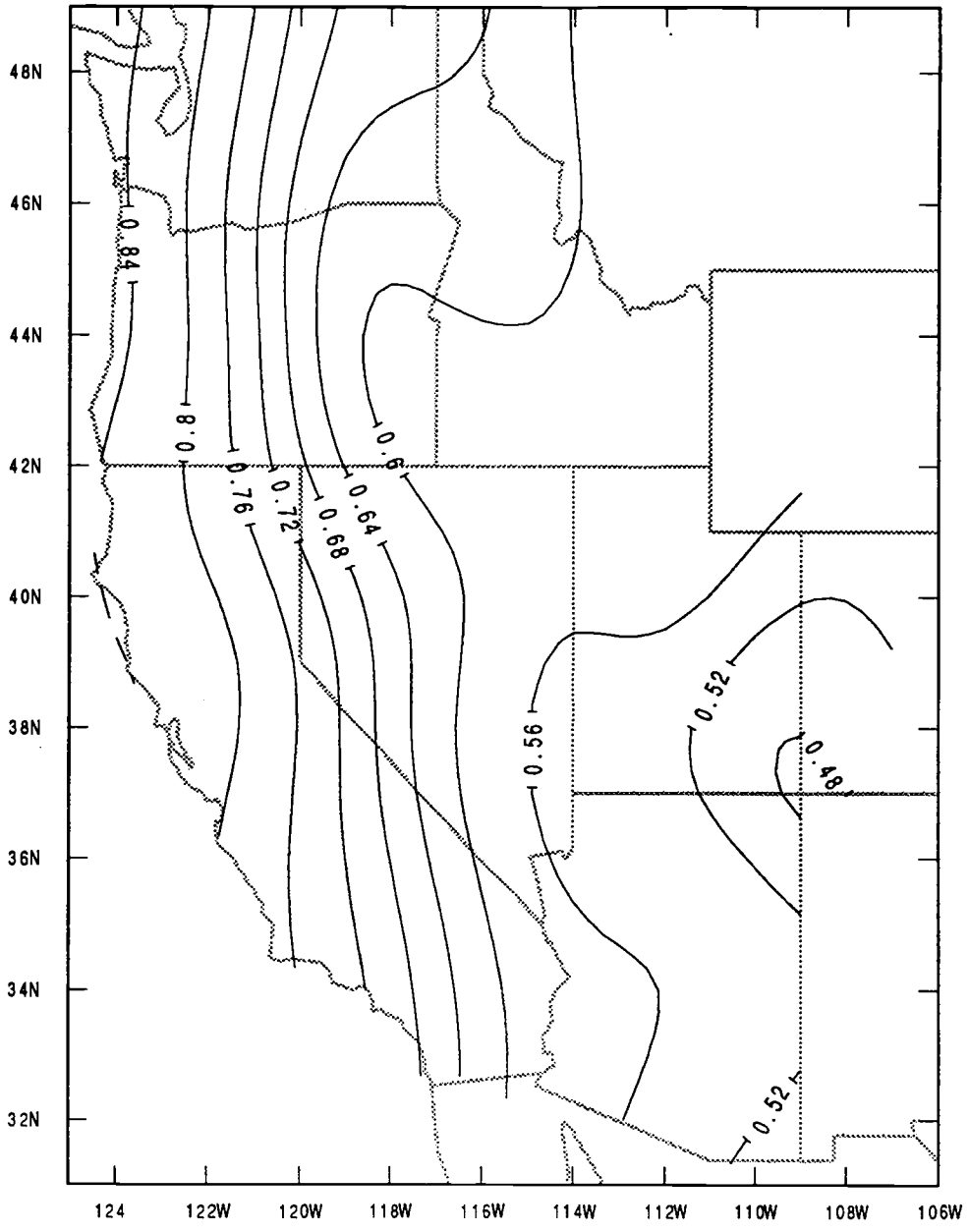

Fig. 4.8 Plot of multiple correlation coefficient of orographic and baroclinic indices vs. observed district precipitation for years 1949-1988. Correlations interpolated to geographic grid for contouring.

interpolated to the geographic grid for presentation. Comparison with Fig. 3.13 shows that the model results are improved considerably over those from direct linear correlation with the height field EOF's. As for the EOF's, the results are better for the western districts. The degradation of model performance in the southeast may be due to the effect of precipitation mechanisms not included in the model, such as the transport of high-level moisture from the subtropical Pacific or from the Gulf of Mexico. As discussed in section 4.1, this model was developed, not as a general precipitation model but rather with the precipitation mechanisms typical of the Pacific coastal states in mind.

With these correlations as a baseline, we now investigate the effect of representing the input 500mb height field by a varying number of EOF's multiplied by their associated PC time-series. The above procedure was repeated and the model re-run with the height fields regenerated using from two to seven EOF's. For comparison purposes, the resulting district correlations were grouped into three regions and averaged. Figure 4.9 shows how these averaged correlations are degraded as the number of EOF's representing the height fields are reduced. The first district group is for those of the coast, coastal valleys (such as the Willamette and Sacramento) and the Sierra and Cascades. The second group consists of the districts of the Columbia Basin, the Great Basin and the Colorado Desert regions. The third group is of the mountainous districts to the east. All three groups show a progressive decline in correlations as the number of EOF's used in the height field representation is reduced. With the exception of the two-EOF case, for which all three correlation averages are below 0.4, the Great Basin group results are a little better than that of the eastern mountains and, in all cases, the Pacific coastal group is considerably better correlated than are the others.

There is almost no fall-off in correlations for any of the groups between the seven-EOF and six-EOF representation, but an accelerating decline thereafter. The six-EOF representation is very little degraded from the actual height field, is essentially the same as that of the seven-EOF representation and is yet a sufficiently compact representation to be convenient for comparisons with potential external forcing effects.

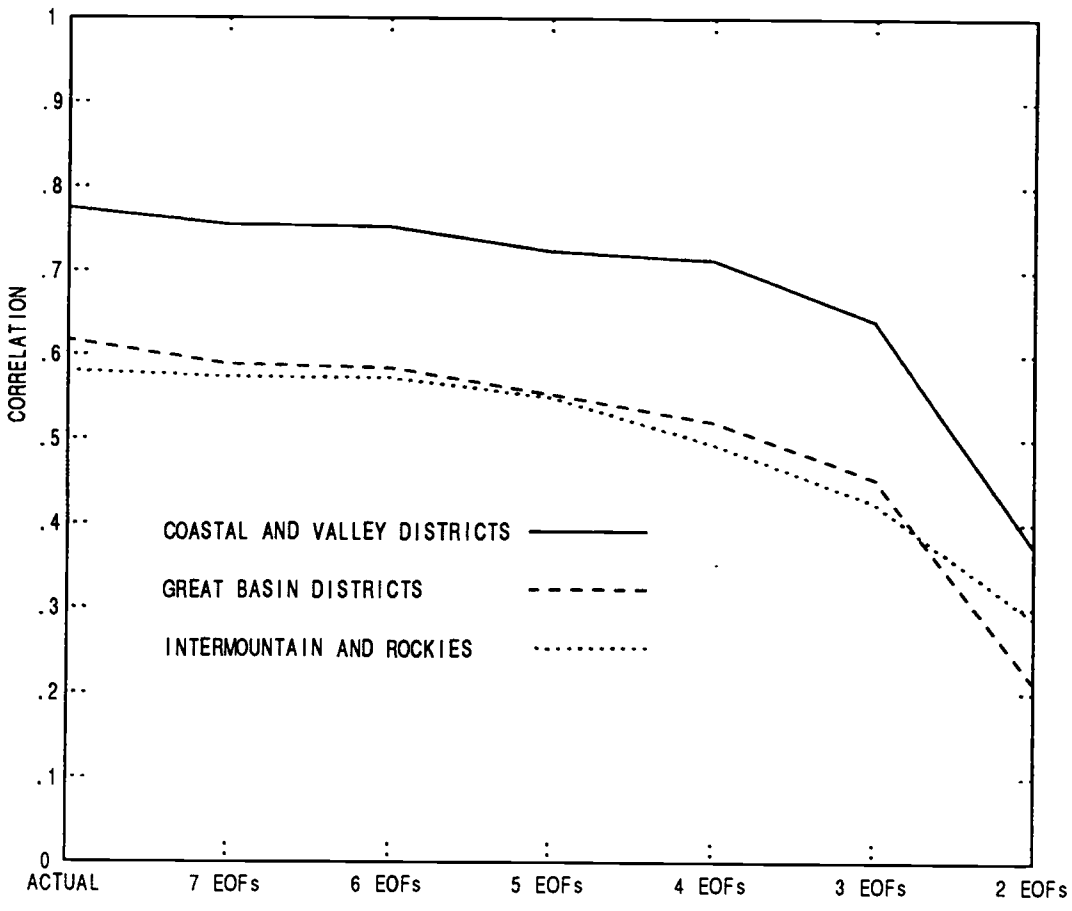

Fig. 4.9 Multiple linear correlation coefficient between the orographic and baroclinic indices and normalized district precipitation as a function of number of EOF's used in reconstructing the 500 mb height field for model input. Solid line is average correlation for coastal, coastal valley and Cascade and Sierra districts. Dashed line is average for districts of the Columbia Basin, Great Basin and southwestern deserts. Dotted line is average for regions to the east of these basins.

Accordingly, we will use the six-EOF height field representation for our evaluation of the model as a forecasting tool and, in the following chapter, will compare these first six-EOF's and associated PC's with the OLR field components of the tropical Pacific.

4.3.2 Evaluation of the model as a forecast aid

To determine how well the precipitation model performs in practice, the record was divided into two approximately equal portions. The first, from November 1949 to March 1969, was used to determine the various statistical relationships. Both the coefficients relating the precipitation indices to the observed precipitation for each district and also those relating the 500mb height field and winds to the intermediate variables needed in the model were tabulated.

With these, the model was then run for the second period, from November 1970 through March 1988 using the first six PC time-series to reconstruct the pentad height fields. The resulting orographic and baroclinic index series were then transformed to a normal distribution and used as inputs to the model equation (4.16). The normalized predicted precipitation series thus generated was correlated with the corresponding observed series for each district. It should be noted that correlations between the normalized series are generally more conservative (with lower apparent correlations) than are those for the original unmodified series. As discussed in Section 4.2.4.1, precipitation series have gamma distributions with (compared to normal distributions) a disproportionate share of near-zero elements. The differences between the pairs of near-zero elements for the compared unmodified series are much less than for the corresponding normalized series. For example, a comparison of 0.01 and 0.03 inches in the unmodified series might become -2.5 and -1.3, respectively, when normalized. In the computation of linear correlation this would have the effect of raising the apparent correlation, unrealistically, for the unmodified series.

Figure 4.10 is a contour plot of these district correlations interpolated to the geographic grid and can be compared to Fig. 3.14. As might be

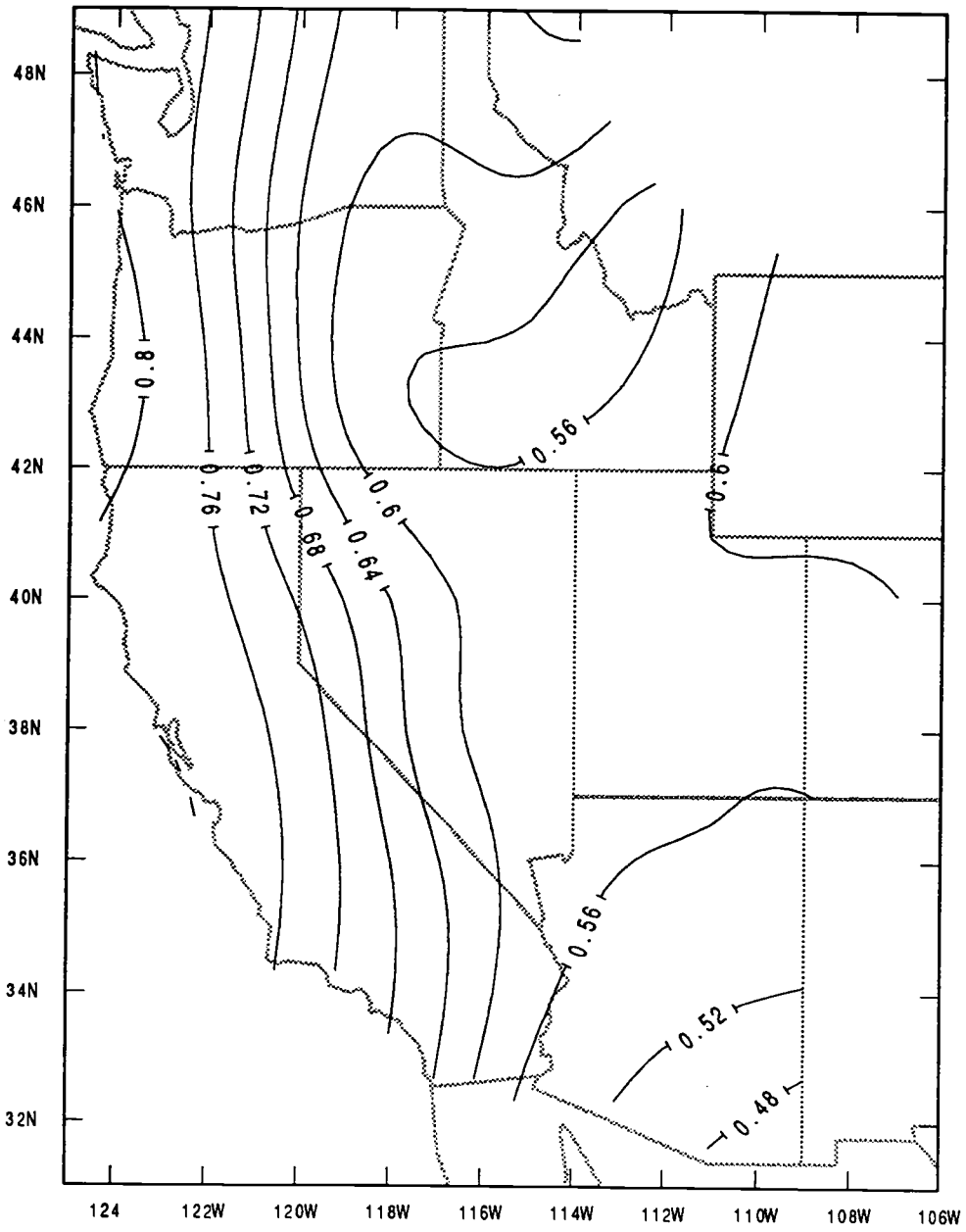

Fig. 4.10 Plot of linear correlation coefficient between precipitation calculated by precipitation model driven by the first 6 500 mb height PC's and observed district wintertime monthly precipitation for years 1970-1988. District correlations interpolated to geographic grid for contouring.

expected, the correlations are a little different from those shown in Fig. 4.8. The split in the record would be expected to result in an increase in the variability due to sampling. It is also possible that in the 20 year time interval between the period used for determining the regression coefficients and the period used in the evaluation, that there has been some short-term climate shift which may have changed relationships between the variables. The gross variations of district correlation, however, appear to be approximately the same as for those in the comparative study (Fig. 4.8). For either case it is useful to make estimates of the magnitude of the correlation variations expected from sampling and to compare them with both the total spatial variability and also to the magnitude of the correlations themselves.

If it were possible to make many repetitions of the forecast experiment, one would expect the correlations between predicted and observed precipitation for a given district to be distributed about some mean correlation, ρ, which should approach the true correlation as the number of repetitions is increased. The distribution of the sample correlation coefficients is not normal, but may be converted to normal by a change in variable. Following Hoel (1947), we note that if $z = 0.5 \ln((1+r)/(1-r))$, where r is the sample correlation coefficient, then z is distributed normally about z_0, where $z_0 = 0.5\ln((1+\rho)/(1-\rho))$ and the standard deviation for z, σ_z, is given by $\sigma_z = 1/(n-3)^{1/2}$, where n is the number of forecast/observation pairs.

We may now determine the probability of a sample correlation, r, differing from ρ by some given amount. From the relationship between r and z it may be seen that high sample correlations are more likely to be close to the true correlations than are low correlations. For the case of this experiment let us assume that a northern coastal district correlation has a true correlation between forecast and observed precipitation of 0.80. Then it can be shown, from the z distribution above, that there is a .10 probability that a sampled correlation will be in excess of 0.84 or less than 0.75. In contrast, for some eastern district for which the true correlation might be 0.40, the corresponding samples would have a .10 probability of being greater than 0.50 or less than 0.29.

Thus, particularly for the eastern districts, a considerable portion of the variability in the correlation coefficients is probably due to sample

variations and the detailed structure in a contour plot of the correlations of this region is likely to be misleading. Nevertheless, the gross features of the variability appear to be statistically significant and the probability of no real correlation at all is vanishingly small ($p = 0.00034$ for the worst case).

4.3.3 The utility of the forecast

The correlations shown by Fig. 4.10 appear to be sufficiently high to be useful, particularly in the western portions of the domain. The linear correlation coefficient, however, is not necessarily the most appropriate indication of utility. The proportion of variance explained is equal to the square of the correlation and falls off much faster than the correlation itself. This may be illustrated by scatter plots of monthly and seasonal precipitation where the predicted precipitation for a given district is compared with that observed on a case by case basis. Figure 4.11 is such a plot for the Oregon Coast, with one of the higher district correlations. The dots show the observed and predicted precipitation for individual months while the numerals identify specific seasons in terms of monthly averaged precipitation. As an artifact of the averaging process for this sort of distribution the correlations for the seasonal averages are somewhat higher than for those of the individual months, approximately .90 in this case. Fig. 4.12 is a plot for the western Washington Cascades, a similar case with the individual months correlated at about .80 and the seasons at about .90. In this case, however, there may be seen a tendency of the model to make occasional gross underpredictions for certain months with high actual precipitation.

The next case shown (Fig. 4.13) is that of the Flathead River Valley of northwest Montana, a major watershed district for the upper Columbia. Even this close to the edge of the model domain the relationship of the predicted to observed precipitation appears close. Here, however, the seasonal correlation (.82) is only slightly better than the monthly (.79).

The last case shown (Fig. 4.14) is for southwest Montana, actually to the southeast of the prior district and much of it in the Missouri drainage. Clearly, the model does not perform as well in this district and the scatter

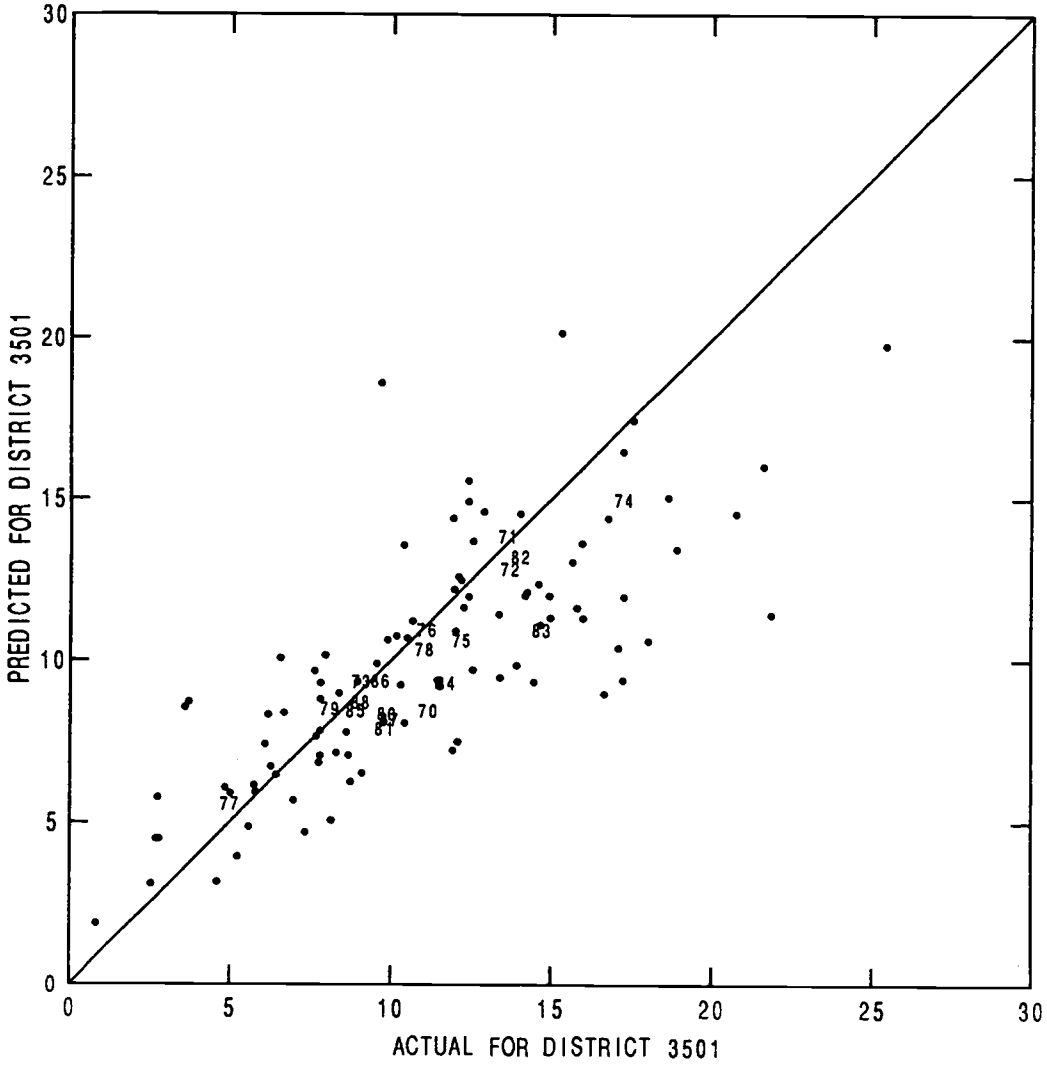

Fig. 4.11 Scatter plot of observed precipitation and that predicted from the precipitation model for the district of The Oregon Coast. Period is from 1970 to 1988. Dots are for individual months. Numerals represent average monthly precipitation for specific seasons.

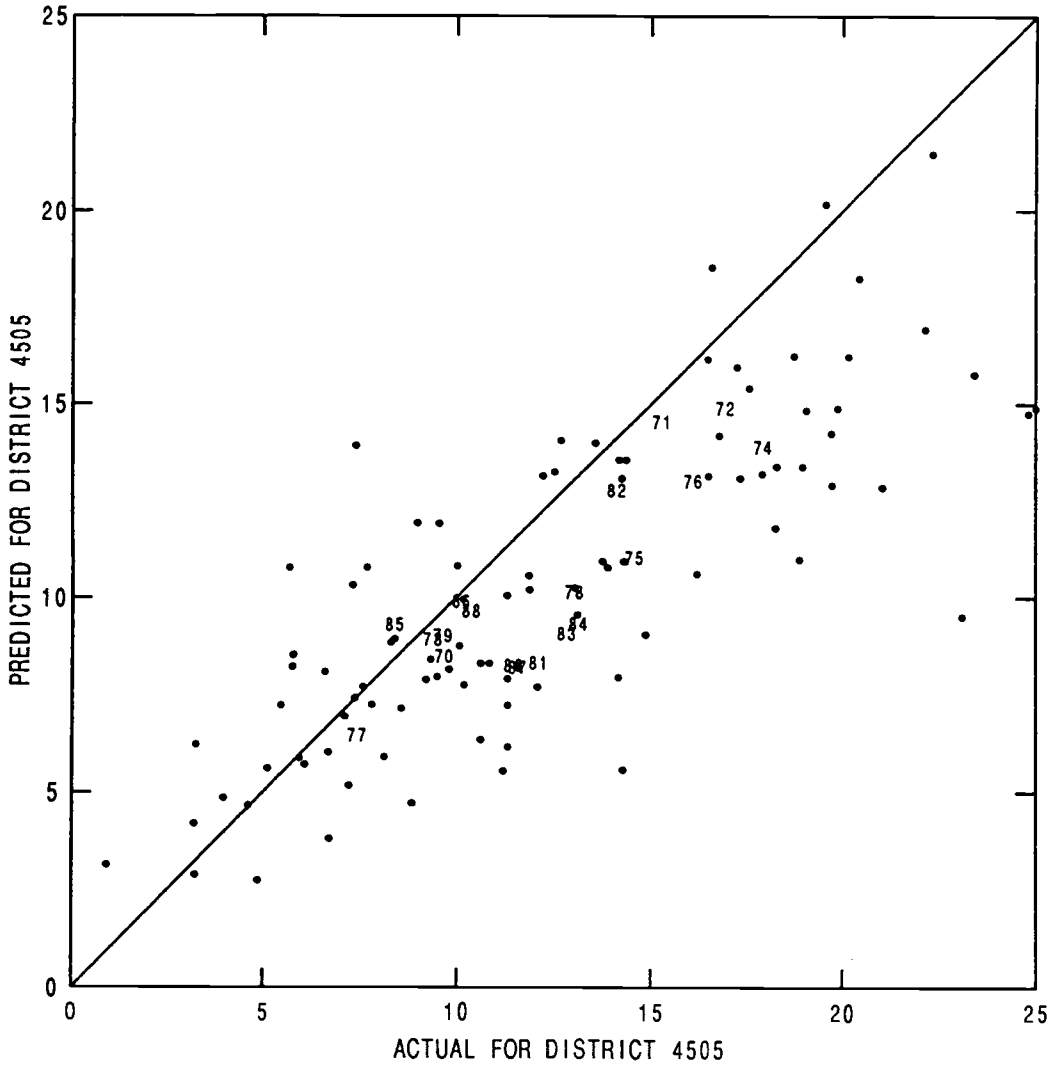

Fig. 4.12 Same as Fig. 4.11 but for the district of the Washington Cascades.

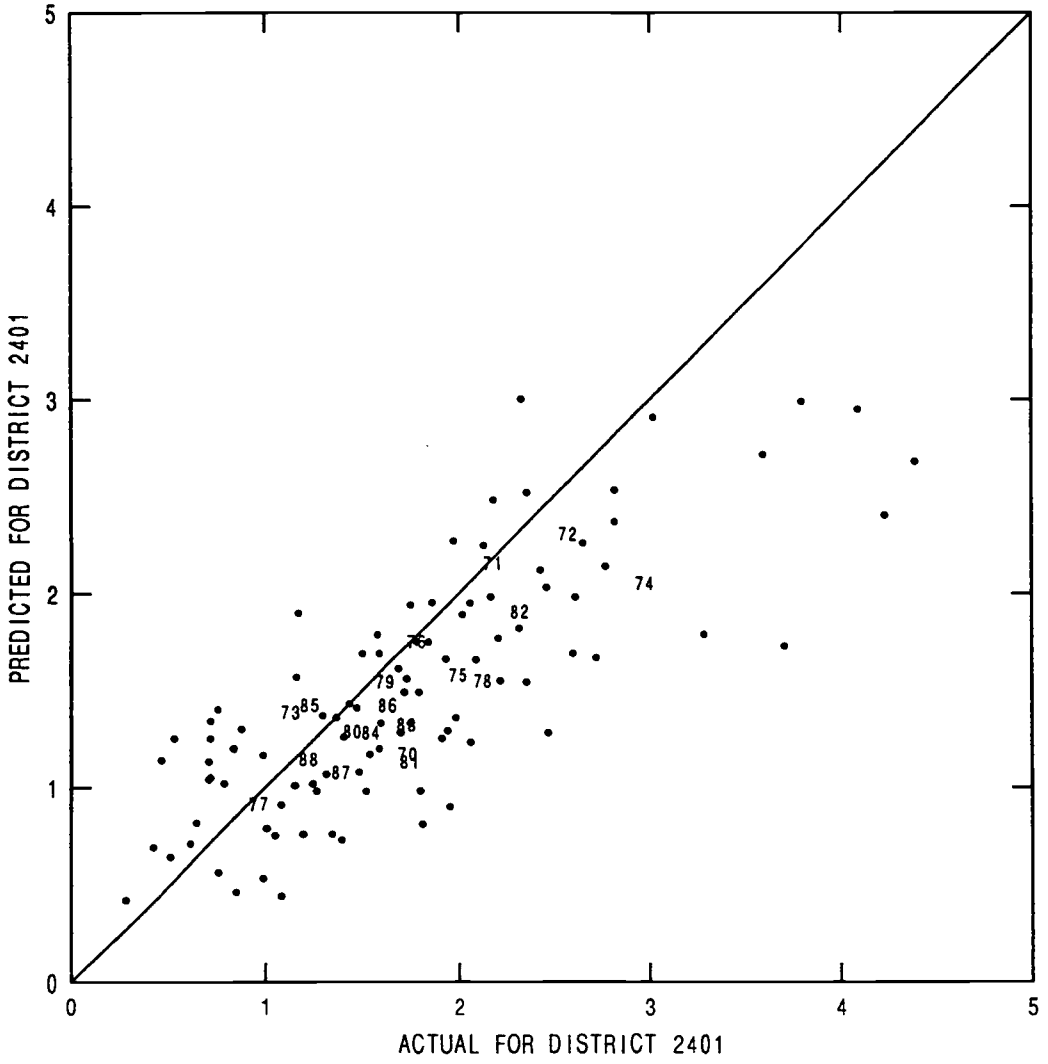

Fig. 4.13 Same as Fig. 4.11 but for the district of the Flathead River Valley of Montana.

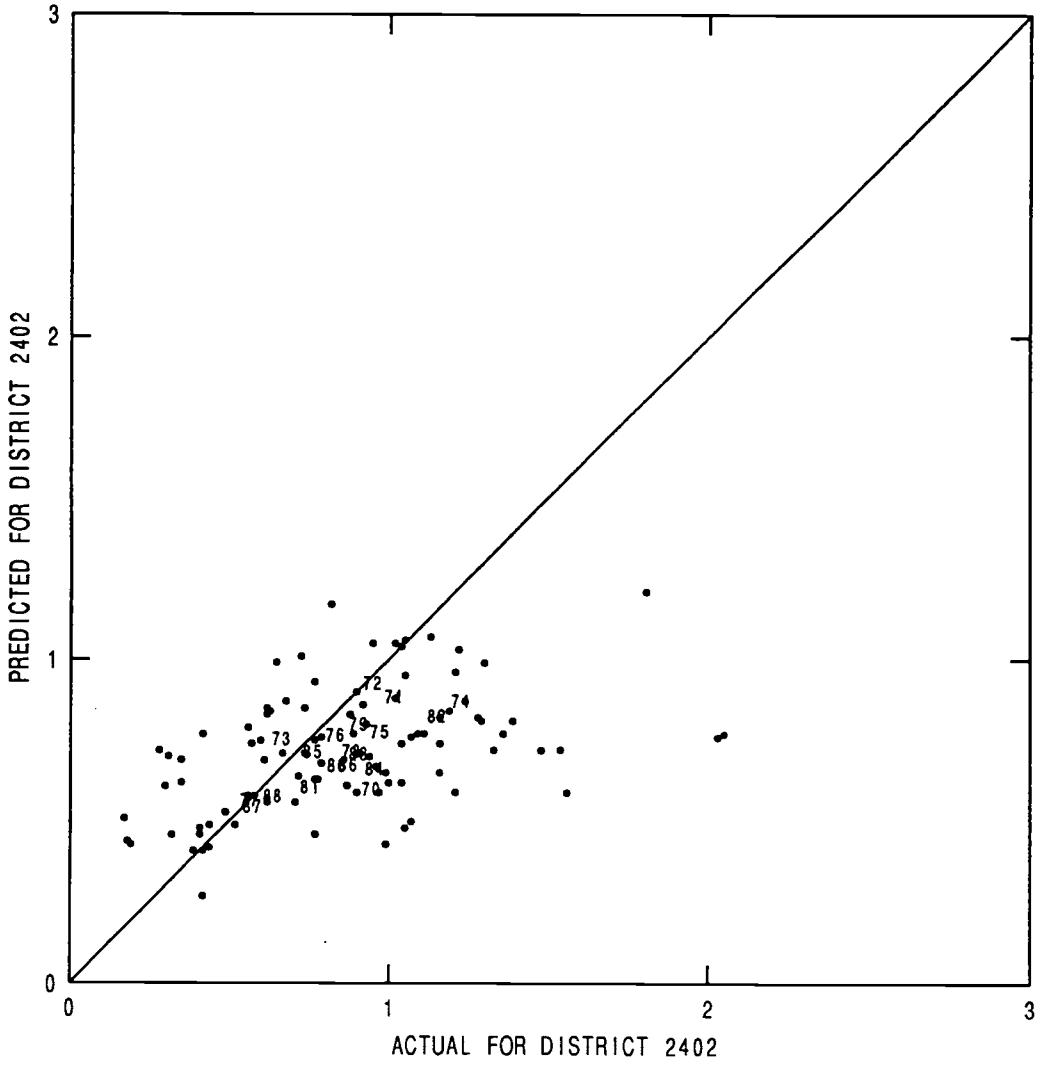

Fig. 4.14 Same as for Fig. 4.11 but for the district of southwestern Montana.

plot gives a visual impression that the predictions are less useful than the monthly correlations of .57 and the seasonal correlation of .68 would indicate. Moreover, the pattern indicates an apparent bias toward overpredicting for months with light precipitation and a stronger bias toward underpredicting for months with heavy precipitation. The coefficients relating the indices to the precipitation were derived from a regression of the indices on the observed precipitation but for the first half of the record. Apparently, there is a difference in the statistical relationship in the second half of the record. The statistical significance of the derived coefficients is, of course, less for cases in which the model index generation does not as well represent the actual precipitation processes. The probability of encountering such problems would thus be greater for such districts as compared to those for which more of the variation in the precipitation is explained by the indices. Nevertheless, more of the cases appear to have biases in this direction than in the reverse and, in fact, fewer of the greatest monthly precipitation amounts for any district are overpredicted and more appear to be underpredicted. It is possible that there might be a non-linear relationship between indices and precipitation not discovered during the development of the model or that additional precipitation processes may have more relative importance in the eastern portions of the study domain.

In the case of the underpredictions for the district of southwest Montana we have looked for precipitation mechanisms not common to the other western districts. The district is mostly to the east of the Continental divide with slopes downward to the northeast. Polar air outbreaks into the central US often result in a layer of cold air over the district, bounded by the higher terrain to the southwest. The situation appears to be similar to the "cold air damming" along the Front Range of the Rockies in Colorado. Dunn (1987) shows that such "damming" is associated with a low-level jet in the cold air, parallel to the mountain obstruction, and further elevating the upper surface of the cold air along the crest. A convergent layer of warmer air above the cold layer is forced to ascend as it approaches the range from the east causing heavy snowfalls from the crest eastward to about 100 km. While the Dunn (1987) study is for Colorado, some of his examples show heavy snowfalls occurring northward along the east slopes of the Rockies into southwestern Montana as well. The upper-level flow

configuration for these situations appears to be that of a deep trough over the Rockies with the jet axis far to the south of the area affected by "cold air damming". Our model would determine that little baroclinic precipitation would be expected so far from the jet axis and that the inferred cross-terrain winds would be insufficient for significant orographic precipitation.

While the scatter plot provides a good subjective impression of the utility of the forecast and appears to be more realistic (or at least more conservative) than that suggested by the correlation coefficient, we should like to have an objective measure for quantitative comparison. The development of such an objective quantitative measure of utility is discussed by Krzysztofowicz (1991). The difficulty in defining any single measure is partly due to the variety of users, each of whom may have different utility functions for activity outcomes. Often, the decision analysis is prepared for a few representative users and the results extrapolated to a population. Using Bayesian decision theory, Krzysztofowicz has developed a measure of utility, which he names the Bayesian Correlation Score (BCS). This includes not only the components of the linear correlation coefficient but also climatology and the slope of the line of regression. He demonstrates how forecasts ordered by this score are in order of their utility to the user despite differences in climatology. The order is not necessarily the same as that by the linear correlation coefficient. The BCS is defined as follows:

$$BCS \equiv \left(\frac{\sigma^2}{a^2 S^2} + 1 \right)^{-\frac{1}{2}} \tag{4.22}$$

It is a number from 0 to 1 with 1 being a perfect forecast (for which forecast and observation variables are identical) and 0 resulting from forecasts generated as if by a random number generator. Here, if the forecast variable, x, is modeled in terms of the regression line on the observation variable, ω,

$$E(x \mid \omega) = a\,\omega + b \tag{4.23}$$

and

$$S^2 = \mathrm{var}(\omega) \tag{4.24}$$

$$\sigma^2 = \mathrm{var}(x \mid \omega) \tag{4.24}$$

For the random forecast it may be seen that a, the slope of the regression line, will vanish, forcing BCS to zero. For the perfect forecast, on the other hand, σ^2, the variance of $x \mid w$, will vanish and BCS will go to unity.

Table 4.1 shows both the linear correlations and the Bayesian Correlation Scores for each district for the comparison of the forecast district precipitation with that observed. It may be noted that the BCS is more variable than is the correlation coefficient with the BCS exceeding the correlation for many of the higher scores but well below for some of the lowest correlations. Moreover it may be seen that the rank order of the BCS is not the same as for the correlations. A number of districts, such as northern Idaho with modest correlation coefficients (.69) have a high BCS (.80) while others, such as the California SE desert with the same correlation, have a low BCS (.39). Evidently, despite the same correlation, the forecasts for the first are far more useful than for the second. Considering the difference in climatology, this is not surprising, as the preponderance of easy no-rain forecasts for the deserts improves the correlation without providing much useful information.

In summary, it should be noted that many of the higher scores are associated with the important watershed districts and, were we able to obtain such results a season in advance, many additional water management decisions could be better justified. The prerequisite is the ability to forecast the approximate five-day time averaged 500mb height field as described by its first 6 PC's and associated EOF's. We are not able to accomplish this but, as described in the next chapter, we are able to forecast a small portion of the variance of these PC's by relating them to external forcing from the tropical Pacific. What we have shown in this chapter is that it is not necessary to provide a precise multi-level forecast of the standard meteorological variables to obtain a useful forecast of monthly precipitation for the western weather districts.

Table 4.1 Correlations and Bayesian Correlation Scores for Districts

Code	District	ST	Correlation	Bayes Score
0201	Northwest Piedmont	AZ	0.5092	0.3163
0202	Northeast Plateau	AZ	0.5508	0.2357
0203	Western Rim	AZ	0.4754	0.2253
0204	Central Rim	AZ	0.5291	0.2499
0205	Southwest Low Desert	AZ	0.4264	0.1746
0206	Central Low Desert	AZ	0.5067	0.2143
0207	Southeast Desert	AZ	0.4308	0.1681
0401	North Coast	CA	0.8208	0.8050
0402	Sacramento Valley	CA	0.7874	0.8118
0403	North Sierra Nevada	CA	0.7282	0.6260
0404	Central Coast	CA	0,8097	0.7983
0405	San Joaquin Valley	CA	0.7265	0.6461
0406	South Coast	CA	0.6664	0.5046
0407	Southeast Deserts	CA	0.6210	0.3792
0502	Western Mountains	CO	0.606	0.3003
1001	Northern Panhandle	ID	0.7302	0.8130
1002	West Central Lowlands	ID	0.6282	0.5992
1003	Clearwater Valley	ID	0.6161	0.5836
1004	Central Highlands	ID	0.7385	0.8020
1005	West Snake River Plain	ID	0.6423	0.4499
1006	Southwest High Desert	ID	0.5020	0.2824
1007	Central Snake River Plain	ID	0.5790	0.3062
1008	Salmon River Valley	ID	0.4809	0.4101
1009	Henrys River Plain	ID	0.5862	0.4886
1010	East Snake River Valley	ID	0.6861	0.5278
2401	Flathead River Valley	MT	0.7654	0.8279
2402	Southwest Highlands	MT	0.5027	0.3493
2601	Northwest Highlands	NV	0.7224	0.6223
2602	Northeast Highlands	NV	0.6346	0.4458
2603	Central Highlands	NV	0.5188	0.3524
2604	Southern Lowlands	NV	0.4644	0.1544
3501	Oregon Coast	OR	0.8068	0.8386
3502	Willamette Valley	OR	0.8057	0.8692
3503	Southwest Interior Valleys	OR	0.7540	0.6536
3504	North Cascades	OR	0.8129	0.8167
3505	South Central Highlands	OR	0.7246	0.6932
3506	Columbia Plateau	OR	0.6033	0.6310
3507	Southeast Highlands	OR	0.5930	0.4510
3508	Blue Mountains	OR	0.6489	0.4839
3509	Owyhee Valley	OR	0.5746	0.3466
4201	Western Desert	UT	0.5624	0.3694
4202	Santa Clara Valley	UT	0.5013	0.2990
4203	Salt Lake Valley	UT	0.5601	0.3275
4204	South Central Uplands	UT	0.5700	0.3645
4205	Uinta Mountains	UT	0.6388	0.5090
4206	Green River Valley	UT	0.5323	0.4044
4207	Southeast Highlands	UT	0.5084	0.2115
4501	Washington Coast	WA	0.7734	0.7747
4502	San Juan Islands	WA	0.6921	0.6954
4503	Puget Sound	WA	0.7498	0.8199
4504	Southwest Interior	WA	0.7784	0.8283
4505	Western Cascades	WA	0.8040	0.8529
4506	Eastern Cascades	WA	0.7320	0.7739
4507	Okanogan Valley	WA	0.6253	0.5107
4508	Columbia Basin	WA	0.5662	0.4601
4509	Northeast	WA	0.6485	0.7260
4510	Southeast	WA	0.6579	0.6285
4801	Yellowstone Plateau	WY	0.5520	0.4198
4802	Tetons and Wind River	WY	0.7152	0.5231
4803	Southwest	WY	0.5704	0.3793

CHAPTER 5: RELATIONSHIP OF THE OLR FIELD OF THE TROPICAL PACIFIC TO THE 500MB HEIGHT FIELD OVER THE NE PACIFIC

As discussed in the introduction, the correlation between precipitation and the Southern Oscillation Index (SOI) for certain regions of the western United States suggests that a portion of the variance in the circulation over the NE Pacific and western North America may be explained by changes in meteorological fields over the tropical Pacific associated with the SOI. Variations in the strength and configuration of the upper-level tropical outflow must affect the tropical boundary of the mid-latitude circulation system, and the Outgoing Long-wave Radiation (OLR) field is closely related to this outflow. It would appear, then, that the OLR field has a high potential for having a demonstrable relationship with the adjacent mid-latitude circulation. Measurements of the OLR field have been made by satellite observation since 1974 with a ten month record gap in 1978.

By choosing OLR to compare with mid-latitude 500mb heights we are not discounting the many other potential causes of mid-latitude height variations such as temporal variations of sea surface temperatures (Webster, 1981), snow and ice extent (Namias, 1985), (Barnett et al., 1989) or polar or stratospheric conditions (McGuirk and Douglas, 1988). These, separately or in combination, have been linked to various aspects of the mid-latitude circulation previously but are beyond the scope of this study. The OLR field has the advantage of variation on a time-scale convenient for comparison with monthly-to-seasonal circulation anomalies and, as discussed in the introduction, the associated tropical weather patterns, coupled as they are to slowly evolving oceanic anomalies, may themselves be more predictable. Moreover, as will be shown in this chapter, there is a fortuitous time lag of several months between changes in the OLR field and those in the 500mb height field which is a further aid to prediction. Accordingly, we have used the OLR field for our comparison.

5.1 The OLR field of the tropical Pacific

Our OLR data set is extracted from the NCAR record, which is a monthly average of outgoing long-wave radiation on a 5° grid. Regions of lower radiation values correspond, in the tropics, to those for which there is extensive coverage of the cold high cloud tops associated with lower-level convergence and upper-level outflow. The regions of higher radiation correspond to those of clear air or clouds with lower tops.

During the winter season the production of kinetic energy in the Hadley Cell far exceeds local dissipation (Hastenrath, 1985) and is exported poleward to power the Subtropical and Polar Jets and, to a large extent, the entire mid-latitude westerly circulation. The energy source, from release of latent heat, is largely concentrated in the meso-scale convective cloud clusters (MCC's) spaced, irregularly, along the ITCZ. Holton (1979), estimates that a few thousand convective "hot" towers, many of which may be embedded in a single MCC, can account for the energy of the Hadley Cell. In the tropical Pacific, for most of the year, the MCC's are normally more extensive in the western region, although their concentration with longitude is quite variable and a net eastward displacement is associated with the El Niño phase of the Southern Oscillation. Maps for specific dates of upper-level cloud concentrations together with 300mb winds (Wallace and Hobbs, 1977) show divergent winds in the vicinity of the MCC's which extend well poleward of the ITCZ and certainly have the potential to affect the configuration of the Subtropical Jet and even more distant circulation systems. In this regard, it should be noted that tropical MCC concentrations are not always along the convergence zone axis, but often appear considerably to the north or south. For these and other reasons discussed in Section 1.2.2, it does not appear that a single index, such as the SOI, would include sufficient information to account for that variability in the OLR field which might be related to the mid-latitude circulation.

As for the 500mb height field, a sufficient proportion of the OLR field variability may be captured, however, by *several* indices, which are the Principal Components (PC's) associated with the first few EOF's of the anomalous OLR field. For the computation of EOF's and PC's, the domain selected was that portion of the Pacific from 15°S to 20°N and from 135°E to

120°W. This is centered roughly on the ITCZ, which averages a few degrees north of the Equator, and is wide enough in latitude to include most of the tropical low radiation regions without also including those associated with the mid-latitude circulation. This can be verified by reference to Fig. 1.20 and Fig. 1.22 from Wallace and Hobbs (1977) which show mean tropical Pacific rainfall and cloudiness, respectively. The latter figure is for the years 1967-1970, when the SOI averaged near zero.

The longitude bounds are set so as to include eastern Indonesia but to exclude the effects of the Asian continent and also to exclude the region just south of Central America. Experiments with shifting these boundaries and expanding or contracting the total area showed little effect other than to decrease slightly the variability per unit area. The tropical Pacific grid used was thus a 176 (22 x 8) point array with 5° between points. Figure 5.1 is a contour plot of the mean January and July OLR fields for the region. For the January plot, the area of depressed OLR over the western Pacific and south of the Equator is indicative of the cold high cloud tops in the region of extensive deep convection over the "Maritime Continent" (Indonesia to New Guinea and southeastward). The nearly cloud free region over the equatorial "cold tongue" of water extending westward from South America shows elevated OLR levels. In the July plot, the area of lowest OLR has migrated northwestward toward SE Asia and a sharply delineated trough of low OLR identifies the ITCZ extending west from Central America across the Pacific at a latitude of about 10°N.

To remove the annual signal and obtain the anomalous OLR field, the mean fields for each month were determined and subtracted from that of each specific month. Next, a 176 x 176 covariance matrix was formed from the time-series at the grid points from which the first five EOF's and associated PC's were extracted. It was determined that these EOF's explained 64% of the total variance while the first three EOF's explained 55% of the total variance. Higher EOF's contributed rather slowly so that the first 20 explained a cumulative 88%. For most of the comparisons between the OLR and 500mb height fields only the first 3 EOF's and PC's were used.

As for the 500mb height field EOF's and the western district precipitation EOF's, we performed a "varimax" rotation on the OLR EOF fields and compared them with the unrotated fields. In this case, there

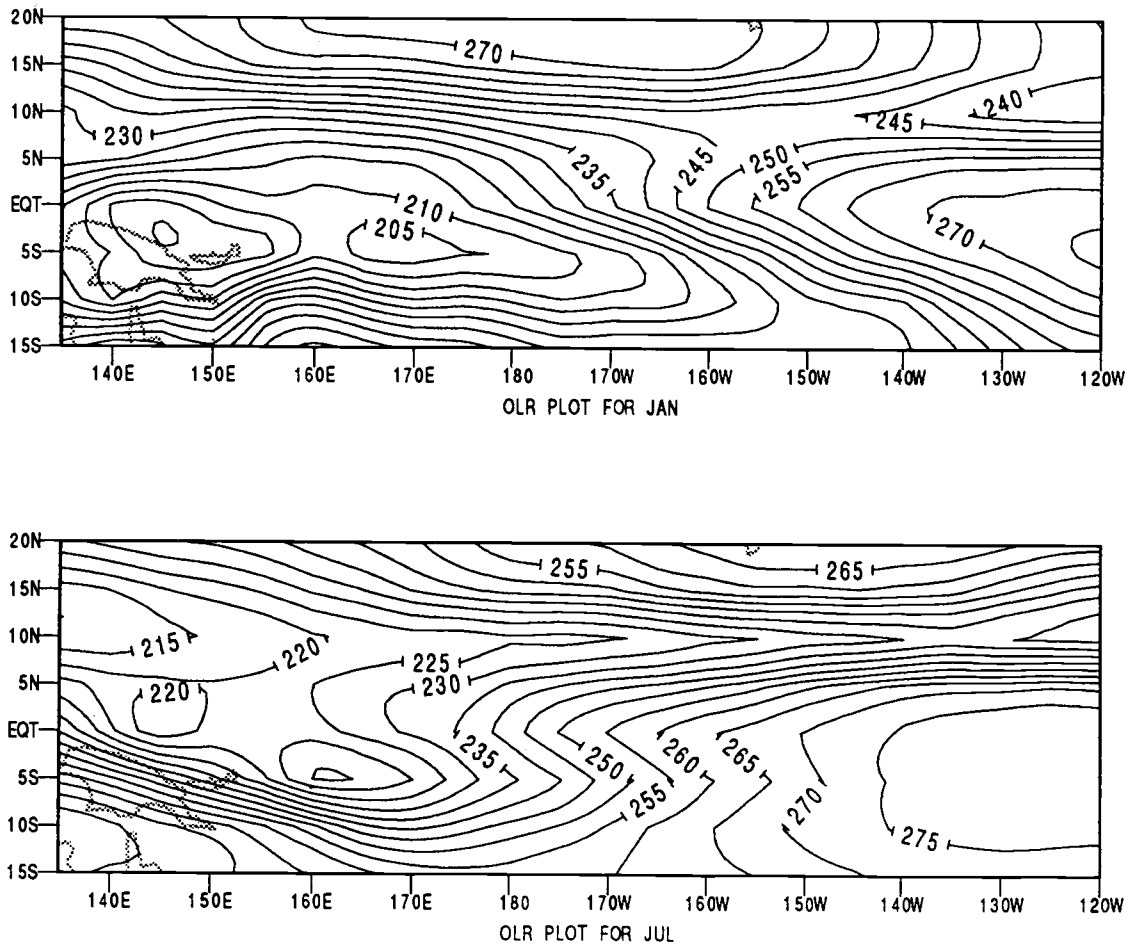

Fig. 5.1 Outgoing Long-wave Radiation (OLR) field over tropical Pacific for mean January and July. Units are in Watts per meter^2.

were few qualitative differences between them and none that were of greater assistance in the analysis of the variance in the OLR fields. Moreover, the variance explained by the first three rotated fields was only about 46% of the total and so it was decided to use the unrotated EOF's, not only for the correlation studies but for the analyses as well.

Figures 5.2 and 5.3 are plots of the first 4 EOF's of the OLR fields. The chief feature of the first EOF is the major equatorial node centered at about 165°W. This corresponds to an anomalous increase in high cloudiness here for a negative value of the first principal component and conversely. This is quite similar to the strongest pattern of anomalous precipitation associated with the ENSO as shown by Ropelewski and Halpert (1987); thus one might expect this principal component to be related to the SOI. The pattern of the second EOF is that of a nodal pair 30° to the east and west of the previous center, with the western node a few degrees north of the Equator and the eastern node about the same distance to the south. In the context of the ENSO, this EOF might be regarded as a measure of a modification in the phase of the displacement of the region of maximum convection and upper-level tropical outflow, in contrast to the first, which would correspond to the amplitude. The pattern shown by the third EOF could be considered as a measure of the north-south displacement of the major node of EOF #1, while EOF #4 might be considered as a measure of tilt for the nodal pair of EOF #2. It should be remarked, however, that there is considerable month-to-month variability in the OLR field (as for other tropical fields) that does not fit the pattern of the "Canonical El Niño" of Rasmusson and Carpenter (1982). The behavior of the various tropical fields during the extended (1993-1994) "mature" phase of the latest warm episode is particularly illustrative.

It is instructive to observe how the PC's vary with time. By autocorrelating each PC at various lag times it was determined that there is a considerable month-to-month persistence for PC #1. At a lag of four months the correlation is still above 0.5 and does not fall to near zero until about nine months. PC #2 has much less persistence, the autocorrelation falling to 0.46 at a lag of three months. PC #3 has still less, 0.37 at a lag of one month, while PC's #4 and #5 have less still. For PC #1 the autocorrelation is consistently negative from 10 to 20 months and is not significant thereafter. This is an indication of the quasi-cyclic nature of

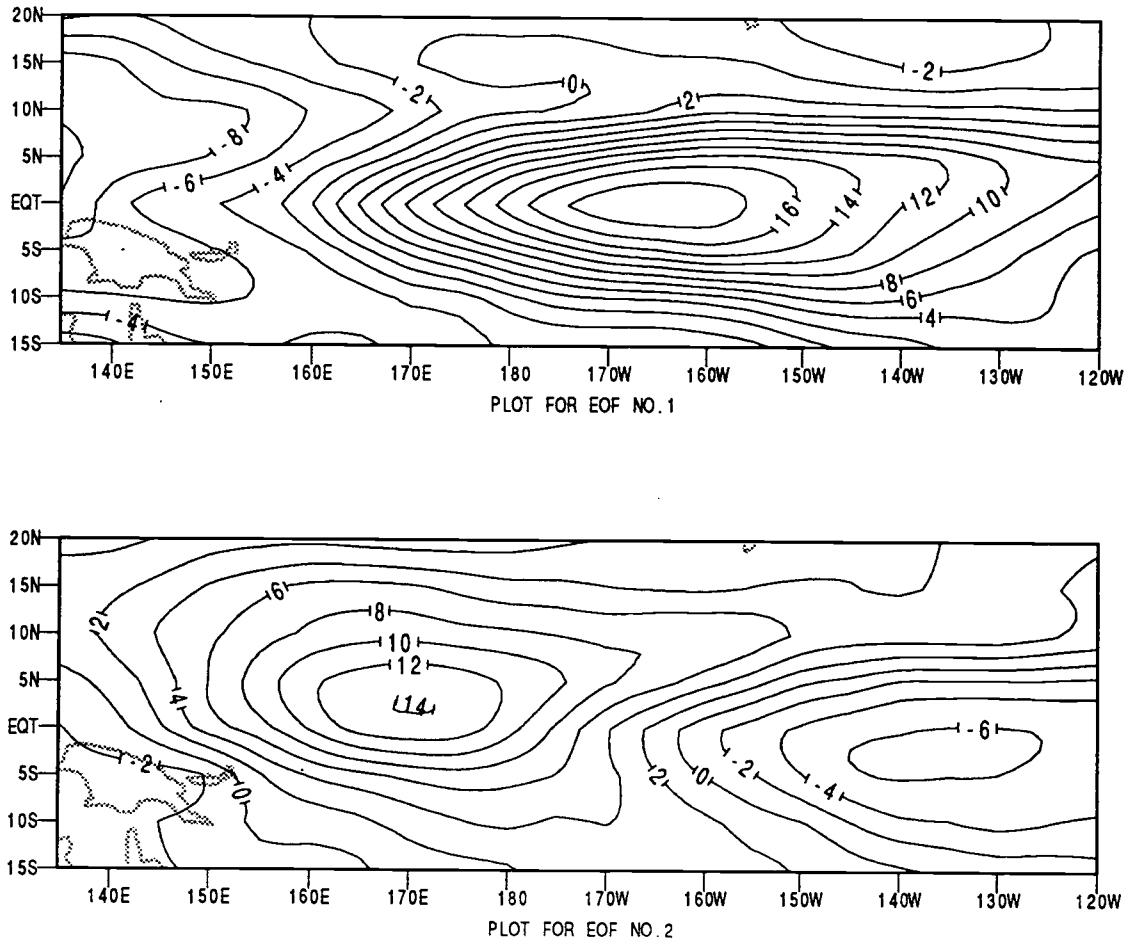

Fig. 5.2 EOF's #1 and #2 of the tropical Pacific OLR field. EOF's are multiplied by rms value of associated Principal Component and units are in watts per meter^2.

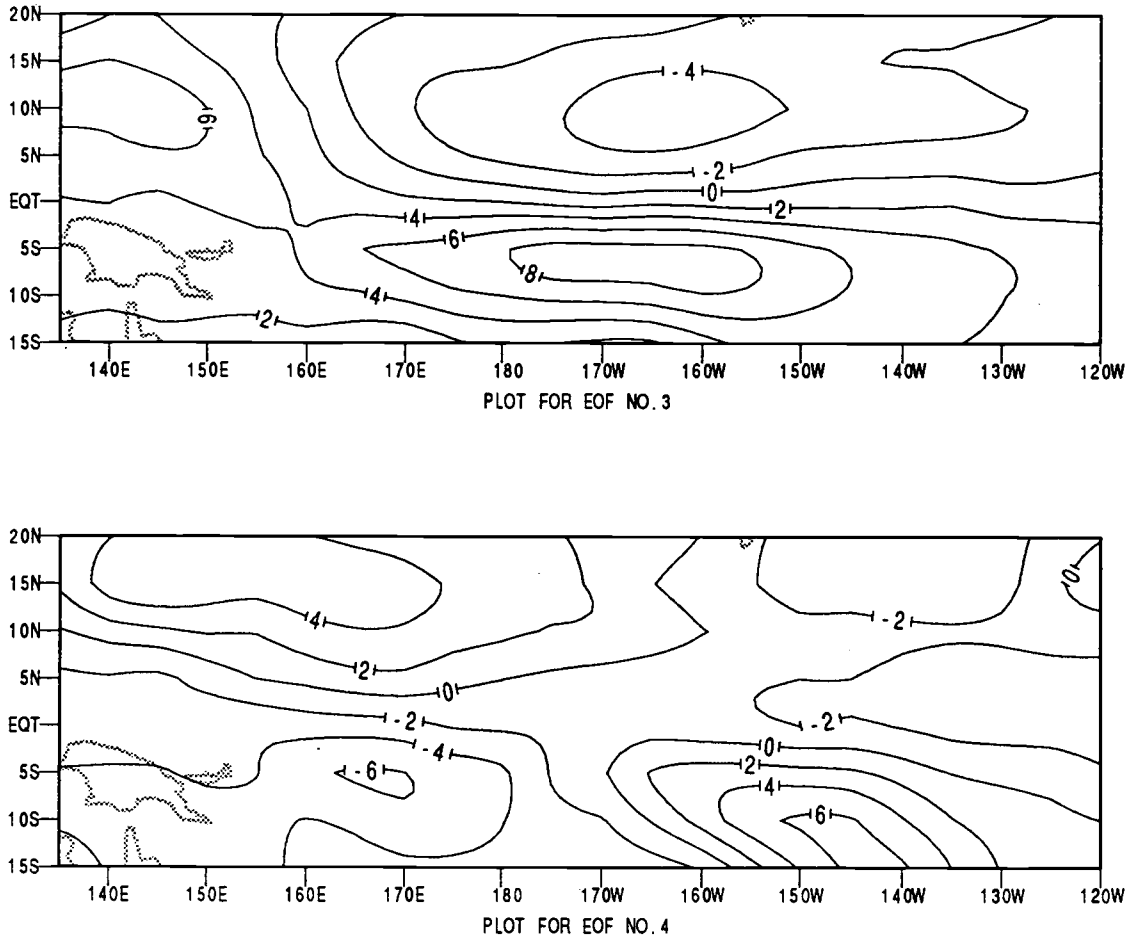

Fig. 5.3 EOF's #3 and #4 of the tropical Pacific OLR field.

the first principal component of the OLR field. As the probability of encountering a reversal of this largest component over a time period of about a year is better than even, the time-scale of OLR transitions can be seen to be on the same order as that of the Southern Oscillation.

The statistical relationship between the OLR PC's and the SOI can be seen by correlating each PC with the SOI for various time lags. Figure 5.4 is a display of these correlations for the first 3 PC's (the remaining PC's appear to have no significant correlations at any time lag). The correlation of PC #1 reaches a maximum of about 0.74, coincident with the SOI. The drop in correlation as the lag time (after the SOI) increases is more gradual than the rise in correlation before the SOI signal. The correlation of PC #2 peaks at 0.37, six months prior to the SOI, while that for PC #3 peaks at 0.36, nine months *after* the SOI signal. The nodes in EOF #2, which may be considered to represent regions of maximum variance in the position of the OLR anomaly shown by EOF #1, apparently are associated with the SOI signal before its peak. This may indicate that in the evolution of an ENSO event, the maximum variation of the OLR anomaly in the east-west direction occurs early, consistent with an east-west irregularity in the field evolution rate. Conversely, the north-south nodal pattern for EOF #3, associated with the SOI signal *after* its peak, may represent a later north-south irregularity in the position of the OLR anomaly. The key finding shown here, however, is that while there is a clear relationship between the OLR field and the SOI, there is much additional information in the OLR PC's which may possibly be relatable to the mid-latitude circulation.

5.2 Correlation of the OLR PC's separately with the 500mb height PC's

The preliminary step in determining the relationship of the OLR field to the 500mb height field is to measure the linear correlation coefficients between the various OLR-height field PC pairs at various time lags between them. As for this comparison there is a maximum of 87 months of data, it is necessary to include a determination of significance as well. The correlation experiments in the previous chapter included a sufficient

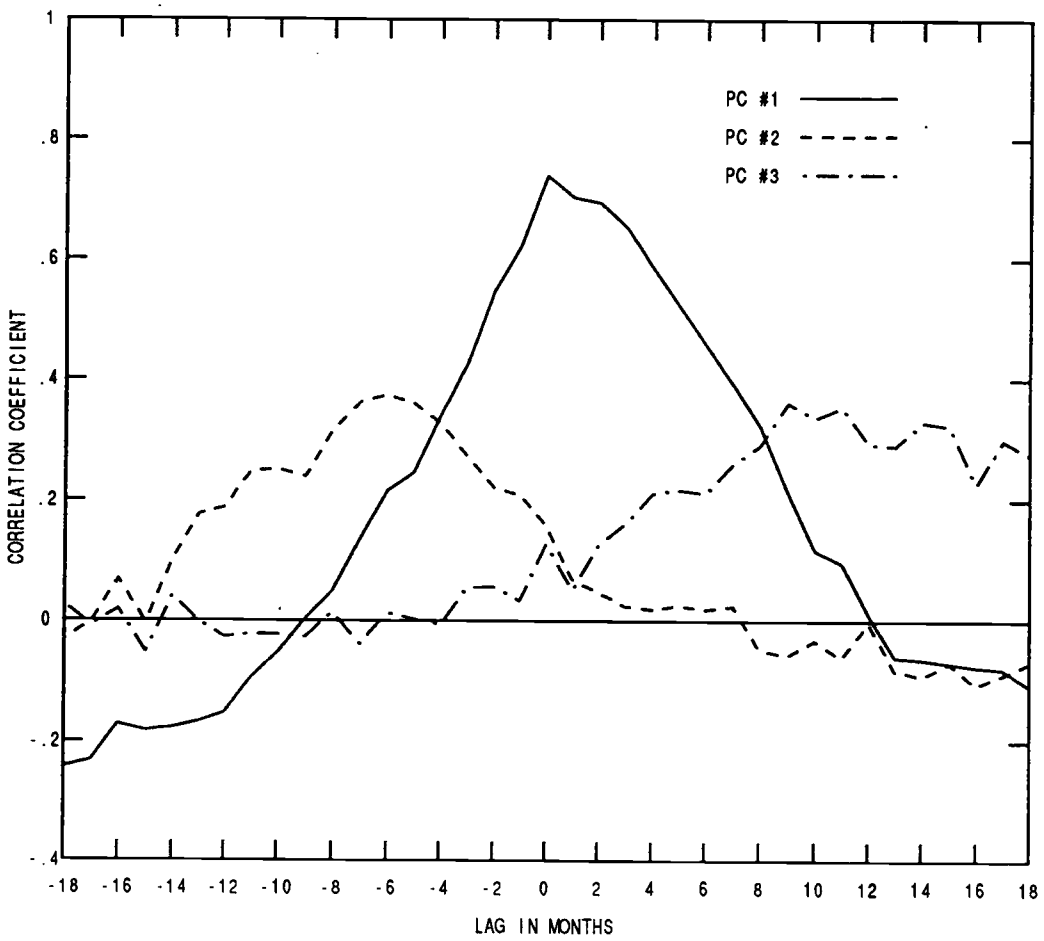

Fig. 5.4 Correlations of the first 3 Principal Components of the OLR field of the tropical Pacific with the Southern Oscillation Index (SOI) as a function of lag-time. Lags are in months after the SOI.

number of events and such high sample correlations that all could be considered highly significant ($p<.01$). For the comparisons of this section, however, due to the lesser number of events and lower apparent correlations, the significance was computed separately for each case.

Table 5.1 is a compilation of the individual correlations of the first six 500mb height field PC's with each of the OLR PC's for time lags of the height PC's behind the OLR PC's varying from zero to twelve months. The significant and highly significant correlations are marked with one and two asterisks, respectively. It can be seen that there are many combinations which show highly significant correlations, but it is difficult to generalize the results. The first OLR PC can be said to be well correlated to height PC's 1,2,3,5 and 6 reaching a broad maximum correlation at lags of between two and five months. The second OLR PC can also be seen to be well correlated with height PC's 2 and 6 at a lag of about six months. Other correlations are scattered but may make some contribution to the overall relationship. Before proceeding further, we will determine an overall measure for this relationship and discuss its significance.

5.3 Multiple regression and canonical correlation analysis

As shown in Table 5.1, the first two OLR PC's are correlated, highly significantly, with five of the first six 500mb height PC's at various lag times. Additionally, the third OLR PC is correlated, to a lesser extent but still significantly, with height PC's 1 and 3 at a lag time of four months. This suggests that each of the height PC's might be modeled as a linear combination of the three OLR PC's with both the weighting coefficients and the coefficient of multiple linear regression determined by multiple regression analysis (MRA) as discussed in Chapter 3 (equations 3.1 to 3.6). In this case, the analysis is repeated for various lag times and the results summarized below in Table 5.2.

Table 5.1 Correlation summary of 500mb height principal components with OLR principal components. Correlations significant at p = 0.05 indicated by *. Those significant at p = 0.01 indicated by **.

Correlations for OLR PC #1

lag	PC #1	PC #2	PC #3	PC #4	PC #6	PC #7
0	0.231	0.117	0.321**	0.168	0.207	0.405**
1	0.156	0.306**	0.399**	0.107	0.222*	0.356**
2	0.311**	0.387**	0.409**	0.150	0.253*	0.416**
3	0.237*	0.332**	0.370**	0.121	0.272*	0.358**
4	0.298**	0.361**	0.355**	0.092	0.321**	0.331**
5	0.286**	0.346**	0.296**	0.196	0.316**	0.170
6	0.160	0.342**	0.237*	0.185	0.283*	0.031
7	0.137	0.215	0.128	0.193	0.194	-.092
8	0.070	0.107	0.074	0.222*	0.118	-.200
9	-.081	0.018	-.023	0.130	0.023	-.254
10	-.127	0.038	-.001	0.144	0.086	-.309**
11	-.149	0.006	-.036	0.011	0.084	-.254*
12	-.044	-.057	0.007	0.055	-.022	-.212

Correlations for OLR PC #2

lag	PC #1	PC #2	PC #3	PC #4	PC #5	PC #6
0	-.228*	-.202	-.308**	0.044	-.163	-.080
1	-.158	-.086	-.149	0.019	-.114	0.030
2	-.203	0.010	-.068	-.100	-.159	0.023
3	-.019	0.107	0.011	0.033	-.082	0.241*
4	-.042	0.226*	0.146	0.047	-.022	0.243*
5	0.051	0.356**	0.264*	-.007	0.045	0.237*
6	0.215	0.289**	0.143	-.085	-.007	0.342**
7	0.184	0.215	0.053	-.075	-.153	0.291**
8	0.092	0.142	0.050	-.123	-.086	0.211
9	0.171	0.070	0.097	-.025	-.054	0.254*
10	0.076	0.107	0.217	0.018	-.111	0.191
11	0.038	-.011	0.205	0.058	0.095	0.307**
12	-.040	0.011	0.107	0.118	-.025	0.116

Correlations for OLR PC #3

lag	PC #1	PC #2	PC #3	PC #4	PC #5	PC #6
0	-.043	0.338**	0.070	-.107	0.061	0.004
1	-.038	-.024	0.066	-.057	0.061	-.068
2	-.088	-.151	-.058	0.079	-.107	-.087
3	-.167	-.085	0.188	-.129	-.025	-.038
4	-.261*	0.118	0.273*	-.056	0.020	0.012

There are no significant correlations at greater lag times for this OLR PC.

Table 5.2 Multiple correlation coefficients for the first six 500mb height PC's with the first three OLR PC's for lags in months of the height PC's behind the OLR PC's. (* indicates significance of the correlation at the p=0.05 level, ** for the p=0.01 level)

Lag	PC #1	PC #2	PC #3	PC #4	PC #5	PC #6
0	0.316 *	0.433 **	0.440 **	0.198	0.265	0.410 **
1	0.224	0.320 *	0.448 **	0.120	0.271	0.359 *
2	0.394 **	0.399 **	0.422 **	0.233	0.317 *	0.418 **
3	0.288	0.339 *	0.481 **	0.177	0.327 *	0.394 **
4	0.425 **	0.377 **	0.438 **	0.115	0.365 *	0.355 *
5	0.339 *	0.416 **	0.357 *	0.228	0.332 *	0.261
6	0.315 *	0.389 **	0.258	0.255	0.304	0.355 *
7	0.269	0.300	0.137	0.229	0.253	0.313 *
8	0.151	0.193	0.098	0.267	0.145	0.272
9	0.224	0.087	0.106	0.149	0.055	0.338 *
10	0.138	0.189	0.222	0.236	0.129	0.363 *
11	0.150	0.061	0.215	0.074	0.145	0.400 **
12	0.128	0.064	0.111	0.142	0.166	0.238

It is seen that the weighted combination of OLR PC's is for all cases better correlated with the height PC's than are the individual OLR PC's. Nevertheless, the increase in correlation is not large. Unlike the full set of OLR PC's, each time-series of which is necessarily uncorrelated with the others, those used in this comparison include only 5 of the 12 values for each year. Consequently, the partial OLR PC time-series are no longer necessarily orthogonal and the resulting cross correlations between them reduce the effect of their combination on the multiple correlation coefficient. It may also be seen that the correlation values required to attain significance are increased, due to a reduction in degrees of freedom.

By applying the set of weighting coefficients, derived by MRA, to the OLR PC series, a composite "predictor" series may be generated for each height PC series and for each time lag. These composite series will necessarily have the same linear correlation with their associated height PC series as the equivalent multiple correlation coefficient for the three

OLR PC's. These composite series are thus both convenient and useful as single comparison measures.

It is noted that while the predictor series have the best fit to the height PC series of any of the possible linear combinations of the OLR PC series, the proportion of the total variance of the height PC series explained by the composite series is small, 0.23 for the best case. Moreover, the total variance of the composite series is much less than that of the associated height series, a factor which must be accounted for in a prediction experiment such as that to be described in Section 5.5.

Although the various combinations of correlations shown in Table 5.2 provide a useful measure of the relationships between the two fields which is more general than the over 200 combinations of individual PC-to-PC correlations for multiple lag times, we should still like to see some measure of the *overall* relationship as a function of lag time. Canonical correlation is a logical extension of the multiple regression technique in accomplishing this task. Used as an analysis tool for comparing monthly and seasonal temperature forecast skill (Barnett and Preisendorfer, 1987), it has more recently been compared with other related methods in finding coupled patterns in climate data (Bretherton et al., 1992) and appears to be a reasonable choice for a comparison of two small sets of variables with a relatively large number of samples. If a relationship exists between two sets of variables, one set represented by the time-series $X_i(t)$ and the other by $Y_j(t)$, then there must be some linear combination of the variables in each set, $\Sigma a_i X_i(t)$ and $\Sigma b_j Y_j(t)$ for which the linear correlation is maximum. This correlation, achieved by the proper selection of the weighting coefficients a_i and b_j, is the canonical correlation coefficient.

As discussed by Harris (1985), the canonical correlation, R_c, can never be smaller than the largest single linear correlation coefficient between any two variables of the sets. Accordingly, one should be cautious in assessing the significance of an apparently large R_c. In the previous section, individual significant correlations were found between the first 3 PC's of the OLR field of the tropical Pacific and PC's 1,2,3,5, and 6 of the 500mb pentad height field over the NE Pacific. We will use these three and five component sets for the canonical correlation. While we would expect to obtain a slightly larger R_c with the inclusion of additional components

with less than significant individual correlations, the overall effect would be to degrade its significance.

The determination of R_c is after Harris (1985). Let $\mathbf{S_{xx}}$ be the 3x3 covariance matrix from the OLR PC amplitude time series, $\mathbf{S_{yy}}$ be the 5x5 covariance matrix from the height field PC's and $\mathbf{S_{xy}}$ be the 3x5 covariance matrix for the two sets of components.
Then let

$$S_{xxy} = S_{xx}^{-1} S_{xy} \tag{5.1}$$

$$S_{xyy} = S_{yy}^{-1} S_{xy}^{T} \tag{5.2}$$

and

$$S_{xxyy} = S_{xxy} S_{xyy} \tag{5.3}$$

$$S_{yyxx} = S_{xyy} S_{xxy} \tag{5.4}$$

The eigenvalues of the matrices defined by (5.3) and (5.4) are the same and the largest eigenvalue, λ_{max}, is the square of the canonical correlation R_c. This overall measure of the field relationships peaks at a lag of four months at 0.6553 and it is this lag that we shall use in the forecast experiment of Section 5.5.

We may also obtain the expansion coefficients, $\mathbf{a_i}$ and $\mathbf{b_j}$, such that, multiplied by the OLR and height field PC amplitudes respectively, the two series formed by the sums of these weighted amplitudes now will have a simple Pearson (linear) correlation equal to R_c. These expansion coefficients are determined by the following sets of homogeneous equations:

$$\left[S_{xxyy} - I\lambda\right]a = 0 \tag{5.5}$$

$$\left[S_{yyxx} - I\lambda\right]b = 0 \tag{5.6}$$

The solutions for both **a** and **b** are underdetermined but, as the correlation is unaffected by the absolute weights, both **a1** and **b1** may be set to some arbitrary value (such as 1) and the remainder of the sets (**a2, a3** and **b2, b3, b4, b5**) are determined in proportion. These weights may be applied to the respective EOF's of the two fields to show related patterns.

Figure 5.5 is a plot of both the tropical OLR and the NE Pacific 500mb height anomaly fields which have been generated by combining the EOF's in these proportions. The anomalous OLR field shown in Fig. 5.5b is seen to be closely related to the cool phase of the ENSO. The positive anomalous OLR values over the central and eastern tropical Pacific are indicative of the less than normal high cloudiness here, associated with this phase. Conversely, a negative amplitude for this same combined EOF would correspond to increased high cloudiness and the warm phase.

The mid-latitude height anomaly field that is best related statistically to this tropical OLR field is seen (Fig. 5.5a) to have a zone of increased heights at a latitude of about 36° N. and decreased heights in the Gulf of Alaska which would appear to result in an intensification of the westerly flow between 40° and 50° N. and a reduced westerly flow over the subtropical Pacific. A negative application of the pattern would produce the opposite effect. This can be better seen by combining the anomaly field with the mean field.

Figure 5.6 is a positive addition of the anomaly field to the mean field for the pentad of 23 January, a typical mid-winter period. The resulting pattern simulates a strong, nearly zonal, westerly jet, crossing the west coast at about the latitude of the Columbia River. South of 40°N., the flow is much weaker, curving anticyclonically to the south. The situation would be consistent with a succession of synoptic storms (with high snow levels as indicated by the elevated 500mb heights) transiting the Pacific Northwest but dry weather for the southwest. The application of the negative anomaly to the same mean field is shown in Fig. 5.7. For this case the flow over the Pacific Northwest is weak and diffluent with a large ridge over the Gulf of Alaska. In this situation one would expect no precipitation for the Pacific Northwest south of northern British Columbia. The subtropical westerly flow is intensified, however, and it would appear that the circulation simulated over Southern and Baja California regions might be conducive to rainfall. The precipitation patterns implied by these height anomalies are thus consistent with those contributing to the correlation map between district rainfall and the SOI shown in Fig. 1.1.

The significance of the canonical correlation is difficult to determine directly for there is no unambiguous way of obtaining a consistent measure of the degrees of freedom for the variables, particularly in such a

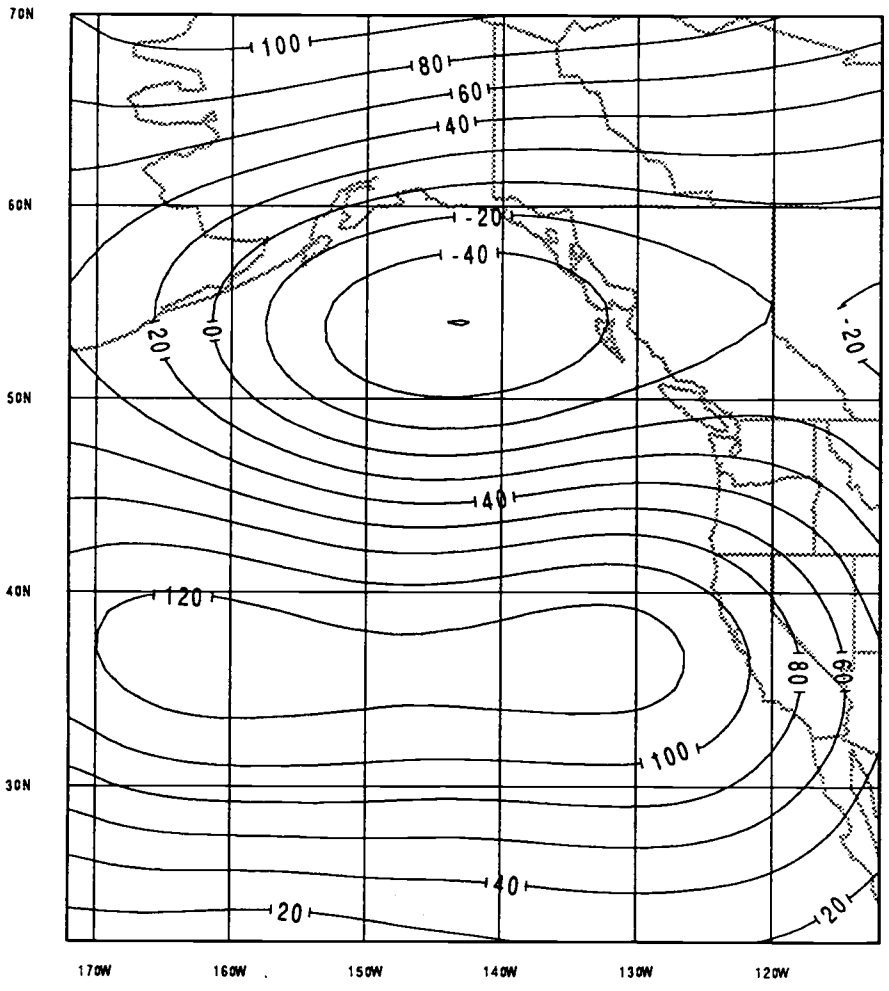

(a) Mid-latitude 500 mb height anomaly in meters.

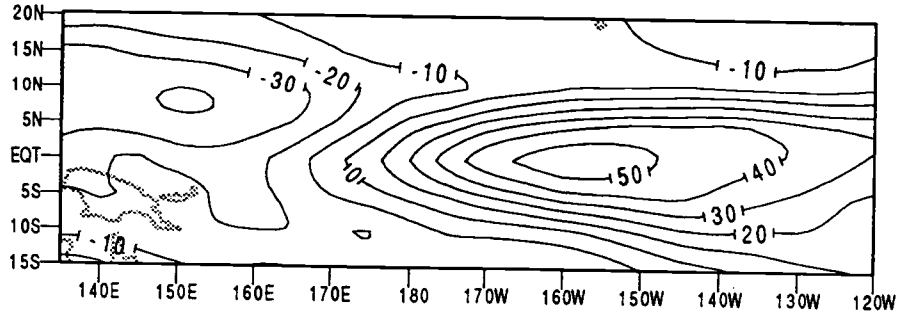

(b) Tropical Pacific OLR anomaly in watts per meter^2.

Fig. 5.5 (a) The mid-latitude 500 mb height anomaly field and (b) the tropical OLR anomaly field best related by canonical correlation. Fields are reconstructed from EOF's multiplied by coefficient sets resulting in the maximum multiple correlation coefficient.

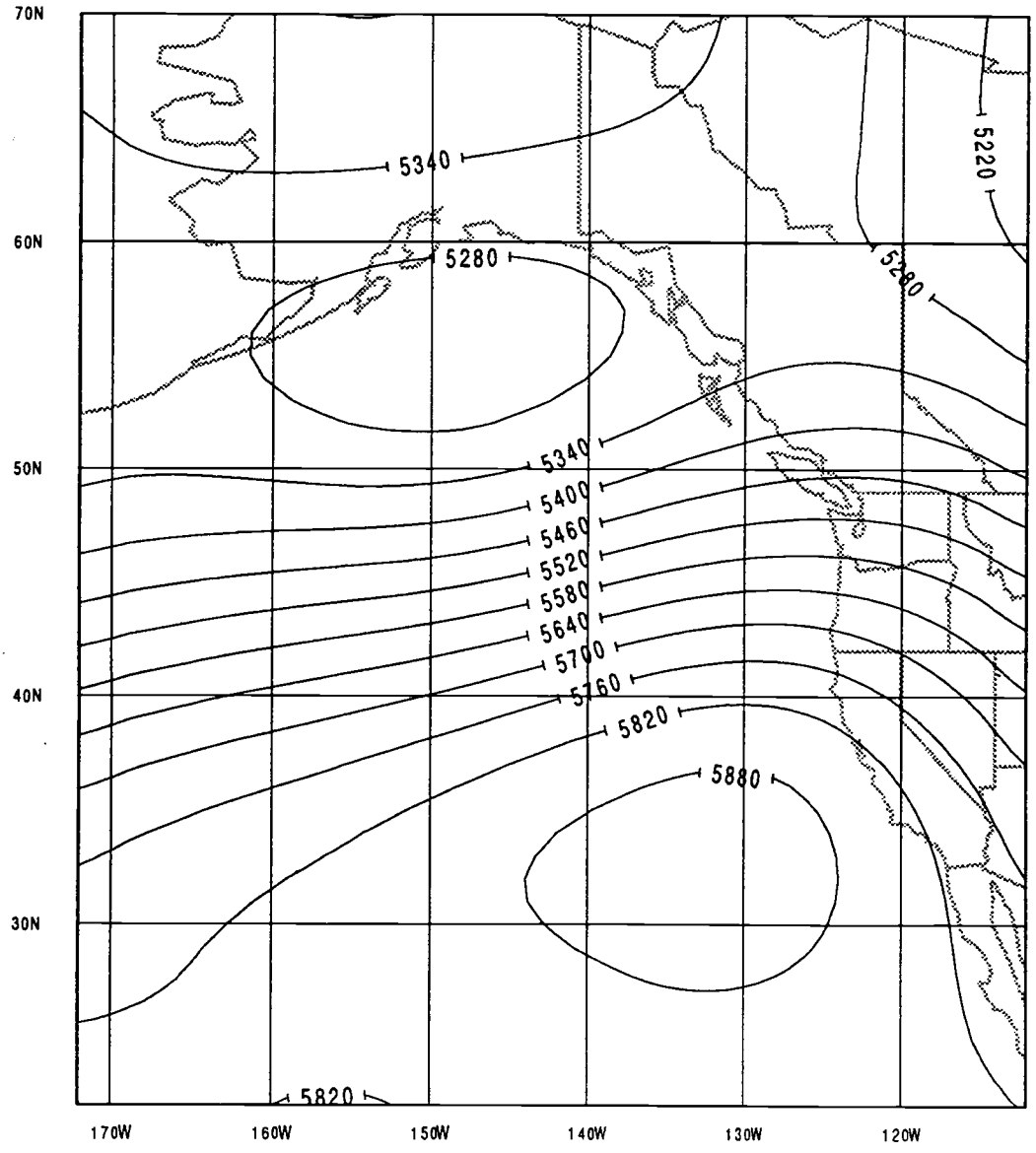

Fig. 5.6 Mid-latitude 500 mb height field reconstructed by adding positive height anomaly from Fig. 5.5 a to mean height field for 23 Jan. Heights are in meters.

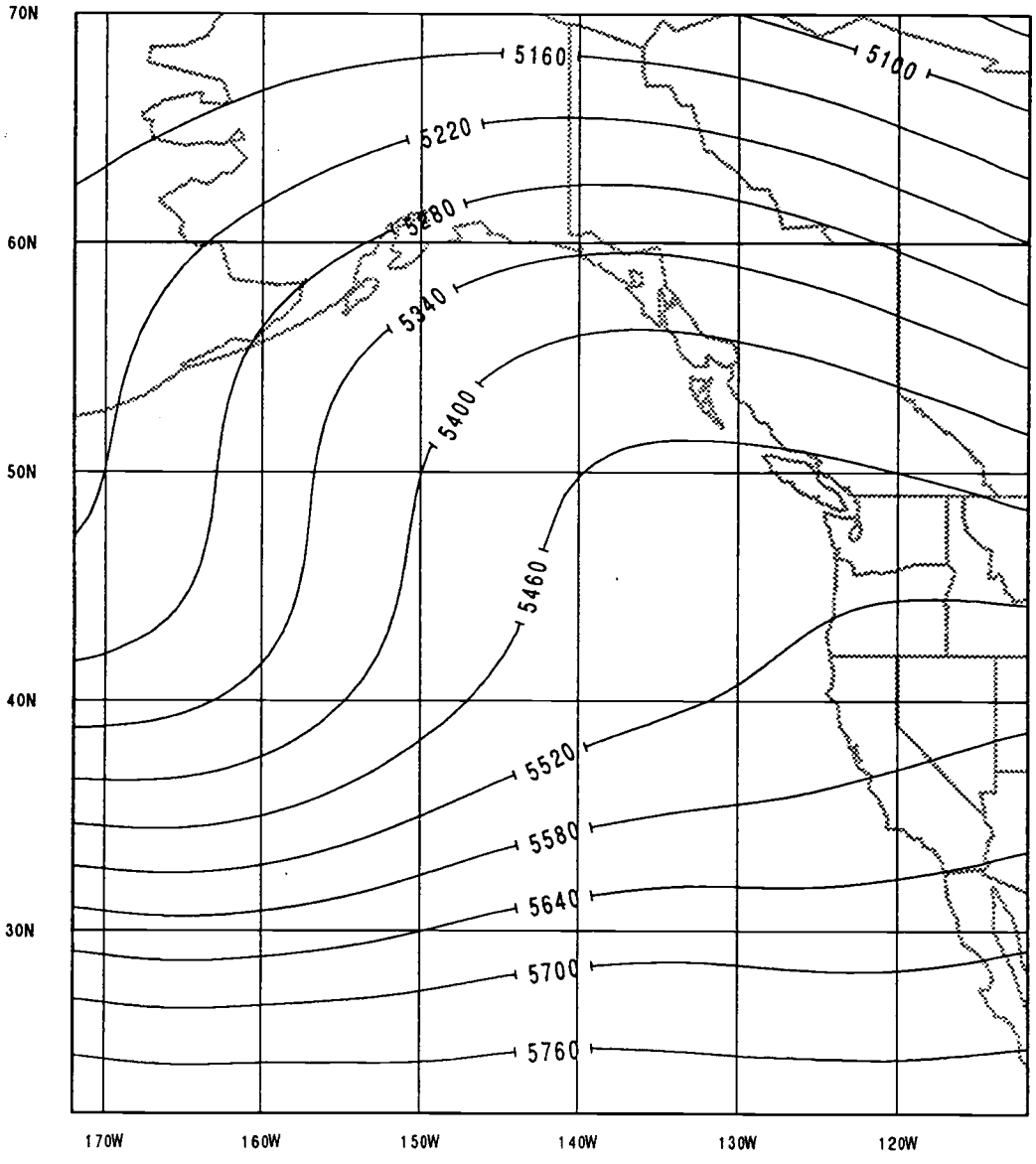

Fig. 5.7 Same as for Fig. 5.6 but for negative height anomaly.

case as this for which there are different and irregular autocorrelations for each time series. Harris (1985) states that in attempting to extend the F-test for significance from the MRA to Canona, results from limited Monte Carlo testing indicated that the F-test (apparently due to an overestimation of the degrees of freedom) attributed higher levels of significance to an apparent correlation than actually was justified.

We have accordingly rerun the canonical correlation test 300 times with the sequence of the OLR PC time series reordered with a random number generator. The mean canonical correlation coefficient for this experiment was found to be 0.3477 with a standard deviation of .0724 (the highest of the 300 Monte Carlo scores was 0.56). This apparently high value is a consequence of the dependence of the variables within each set and the probability that, in the 15 combinations for each run, some of the pairs of variables will be highly correlated by chance. Nevertheless, from the results of this Monte Carlo experiment it can be seen that, assuming a normal distribution of the random correlations, there is a probability of only 0.01 of exceeding a canonical correlation in excess of 0.52 by chance and far less for the 0.6553 which was actually measured. We thus conclude that the overall relationship between the two sets of PC time series is established to a very high degree of confidence.

5.4 Analysis by stratification of OLR PC's

The simple, multiple and canonical correlation measurements of the previous sections have shown a highly significant relationship between the 500mb height field over the NE Pacific and western North America and the OLR field over the tropical Pacific. In Figure 5.5 we have shown the most probable configurations of *overall* related patterns for these two fields. We should like, however, to be able to associate *specific* differences in the attributes of the 500mb height field with those of the OLR field. As we have shown a time lag of two to five months of the height field PC's behind the OLR PC's for the closest relationship there would also be a forecasting implication, should such specific relations be sufficiently close.

As discussed in the previous section, much of the variance in the height PC's is unexplained by the OLR PC's, and there is also much more total variability in the height PC's. Thus, the differences in the height field predicted by the OLR PC's are subtle and obscured somewhat by the unexplained variations. One method of emphasizing such differences is the separation of means. Additionally, there is the possibility that a change in the OLR field might be related to a different *distribution* of the height PC's and it is also possible that such a change in distribution of the height PC's would be more distinctive than the change in the mean value. There is, at least, additional information to be obtained by examining the height PC distributions associated with differences in the OLR PC's.

Both of these methods require that the height PC's be associated with a block or "strata" of the OLR PC's. Had the height PC's been shown to be correlated with only OLR PC #1, one might have stratified the height PC's by association with the upper and lower thirds of this OLR PC. This would have retained a small but (as shown below) sufficient sample size in the upper and lower blocks to form a reliable mean, although the significance of the details of the distribution would be questionable. However, this would also have discarded the contributions of the other two OLR PC's. If there were sufficient data the height PC's could be stratified by all three of the OLR PC's jointly. This would require a division of the height PC's into nine OLR categories and, with the commensurate reduction in PC occurrences per category, would have reduced unacceptably the significance of any apparent separation of means. We have, instead, stratified each height PC by its associated composite "predictor" OLR series, discussed previously in section 5.3. This includes more of the OLR information than would a single OLR alone without further reducing the sample size.

5.4.1 Separation of means.

To examine the difference in the mean values of the height PC's associated with the upper and lower thirds of the composite OLR series, we may represent the differences in means in a standardized measure which

may be directly related to its significance. The students t-test for the difference between two means is well suited for this purpose. Here,

$$t = \frac{\bar{x} - \bar{y}}{\sqrt{n_x \sigma_x^2 + n_y \sigma_y^2}} \sqrt{\frac{n_x n_y (n_x + n_y - 2)}{n_x + n_y}} \qquad (5.7)$$

where x and y are the different groups, n_x and n_y are the numbers in each group and σ_x and σ_y are the standard deviations for each group. The resulting value for t is then tested for significance using ν degrees of freedom where $\nu = n_x + n_y - 2$. The resulting probability that the difference between means might have been drawn from a random selection of means from a single population assumes a normal distribution. While this assumption of normality is not strictly supported by the actual distributions of the 500mb height PC's, it is not so grossly violated as to invalidate the results of the t-test. Harris (1985) states that, provided the number of observations exceeds about 10 and the ratio of the sample variances for the two groups is no greater than 20:1, the t-test is valid even for U-shaped population distributions. Clearly, with much larger sample sizes and near equal variances, the distributions (as shown in the following section) should not invalidate the test. Although the sizes of the different groups vary slightly from case to case, ν always equals or exceeds 43 for which the significant (0.05) value of t is 1.67 and the highly significant (0.01) value of t is 2.41.

The separations of the means of the five 500mb height PC's found to be correlated significantly with the OLR PC's, expressed as the above t-statistic, are plotted against lag time in Fig. 5.8. The separation of means is seen to be significant for all PC's and for all time lags up to six months. With the exception of the lag time of one month, the separation for the means of PC's 1, 2 and 6 were highly significant and those of PC's 3 and 5 were highly significant for lags in excess of two months. It is noted that t-scores of 5 or better, attained by PC's 1 and 2 at two months and 3 at four months are so high that the probability of occurrence by chance is vanishingly small, being less than 4×10^{-7}. The relationship as a function of lag time is roughly similar to the pattern of the correlations shown in table 5.2 but there are some considerable differences. In particular, the significance's of the separation of means, when stratified by the

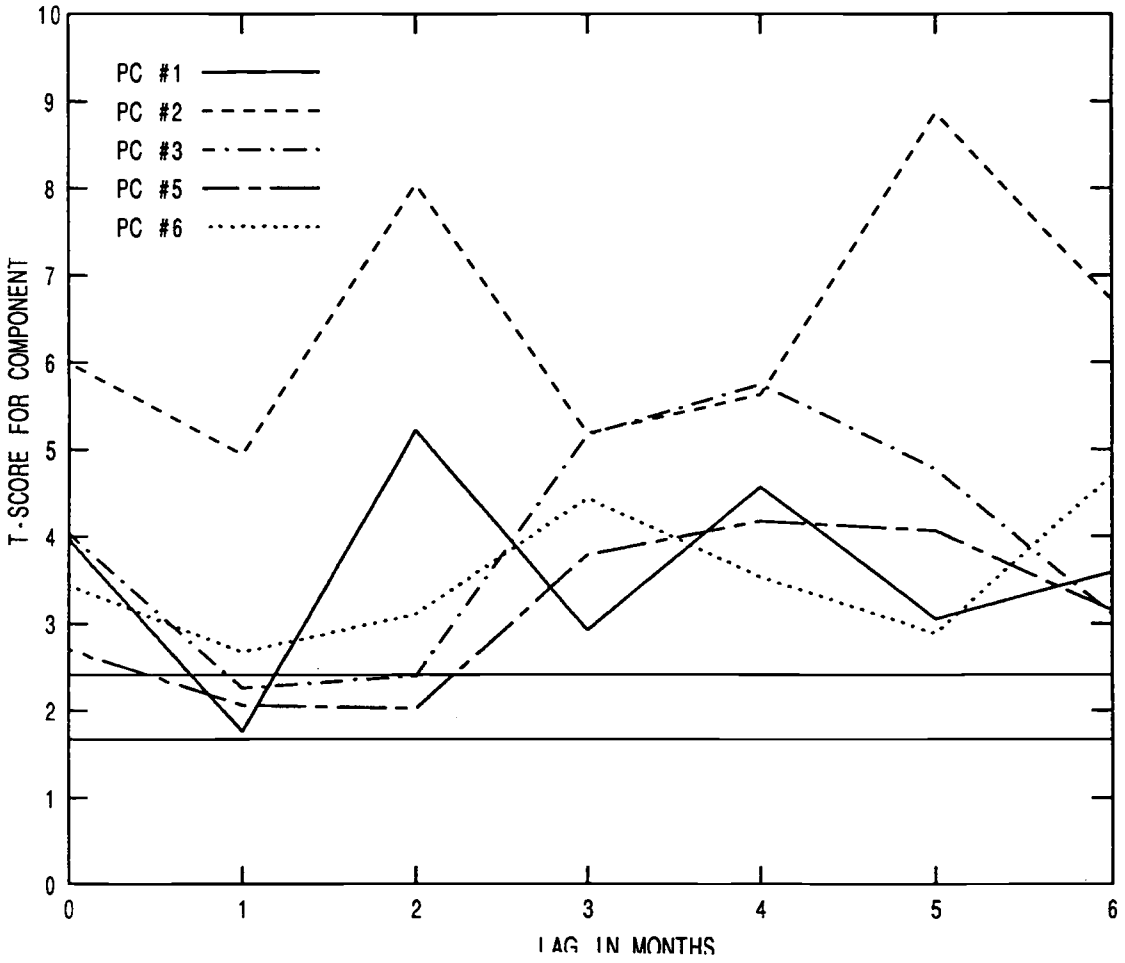

Fig. 5.8 T-scores of separation of means of 500 mb height PC's 1-6 stratified by upper and lower thirds of composite OLR PC as function of lag in months after OLR. Lower horizontal line represents level of significance ($p = 0.05$), upper line is highly significant level ($p = 0.01$).

corresponding OLR PC's, are much greater than those of the direct correlations.

5.4.2 Frequency distributions of height PC's stratified by OLR PC's

As previously discussed, the variance of the pentad 500mb height PC's exceeds considerably that of the monthly OLR PC's. Although, as shown in section 5.4.1, the means of the height PC's are strongly related to the composite OLR PC values, there is much variation of the height PC's that may occur while the corresponding OLR PC remains relatively unchanged. It was remarked in section 5.1 that the first OLR PC exhibited an autocorrelation exceeding 0.5 at a lag of 4 months, PC #2 had an autocorrelation of 0.46 at three months and that the next few PC's had at least a significant positive autocorrelation for one month. In contrast, for the pentad 500mb height PC's, only PC #2 has a significant autocorrelation extending beyond the subsequent pentad and that only for two pentads. Thus, there is little statistical relationship in 500mb height fields separated in time by more than a week or two, while major features of the tropical OLR field often persist for many months.

This behavior appears to be in conflict with the perception of frequent instances of near stationary circulation states and, in particular, episodes of persistent blocking that are observed over the NE Pacific. Observation of such events, however, reveals that many of the apparently very long term quasi-stationary circulation states are interrupted by temporary circulation events followed by a return to the quasi-stationary state. Statistics on the persistence of 500mb height anomalies were obtained by Dole (1985) which show that for 14 winter seasons there were only about 100 events for the mid-latitude Northern Hemisphere which exceeded 10 days (two pentads) in length. For 14 days duration the number of events had fallen to less than 50. The definition of the persistent anomaly included the requirement that the height departure above threshold be *continuous*. As defined by Dole, then, the frequency and persistence of the anomalies is not inconsistent with our observation of autocorrelation of the height PC's. Longer lasting but discontinuous anomalies, while very important factors

in seasonal precipitation and impressive to the observer, apparently do not have a substantive effect on the autocorrelations of the height PC's for lags of a month or more.

There remains the possibility, however, that a particular value of the composite OLR PC is associated not only with the *means* of the height PC's but also with a distinctive *frequency distribution*. For this determination it must be recognized that the total of the events is divided by the number of frequency bands selected and thus, as the resolution of PC amplitude is increased, we necessarily lose confidence in the validity of the frequency of any particular amplitude. We have chosen 21 amplitude bands, normalized by standard deviation, such that each band is 0.25 σ in width.

With this necessary fragmentation of the already brief OLR record, it is not possible to demonstrate that the apparent distributions could not be drawn by chance from a single population. The χ^2 test probabilities of such an occurrence are no less than 0.12. It would seem likely, in fact, that the apparent details of the distribution structures are fortuitous. On the other hand, the gross structure differences are probably real. For example, a distribution associated with the upper third of the OLR PC's might differ from that of the lower third principally due to an increase in frequency near the extreme upper end of the distribution but be essentially normal elsewhere. As, in this case, it is this aberration that causes the difference in means between the two, and as in the previous section we have shown very high confidence in the separation of means, we must have a reasonable degree of confidence in at least the gross features of the aberration.

In the distributions we focus particularly on aberrations near the extrema. The PC's in these amplitude bands are associated with the anomalous circulation events (such as blocking ridges) which may have a profound effect on western precipitation patterns. Three examples are displayed in Figs. 5.9, 5.10 and 5.11. These compare the distributions of height PC #5 at lags of 3 and 4 months and PC #3 at a lag of 6 months when associated with the upper and lower thirds of the composite OLR PC. For Fig. 5.9 it can be seen that the values of the height PC for the lower third fall off steadily from the median compared with those for the upper third, which have similar frequencies between plus and minus one standard deviation. In Fig. 5.10 the upper-third plot shows split maxima

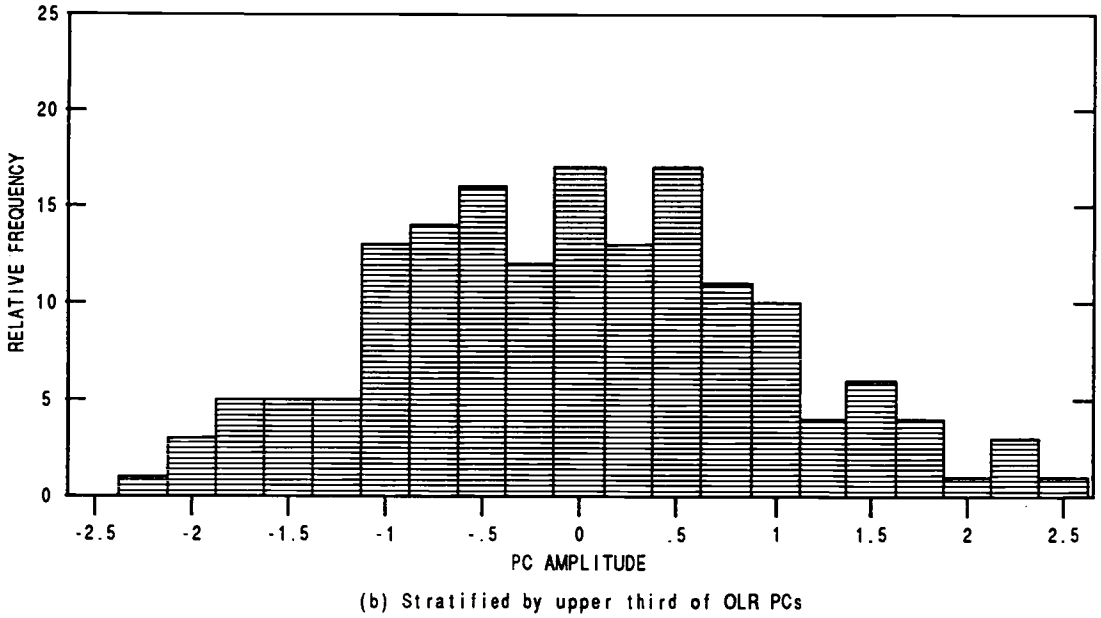

(b) Stratified by upper third of OLR PCs

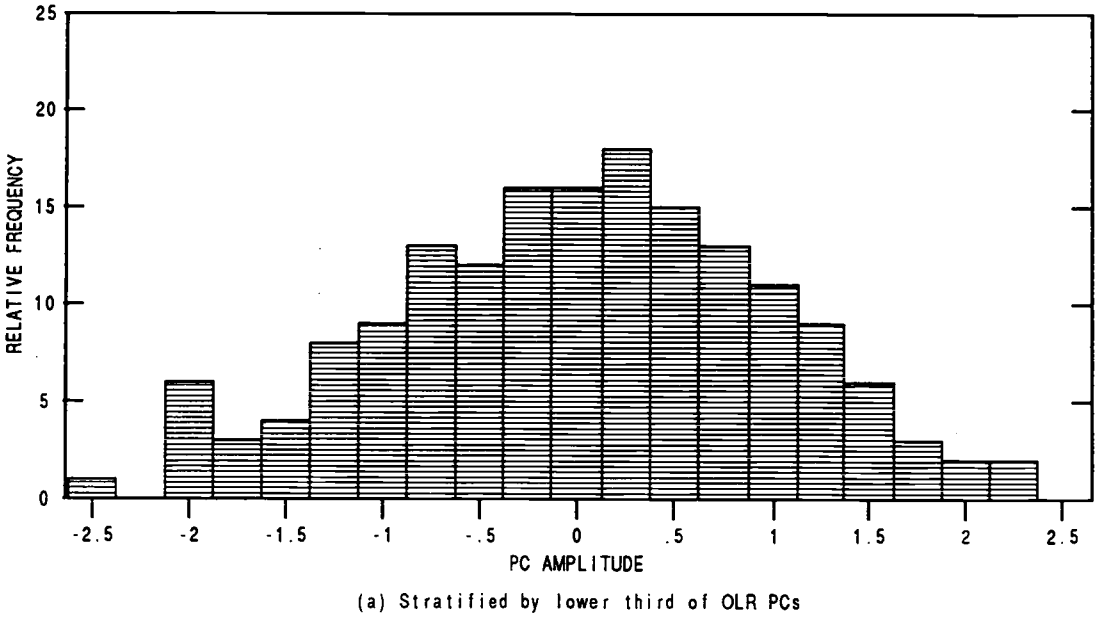

(a) Stratified by lower third of OLR PCs

Fig. 5.9 Frequency distribution of normalized amplitudes of PC #5 at a lag of three months after OLR. Distributions stratified by upper and lower thirds of composite OLR PC.

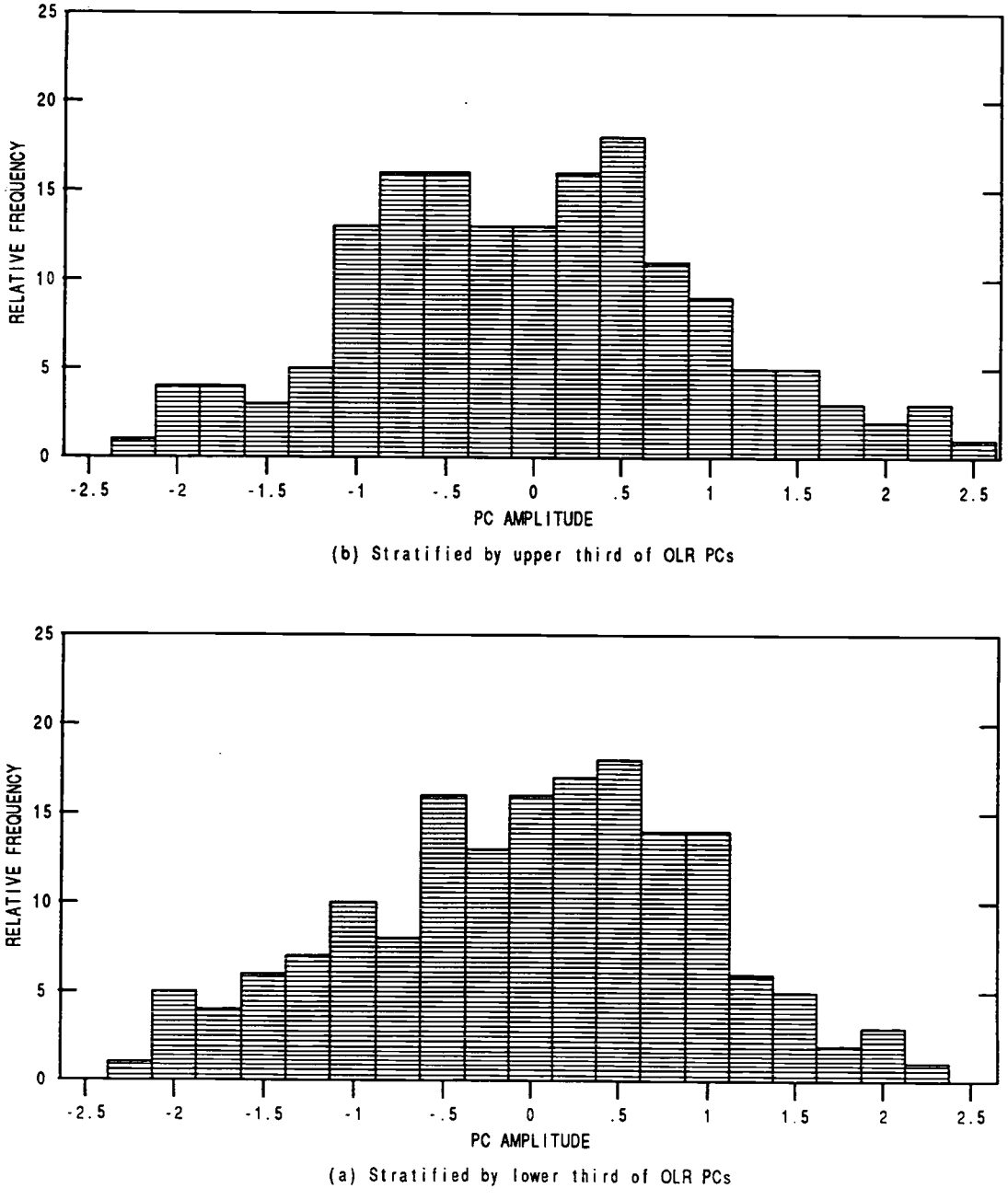

Fig. 5.10 Same as for Fig. 5.9 but for a lag of four months.

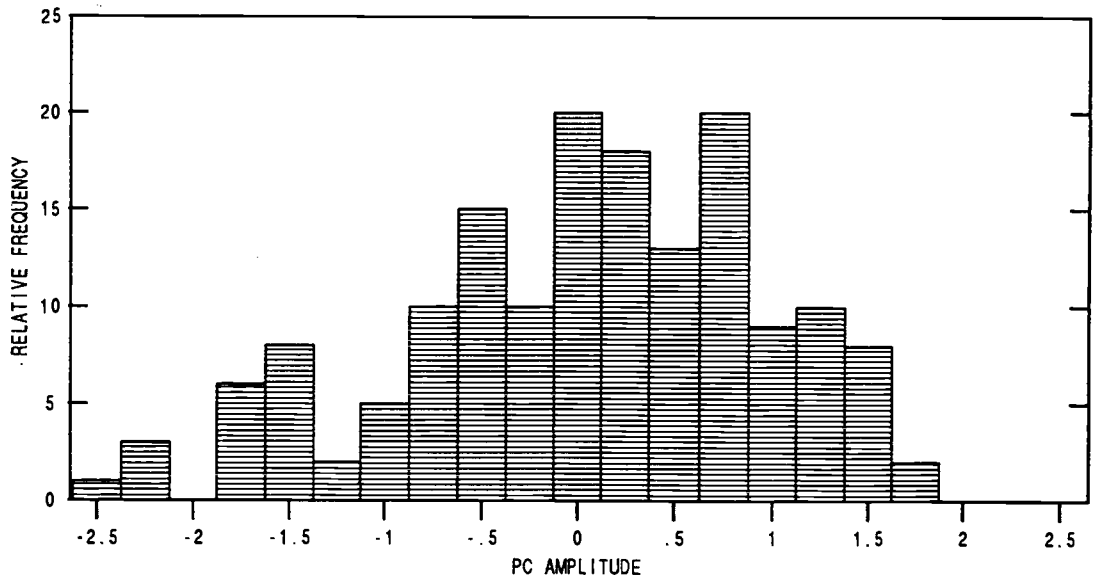

(b) Stratified by upper third of OLR PCs

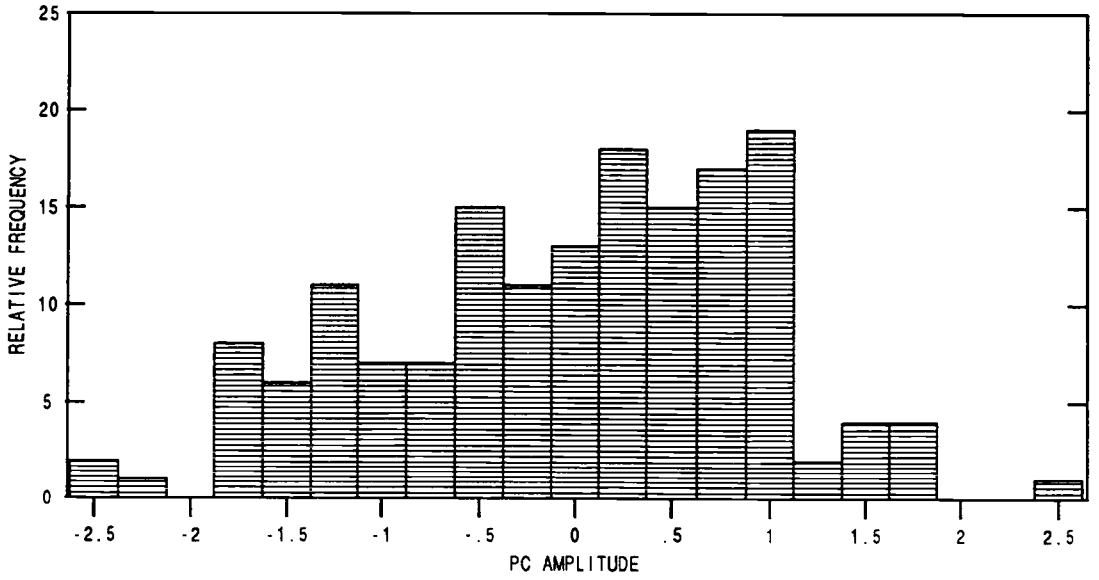

(a) Stratified by lower third of OLR PCs

Fig. 5.11 Same as for Fig. 5.9 but for PC #3 and at a lag of six months.

at plus and minus .5 standard deviations, while the frequency for the lower-third plot is negatively skewed. Fig. 5.11 is an example of relatively high frequencies of PC amplitudes well removed from the mean. In the case of the lower-third plot the maximum number of occurrences is a full standard deviation above zero, while for the upper-third plot a cluster of occurrences are found near 1.5 standard deviations below zero. Thus, associated with the upper and lower thirds of the composite OLR PC are not only differing mean values of the height PC's but also occasional but distinctive occurrences of PC's corresponding to circulation states well removed from those which are defined by the modestly shifted mean. We now wish to determine if the different distributions can aid us in forecasting western district precipitation from the variation in the tropical OLR field.

5.5 A precipitation forecast experiment

In Chapter 4 the monthly U.S. western district precipitation pattern was related to the 500mb height field over the NE Pacific and western North America and it was demonstrated that the precipitation for some of the districts could be reasonably forecast (with correlations of about 0.80) if only the first 6 EOF's of the height field were known. In the previous sections of Chapter 5, a small but significant portion of the variance of the 500mb height field has been shown to be explained by the first three principal components of the OLR field of the tropical Pacific, some months before the date of the height field record. It might therefore be expected that a certain portion of the variance of the western district precipitation pattern might be forecast by the OLR field.

It has been an underlying assumption of this study that the well known correspondence between the SOI and winter season western precipitation (discussed in the introduction and plotted as a correlation map in Fig. 1.1) has the circulation over the west as its principal intermediary. We have assumed that conditions in or over the tropical Pacific have an effect on the mid-latitude circulation which in turn affects western precipitation patterns. It is quite possible that there are additional

links in the chain, such as mid-latitude sea surface temperatures, perhaps influenced by tropical currents, but it appears that the principal ultimate link to precipitation must be the circulation pattern. If this were not so it would be difficult to account for such a large proportion of the variance in the precipitation pattern explained by an approximation to the 500mb level of the circulation alone.

We have also assumed that the OLR field over the tropical Pacific, being closely related to the upper-level outflow from the tropics, should be a more direct predictor of the mid-latitude circulation than the SOI, which is merely an index of sea-level pressures at the extreme ends of the tropical Pacific basin.

In consonance with these assumptions, we now wish to show that a four month circulation forecast, determined from prior values of the OLR PC's, will result in a district precipitation pattern better correlated with the observational record than is the SOI. There are two different types of comparisons that will be made. The first is that of the correlation of observed precipitation with the indices predicted by the model of Chapter 4. The input height field PC inputs are to be inferred from the OLR-height field relationship of the entire record. These correlations will be compared to those based on the SOI. It should be noted that these correlations are *not* of forecasts. The second is a comparison of actual forecasts; one generated by the OLR field and the other from the SOI. For these, the data sets applied to the respective models are segregated from those used in generating model coefficients.

5.5.1 Comparison of observed precipitation correlations with model indices from the OLR inferred height field and equivalent correlations with the SOI

In section 5.3 we discussed the consequence of the relatively small variability of the OLR PC's in comparison with those of the 500mb height field. As only a small fraction of the height PC variance is explained by the composite OLR PC series, even extreme values of the OLR PC's will infer only modest departures of the height field from its seasonal mean. The use of such a single predicted anomaly combined with the mean field for that

date will produce an unrealistic precipitation forecast, for the same reason that the mean circulation state does *not* result in a precipitation pattern that resembles the climatological mean. The mean precipitation pattern is the result of many different circulations, the *average* of which defines the circulation mean. This distinction is of sufficient importance to illustrate with an example. We have applied the mean circulation to the precipitation model by setting the input height PC's to zero for the six pentads of a given month and have plotted the resultant normalized precipitation as a percentage of the mean as shown in Fig 5.12. Precipitation in most of the region is far below the climatological average. In the far southwest it is seen to be less than 10% of the mean. It approximates the mean only along a narrow band from northwest Oregon to northeast Washington and is well above the average in the extreme northwest corner of the domain.

A much more realistic inference of the circulation associated with a particular set of OLR PC's can be obtained by use of the many different circulations found, as in section 5.4, to be associated with some range of OLR PC values. In this manner, not only will the particular mean circulation related to an OLR PC in this range be represented (by the average of the height PC ensemble) but the many additional circulation states, also associated with this range, will be included.

For these experiments we have stratified the composite OLR PC time-series into five levels, each containing approximately the same number of OLR values. This permits a reasonable degree of discrimination in the state of the OLR field without unduly limiting the size of the pentad height PC sample associated with each OLR level. The height PC's are those associated with the OLR field four months before in accordance with the four month forecast period selected and also in consonance with the results of the earlier discussed correlation tests. For the each of the six height PC's used, 40 characteristic values are associated with each OLR level.

Corresponding to each successive monthly value of the composite OLR PC level, 40 height fields were generated by combining the PC's of each of the six distributions for that level. As the PC's defining these 40 height fields then each had distributions characteristic of the OLR level for the designated month (four months prior to the forecast), the 40 constructed

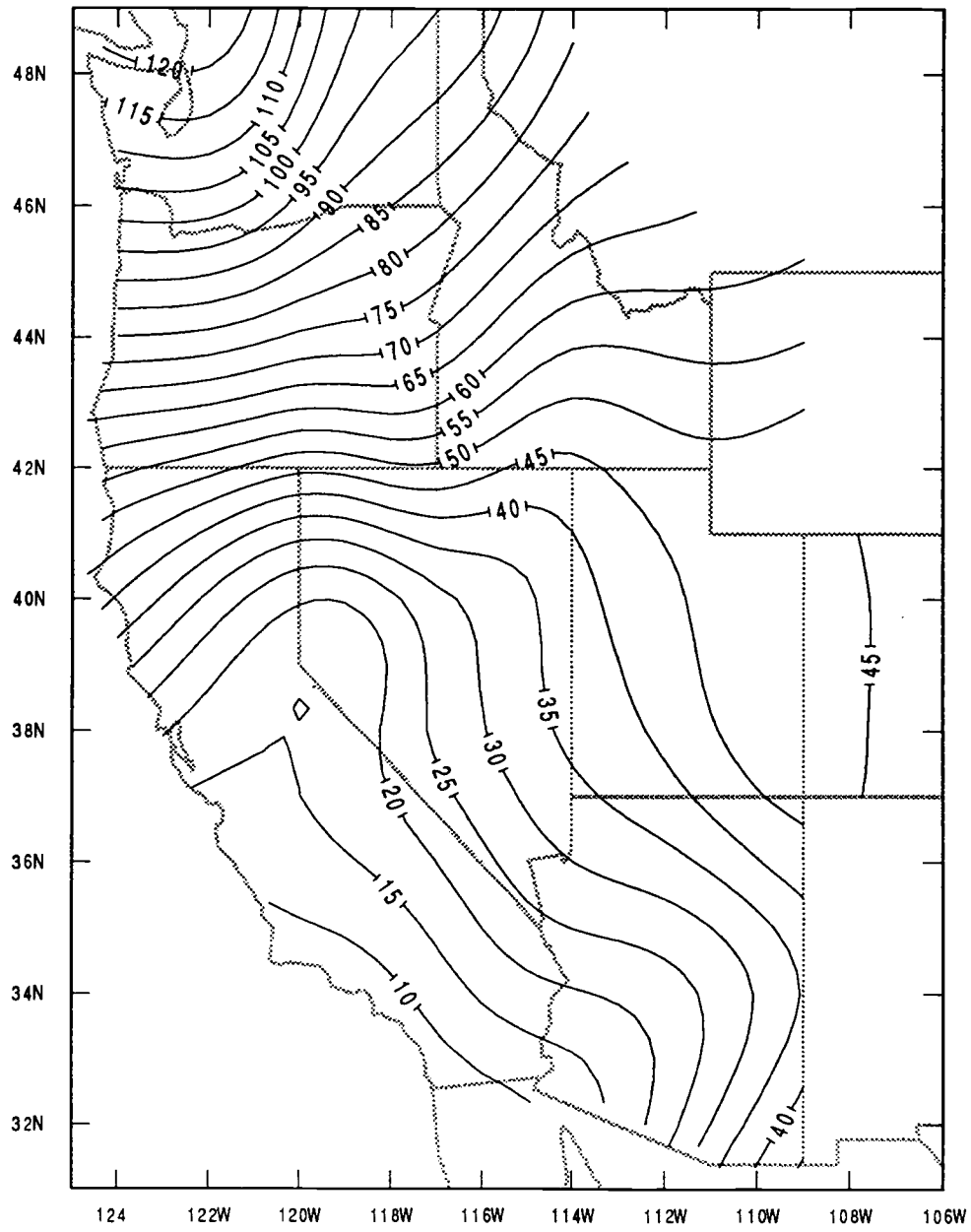

Fig. 5.12 Percentage of normal monthly precipitation resulting from mean height field being applied to precipitation model for entire month.

height fields were likewise representative of the height field distribution associated with that level. With the 40 height fields as inputs, the precipitation model of Chapter 4 was run and the 40 resulting pairs of precipitation indices (for each district) averaged to form district orographic and baroclinic indices for the month. In this manner, the predictant OLR was associated with a precipitation pattern corresponding to the *ensemble* of circulation states for that OLR level, rather than to that of a single mean circulation state. The procedure was repeated for each of the forecast months. The observed district precipitation record was then regressed against the 65 month time-series of these index pairs for the November through March months from 1974 to 1988.

The coefficient of multiple correlation, interpolated to the geographic grid, is shown in Fig. 5.13 and can be compared to Fig. 5.14, which is an equivalent plot of the correlation of the SOI to district precipitation for the years 1950 through 1988. The correlation pattern of Fig. 5.14 is similar, qualitatively, to that of Fig. 1.1, for which the correlations were for the entire winter season (at a lag of five months) and consequently somewhat higher. With the SOI to district precipitation correlations plotted for a five month lag (as in Fig. 1.1, but for the years 1974 to 1988) the plot (not shown) is very little different from Fig. 5.14, but the correlations are generally lower. For the month-to month record, in contrast to the October through February seasonal comparison of Fig. 1.1, the correlations are highest for a lag of four months for the SOI as well.

In any comparison of multiple with linear correlation it should be noted that the coefficient of multiple correlation cannot be negative and that the significance of equivalent values of the multiple correlation coefficient is lower. As discussed in Section 5.3, the effect of regression against multiple variables is to increase the probability of higher values of the sample correlation coefficient. The relative difference in significance is greater for the smaller apparent correlations such as those in the band from northern California to Colorado. This is just to the south of the line of zero linear correlation between the SOI and district precipitation. By transforming the district SOI-precip correlations to the normally distributed z statistic, where $z=(\ln((1+r)/(1-r))/2$, it was determined that absolute values of correlations in excess of 0.15 were significant and those in excess of 0.20 were highly significant. An inspection of Fig. 5.14 shows

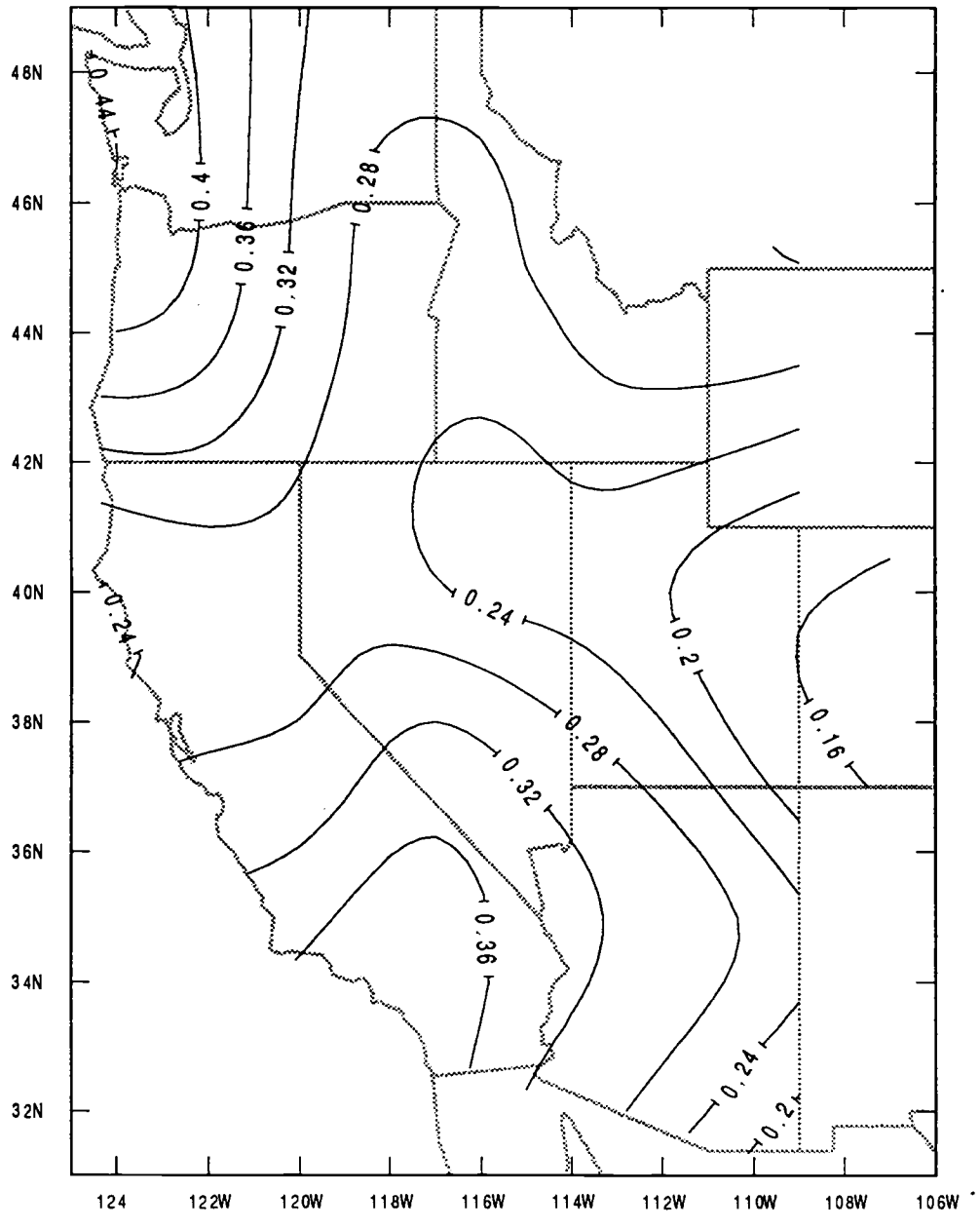

Fig. 5.13 Multiple correlation coefficient of precipitation indices with observed district winter month precipitation for years 1974-1988. Indices from precipitation model with input height fields from distributions characteristic of composite OLR level four months before forecast date.

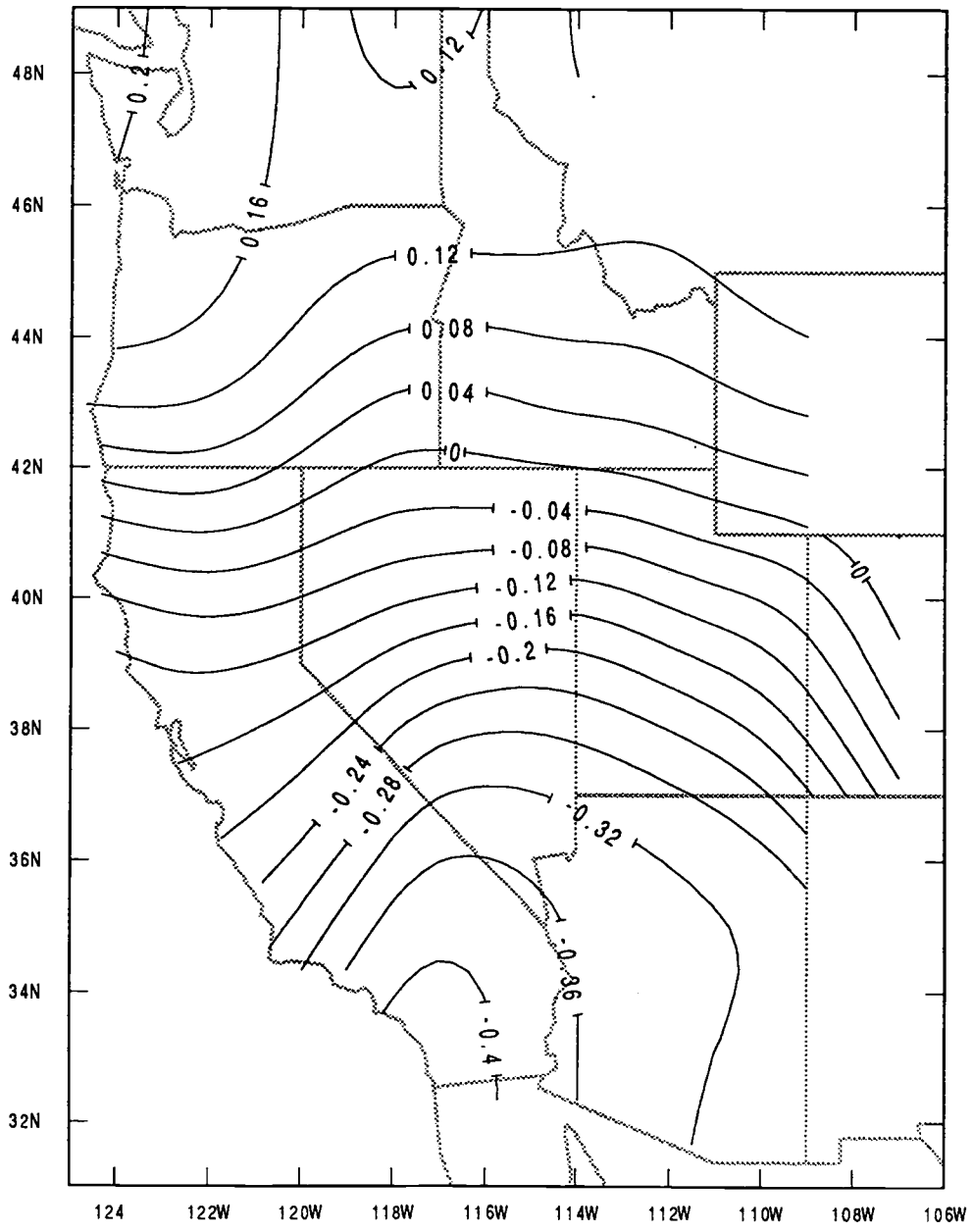

Fig. 5.14 Correlation of SOI with observed district winter month precipitation for years 1950-1988. Precipitation four months after SOI measurement.

that the negative correlations in the southwest are highly significant while the positive correlations are only significant in the far northeastern and northwestern corners of the domain.

An equivalent examination of the multiple correlation coefficient, plotted for the OLR based precipitation indices in Fig. 5.13, was made with the aid of the F-statistic, where $F=(N-3)R^2/2(1-R^2)$ for a two variable MRA with N events. With this it was found that individual district correlations were significant for values greater than 0.35 and highly significant for values in excess of 0.42. Thus, for this case, the correlations along the Pacific Northwest Coast were highly significant and those in Southern California significant.

5.5.2 Comparison of an OLR based forecast with that from the SOI

A more rigorous examination of the utility of the OLR field of the tropical Pacific as an aid in the prediction of western district precipitation was made by segregating the data used in developing the model statistics from that used as input to the model for the forecast. Similarly, for the comparative SOI based forecast, the SOI and district precipitation data used to determine the regression line coefficients were taken from a different portion of the record (years 1950-1968) from the SOI input to the forecast (years 1969-1988). The results for the SOI forecast are plotted in Fig. 5.15. In contrast to the previous SOI plot, this is a correlation of the precipitation predicted by the application of new data to the regression coefficients with the observed district precipitation. It may be seen that the correlation pattern of Fig. 5.15 is qualitatively similar to that of Fig. 5.14, with consideration given to the necessity that all correlations are positive, because the correlations are now between the observed precipitation and the SOI *forecast precipitation* (rather than the SOI itself). The correlations of Fig. 5.15 are slightly reduced, the regions with significant forecasts being a little smaller than those for significant SOI-to-precipitation correlations in Fig. 5.14. Nevertheless it is notable that the true forecast is only slightly degraded, demonstrating that the statistical relationship of the SOI to precipitation is almost unchanged between the period used for

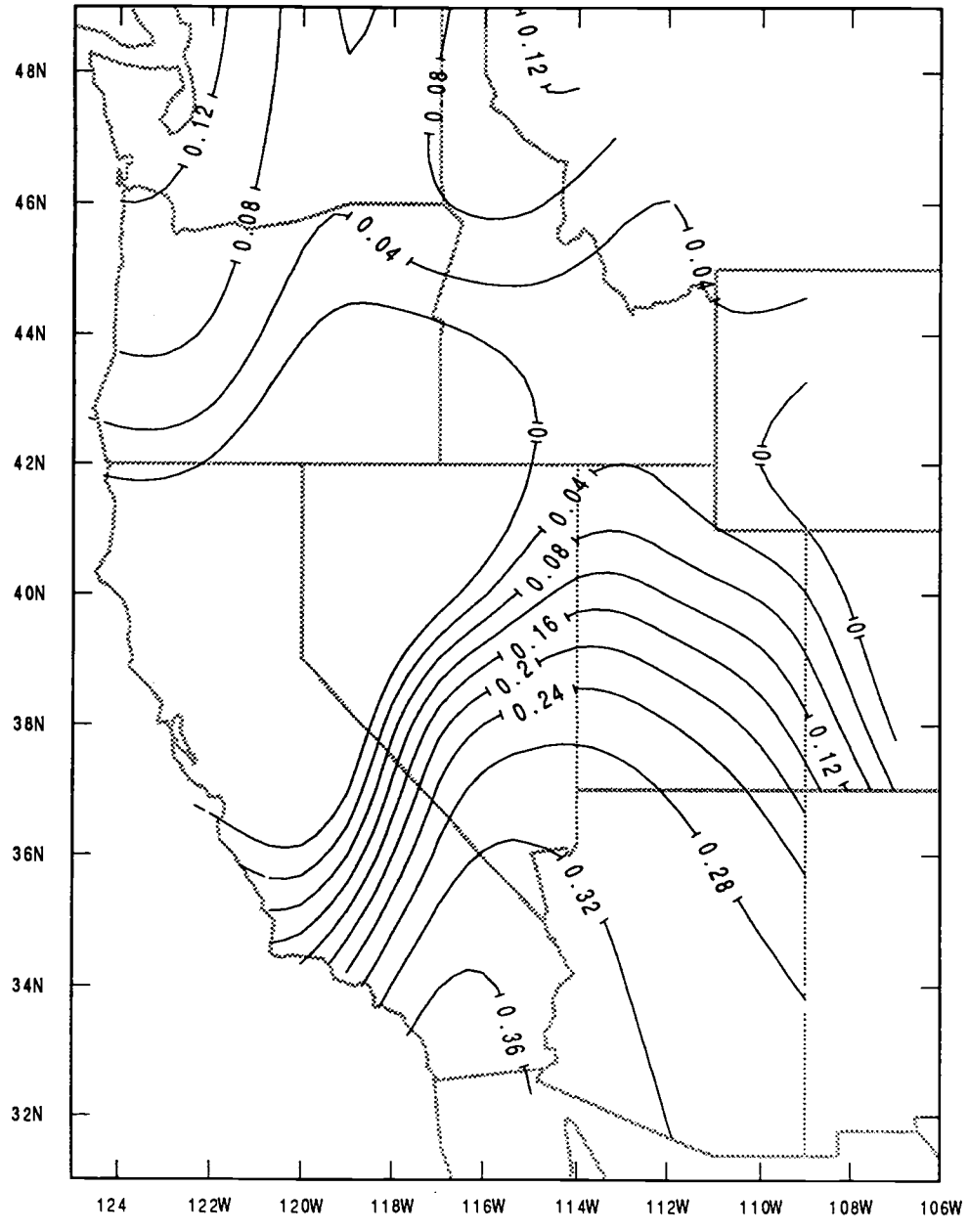

Fig. 5.15 Correlation of winter month district precipitation with that forecast by SOI four months before. Forecast for years 1970-1988.

model development and that for the forecast.

To make a precipitation forecast based on the shorter OLR record we have divided the data into the six year section (1974-1981) not including the record gap and the seven year section (1982-1988). Because of the shortness of the record we have made one forecast for the second period using model coefficients from data of the first period and another forecast for the first period developed using data from the second period. The two forecasts were combined into a nine year (65 winter months) forecast which was then correlated with the actual record.

As discussed in the previous section, the procedure was to form distributions of each of the first 6 height PC's associated with the five stratified OLR PC levels (all from the data sets of one period) and then to use these distributions to forecast a set of height PC's for the monthly OLR level from the other period. As before, 40 height fields (generated from these PC's) were forecast to occur four months after the OLR measurement and used as the only variable input to the precipitation model.

The resulting 40 precipitation index pairs per month were averaged and applied to the linear model developed, as discussed in Chapter 4, by multiple regression of the index set from *actual* height PC's against each district precipitation record. The coefficients of the linear model were derived, therefore, from indices based on actual height data and applied to indices resulting from OLR *forecast* heights. The predicted monthly district precipitation was correlated to that observed, interpolated to the geographic grid and plotted as shown in Fig. 5.16.

There is less geographic variation in the correlation coefficient than for that of the equivalent correlation plot for the SOI based forecast shown in Fig. 5.15. The lowest correlations in both are seen along the northern California coast and in the eastern or southeastern region. The region of highest SOI correlation, in Southern California, is shifted somewhat to the north and west, with a broad band of correlations approximating 0.4 extending from eastern Nevada northward into western Montana. The low correlations in the southeast may be related to the poor performance of the model in that region. It is possible that the minimum in the SOI/precip correlation in northern California and southern Oregon, and that roughly coincident with the lower correlated OLR based forecasts in

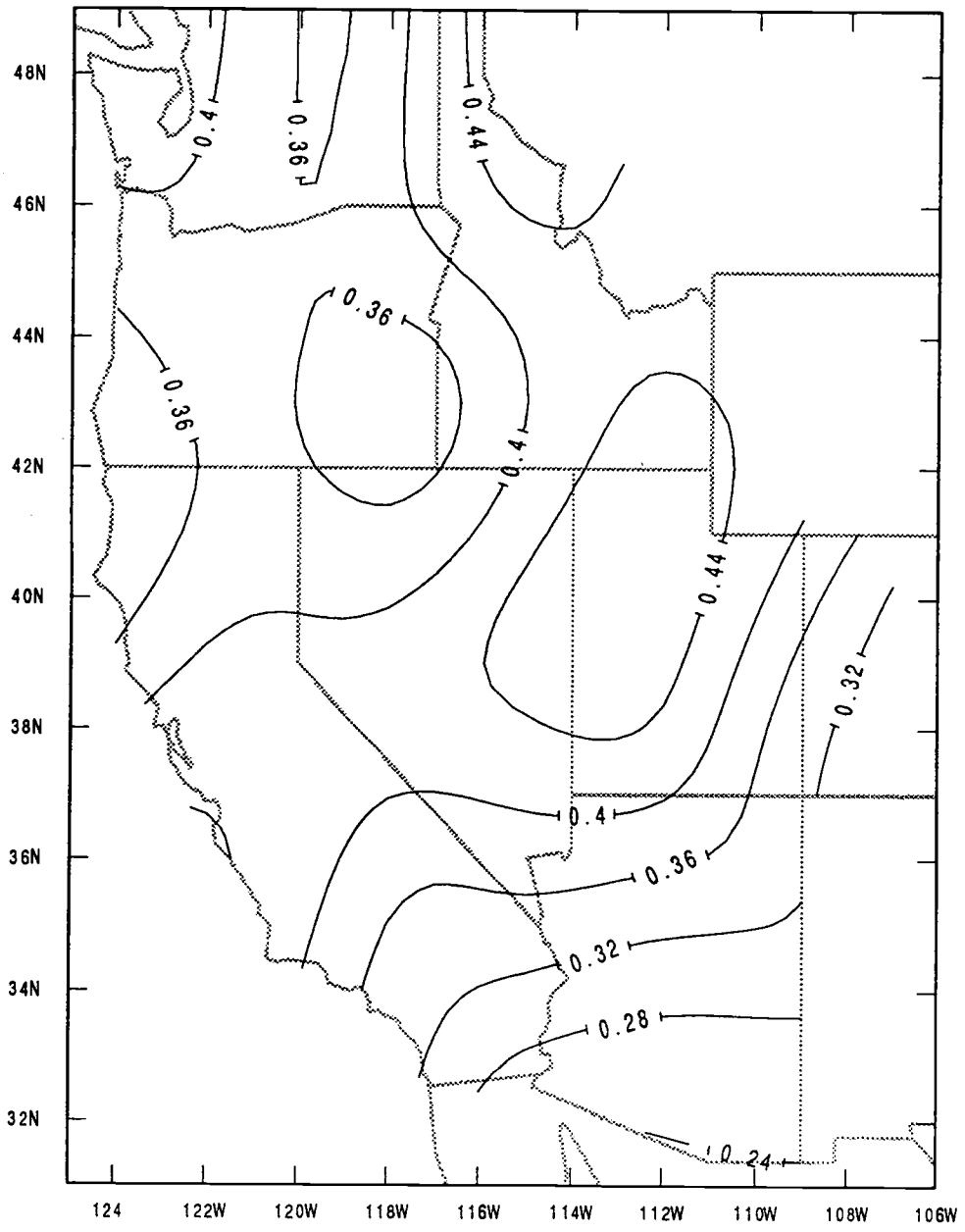

Fig. 5.16 Correlation of winter month district precipitation with that forecast by precipitation model with input 500 mb heights predicted from OLR four months before. Forecast for years 1974-1988.

the same area, may share a common physical cause. For almost all of the west, however, the apparent correlations of the OLR based forecasts are considerably higher than are those based on the SOI.

We still need to consider the relative significance of these apparent correlations, considering the different record lengths. Again, applying the z-statistic significance test to the OLR based forecast correlations, we now find that correlations above .29 are significant and those above .36 are highly significant. The corresponding values for the SOI based forecast are .22 and .30 respectively, due to the longer record.

As there are possible dependencies between members of both the observation and the forecast time-series which might alter this computed determination of significance, we have again made an empirical Monte Carlo determination by reordering the precipitation record at random and rerunning the correlation calculation for 500 repetitions. As would be expected, the mean value of correlation for every district was near zero, the maximum being 0.01. The mean district standard deviation of the correlations was about 0.14 and the maximum was less than 0.16. There were no districts for which there were more than two occurrences of correlations greater than 0.28. Based on the number of occurrences of various random correlation scores it was determined that, for the average district, the probability of a chance score greater than 0.16 was less than 0.05 (significant) and greater than 0.24 was less than 0.01 (highly significant). This is a somewhat better than the theoretical significance and increases our confidence in the presence of a real correlation between the forecast and observed precipitation records.

We must remain cautious in our interpretation of these results due to the brevity of the record but nevertheless can conclude that our forecast methodology is a superior means of including the effect of the tropical Pacific to that of the SOI correlation. Not only are most district correlation scores higher, even after making allowance for the decreased significance, but the significant correlations cover the entire western region with the exception of southern Arizona. In contrast, the SOI based forecasts have significant correlations with the observations only in Southern California and the lower Colorado Valley.

The improvement in the skill of the OLR based precipitation forecast over that of the SOI cannot be due solely to the inclusion of the mid-latitude

circulation as an intermediary. In fact, a two-stage *linear* statistical model, linking the SOI with western district precipitation via the mid-latitude circulation alone, must necessarily have a lesser forecast skill unless those aspects of the circulation variability explained by the SOI are the *only* SOI connected features to influence precipitation.

Part of the improvement may be due to the closer linkage of the OLR field (representative of the tropical upper-air outflow) with the mid-latitude circulation. Additionally, the inclusion of three OLR indices (PC's) rather than the single index of the SOI has the potential for explaining more of the mid-latitude circulation variability. An important component of the improvement, however, is due to the insertion of the circulation; for its inclusion permits the physical modeling of non-linear precipitation mechanisms as a crucial link in an otherwise linear statistical chain. As shown in Chapter 4, the alternative of a direct statistical model, with precipitation PC's linear functions of the height PC's, results in a lesser forecast skill.

We have no comparable physical model to link the tropical upper-air outflow with changes in the density distribution of the circulation state ensemble. It is quite probable that the linear statistical model, here described, does not make maximum use of the information contained in the OLR PC's. A non-linear statistical model would almost certainly be superior but objective methods for determining the specific functions and associated coefficients for an optimum fit would require far more extensive data sets than are available from the brief historical record.

CHAPTER 6: SUMMARY, CONCLUSIONS AND SUGGESTIONS FOR FURTHER STUDY

The focus of this study has been two-fold. The first and original purpose was to investigate relationships between features of the mid-latitude circulation over the NE Pacific and western North America and of the OLR field over the tropical Pacific. This comparison was made with the hope that the already established statistical relationship between the Southern Oscillation Index (SOI) and western district precipitation, along with its fortuitous time-lag, could be better understood and improved upon through the intermediary of the mid-latitude circulation. Additionally, it was believed that because of the additional information contained in the OLR field over that in the SOI and the closer linkage to the upper-level circulation of the OLR field (which may be considered a surrogate for the upper-level tropical outflow) that its association to western precipitation might be stronger.

The second purpose, which arose from the first, was to determine a method to infer precipitation from that minimum set of mid-latitude circulation parameters which might be expected to be forecast from the OLR field. If a model that would produce a sufficiently accurate precipitation forecast from minimal upper-air circulation inputs alone could be devised, then not only could we better forecast precipitation from the OLR field but we would also have a model which could be used in conjunction with other circulation forecasting methods and perhaps for other purposes as well.

6.1 Summary of results

6.1.1 Relationship of the 500mb height field to the OLR field

- Field representation. In order to capture the major portion of the variability of both the mid-latitude circulation and OLR fields we have represented each field by a small number of

EOF's and associated Principal Components (PC's). In so doing, we have been able to simplify the statistical relationship which would have otherwise been so complex as to obscure the analysis. As verified with the precipitation model it was determined that the 500mb height field could be represented adequately with 6 EOF's. For the OLR field, the first 3 EOF's were used.

- The PC's of the height and OLR fields are statistically related. The two sets of PC's were found to have highly significant linear correlations when compared by various individual pairs and at various lag times. By modeling each height field PC as a linear combination of all three OLR field PC's their multiple correlation was found to be highly significant for all but height PC #4.
- The best related height PC's lag the OLR PC's by four months. By determining the canonical correlation between the five well-related height PC's and the three OLR PC's, as a function of lag time, it was found that the correlation peaked at 0.6553 at a time lag of four months. This highly significant canonical correlation at that lag implies a forecasting potential.
- Differing mean values of the height PC's were associated with stratifications of the OLR PC's. The differences in the means of each of the five well-related height PC's associated with the upper, as compared to the lower thirds of the OLR PC's were found to be highly significant.
- Differing frequency distributions of the height PC's were associated with stratifications of the OLR PC's. The upper and lower thirds of the OLR PC's were found to be associated, after time lags of three to six months, with distinguishable frequency distributions of the height PC amplitudes. The differences at the extrema of the distributions were considered indicative of uncommon circulation regimes.
- Height fields forecast from the OLR PC's could be used to forecast western district precipitation. Such forecasts, four months in advance, when used as inputs to the precipitation

model were found to be better correlated to the observations than were equivalent forecasts based on the SOI.

6.1.2 The precipitation model

- The purpose of the model was to infer monthly precipitation for the western districts from an approximation to the 500mb height field. On the assumption that long-range circulation forecasts will remain limited (in the foreseeable future) to a rudimentary representation, the model input was constrained to a sequence of pentad averages of the 500mb height field approximating the long-wave circulation structure. The role of the model was to make maximum use of this limited information.
- Model precipitation is categorized into orographic and baroclinic components. Due to the time-scale of the model precipitation, no resolution of individual storms is possible. Based on the flow configuration and district topography, the expectation of orographic precipitation is computed. The expectation of precipitation due to storms resulting from baroclinic instability is determined from the configuration and strength of the jet in relation to the district.
- Statistical inference is combined with physical modeling. Unlike current long-range methods which model precipitation as a direct linear combination of height field values, this model limits statistical inference to obtain only those intermediate variables which are well correlated with the height field. The non-linear precipitation processes are then modeled physically, using these intermediate variables.
- Orographic precipitation component. The 850mb wind, relative humidity, sea-level pressure and stability are inferred statistically from the 500mb height field. Correlations for these range from about .8 for the low-level winds to about .4 for the stability index. The coefficients for the linear models

are obtained by regression from the appropriate records. Although much of the variance of the relative humidity and stability index is not explained by the 500mb components, the method is considered superior to that of using standard profiles. From the 500mb winds and heights plus the inferred variables, the temperature and moisture profiles are computed directly. Orographic lifting is computed from the 850mb flow over the model terrain. Layers in the vertical atmospheric column are lifted as a function of wind, surface elevation change and relative position in the column. Cooling is computed at either the dry or moist adiabatic rate depending on saturation, and condensed moisture summed for the column.

- Baroclinic precipitation component. Precipitation expected as a result of baroclinic instability is calculated from the 500mb winds (approximating the Polar Jet at the 300mb level) using the wind maximum and the cross-"jet" velocity profile. The jet orientation and the geographic separation of the "jet" axis from the district center is determined. The expectation of precipitation from systems developing in the baroclinically unstable flow in the vicinity of the jet is modeled from data taken from many case histories and considerations of the results of a number of theoretical and observational studies relating the position and meridional extent of the baroclinic precipitation band to the upper-airflow configuration. Precipitation mechanisms such as lifting due to frontal convergence are included implicitly through the baroclinic component.
- Combining baroclinic and orographic precipitation for a specific district. Both of the components are geographic specific and orographic precipitation is a function of the particular terrain in a given district. Nevertheless, there is much variation in the relative contributions of the precipitation mechanisms as a result of district characteristics which could not easily be included in the physical model. As is commonly done in day-to-day forecasting for a specific

station, a Model Output Statistics (MOS) approach is taken as the final stage in predicting district precipitation. For each district the component set was regressed against the observed precipitation record to obtain a set of district specific coefficients. These are then used as weighting factors to obtain the forecast precipitation.

- The precipitation model forecasts were better correlated with the observations than for systems currently in use. In evaluations of the ability of the model to forecast, the data sets used to create the various model coefficients by regression were segregated from those used to test the model. The winter seasons from 1950 to 1969 were used for obtaining these model coefficients. Using actual pentad height fields from 5-day averages of the NCAR compiled NMC 500mb twice-daily Northern Hemisphere data set, the precipitation monthly predictions for the winters of 1970-1988 were found to have correlations with the observations of over 0.80 for the western coastal districts falling off to about 0.60 in the eastern Great Basin and below 0.50 in the far southeastern portion of the domain. In comparison, the purely linear statistical model comparable to that of Klein and Bloom (1989), used by the NMC and based on 700mb heights, has correlations ranging from about 0.50 along the northern California coastal districts to about 0.15 in western Colorado.
- Forecast accuracy is maintained with a 6 EOF representation of the 500mb height field. When the height fields are replaced by those reconstructed from the first 6 EOF's and associated PC's, the correlations fall off, but only very slightly, demonstrating that the details of the fields not resolved by the first 6 EOF's do not contribute significantly to the ability of the model to forecast. Using fields reconstructed with fewer than 6 EOF's, mean correlations progressively decline and fall below significance for 2 EOF's. Increasing the representation to 7 EOF's, however, results in little measurable improvement.

6.2 Discussion and conclusions

We have shown that a representation of the atmosphere by a six PC component state vector for each pentad is sufficient to infer district monthly winter season precipitation to a useful degree of accuracy. In terms of the Bayesian Correlation Score, which is a more utility oriented measure than is linear correlation, the forecasts are particularly successful in the districts with large contributions to the major watersheds.

It would appear likely that as progress is made in the understanding and ability to forecast the state of the atmosphere, it will be in the large-scale features of the upper-level circulation, rather than in the small-scale details of wind, moisture and temperature at many levels. Therefore, a successful precipitation model of this sort which needs only a minimal input has a better potential to be useful in a true extended-range forecasting system than one which requires a detailed, multi-layered representation of the atmosphere.

The "forecast experiment" as discussed in section 5.5, is based on a very limited OLR record, of necessity further fragmented to segregate the regression coefficient forming portion from that applied to the forecast experiment. Nevertheless, the apparent improvement in the forecast over that based on a linear statistical model driven solely by the SOI is demonstrated to a reasonable degree of confidence. This result appears to further verify the existence of a quantifiable relationship between the OLR field and the mid-latitude circulation. Moreover, it demonstrates that the linkage between the tropical variations and the precipitation of the western US can be explained through its *effect* on the mid-latitude circulation.

Some of the improvement in the ability to forecast western precipitation from conditions over the tropical Pacific may be the result of the inclusion of more tropical information by use of the three OLR PC's as compared to the single index of the SOI. The more direct physical link between tropical outflow and the mid-latitude circulation may also be a factor. A considerable portion of the improvement, however, is probably due to the inclusion of non-linear processes in the precipitation model. The historical OLR record is far too short to develop, objectively, a non-linear statistical model to forecast the precipitation field directly from the multiple tropical

indices. The insertion of the circulation as an intermediary can add no new information to the tropical-to-precipitation association. What it does permit is the incorporation of non-linear physical processes which partially compensate for the deficiencies in the linear statistical part of the linkage.

The cause and dynamics of the demonstrated relationship between the tropical and mid-latitude fields is beyond the scope of this study. We have speculated that changes in the tropical upper-level outflow related to those in the OLR field may influence conditions along the tropical boundary of the mid-latitude circulation; this appears reasonable as the outflow may be detected well poleward of its source near the ITCZ. As discussed in the introduction, upper level poleward flow is related to Subtropical Jet acceleration which may be further linked to changes in the modes of the mid-latitude circulation.

The lag between a change in the tropical OLR field and the corresponding maximum in the change of the mid-latitude circulation may possibly be due to the period required to settle into a new equilibrium in the mean state and a new pattern of variability following the imposition of different boundary conditions. It is also possible that the mid-latitude circulation may be responding to some aspect of the tropical atmosphere-ocean system that peaks earlier in the typical ENSO evolution than does the OLR anomaly. While the amplitudes of the wind and SST anomalies appear to be greatest over the most extensive areas during the "transition phase" of the ENSO (Rasmusson and Carpenter, 1982), roughly coincident with the OLR anomaly maximum; there are certain, more limited, regions for which there are different, but comparable amplitudes in these fields for the earlier "onset" and peak" phases of the canonical El Niño. The mid-latitude atmosphere may be particularly sensitive to anomalies in such regions.

Still another possibility is that conditions along other boundaries with systems of longer time constants may be affected by an initial change in the mid-latitude circulation. The period required for the feedback mechanisms between these other systems and the mid-latitude circulation to establish a state of joint equilibrium would be controlled by the system with the longer time constant. For example, a low-level cyclonic circulation over the mid-latitude ocean as part of an initial change related to the tropical influence will cause upwelling and cooling of the local oceanic surface. A study by

Alexander (1992), using the NCAR Community Climate Model, discussed such mid-latitude forcing of the North Pacific. The feedback to the circulation is complex. Following the discussion by Hendon and Hartmann (1982), if the lower atmosphere, which is presumably colder than normal due to the cyclonic circulation, is none the less warmer than the surface there will be additional atmospheric cooling balanced by warm advection from the south with higher pressure to the east. On the other hand, if the air is sufficiently cold there will be heating from the surface, cold advection from the north and lower pressure to the east. A possible scenario would be the latter situation followed by the former as the surface gradually cooled. The time required to reach some sort of equilibrium would appear to be on the order of the time lags observed. It should be again remarked that the "equilibrium" discussed here is that of the envelope or distribution of circulation phase state density, rather than some steady state for, whatever the boundary condition, the phase state of the circulation will continue to change quasi-chaotically.

6.3 Recommendations for further study

The problem of determining, analytically, the dynamics of the effect of the tropical outflow on the mid-latitude circulation appears very difficult and would seem to require the study of examples in isolation from other effects. As a next step in this study, a model of the tropical and mid-latitude circulation systems might be devised. The other mid-latitude system boundary conditions would be fixed and the tropical system forced into various configurations. With such controls, sufficient data could be collected for different tropical configurations so that the manner in which the structure of the phase state distributions change would be better understood. This has already been done for other boundary conditions such as the sea surface effect mentioned above by Hendon and Hartmann (1982) but not, as far as this observer knows, with tropical forcing in the context of comparing the resultant circulation phase-state ensembles. At the least, such an effort should result in data sets sufficiently extensive so that a non-

linear statistical model, linking tropical indices to the mid-latitude circulation, could be developed.

For the precipitation model there are a number of additions and alterations which might be tested: The model for the intermediate variables uses for inputs the 500mb winds and height at the single point for which the variables are required. The alternative of modeling these variables by incorporating, in addition, the *configuration* of the 500mb field was not attempted due to the added complexity. Many new input variables would be required for a full representation of the field configuration; however it is possible that a single parameter representative of local streamline curvature might improve the model. Another possible alteration would be the inclusion of a quadratic term in some of the statistical models for variables such as relative humidity and stability (for which the linear model explains less of the variance than they do for the 850mb winds or mean temperature). As explained in the introduction to Chapter 4, such a departure from linearity would require more data to determine weighting coefficients with the same confidence limits attained for the weights in the linear models.

One of the problems in the model development was the necessity to compare a single monthly precipitation value with the index values generated from 6 pentad averaged height fields. With considerable additional effort the daily precipitation records of individual stations could be combined into district *pentad* precipitation records. For Oregon alone, there are more than 1800 reporting stations with reporting periods of varying length and much missing data. In the preparation of a small portion of these data for use in Appendix B it was found necessary to manipulate very large data bases; nevertheless it is a feasible approach and should provide better discrimination for the upper-air relationships with orographic and baroclinic precipitation.

Another alternative to the present model might be the recomputation of the vertical profile of water content along the trajectory passing over a district, with additions and subtractions determined by an evaporation and precipitation budget. This approach was originally attempted using trajectories initialized at the domain boundaries and was found to consume excess computer time; additionally, the original budget algorithm resulted in very dry moisture profiles over the interior districts, precluding any

orographic precipitation there. The algorithm could be made more realistic, however, and the trajectories shortened.

Finally, the precipitation model, or appropriate portions of it, might be modified for use in more climatologically oriented studies. Combined with the PRIZM model (Daly, et al., 1994) approach to improvement in the determination of precipitation distribution, for example, there might be an opportunity to relate small-scale anomalies in precipitation to upper-air flow regimes. Given the upper-air circulation patterns for the previous month or season, one might be better able to infer snow depths or stream flows in specific basins.

BIBLIOGRAPHY

Abbot, C. G., 1935: Solar radiation and weather studies. *Smithsonian Misc. Coll.*, **94**.

Alexander, M. A., 1992: Mid latitude atmospheric-ocean interaction during El Niño. Part I: The North Pacific Ocean. *J. Climate*, **5**, 944-957.

Anderson, J. R. and J.R. Gyakum, 1989: A diagnostic study of Pacific Basin circulation regimes as determined from extratropical cyclone tracks. *Mon. Wea. Rev.*, **117**, 2672-2686.

Barnes, S. L., 1964: A technique for maximizing details in numerical weather map analysis. *J. Appl. Meteor.*, **3**, 396-409.

Barnett, T. P. and R. W. Preisendorfer, 1987: Origins and levels of monthly and seasonal forecast skill for United States surface air temperatures determined by canonical correlation analysis. *Mon. Wea. Rev.*, **115**, 1825-1850.

Barnett, T. P., L. Dumenil, U. Schlese and E. Roeckner, 1989: The effect of Eurasian snow cover on regional and global climate variations. *J. Atmos. Sci.*, **46**, 661-685.

Baur, F., 1951: Extended range weather forecasting. *Compendium of Meteorology, Amer. Meteor. Soc.*, 814-833.

Blackmon, M. L., 1976: A climatological spectral study of the 500mb geopotential height of the Northern Hemisphere. *J. Atmos. Sci.*, **33**, 1607-1623.

Bonner, W. D., 1989: NMC overview: Recent progress and future plans. *Wea. and Forecasting*, **4**, 275-285.

Bretherton, C. S., C. S. Smith and J. M. Wallace, 1992: An intercomparison of methods for finding coupled patterns in climate data. *J. Climate,* **5** 541-560.

Brier, G. W. and D. A. Bradley, 1964: The lunar synodical period and precipitation in the United States. *J. Atmos. Sci.*, **21**, 386-395.

Browning, K. A. and T. W. Harrold, 1969: Air motion and precipitation growth in a wave depression. *Quart. J. Roy. Meteor. Soc.*, **95**, 288-309.

Cane, M.A. and S.E. Zebiak, 1987: Deterministic prediction of El Niño events. Atmospheric and Oceanic Variability. *H. Cattle, Ed., Roy Meteor. Soc. / Amer. Meteor. Soc.* ., 153-182.

Caplan, P. M. and G. H. White, 1989: Performance of The National Meteorological Center's medium-range model. *Wea. Forecasting,* **4**, 391-400.

Carter, G. M., J. P. Dallavalle and H. R. Glahn, 1989: Statistical forecasts based on the National Meteorological Center's Numerical Weather Prediction System. *Wea. Forecasting*, **4**, 401-412.

Charney, J. G., 1963: A note on the large-scale motions in the tropics. *J. Atmos. Sci.*, **20**, 607-609.

Charney, J. G. and J.G. DeVore, 1979: Multiple flow equilibria in the atmosphere and blocking. *J. Atmos. Sci.*, **36**, 1205-1216.

Charney, J. G. and D. M. Straus, 1989: Form-drag instability, multiple equilibria and propagating planetary waves in baroclinic, orographically forced, planetary wave systems. *J. Atmos. Sci.*, **37**, 1157-1176.

Clayton, H. H., 1934: World weather and solar activity. *Smithsonian Meteor. Coll.*, **89**.

Clayton, H. H., 1936: Long-range weather changes and methods of forecasting. *Mon. Wea. Rev.*, **64**, 359-376.

Craddock, J. M., 1958: Research in the meteorological office concerned with long-range forecasting. *Meteor. Mag.*, **87**, 239-249.

Crowley, T. J., 1983: The geologic record of climate change. *Rev. Geophys. Space Phys.*, **2**, 827-877.

Daly, C., R. P. Neilson and D. L. Phillips, 1994: A statistical-topographical model for mapping climatological precipitation over mountainous terrain. *J. Appl. Met.*, **33**, 140-158.

Dole, R. M., 1985: Persistent anomalies of the extratropical Northern Hemisphere wintertime circulation: Structure. *Mon. Wea. Rev.*, **114**, 178-207.

Dunn, L., 1987: Cold air damming by the Front Range of the Colorado Rockies and its relationship to locally heavy snows. *Wea. and Forecasting*, **2**, 177-189.

Egger, J. and H-D. Scilling, 1983: On the theory of the long-term variability of the atmosphere. *J. Atmos. Sci.*, **40**, 1073-1085.

Eliassen, A., 1956: Instability theories of cyclone formation. *Chapter 15, Petterssen (1956)*, q.v.

Elliot, R. D., 1944: Extended weather forecasting by weather type methods. *Long Range Weather Forecasting Unit 10-13,* U. S. Navy Dept., Washington DC.

Elliot, R. D. and T. B. Smith, 1949: Long period variations in the index cycle. *J. Meteorology* **6**, 67-87.

Epstein, E. S., 1988: Long-range weather prediction: Limits of predictability and beyond. *Wea. Forecasting.*, **3**, 69-75.

Farrel, B. F., 1990: Small error dynamics and the predictability of atmospheric flow. *J. Atmos. Sci.*, **47**, 2409-2416.

Garrity, J., 1977: The LFM Model-1976: A documentation. NOAA Technical Memorandum NWS NMC-60 (NTIS PB-279-419), 68 pp.

Glahn, H. R. and D. A. Lowry, 1972: The use of model output statistics (MOS) in objective weather forecasting. *J. Appl. Meteor.*, **11**, 1203-1211.

Hasler, A. F., W. A. Skillman and W. E. Shenk, 1979: In situ aircraft verification of the quality of satellite cloud winds over oceanic regions. *J. Appl. Meteor.*, **18**, 1481-1489.

Hastenrath, S., 1985: Climate and Circulation of the tropics. *D. Reidel Publishing Company*, 455 pp.

Harris, R. J., 1985: A primer of multivariate statistics. *Academic Press, Orlando*, 576 pp.

Hendon, H. H. and D. L. Hartmann, 1982: Stationary waves on a sphere: Sensitivity to thermal feedbacks. *J. Atmos. Sci.*, **39**, 1906-1920.

Hobbs, P. V., 1974: Ice physics. *Oxford University Press*, 461-724 pp.

Hobbs, P. V., R. A. Houze, Jr. and T. J. Matejka, 1975: The dynamical and microphysical structure of an occluded frontal system and its modification by orography. *J. Atmos. Sci.*, **32**, 1542-1562.

Hoel, P. G., 1947: Introduction to mathematical statistics. *John Wiley & Sons, New York*, 258 pp.

Hoke, J. E., N. A. Phillips, G. J. DiMego, J. J. Tuccillo and J.G. Sela, 1989: The regional analysis and forecast system of The National Meteorological Center. *Wea. and Forecasting*, **4**, 323-334.

Holton, J. R., 1979: An introduction to dynamic meteorology. *Academic Press, New York,* 391 pp.

Horel, J. D., 1981: A rotated principal component analysis of the interannual variability of the Northern Hemisphere 500mb height field. *Mon. Wea. Rev.*, **109**, 2080-2090.

Horel, J. D. and J. M. Wallace, 1981: Planetary scale atmospheric phenomena associated with the interannual variability of sea-surface temperature in the equatorial Pacific. *Mon. Wea. Rev.*, **109**, 813-839.

Hoskins, B. J., I. Draghici and H. C. Davies, 1978: A new look at the ω equation. *Quart. J. Roy. Meteor. Soc.*, **104**, 31-38.

Hoskins, B. J. and D. J. Karoly, 1981: The steady linear response of a spherical atmosphere to thermal and orographic forcing. *J. Atmos. Sci.*, **38**, 1179-1196.

Hoskins, B. J. and R. P. Pearce, 1983: Large-scale Dynamical processes in the atmosphere. *Academic Press, London*, 397 pp.

Hoskins, B., J. and M., A. Pedder, 1980: The diagnosis of middle latitude system development. *Quart. J. Roy. Meteor. Soc.*, **106**, 707-719.

Hubert, L. F. and L. F. Whitney, Jr., 1971: Wind estimation from geostationary satellite pictures. *Mon. Wea. Rev.*, **99**, 665-672.

IMSL, 1979: International mathematical and statistical laboratory, Edition 7, volume 3. *IMSL publ.*, Houston, TX.

James, I, N., 1987: Suppression of baroclinic instability in horizontally sheared flows. *J. Atmos. Sci.*, **44**, 3710-3720.

Jenne, R. L., 1975: Data sets for meteorological research. *NCAR technical note TN/1A-111, NCAR,* Boulder Co., 194 pp.

Jenne, R. L., 1989: Data availability at NCAR. *Data Support Section (Scientific Computing Division) NCAR,* Boulder Co., 45 pp.

Julian, P. R., 1966: The index cycle: A cross-spectral analysis of zonal index data. *Mon. Wea. Rev.*, **94**, 283-293.

Junker, N. W., J. E. Hoke and R. H. Grumm, 1989: Performance of NMC's regional models. *Wea. Forecasting*, **4**, 368-390.

Klein, W. H. and H. J. Bloom, 1989: An operational system for specifying monthly precipitation amounts over the United States from the field of concurrent 700 mb heights. *Wea. Forecasting,* **4**, 51-60.

Krishnamurti, T. N. and S. Low-Nam, 1986: On the relationships between the outgoing long wave radiation and the divergent circulation. *J. Meteor. Soc. Jap.*, **66**, 709-719.

Krzysztofowicz, R., 1991: Bayesian Correlation Score: a utilitarian measure of forecast skill. *Mon. Wea. Rev.*, **120**, 208-219.

Kushnir, Y. and N-C. Lau, 1992: The general circulation model response to a north Pacific SST anomaly: Dependence on time-scale and pattern polarity. *J. Climate,* **5**, 271-283.

Kutzbach, J. E., 1967: Empirical eigenvectors of sea-level pressure, surface temperature and precipitation complexes over North America. *J. Appl. Meteor.*, **6**, 791-802.

Kutzbach, J. E., 1976: The nature of climate and climatic variations. *Quat. Res.*, **6**, 471-486.

Kutzbach, J. E., 1981: Monsoon climate of the early Holocene: Climate experiment with the Earth's orbital parameters for 9000 years ago. *Science*, **214**, 59-61.

Kyle, H. L., 1990: The Nimbus-7 Earth Radiation Budget (ERB) data set and its uses: SPIE Vol. 1299 Long-term Monitoring of the Earth's Radiation Budget. *NASA/Goddard Space Flight Center, Greenbelt, Md.*, 39 pp.

Leathers, D. J., B. Yarnal and M.A. Palecki, 1991: The Pacific/ North American teleconnection pattern and United States climate. Part I: Regional temperature and precipitation associations. *J. Climate*, **4**, 517-528.

Lim, G. H. and J. M. Wallace, 1991: Structure and evolution of baroclinic waves as inferred from regression analysis. *J. Atmos. Sci.,* **48**, 1718-1732.

Lorenz, E. N., 1952: The flow of angular momentum as a predictor for the zonal westerlies. *J. Meteor.*, **9**, 152-157.

Lorenz, E. N., 1963: Deterministic nonperiodic flow. *J. Atmos. Sci.*, **20**, 130-141.

Lorenz, E. N., 1969a: Atmospheric predictability as revealed by naturally occurring analogues. *J. Atmos. Sci.*, **26**, 636-646.

Lorenz, E. N., 1969b: The predictability of a flow which possesses many scales of motion. *Tellus*, **21**, 289-307.

McGuirk, J. P. and D. A. Douglas, 1988: Sudden stratospheric warmings and anomalous U.S. weather. *Mon. Wea. Rev.*, **116**, 162-174.

Merkine, L.-O., 1975: Steady finite amplitude flow over long topography in a rotating stratified atmosphere. *J. Atmos. Sci.*, **32**, 1881-1893.

Milankovitch, M., 1941: Canon of insolation and the ice-age problem. *The U.S. Department of Commerce and The National Science Foundation,* Washington, D. C., 484 pp.

Molteni, F., S. Tibalbi and T. M. Palmer, 1990: Regimes in the wintertime circulation over northern extratropics. I: Observational evidence. *Quart. J. Roy. Meteor. Soc.*, **116,** 31-67.

Molteni, F. and T. N. Palmer, 1993 : Predictability and finite-time instability of the northern winter circulation. *Quart. J. Roy. Meteor. Soc.*, **119**, 269-298.

Mukougawa, H., 1988: A dynamical model of "quasi-stationary" states in large-scale atmospheric motions. *J. Atmos. Sci.*, **45**, 2868-2888.

Mureau, F., F. Molteni and T. M. Palmer, 1993: Ensemble prediction using dynamically conditioned perturbations. *Quart. J. Roy. Meteor. Soc.*, **119**, 299-323.

Namias, J., 1947: Extended forecasting by mean circulation methods. *US. Weather Bureau*, Washington D. C.

Namias, J., 1950: The index cycle and its role in the general circulation. *J. Met.*, **7**, 130-139.

Namias, J., 1951: The great Pacific anticyclone of winter 1949-50: A case study in the evolution of climatic anomalies. *J. Met.*, **8**, 251-261.

Namias, J., 1968: Long-range weather forecasting-History, current status and outlook. *Bull. Amer. Meteor. Soc.*, **49**, 438-470.

Namias, J., 1976: Negative ocean air feedback systems over the North Pacific in the transition from warm to cold season. *Mon. Wea. Rev.*, **104**, 1107-1121.

Namias, J., 1985: Some empirical evidence for the influence of snow cover on temperature and precipitation. *Mon. Wea. Rev.*, **113**, 1542-1553.

Opsteegh, J. D. and H. M. Van Den Dool, 1980: Seasonal differences in the stationary response of a linearized primitive equation model: Prospects for long-range weather forecasting? *J. Atmos. Sci.*, **37**, 2169-2185.

Palmen, E. and E. O. Holpainen, 1962: Divergence, vertical velocity and conversion between potential and kinetic energy in an extratropical disturbance. *Geophysica (Helsinki)*, **8**, 88-113.

Palmén, E. and C. W. Newton, 1969: Atmospheric circulation systems. *Academic Press, New York,* 245 pp.

Pauley, P. M. and S. J. Nieman, 1992: A comparison of quasigeostrophic and nonquasigeostrophic vertical motions for a model-simulated rapidly intensifying marine extratropical cyclone. *Mon. Wea. Rev.*, **120**, 1108-1134.

Pedlosky, J. and C. Frenzen, 1980: Chaotic and periodic behavior of finite amplitude baroclinic waves. *J. Atmos. Sci.*, **37**, 1177-1196.

Penland, C. and M. Ghill, 1993: Forecasting Northern Hemisphere 700 mb geopotential height anomalies using empirical normal modes. *Mon. Wea. Rev.*, **121**, 2355-2372.

Petersen, R. A. and J. D. Stackpole, 1989: Overview of the NMC production suite. *Wea, and Forecasting*, **4** , 313-322.

Petterssen, S., 1955: A general survey of factors influencing development at sea level. *J. Meteor.*, **12**, 36-42.

Petterssen, S., 1956: Weather analysis and forecasting. *McGraw-Hill, New York*, 505 pp.

Phillips, N. A., 1979: The nested grid model. *NOAA Tech. Report NWS*, **22**, U.S. Department of Commerce, Washington, DC, 80 pp.

Pickard, G. L. and W. J. Emery, 1982: Descriptive physical oceanography: An introduction. *Pergamon Press, Oxford.*, 249 pp.

Press, W. H., B. P. Flannery, S. A. Teukolsky, and W. T. Vetterling, 1988: Numerical recipes: The art of scientific computing. *Cambridge University Press.*, 818 pp.

Prohaska, J., 1976: A technique for analyzing the linear relationships between two meteorological fields. *Mon. Wea. Rev.*, **104**, 1345-1353.

Puri, K. and M. J. Miller, 1990: The use of satellite data in the specification of convective heating for diabatic initialization and moisture adjustment in numerical weather prediction modes. *Mon. Wea. Rev.*, **118**, 67-93.

Rasmusson, E. M. and T. H. Carpenter, 1982: Variations in tropical sea surface temperatures and surface wind fields associated with the Southern Oscillation/El Niño. *Mon. Wea. Rev.*, **110**, 354-384.

Rasmusson, E. M. and K. Mo, 1993: Linkage between 200 mb tropical and extratropical circulation anomalies during the 1986-1989 ENSO cycle. *J. Climate*, **6**, 595-616.

Reference Technology, Inc., 1988: World Weather Disc CDRM 075200 , *Weather Disc Associates, Inc.*, 4584 89th NE., Seattle, WA. 98115

Richman, M. B., 1986: Rotation of principal components. *J. Climatology*, **6**, 293-335.

Ropelewski, C. F. and M. S. Halpert, 1987: Global and regional scale precipitation patterns associated with the El Niño/Southern Oscillation. *Mon. Wea. Rev.*, **115**, 1606-1626.

Ropelewski, C. F. and M. S. Halpert, 1989: Precipitation patterns associated with the high index phase of the Southern Oscillation. *J. Climate*, **2**, 268-284.

Rossby, C.-G., 1939: Relations between variations in the intensity of the zonal circulation and the displacements of the semi-permanent centers of action. *J. Marine Res.*, **2**, 38-55.

Rossby, C.-G., 1945: On the propagation of frequencies and energy in certain types of oceanic and atmospheric waves. *J. Meteor.*, **2**, 187-204.

Sansom, H. W., 1951: A study of cold fronts over the British Isles. *Quart. J. Roy. Meteor.*, Soc., **77**, 96-120.

Saucier, W. J., 1959: Principles of meteorological analysis. *University of Chicago Press*, Chicago, 438 pp.

Sawyer, J. S., 1970: Observational characteristics of atmospheric fluctuations with a time scale of a month. *Quart. J. Roy. Meteor. Soc.*, **96**, 610-625.

Schubert, S, D., M. T. Suarez, and J-K. Schemm, 1992: Persistence and predictability in a perfect model. *J. Atmos. Sci.*, **49**, 256-269

Sela, J. G., 1982: The NMC spectral model. *NOAA Tech. Report NWS,* **30**, U. S. Department of Commerce, Washington, DC, 36 pp.

Sela, J. G., 1988: The new T80 NMC operational spectral model. *Preprints Eighth Conf. on Numerical Weather Prediction,* Baltimore, Md., Amer. Meteor. Soc., 312-313.

Shuman, F. G., 1989: History of numerical weather prediction at the National Meteorological Center. *Wea. and Forecasting*, **4**, 286-296.

Simmons, A., J.1974: The meridional scale of baroclinic waves. *J. Atmos. Sci.*, **31**, 1515-1525.

Simmons, A. J. and B. J. Hoskins, 1977a: The life cycles of some nonlinear baroclinic waves. *J. Atmos. Sci.*, **34**, 414-431.

Simmons, A. J. and B. J. Hoskins, 1977b: Baroclinic instability on a sphere: Solutions with a more realistic tropopause. *J. Atmos. Sci.*, **34**, 581-588.

Simmons, A. J., J. M. Wallace and G. W. Branstator, 1983: Barotropic wave propagation and instability, and atmospheric telecommunication patterns. *J. Atmos. Sci.*, **40**, 1363-1392.

Starr, V. P. and R. M. White, 1951: A hemispherical study of the atmospheric angular momentum balance. *Quart. J. Roy. Meteor. Soc.*, **77**, 215-225.

Stone, P. H., 1969: The meridional structure of baroclinic waves. *J. Atmos. Sci.*, **26**, 376-389.

Stone, P. H., 1978: Baroclinic adjustment. *J. Atmos. Sci.*, **35**, 561-571.

Stout, J. E. and J. A. Young, 1983: Low-level monsoon dynamics derived from satellite winds. *Mon. Wea. Rev.*, **111**, 774-798.

Sutcliffe, R. C., 1947: A contribution to the problem of development. *Quart. J. Roy. Meteor. Soc.*, **73**, 370-383.

Sutera, A., 1986: Probability density distributions of large-scale atmospheric flow. *Adv. Geophys.*, **29**, 227-249.

Thom, H. C. S., 1958: A note on the gamma distribution. *Mon. Wea. Rev.*, **86**, 117-122.

Teisserenc de Bort, L., 1883: Etude sur l'hiver de 1879-1880 et recherches sur position des centres d'action de l'atmosphere dans le hivers anormaux. Bureau centre de Meteorologique de France. *Annales*, 1881, pt. **4**, 17-62.

Thorncroft, C. D., B. J. Hoskins and M. E. McIntyre, 1993: Two paradigms of baroclinic-wave life cycle behavior. *Quart. J. Roy. Meteor. Soc.*, **119**, 17-55.

Tracton, M. S., M. O. K. Mo., W. Chen, E. Kalnay. R. Kistler and G. White., 1989: Dynamical extended range forecasting (DERF) at the National Meteorological Center. *Mon. Wea. Rev.*, **117**, 1604-1635.

Van Den Dool, H. M. and S. Saha, 1990: Frequency dependence in forecast skill. *Mon. Wea. Rev.*, **118**, 128-137.

Van Loon, H. and J. C. Rogers, 1981: The Southern Oscillation. Part II: Associations with changes in the middle troposphere in the northern winter. *Mon. Wea. Rev.*, **109**, 1163-1168.

Vautard, R. and B. Legras, 1988a: On the source of mid-latitude low frequency variability. Part I: A statistical approach to persistence. *J. Atmos. Sci.*, **45**, 2811-2843.

Vautard, R. and B. Legras, 1988b: On the source of mid-latitude low frequency variability. Part II: Nonlinear equilibration of weather regimes. *J. Atmos. Sci.*, **45**, 2845-2867.

Wade, J. E., K. Redmond and P.C. Klingerman, 1989: The effects of climate change on energy planning in the Pacific Northwest: Bonneville Power Administration Report. *Energy Resources Research Laboratory, Office of the (Oregon) State Climatologist and Water Resources Research Institute.* 152 pp.

Wagner, A. J., 1989: Medium- and long-range forecasting., *Wea. and Forecasting*, **4**, 413-426.

Walker, G., 1915: Correlations in seasonal variations of weather IV. *Mem. India Met. Dept.*, **21**, Part X, 17-60.

Wallace, J. M. and D. S. Gutzler, 1981: Teleconnections in the geopotential height field during the Northern Hemisphere winter. *Mon. Wea. Rev.*, **109**, 784-812.

Wallace, J. M and P. V. Hobbs, 1977: Atmospheric science: An introductory survey. *Academic Press, New York,* 467 pp.

Ward, F. and R. Shapiro, 1961: Meteorological periodicities. *J. Meteor.*, **5**, 635-656.

Webster, P. J. , 1981: Mechanisms determining the atmospheric response to sea surface temperature anomalies. *J. Atmos. Sci.*, **38**, 554-571

Webster, P. J., 1983: Large-scale structure of the tropical atmosphere, 235-275. From *Large-scale Dynamical processes in the atmosphere.*(Hoskins and Pearce) *Academic Press, London*, 397 pp.

Wilks, D. S. and K. L. Eggleston, 1992: Estimating monthly and seasonal precipitation distributions using 30- and 90-day outlooks. *J. Climate*, **5**, 252-259.

APPENDICES

APPENDIX A: Description of the Western District Precipitation Model

A.1. General

This model combines statistical inference and physical processes to compute expected five-day (pentad) precipitation for each of 60 western weather districts consistent with the pentad averaged 500mb height field. The input variable is a 500mb height field principal component (PC) amplitude vector of n components (corresponding to the first n PC's) where n may be set from one to seven. This vector, also called the circulation state vector (CSV), has a value for each pentad which may be either derived from an EOF analysis of the series of observed pentad height fields or forecast by a predictive model.

The non-variable inputs, loaded into the program data base from external files, include the seven EOF fields corresponding to the PC's, the US western terrain height data base and a number of files containing coefficients of regression lines for the inference of secondary variables necessary to the computation. These will described below.

The model is run in two stages: In the first stage, two components, or indices of precipitation (Io and Ic), proportional to orographic and baroclinic storm system contributions, are computed. In the second stage the indices are combined linearly, using district specific weights, to compensate for biases which are not determined explicitly. The weights are determined by regressing the observed monthly district precipitation record against the six model generated pentad index sums for the corresponding month.

As both precipitation and the proportional indices have gamma distributions and linear regression is best accomplished with variables of normal distributions, the indices and the observed precipitation series are mapped into corresponding normal distributions prior to regression and combination. The computed normalized precipitation is then remapped into its original gamma distribution. A full discussion of this process is given in section 4.3.1.

A.2. The primary variables

The primary variables for the model are the 500mb height and the 500mb u and v geostrophic winds computed from the input PC amplitude vector (CSV) and interpolated to the location of the district centroid. The computational domain for the height and wind fields is from 22°N to 70°N and from 106°W to 172°W and the Cartesian grid spacing is 3°.

a) The height field

The height field is generated from the CSV as follows:

$$Z_{i,j} = \sum_{n=1}^{7} P_n E_{i,j,n} \qquad \text{(A.1)}$$

where Z i,j is the geopotential height at i,j, Pn is the amplitude of the nth PC and E i,j,n is the value of the nth EOF field at i,j. (i=1,23, j=1,17, n=1,7). For a particular location the height is found from that at the four surrounding grid points by bilinear interpolation.

b) Winds

The geostrophic wind is computed on the interior grid (i= 2,21, j= 2,16) from:

$$u = -\frac{g}{f}\frac{Z_{i,j+1} - Z_{i,j-1}}{2\Delta y} \qquad \text{(A.2)}$$

$$v = \frac{g}{f}\frac{Z_{i+1,j} - Z_{i-1,j}}{2\Delta x} \qquad \text{(A.3)}$$

where $f = f_0 \sin(\phi)$ and ϕ is the latitude, Δy is the grid interval of 3° , 333 km, and $\Delta x = \Delta y \cos(\phi)$

On the domain edges (i=1, i=23 and j=1, j=17) the winds are extrapolated from those on the interior grid. For any particular location the winds are interpolated, bilinearly, from those at the surrounding four grid points.

A.3. Computation of secondary variables

A number of variables are inferred from the local primary 500mb winds and height assuming a linear model. These include the 850mb u and v wind components, sea-level pressure, P_0, mean relative humidity of the vertical profile, RH, and a vertical stability index, S. To determine the coefficients of the regression lines, records for each secondary variable were regressed against the 500mb Z, u-wind and v-wind components at each location for which the data had been recorded or could be derived. The data sets are cited in section 2.2.4. Winds, height or both were retained in the linear model for each secondary variable depending upon the incremental significance of the inclusion. The 500mb wind components were retained for 850mb winds, RH and P_0. The 500mb height was also included for the stability index. The general model for a variable, V, is:

$$V = a_0 + a_1 Z_{500} + a_2 u_{500} + a_3 v_{500} \qquad (A.4)$$

The coefficient sets for the 850mb winds and sea-level pressures were determined for each of 20 grid points in a 4x5 array with 5° spacing across the western US.(125°W, 120°W, 115°W, 110°W and 30°N, 35°N, 40°N, 45°N, 50°N). The humidity and stability index data were taken from records of RAOB profiles at Tucson and Winslow, AZ, Oakland, CA, Boise, ID, Great Falls, MT, Ely, Las Vegas and Winnemucca, NV, Salem and Medford, OR, Salt Lake City, UT and Quillayute and Spokane, WA. All linear model coefficients are archived in external files and read into coefficient arrays at the startup of the precipitation model program run. When a particular district is called up, local values for all of these coefficients are determined by linear interpolation from nearby tabulated values and local values of each secondary variable are then inferred from (A.4). The multiple correlation coefficients relating these secondary variables estimated by the linear model to actual values averaged about .8 for the 850mb winds, .75 for sea-level pressure, .6 for relative humidity and .4 for the stability index. While relatively little of the total variance was explained for the latter two variables, use of the modeled estimations was considered superior to the alternative of standard profiles.

A.4. Derived variables needed for the orographic index

To determine the orographic precipitation index for a given district the model requires not only the speed and direction of the 850mb wind through the district center and the corresponding terrain height profile along the wind vector but also the temperature and mixing ratio at various levels above the surface. These are derived from the primary and secondary variables as shown below.

A.4.1 Vertical mean (mass weighted) temperature, T

This is the temperature corresponding to the 1000mb-500mb thickness and is computed as follows:

(1) From the sea-level pressure, P_0, the 1000mb height, Z_{1000}, is computed from $Z_{1000} = H_o \ln(1000/P_0)$ where $H_o = 8321$ m is a characteristic low-level scale height, assuming a mean wintertime low-level temperature of 11°C.

(2) The 500mb-1000mb thickness, $\Delta Z = Z500 - Z_{1000}$, is then equated to the mean 500mb-1000mb temperature, T, from

$$T = \frac{g}{R_d} \frac{\Delta Z}{\ln\left(\frac{1000}{500}\right)} = 0.0493°c / m\, \Delta Z \qquad (A.5)$$

Departures from the assumed 11°C for a low-level temperature by as much as 10°C would have only a 9 meter effect on Z_{1000} assuming a SLP of 1030mb and an effect on T of only about 0.5°C. It is also noted that (A.5) is actually an expression for *virtual* temperature, T_V, but for the vertically averaged mid-latitude wintertime moisture content, which can not be expected to exceed about 3 g/kg, the worst case correction would be on the order of 1°C.

A.4.2 Construction of vertical profile of temperature

The vertical profile of temperature required for the model is constructed by applying computed vertical mean temperature and stability

to a standard profile obtained from an averaging of the RAOB profiles. The recorded temperature profiles range from the very stable to those approximated by the dry adiabatic lapse rate. For purposes of computation in this model stability is designated by an index, defined by differences in temperature at the 1000mb, 850mb and 500mb levels. The non-dimensional stability index, S, for a profile is a function of the temperature differences between the 1000mb and the 850mb levels and between the 850mb and the 500mb levels as compared to those for the moist adiabatic lapse rate. The stability index for this reference profile, which begins with $T_{1000} = 10°C$ (the mean base temperature for the computed profiles), is zero. Temperature drops between these levels are 7°C and 28°C, respectively. On this model scale, the stability index for a profile with a dry adiabatic lapse rate is designated -1, for which the equivalent temperature drops are 13.8°C and 38°C. Our model profiles have two slopes. Using the index to generate a temperature profile we use:

$$T_{1000} - T_{850} = 7.0° - 6.8° S \qquad (A.6)$$

$$T_{850} - T_{500} = 28.0° - 10.0° S \qquad (A.7)$$

The constructed profiles have a fixed relationship between the upper and lower slopes for a given stability index. In computing stability indices from *observed* profiles we combine (A.6) and (A.7), weighted by the pressure difference between levels to obtain

$$S = .0551(7.0° - T_{1000} + T_{850}) + .0625(28.0° - T_{850} - T_{500}) \qquad (A.8)$$

From an average of the wintertime soundings for the 13 RAOB stations the mean stability index, so defined, is +0.22, for which the temperature drops across the lower and upper layers are 5.2°C and 26°C, respectively. The stability indices, compiled from the RAOB station soundings and regressed against the 500mb winds and heights are used to obtain the weighting coefficients from which, in the model runs, the stability index may be inferred.

The next step in the computation is to determine temperatures at all levels which both conserve the profile slopes and also are consistent with the thickness temperature previously computed. To do so, an initial vertically averaged temperature, T_i, is approximated from the profile temperatures, considering an arbitrary T_{1000} of 0°C, and then each profile temperature is incremented by $T - T_i$. The resulting profile will then have

both the correct stability and a vertically averaged temperature corresponding to that specified from (A.5).

The computation of the pressure averaged temperature is by a finite difference approximation to the thickness equation and mean temperature equivalent.

$$\Delta Z = \frac{R_d}{g}\int_{p_2}^{p_1} T(p)\frac{dp}{p} = \frac{R_d}{g}\ln\left(\frac{p_1}{p_2}\right)\overline{T} \qquad \text{(A.9)}$$

$$\text{then:} \quad \overline{T} = \frac{1}{\ln\left(\frac{p_1}{p_2}\right)}\int_{p_2}^{p_1} T(p)\frac{dp}{p} \qquad \text{(A.10)}$$

This is the pressure weighted vertical mean which, in this model, is approximated by its finite level equivalent,

$$\overline{T} = \frac{1}{\ln\left(\frac{1000}{500}\right)}\sum_{l=1}^{4} T_l\frac{\Delta p_l}{p_l} \qquad \text{(A.11)}$$

summed over the 1000mb, 850mb, 700mb and 500mb levels.

For the districts above the height of the 1000mb level, the final temperature profile is truncated at Ps by linear interpolation. In conclusion of this section, it is noted that the constructed temperature profile is linear with two slopes: one from Ps to 850mb and the other from 850mb to 500mb. In later computations in the model the temperatures may then be interpolated, linearly, to intermediate levels.

A.4.3 The construction of the moisture profile

As stated in section A.3, the mean, or vertically mass-averaged relative humidity, RH, for a particular pentad and district is inferred from the 500mb u and v winds. Additionally, from the RAOB data, standard vertical relative humidity profiles, R(p), dependent on location but independent of time, are interpolated to each district location. As for the temperature profiles, the relative humidity profiles are estimated by computing an initial vertically averaged RH_i from the standard profile and

then adjusting each level value of the standard profile by RH - RH_i. RH_i is determined from:

$$RH_i = a_1 R_{1000} + a_2 R_{850} + a_3 R_{700} + a_4 R_{500} \quad \text{(A.12)}$$

where the weighting coefficients are the same as those used for computing the mean temperature as in (A.11).

Later in the model computation it is necessary to determine the mixing ratio at various levels. This is done by multiplying the saturation mixing ratio, w_S, by the relative humidity. The saturation mixing ratio is computed from the saturation vapor pressure, e_S, from the integrated form of the *Clausius-Clapeyron equation*, using the temperature at the level designated.

$$e_s = 6.11 Exp\left[\frac{L}{R_v}\left(\frac{1}{273} - \frac{1}{T}\right)\right] \quad \text{where } e_s \text{ is in mb.} \quad \text{(A.13)}$$

and

$$w_s = 0.622\frac{e_s}{p - e_s} \quad \text{(A.14)}$$

A.4.4 Accommodation for unexplained variance in relative humidity

As noted in Section 4.2, the model relating relative humidity to the 500mb winds explains about 30% of the variance. Considering the extremes in the 500mb configuration likely to be encountered, the model-computed pentad mean relative humidity may be expected to vary from a low of about 35% to a high of about 70%. Applied to the standard profile, as discussed in A.3, the maximum RH computed for any level may reach about 75%.

In an actual situation, for a given 500mb configuration, there is a considerable variability (the unexplained variance) in RH, not associated with differences in the 500mb flow, as bands of varying moisture content move across a district. For generally dry flow configurations individual soundings typically are observed with relative humidities at certain levels from as high as 60% to as low as near zero. For wet flow configurations, with strong southwesterly flow aloft, certain levels often become saturated.

The time averaged RH for such circulations, however, is on the order of 65%. As this corresponds, at a 10°C surface temperature, to a specific humidity of about 5 g/kg and a lifting condensation level of 1100 meters, the modeling of orographic precipitation from the mean RH alone would be unrealistically limited to the higher mountain ranges, such as the Cascades or Sierra Nevada.

For each topographical situation there is, thus, a threshold RH for orographic precipitation, in most cases never exceeded by the time averaged RH but often exceeded by particular RH values distributed about the mean. We model this situation by approximating this distribution as normal with a standard deviation measured from those of the actual soundings. To do this, 25 values of deviations from the mean are selected corresponding to the frequency of occurrence for such deviations. Specifically:

-1.80 σ	1 case	run #1
-1.36 σ	2 cases	run #2
-1.01 σ	3 cases	run #3
-.66 σ	4 cases	run #4
0.0 σ	5 cases	run #5
.66 σ	4 cases	run #6
1.01 σ	3 cases	run #7
1.36 σ	2 cases	run #8
1.80 σ	1 case	run #9

For each run of the model (nine per pentad), the computed pentad time averaged value of RH is modified by the coefficient times the RH standard deviation and the result is weighted by the frequency factor (number of cases), summed and then divided by 25. Of the 25 cases, an appropriate number will exceed the orographic threshold and at least some orographic precipitation will be modeled for even modest terrain height rises, such as the Oregon Coast Range, as would be expected in an actual situation.

A.5 The orographic precipitation mechanization

With the necessary variables inferred or calculated at the district centroid coordinates, the expected orographic precipitation for the pentad is computed by determining the lift, consequent pressure drop, resultant dry and moist adiabatic cooling and condensation for incremental layers in the air passing across the district. We employ a rigid-lid approximation at 250mb. Consequently, the upper portions of the air flow are not lifted as much as those near the terrain surface. The computation of this lift is described in section A.5.2. The computation of effective terrain elevation change is discussed below.

A.5.1 Effective terrain elevation change

A consideration of different terrain situations shows that elevation change consistent with orographic precipitation cannot be as simple as the difference between some start and end point along the air flow trajectory. For example, the district centroid might be on the highest elevation of the district with the start and end points of the trajectory at equal, lower elevations. Nevertheless, the air is lifted for the first half of its path and orographic precipitation may be expected over the windward portion of the district. Therefore, effective terrain height rise is calculated as the difference between the high point along the profile and the upstream start point. Furthermore, as the desired precipitation is not just along a line through the district centroid but across the entire district, a band average elevation is estimated by averaging the elevation at points 20 km to either side of the trajectory. The trajectory profile is 75 km long, its mid point on the district centroid, and oriented along the angle of the 850mb wind. The band average is taken at nine points along the trajectory to form the elevation profile. This point density is sufficient to capture the key elevations, considering the spatial resolution of the terrain model. Fig. A.1 illustrates the profile construction.

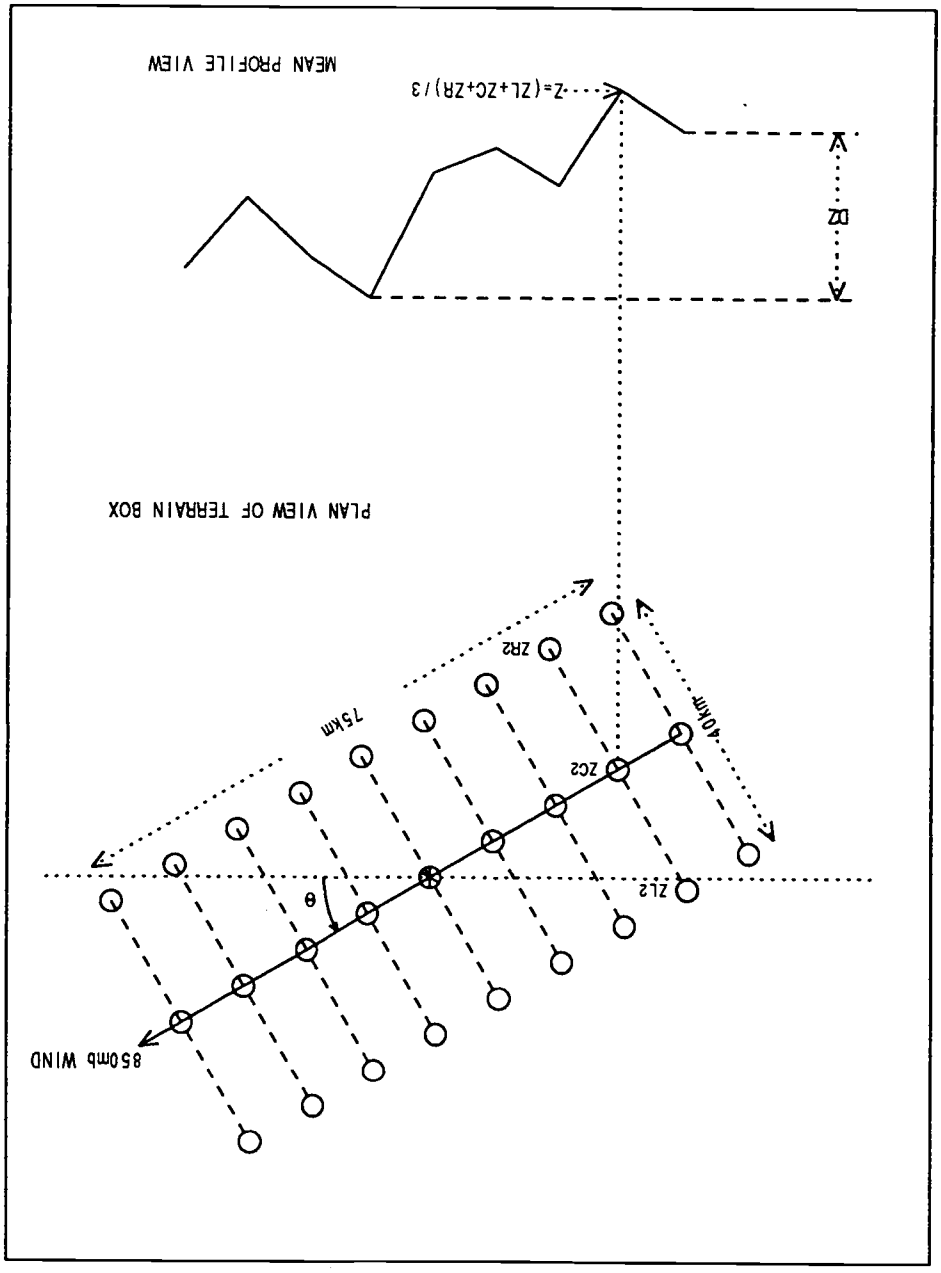

Fig. A. 1 Plan and profile views of geometry for determining topographic elevation change along track of 850mb wind.

A.5.2. Computation of atmospheric lifting

The air flowing over the terrain is approximated by 20 layers divided by sigma surfaces, all moving at the 850mb wind velocity. A discussion of the appropriate assumptions for this approximation is given in Section 4.2. As shown in Fig. A.2, the lift for each layer decreases with increased height above the terrain. At a surface elevation of sea-level, the sigma surfaces separating the layers are set such that the 1013mb to 250mb model tropospheric column is divided into 20 layers of equal pressure difference. As the air moves across terrain of varying elevation, the pressure at the bottom of each layer varies in proportion to that of the surface such that for the bottom of the nth layer, $P_n = P_s-(n-1)(P_s-250)/20$, where P_s is the surface pressure.

The surface pressure is computed as a function of SLP, terrain elevation and a scale height, Ho, calculated from the surface temperature as $H_o = 29.3\ T_s$. Then:

$$P_s = P_{1000} \exp (-Z_s/H_o) \qquad \text{(A.15)}$$

where $Z_s = Z - Z_{1000}$, and Z is the actual terrain elevation. As the terrain elevation changes, P_s changes and each level pressure P_n changes to a lesser degree in proportion.

Before the computation of elevation change across the district, the temperature and relative humidity of each of the 20 layers is interpolated from the original profile discussed in A.4. The mixing ratio for each layer is then computed from (A.13), (A.14) and RH. Next, the dewpoint for each layer is approximated from the layer pressure and vapor pressure (A. 14) from a rearrangement of the *Clausius-Clapeyron equation*,

$$T_d = \frac{1}{\frac{1}{273.15} - \frac{R_v}{L} \ln\left(\frac{e_s}{P_n}\right)} \qquad \text{(A.16)}$$

where T_d is in degrees K and e_s and P_n are in millibars.

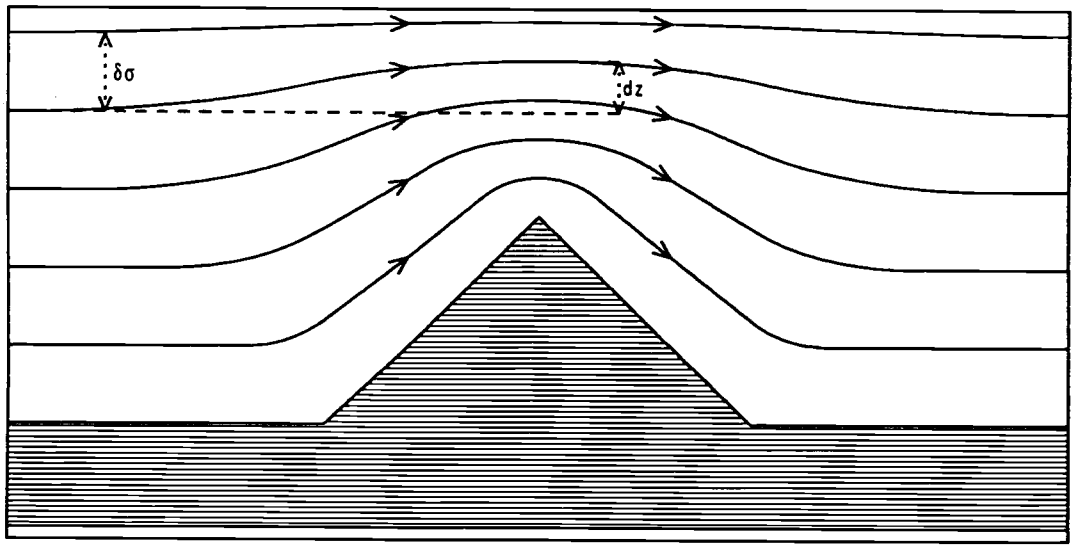

Fig. A. 2 Profile view of air flow over ridge showing change in elevation rise as function of terrain height and sigma surface.

After setting these initial conditions at the start of the trajectory the pressure change is computed for each layer as a consequence of the effective elevation change as discussed above. A new trial temperature, T_1 is set assuming a dry adiabatic lapse rate from:

$$T_1 = T_0\left(\frac{p_1}{p_0}\right)^{\frac{R}{C_p}} \qquad \text{(A.17)}$$

where P0 and P1 are the initial and final layer pressures and T_0 is the initial temperature.

If T_1 is greater than T_d the routine returns with no condensation. If T_1 is less than T_d the fall of temperature below T_d is computed from an approximation of the moist adiabatic lapse rate. The difference between the dry and moist lapse rates is a complex function of pressure and temperature. Here, it is approximated as a linear function of temperature so that the final temperature, T_f, is modeled as:

$$T_f = T_d - \left(\frac{353 - T_1}{393}\right)(T_d - T_1) \qquad \text{(A.18)}$$

Over the range of pressures and incremental temperature changes encountered in the model, this function provides an approximation to about a 1° C accuracy of the final temperature as would be computed on the pseudo-adiabatic diagram.

With this final temperature, a new saturation mixing ratio is calculated from (A. 13) and (A. 14). The difference between the original and final mixing ratios represents the water condensed from this layer over the entire trajectory. The water loss sum for all the layers is the total condensation from the entire column over the trajectory. Multiplying by 850mb wind speed then yields the orographic precipitation rate.

A. 6. Convective augmentation

We model precipitation due to convective instability as an augmentation to that produced by orographic lifting, due to the influence of

orography on the probability of convective precipitation for any particular vertical stability of the atmospheric column.

The modeling is a parameterization of three influential factors appropriate to the scale of the model. These are air mass stability, moisture content and elevation change of the atmospheric column base due to passage over terrain. We consider convective augmentation proportional to the moisture content for, while it is actually more complex, involving positive feedback due to its effect on the energy of the overturning, we lack the temperature and moisture profile detail necessary for the computation of its influence. The relationship between stability and elevation change as factors in the probability of convective overturning is highly non-linear, even for the greatly simplified model profiles. To formulate the relationship we examine the behavior of various ensembles of profiles whose mean vertical stability (stability index) is of some particular value, for various elevation change forcing. We conduct trial convection experiments with each member of the ensemble and for different elevation change forcing using a numerical model approximation of the pseudo-adiabatic diagram and determine the proportion of ensemble cases, for various stability index-elevation rise combinations, which should result in convection.

Eight ensembles of 25 profiles each were taken from the western RAOB data with mean stability indices stratified in bands of .25 stability units each and with band centers ranging from -0.25 to +1.50. These were tested for convection using forced base elevation rises of 0, 250, 500, 1000 and 2000 meters. The first 25 cases from each stability index band were extracted from the approximately 20,000 profiles in the NCAR archived data base. These 200 cases were subjected to a program which simulated the lifting of air parcels at nine 50mb intervals at the dry adiabatic lapse rate to an intersection, if any, with the Td profile and along an approximate moist adiabat thereafter. The temperature of each parcel was then compared with the environmental temperature at that level and, if four or more of the nine parcels had temperatures greater than the environmental, the profile was scored as convective. Table A.1 shows the number of cases out of a possible 25 for which convection was determined as a function of mean stability index and forced elevation change. To include the effect of mechanical (wind generated) turbulence, which would

be expected to induce lifting in addition to that from terrain rise, we also added a 250 meter lift to all cases. This is 25% of the nominal boundary layer thickness and appears to provide the right order of initiating perturbation without which convection would not be possible for flows over flat terrain(for air masses which are not mechanically unstable).

Table A. 1 Number of cases out of 25 experiments for which convection resulted for different stability indices as a function of forced elevation rise

elev index	0	250	500	1000	2000
-.25	25	25	25	25	25
0.00	24	24	25	25	25
0.25	20	22	23	24	25
0.50	15	17	19	21	23
0.75	10	12	13	16	19
1.00	4	6	7	10	13
1.25	0	0	2	4	7
1.50	0	0	0	0	2

It may be noted that the probability of convection was found to be greater than that expected from the stability index. This is due to the frequent occurrence of both high-level and shallow low-level layers of stable air that raise the *computed* mean stability index of an otherwise unstable profile. The high-level stability is often found to cap unstable polar maritime air masses at levels of 550mb-650mb, still having unstable air of sufficient depth to allow the tops of wintertime convective clouds to become glaciated, the condition for significant precipitation. The low-level stability is normally the result of the 1200Z early morning observations, about half of the total, which often have a cooled surface layer and a low-level temperature inversion with little influence on convection above it. Accordingly, and as verified by the trial convection experiments, the stability index, computed from the surface, 850mb and 500mb levels, is

biased and air masses with mean profile stability indices of +0.6, for example, have an approximately even chance of convective activity. By plotting the data from Table A. 1, as shown in Fig. A. 3, we find a non-linear relationship between the stability index and the probability of convection for various forced elevation changes, which can be well represented by a family of sigmoid-like curves. The lateral (stability index) separation of the curves due to differences in forced elevation change appears to be independent of the stability index and may be modeled as a bias, SB, which can be represented as a logarithmic function of the forced elevation change. Each curve can then be considered as the same function of a stability index altered by the elevation bias, x, such that x = SI + SB. Then, the matching sigmoid function may be determined empirically from the constraints of the data. We designate the general function for the probability of convection, Pc, as

$$Pc = a(\exp(-bx^2) - c) \qquad \text{(A. 19)}$$

where a, b, and c are to be determined. The bias is set so that x is greater or equal to zero and SB, for the zero elevation case, is -0.2. From the data points for this case we see that for x = 0, Pc approaches 1. Then, from (A. 19) we obtain the relation a = 1/(1 -c). Next, we note that the probability of convection cuts off at about SI = 1.2 or x=1.4. Again, from (A. 19) we obtain the relation b = -ln(c)/1.42. To determine c, these relations are substituted back into (A. 19) and some intermediate data point is selected. We use, say, Pc = 0.40 (10 cases out of 25) at a value of x of 0.95 (SI = 0.75) for the zero elevation set. Substituting, we find an equation for c alone as

$$c^{.46} - 0.6c - 0.4 = 0 \qquad \text{(A. 20)}$$

This is solved, numerically, to obtain c = 0.2997. Then a = 1.428 and b = .6148.

We now must derive, by a similar method, an empirical expression for the stability bias, SB, which we have set, for convenience at -0.2 for a zero elevation change and, noting that the data configuration, -.20, -.12, -.06, +0.05, and 0.20 for ΔZs of 0,250,500,1000 and 2000 meters, respectively, suggests a logarithmic function. We use the general form:

$$SB = -0.2 + a\left[\ln\left(\frac{\Delta Z + Z_0}{b}\right) - 1\right] \qquad \text{(A.21)}$$

and the constraints from the data to evaluate a, b and Zo. For zero

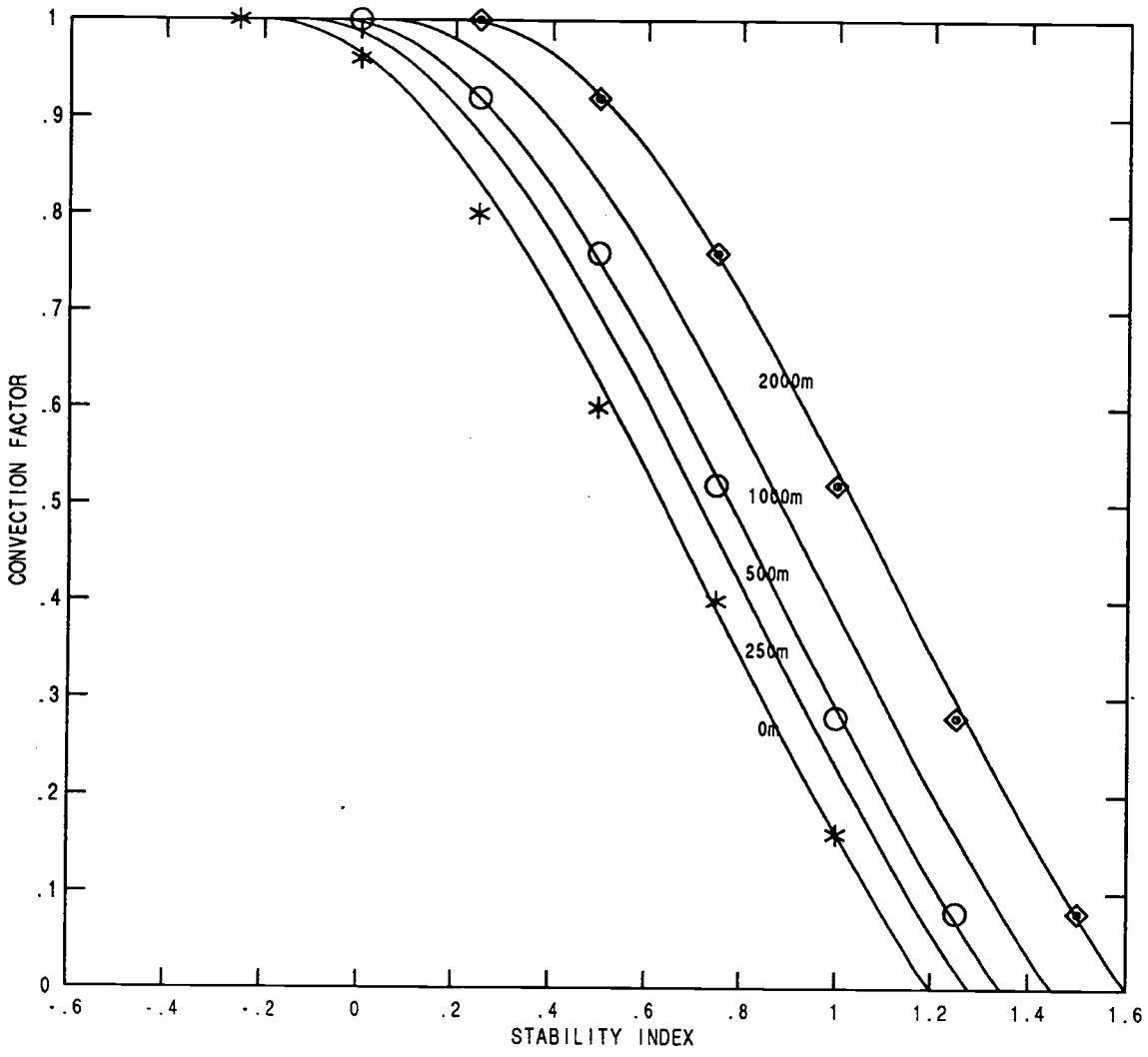

Fig. A. 3 Plot of data from Table A. 1 of convection factor vs. stability index showing match of empirical convection function to data for various elevation changes.

elevation change, the value within the brackets must also be zero, hence Zo/b = e. Then, from any other two elevation change data pairs, say for 500 and 2000 meters, we obtain two equations in a and b which can be reduced to a single equation in a:

$$4e^{\frac{0.94}{a}} - e^{\frac{1.4}{a}} - 3e = 0 \qquad \text{(A. 22)}$$

This is solved, numerically, to yield a=0.399. Then, by substitution, b = 428 and Zo =1163 m.

With the stability bias and convective probability functions thus determined, empirically, to match the experimental data points, we may generate the model curve family, which, as shown in Fig. A. 3, verifies that the functions are representative and can be used in the model computation of convective precipitation.

A. 7 Inclusion of convective precipitation in the orographic index

Before combining the convective precipitation component with the orographic, there are several questions which must be resolved. It should be determined whether or not the additional complexity introduced actually improves the performance of the model as compared to the observations and, if so, is there some additional proportionality factor relating the two components which should be introduced.

From the monthly district precipitation record there is no way of isolating observed convective precipitation events to test the model directly. We know, however, that the record must include cases for which convection has increased the total precipitation. Then, if the model results are better correlated with the observations by including the convective portion of the model, the convective augmentation is an improvement. Furthermore, by varying the proportional contribution of convective precipitation to the orographic index and comparing correlations of the orographic index with the observations, the optimum proportionality factor may be determined as well.

This experiment was made, varying the proportionality constant from zero (no convection computed precipitation added) to 2.0, in a series of nine runs (0.,.3, .6, .8, 1.0, 1.2, 1.4, 1.7 and 2.0). The correlations were averaged

across the districts and compared. The resulting correlations were .52, .56, .59, .61, .62., .60., .58, .57 and .55 respectively. With the broad maximum at 1.0, it was determined to combine the orographic and convective contributions equally. It should be noted that this result does *not* imply that the average contribution of convective precipitation equals that of the orographic component. In fact, in the majority of cases for which the model indicated orographic precipitation, the model computed stability index was too high for the inference of convection and the total model convective precipitation contribution was considerably less than that of the orographic component. It does imply, however, that the model computations for the two components appear to be in the correct proportion.

A. 8. Computation of the baroclinic index

As discussed in Section 4.2.2, the precipitation resulting from dynamic lifting associated with extratropical disturbances developing along the baroclinic zone can be considered as a function of the strength and configuration of the jet and of the location of the target district relative to the jet axis. The nature of this function is derived from a consideration of the theoretical studies discussed in Section 4.2.2, primarily that of Simmons (1974), and two observational studies. The first (Anderson and Gyakum, 1989) includes observations of storm tracks in relation to the axis of the belt of maximum 500mb winds by and the second, by Lim and Wallace (1991), yields representative scales of height and vertical motion fields for baroclinic disturbances from simulations by GCMs. We also include the results of our own study of Oregon precipitation patterns associated with the tracks of baroclinic systems (Appendix B).

In summary, these studies indicate that baroclinic storm precipitation can be modeled by incorporating in the algorithm the following factors: (1) The expectation of occurrence of baroclinic systems increases with the strength (maximum wind speed) of the jet. (2) The precipitation rate increases with the rate of growth of the system and this is also a function of the jet strength. (3) The center of the precipitation

pattern is slightly to the north (left) of the track of the surface center. (4) The meridional positions of the tracks of the surface centers average about 3° north of the pentad average latitude of the 500mb wind maximum, called the "jet" hereafter in this appendix for convenience, and are distributed with an approximately normal distribution with a standard deviation of about 5°. (5) The width (meridional) scale of the precipitation pattern is less than that of the height perturbation and both are limited by the width of the baroclinic zone; the meridional scale also appears to be a function of latitude.

A.8.1 Theoretical and observational basis for the baroclinic precipitation algorithm parameters

From the Anderson and Gyakum (1989) study of cyclone tracks for various large-scale 500mb flow patterns it can be seen that for zonal flow, at least, the tracks are typically initiated near or slightly south of the 500mb flow maximum. By two days after their detection, however, the storm centers have moved an average of about 3.5° to the north of the flow axis and this northward departure increases with further development. This displacement from the averaged jet axis corresponds to a time of near maximum growth (Thorncroft et al., 1993),with heavy precipitation, and we consider it a significant factor in determining the displacement of the precipitation band center from the jet in our precipitation model.

Lim and Wallace (1991) have studied mid-Pacific baroclinic systems using regression analysis. Their results show mean meridional scales for the height field perturbation and vertical velocity fields to be approximately 8° and 5° of latitude, respectively. We consider the latter figure to be a reasonable surrogate for the scale of the precipitation field but also require an algorithm to modify this scale as a function of latitude. The theoretical study of meridional scales of baroclinic systems by Simmons (1974) is helpful in this regard. He determines that the meridional scale of the height field perturbation, Y, should be the geometric mean of the radius of deformation, L, and a length scale, R, related to the curvature of the cross-jet velocity profile.

Then:

$$Y = \sqrt{LR} \tag{A.23}$$

where

$$L = \frac{NH}{f} \tag{A.24}$$

and

$$R = \left(U_{\max} \Big/ \frac{d^2u}{dy^2} \right)^{\frac{1}{2}} \tag{A.25}$$

where the curvature of the velocity profile is restricted to that of a quadratic. The *Brunt-Väisälä frequency*, N, is a function of vertical stability and its relationship to latitude is not consistent. The scale height, H, can be related to latitude through the mid-latitude dependence of vertically averaged temperature, while f is proportional to the sine of the latitude. As an example of the dependence of meridional scale on latitude let us assume a parabolic velocity profile with a jet width of 12°, a U_{max} of 50 m/s and a nominal N^2 of 0.00015 sec^{-2}. With the scale height determined as a function of latitude from the Palmen and Newton (1969) data of 8120 m and 7580 m for 30°N and 50°N, respectively, the meridional scale is 10.2° at 30°N and 7.9° at 50°N by the above formulation.

As discussed above, the meridional (width) scale of the precipitation band in mid-Pacific storms appears to be approximately 70% of that of the pressure perturbation; however, this is still considerably wider than the precipitation bands commonly observed with developing baroclinic systems along the west coast of the United States. This may be due to a large proportion of such storms being in an early stage of development, with waves of small amplitude. If true, this would require that a smaller scale be used in the precipitation model for representing baroclinic precipitation. Accordingly, we conducted a separate study, compositing precipitation from a dense network of precipitation reporting stations in reference to 52 individual baroclinic storm tracks which transited Oregon during 12 winter seasons (1976-1987).

This study, which is discussed in detail in Appendix B, showed that the typical baroclinic precipitation band is roughly normal in its cross-track distribution, with a standard deviation of 1.24° of latitude and a center 0.87° left (north) of the storm track. As further discussed in

Appendix B, the addition of the variances and lateral biases of the storm track in reference to the instantaneous jet position and also those of the instantaneous jet in reference to the pentad averaged jet resulted in a combined bias of 3.3° to the left and a standard deviation of 5.3°. While this standard deviation is comparable to the meridional scale of the precipitation patterns observed by Lim and Wallace (1991), it is only so due to the diffusion caused by the uncertainty in the instantaneous jet position. Nevertheless, this larger meridional scale (σ) due to the inclusion of these uncertainties is appropriate for implementation in the model. When compared with different precipitation width-scales by regressing the model computed baroclinic index against observed precipitation, a single σ value of 5.5° yielded slightly higher correlations than did values of 5.0° or 6.0°. Moreover, the addition of the theoretically determined latitude dependence, such that σ was made to vary between 6.0 at 34°N and 5.0° at 48°N (in proportion to the theoretical latitude variation), further improved the correlation.

A.8.2 Implementation of the baroclinic algorithm

A cross-jet velocity profile is determined by constructing a line through the district centroid perpendicular to the closest jet axis and determining the wind velocity at 0.2° intervals. The distance, d, between the position of the velocity maximum and the district is determined. The ratio between the maximum velocity, Vmax, and that at a point 6° from the peak (on the side of the district), Vs, is a measure of the profile curvature such that C = Vs/0.85Vmax, but is limited to a maximum of 1.0.

The width-scale, σ, is approximated by a linearized application of the latitude variation discussed in the previous section and further modified by the profile curvature factor. Specifically :

$$\sigma = C\left[6.0 - \left(\frac{lat - 34^\circ}{14^\circ}\right)\right] \qquad \text{(A.26)}$$

Then, biasing d by the offset of b=3.3° (from the observations), the sign depending on which side of district is the jet, a preliminary value of the baroclinic index is computed from

$$I_0 = 0.035 \exp\left[-\frac{1}{2}\left(\frac{d \pm b}{\sigma}\right)^2\right] \qquad \text{(A.27)}$$

As discussed in Appendix B, we have found greatly diminished baroclinic system occurrence for meridional flow regimes for which the inclination of the streamlines to the latitude parallels exceeds 45°. We incorporate this behavior in the model by including a cosine-squared factor going to zero at an inclination of 75°:

$$I_c = I_0 \cos^2\left(\frac{90\alpha}{75}\right) \qquad \text{(A.28)}$$

where α is the inclination angle of the streamlines.

As discussed in the previous section, the values of many of the constants and other parameters were adjusted by repetitive runs of the model, correlating the computed baroclinic index, Ic, with a portion of the actual district precipitation records, using the actual 500mb pentad height fields as model inputs.

APPENDIX B: A Study of Oregon Precipitation Patterns Resulting from Passages of Baroclinic Storm Systems

In order to better model the effect of the configuration and intensity of the Polar Jet on precipitation patterns we have compared both daily and pentad averaged 500mb circulation configurations with the daily precipitation record for 103 reporting stations in Oregon. The stations selected form a grid of approximately even density across the state and the resultant precipitation patterns associated with the tracks of individual storm systems are indicative of the distribution of precipitation to be expected. We distinguish, here, between the statewide, light to moderate precipitation associated with large, fully developed or decaying systems and the smaller scale, more intense precipitation pattern associated with developing baroclinic disturbances. From observation of these systems it appeared that while there were relatively few that affected any given region, as compared to the larger decaying systems, they had a disproportionate effect on the seasonal precipitation totals.

The purpose of the study was to quantify this effect, to associate the frequency of occurrence of the baroclinic storms with different large-scale circulation configurations and to determine the lateral scale and centers of their related precipitation bands in relation to the 500mb axis of maximum winds. The precipitation data, extracted from the records of the Oregon State Climatologist, extended from January, 1976 through December, 1987 for the months of November through March. For each of the 1815 days in this series, the surface and 500mb analyses were examined.

B.1 The distribution of precipitation associated with baroclinic systems

The occurrence of baroclinic systems was determined by the presence of a surface depression in advance of an open 500mb trough. These systems were usually, but not invariably, associated with an open-wave frontal pattern. The presence of a frontal occlusion, closed 500mb low over the surface low, or even a deep 500mb trough vertically aligned over the

surface low disqualified the system as baroclinic. For the 12 winter seasons there were 120 days for which baroclinic systems were detected between 40°N and 47°N and between 125°W and 117°W. Of these, only 52 systems had tracks that resulted in precipitation over a sufficient portion of the Oregon reporting station grid to be useful in our analysis. These storms, however, were found to be responsible for about 10% of the total winter precipitation. When normalized (by dividing by the number of days for which baroclinic systems transited at least a portion of Oregon and, in contrast, by the number of days for which they did not), the relative "proportional" expectations of precipitation were found to be 0.78 and 0.22, respectively. For a specific reporting station, Corvallis, it was found that days with heavy precipitation were associated with days of baroclinic transit. For the 12 winter seasons there were 1086 days for which there was measurable precipitation. Table B.1 shows the distribution of these days by precipitation amount and association with baroclinic system transit.

Table B.1 Days for 12 winter seasons in Corvallis, Oregon for which precipitation exceeded certain values categorized by occurrence of baroclinic system transit across state. Precipitation in inches

	total	Baroclinic	non-baroclinic
total days	1815	52	1763
meas precip	1086	52	1034
precip < 1.00	1030	7	1023
1.0<precip<1.5	38	31	7
1.5<precip<2.0	11	7	4
precip>2.0	7	7	0

It can be seen that the great majority of precipitation events are of less than 1 inch and also that the few major precipitation events are increasingly likely to be associated with the passage of baroclinic systems as the precipitation category becomes greater.

The tracks of the individual baroclinic systems were approximated by straight lines with slopes and latitudes at the crossing of the 125°W meridian estimated from successive surface analyses. For each track, the

perpendicular distance of each of the 103 Oregon reporting stations was determined (the cross-track distance) and precipitation from each station was accumulated in 40 cross-track distance bins. This procedure was repeated for each system to form a composite cross-track distribution. All station precipitation contributions were normalized by division by the mean daily precipitation for that station during the November-March winter season. The result is a precipitation distribution for a "canonical" baroclinic system, typical of those transiting Oregon. The meridional extent of the pattern is less than that of the "generic" system found in the mid-Pacific by Lim and Wallace (1991), perhaps due to being, on the average, at an earlier stage of development.

Figure B.1 is a bar chart showing the composite distribution of precipitation relative to the track of the system low pressure center. The cross-track distances are in degrees of latitude to the left of the track (designated in the figure as "north"). The values of precipitation on the ordinate are relative, for there is no reasonable way of interpreting an absolute value from an accumulation of normalized station precipitation increments. The distribution is seen to be approximately normal, with a slight positive skewness (computed to be +0.085) and a negative (flattened) kurtosis of -0.989 (referenced to zero for a normal distribution). The mass weighted center of the distribution is .87° left of the track and the standard distribution of the pattern is 1.24°.

We have also found and composited the latitude of the 500mb axis of maximum winds relative to the storm track at 123°W. The mean "jet" relative latitude is shown on the figure although, for the sake of clarity, the complete distribution is not. This distribution is peaked, somewhat, at the mean (a kurtosis of +2.5) with long tails, particularly to the south (a skewness of -0.5). The mean is 0.25° to the right of the storm track and the standard deviation is 2.54°. In the model, we compute the configuration of the pentad 500mb wind maximum rather than that of an individual 500mb analysis. This contributes an additional uncertainty in the position of the storm track, in reference to the pentad wind axis maximum. Comparing the individual "jet" positions with that of the pentad jets, we find the mean position of the individual jets to be 2.2° north of the pentad jet and with a standard deviation of 4.5°.

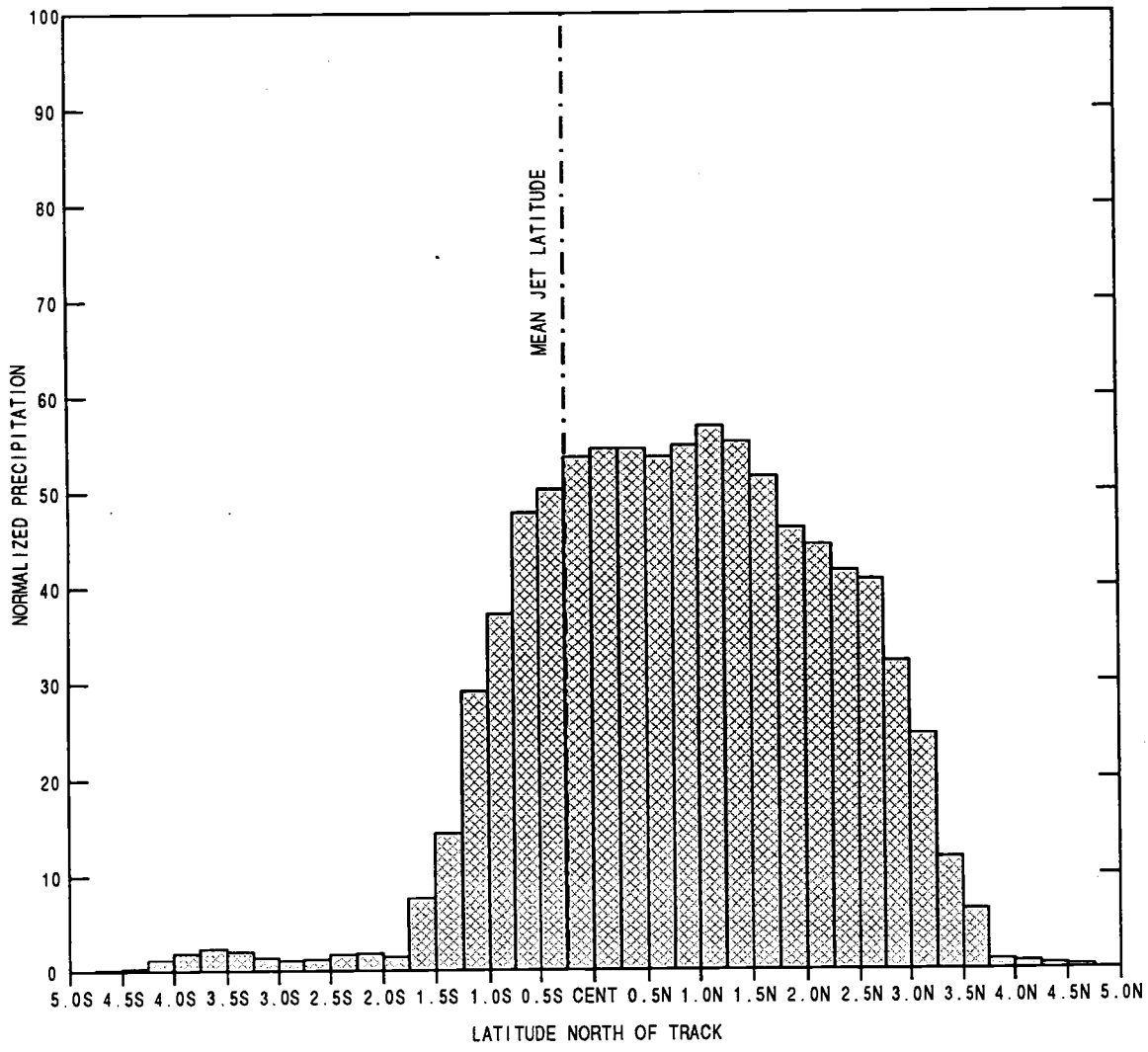

Fig. B. 1 Bar chart of distribution of precipitation across track of composite of 52 baroclinic storm systems transiting Oregon for the 12 winter seasons from 1976 through 1987.

In application to the precipitation model, we may summarize these findings by observing that a knowledge of the position of the pentad "jet" axis is useful in locating the track of many (but not all) of the expected baroclinic systems and also of the position and relative width of the expected precipitation associated with these systems. The lateral extent of the baroclinic precipitation band used in the model must be increased by the uncertainty in the relative jet position by summing the respective variances. The result is a precipitation center offset (from the jet) of 3.3 ° to the left and a precipitation scale-width of 5.3°. It is noted that the findings of this study apply to Oregon and modifications must be considered for other regions. As discussed in Appendix A, such modifications, based on a number of both theoretical and observational studies (also discussed in Chapter 4), include the effects of latitude dependence and also jet strength and width.

B.2 Circulation configurations and Oregon precipitation

In addition to the determination of baroclinic system tracks for the 12 winter seasons of this study, we have found it instructive to compare both precipitation and the occurrence of baroclinic systems with the daily configuration of the long-wave circulation pattern. While there is an apparent continuum of flow configurations, we have found it useful to categorize them into a number of "types", related to the Caltech circulation types (Elliot, 1944) but with a positional reference to Oregon for which the precipitation comparison is made.

The low-amplitude long-wave troughs and ridges in zonal flow appear to be less persistent than are their high amplitude counterparts in meridional flow and have less relative effect on precipitation. Vigorous short-wave disturbances are observed to propagate rapidly through the long-wave pattern with little difference in precipitation intensity or developmental rate due to position relative to the long-wave crests or troughs. For this comparison, then, it is convenient to consider all zonal flow situations as a single category (I). We limit this first category to cases for which the maximum north-south inclination of the streamlines is less

than 45° and with the further restriction that a significant portion of the flow must be over Oregon. In practice, we find that when the axis of maximum winds is north of 50°N there is little zonal flow component over Oregon. For most such cases however, this condition is associated with meridional flow.

In contrast to zonal flow, the high-amplitude long-wave troughs and ridges of meridional flow are more often quasi-stationary. Moreover, as the phase of these long-waves relative to a particular region has a pronounced effect on the weather regime, it appeared appropriate to further categorize meridional flow by wave-phase relative to the target area (Oregon). We use the 121°W meridian as our reference longitude.

Category II is designated for those cases in which the ridge axis is closer to the reference longitude than are either the ascending or descending nodes. Upper winds over Oregon are generally light and anti-cyclonic; there is little expectation of rain. Cases for which the ridge axis is sufficiently far to the east that the ascending node is closer to the reference longitude than are either the ridge axis or the western trough are designated as Category III. Although Oregon is generally under a strong southwesterly flow for this condition, precipitation appears to be less than for westerly zonal flow and is often confined to the immediate coastal area.

For cases in which the trough line is nearest the reference longitude we also find that there is a strong tendency for a developing tilt to a NE-SW axis. The southwest extremity of the trough usually becomes a "cutoff " low with northeasterly flow over Oregon. While this situation commonly results in rain over Southern California and Arizona there is generally little rainfall in Oregon despite the subnormal 500mb heights. We designate this flow as Category IV.

With the ridge over the eastern Gulf of Alaska but the descending node to the east of the reference longitude, the upper flow over Oregon is generally anti-cyclonic with the streamlines over land. This configuration, which we designate as Category V, is only slightly wetter than that of Category II. Our final Category (VI) is also for flows from ridges over the Gulf of Alaska but with the descending node to the *west* of the reference longitude. The flow over Oregon is normally cyclonic and the streamlines are over the ocean. While precipitation is seldom heavy for

this category, 500mb heights are low, the air often unstable and snow levels occasionally drop to sea-level. An example of each of these circulation categories from the pentad 500mb height fields is shown in Fig. B.2.

We have assigned each of the 1815 analyses of the 500mb height field to one of these circulation categories and have associated them with two daily values of Oregon precipitation, one east of the Cascades and the other to the west. Each value is a composite of 20 representative stations, approximately evenly spaced across the region and normalized by division by that station's mean daily wintertime precipitation. Table B.2 is a summary of the results which also includes the number of baroclinic systems (discussed in the previous section) corresponding to each circulation category.

Table B. 2 Precipitation of eastern and western Oregon associated with different circulation categories. Column two is the number of occurrences of category out of 1815 days. Columns three and four represent proportion of total precipitation for each category for eastern and western Oregon respectively, normalized by number of days in category. Column five is number of baroclinic systems for 12 winter seasons in each category.

Category	Occurrences	Eastern Oregon	Western Oregon	Systems
I	622	.3387	.4399	45
II	411	.0452	.0584	1
III	281	.2226	.2350	5
IV	173	.0978	.0558	1
V	181	.0717	.0660	0
VI	177	.1705	,1448	0

There appears to be little difference in the response of precipitation to various circulation categories east and west of the Cascades. There is a slightly higher expectation of precipitation in eastern Oregon for the northerly flow categories of IV, V, and VI, perhaps due the greater

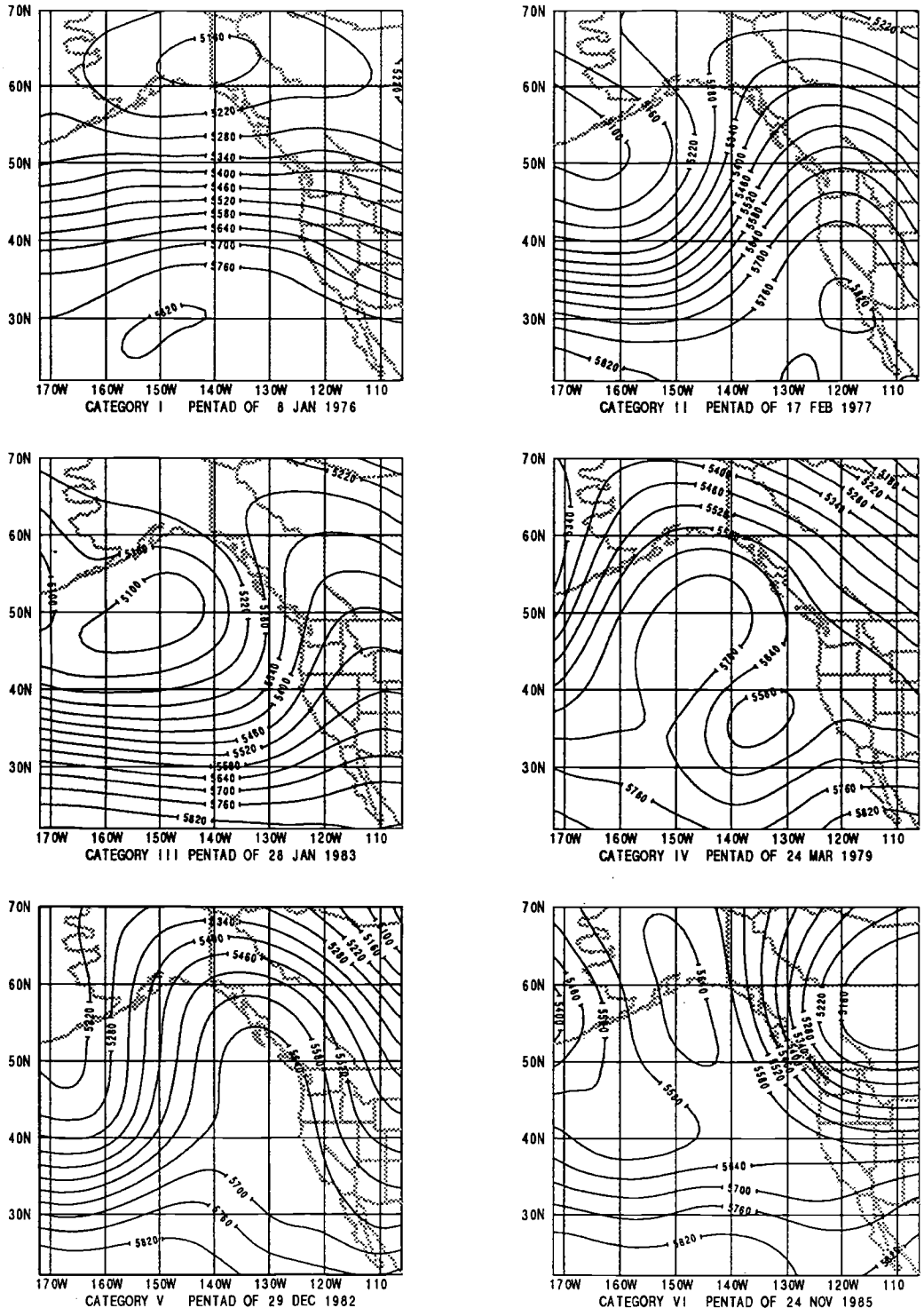

Fig. B. 2 Examples of pentad 500mb height fields corresponding to circulation types. Circulation categories I to VI are discussed in text.

distance from the western ridge, and a greater expectation of precipitation in western Oregon for Category III, perhaps due to the closer proximity of the western trough. The difference in the Category I response may be due to the orographic effect of the Cascades, with the greater probability of forced rise in the west for zonal flow.

The great preponderance of baroclinic systems in westerly flow and the total absence of such systems in the northwesterly flows of Categories V and VI in particular, is a little surprising. Baroclinic development in similarly directed flows along the lee slopes of the Rockies is commonly observed. One possible contributing effect may be that of the cross-flow topographic height gradient, which is in the opposite direction for the two cases. Another may be that the low-level cross-flow temperature gradient is generally greater east of the Rockies. For flows crossing the Rockies and hence subjected to vertical stretching on descent, there is also the vorticity enhancement effect (lee cyclogenesis) to contribute to system development. Furthermore, as discussed by Merkine (1975), the temperature field is concentrated and the vertical shear intensified on the lee side of the range.

We incorporate this apparent dependence of baroclinic system occurrence on flow direction into the precipitation model by reducing the expectation of baroclinic precipitation for flows inclined to the east-west direction. We reduce the expectation by one half at 50° and to zero at 75° inclination using a cosine squared function.

APPENDIX C: Glossary of Special Terms

Ageostrophic Wind. The component of wind for which the Coriolis force is not in balance with the pressure gradient force; cross isobaric.

Baroclinic. Situation for which the wind field changes with height. Associated with a horizontal gradient in the mean temperature field.

Barotropic. Situation for which the wind field is invariant with height. No horizontal gradient in the mean temperature field.

Beta-Plane (β-plane). A linear approximation to the sinusoidal variation of the Coriolis force with latitude ($f = 2\Omega \sin(\text{lat})$) represented by $f = f_o + \beta y$, where y is the north-south distance and β and f_o are constants.

Categorical Forecast. A forecast, usually of precipitation or temperature, for which the forecast variable is characterized by category (e.g. rain or no rain). More recently used as a component of a Probabilistic Forecast depicting the probability of precipitation being in the above normal or below normal category over some designated region.

CSV (Circulation State Vector). Used in this paper as an ordered array of real numbers, each representing the amplitude of the principal components which can be summed to approximate a 500mb height field for a particular pentad. The CSV's used here are members of a time-series.

Dynamic Predictability. The ability to predict a future state of the atmosphere by extrapolating its variables using the appropriate equations of motion and thermodynamics which relate incremental changes to instantaneous variable values.

ENSO (El Niño-Southern Oscillation). The El Niño, which was historically considered a local phenomenon (off the west coast of tropical South America) with unusually warm ocean surface water, was found to be connected to the later discovered Southern Oscillation for which unusually high surface barometric pressures over the western tropical Pacific were related to low pressures over the eastern tropical Pacific and conversely. These two phenomena, together with anomalous winds, sea surface temperatures, sea level elevations, currents and rainfall patterns are now considered as a single entity.

EOF's (Empirical Orthogonal Functions). The normalized eigenvectors of the covariance matrix formed by comparing, point by point, the time series of a field.

FGGE (First GARP Global Experiment).

GARP (Global Atmospheric Research Program).

GATE (GARP Atlantic Tropical Experiment). An intensive 3-dimensional data collection effort off the coast of North Africa made with closely spaced ships using extensive radar coverage and with frequent radiosonde launches

Geostrophic Wind. Wind computed by equating the Coriolis force to the pressure gradient force.

ITCZ (Inter Tropical Convergence Zone). A relatively narrow and often interrupted band, usually within about 10° of the Equator, of convergent trades, lowered surface pressures and heavy cloud systems extending to high altitudes.

LFM (Limited-area Fine Mesh). A grid system used in a synoptic-scale short-range forecast model with 6 (now 7) levels and a grid spacing of 190.5 km.

Long-wave-Scale. A scale suitable for depicting waves in the circumpolar circulation with lengths such that one to five waves would encircle the globe. These are normally slow moving, large amplitude waves which may propagate either west to east or east to west. They are associated with weather regimes, rather than with individual storms.

MCC (Meso-scale Cloud Cluster). In the tropics, often along the ITCZ, many individual convective storms are clustered rather than being evenly dispersed. Over such clusters, the rising air associated with each cell is not compensated for in the narrow regions of sinking air between the cells; thus the net upper-air flow in the vicinity of the MCC is divergent.

Meso-Scale. A scale suitable for the resolution of such meteorological features as fronts, rainbands and clusters of convective cells.

MONEX (Monsoon Experiment). An extensive study of both summer and winter monsoons over S. E. Asia and the western tropical Pacific during the 1973-1974 time period.

MOS (Model Output Statistics). Statistics ordinarily relating various synoptic-scale circulation parameters from the output of a dynamic model to local (point) variables such as station temperature or precipitation. The statistics, accumulated over a long period of comparison, are used to generate weighting coefficients for the inference of the point variables from a combination of the circulation model output variables.

NGM (Nested Grid Model). A forecast model using a 16 level grid with horizontal spacing of 2° longitude and 1.5° latitude over the forecast area and with larger spacing, comparable to the LFM, outside of the forecast area.

NMC (National Meteorological Center).

OLR (Outgoing Long-wave Radiation). Usually measured by satellite, this radiation is indicative of the temperature of the radiating surface. High OLR levels for the tropics are associated with either cloudless regions which permit direct radiation from the surface or low clouds, the tops of which are relatively warm. The lowest tropical OLR indicates cloud cover extending to the highest levels, with temperatures consistent with that of the tropopause

PC (Principal Component). When the normalized eigenvectors comprising empirical orthogonal functions (EOF's) are multiplied by the square roots of their associated eigenvalues they form what is known as a principal component *loading* matrix. When an eigenvector is multiplied point by point with the original anomalous field at a given time and summed, the result is a point in a matrix known as a principal component *score* matrix. Each column in the PC score matrix is a time series representing the amplitude of that particular EOF as a contribution to the total anomalous field. In this study, for convenience and to avoid excess repetition, the term PC is used here, in the latter sense, to refer to the amplitude or score time-series.

Primitive Equation Model. A model, often a forecast model, which integrates the momentum equations to extrapolate the evolution of atmospheric variables. The horizontal equations are the fundamental Newtonian equations, referenced to a rotating spherical Earth (but not including the "curvature" terms, which are several orders of magnitude less in effect

than are the pressure gradient), Coriolis and acceleration terms. The vertical equation of motion is replaced by that of the hydrostatic approximation.

QBO (Quasi-Biennial Oscillation). A wind alternation in the equatorial stratosphere of easterly and westerly flows which propagates downward at about 1 km per month. The opposing flows are most prominent from about 10mb to 40mb and the cycle, which is not strictly regular, has a period of roughly two years.

RAOB (Radiosonde Observation). Observation of winds, altitude of pressure levels, temperatures and humidities telemetered back to a ground station by radio from a free balloon. Taken normally twice daily (00Z and 12Z) from widely separated stations. There are only 7 such stations in the Pacific Northwest.

SOI (Southern Oscillation Index). The index most often used to characterize the state of the tropical Pacific. It is the monthly averaged surface pressure at Tahiti, divided by the standard deviation of this pressure minus the corresponding measure at Darwin, Aus. Positive values of the SOI are associated with "cool" episodes with strong easterlies over the eastern tropical Pacific and cold upwelling ocean water. Negative values are associated with "warm" or El Niño events.

SST (Sea Surface Temperature). Temperature of the sea surface, typically the "skin" temperature at the interface with the atmosphere.

Synoptic-Scale. A scale suitable for the resolution of the gross structure of extratropical cyclones. Tropical cyclones are generally considered to be at the small-scale limit of the synoptic-scale in their overall pressure structure but the major constituents, such as rain bands and eye wall are

meso-scale. The term "synoptic", as applied to meteorology, was used originally to refer to an analysis for which all variables were presented as a function of space but were simultaneous, or *synoptic*. The resolution of such analyses was limited by the reporting station density, ranging from about 10 to 200 miles. To distinguish this scale from other larger or smaller scale analyses, which were also simultaneous, the scale itself was named synoptic.